



## UNIVERSIDAD NACIONAL AUTÓNOMA DE MÉXICO

### Maestría y Doctorado en Ciencias Bioquímicas

Efecto de la Glucosa-6-fosfato, Fructosa-6-fosfato y Fructosa-1,6-bisfosfato en la modulación del canal mitocondrial inespecífico de *Saccharomyces cerevisiae* (<sub>Sc</sub>MUC).

TESIS

QUE PARA OPTAR POR EL GRADO DE:

Doctor en Ciencias

PRESENTA:

Mónica Rosas Lemus

TUTOR PRINCIPAL:

Dr. Salvador Uribe Carvajal  
[Instituto de Fisiología Celular, UNAM](#)

MIEMBROS DEL COMITÉ TUTOR:

Dra. María Soledad Funes Argüello  
[Instituto de Fisiología Celular, UNAM](#)

Dr. Edmundo Chávez Cossío  
[Instituto Nacional de Cardiología](#)

MÉXICO, D. F., NOVIEMBRE, 2015



**UNAM – Dirección General de Bibliotecas**

**Tesis Digitales**  
**Restricciones de uso**

**DERECHOS RESERVADOS ©**  
**PROHIBIDA SU REPRODUCCIÓN TOTAL O PARCIAL**

Todo el material contenido en esta tesis está protegido por la Ley Federal del Derecho de Autor (LFDA) de los Estados Unidos Mexicanos (México).

El uso de imágenes, fragmentos de videos, y demás material que sea objeto de protección de los derechos de autor, será exclusivamente para fines educativos e informativos y deberá citar la fuente donde la obtuvo mencionando el autor o autores. Cualquier uso distinto como el lucro, reproducción, edición o modificación, será perseguido y sancionado por el respectivo titular de los Derechos de Autor.

## **AGRADECIMIENTOS**

A la **Universidad Nacional Autónoma de México** (UNAM) y al **Programa de Maestría y Doctorado en Ciencias Bioquímicas**, por la formación y apoyos recibidos.

Al **Consejo Nacional de Ciencia y Tecnología** (CONACYT) por la beca de manutención para desarrollar este trabajo (CVU: 297126).

Al **Programa de Apoyo a los estudios de Posgrado** (PAEP) por los apoyos otorgados para la asistencia a congresos nacionales e internacionales.

A los programas que apoyaron la realización de este proyecto: **CONACYT** (239487) y **DGAPA-PAPIIT** (IN204015).

Al **Dr. Salvador Uribe Carvajal** por su apoyo y guía durante mi formación en el posgrado.

Al **Dr. Marcos Hernández Rodríguez** del Instituto de Química, UNAM por su colaboración para la síntesis del 1,4-bisfosfobutano.

A la **Dra. Anne Devin** de la Université de Bordeaux, France por su cotutela y apoyo durante mi estancia en su laboratorio.

A las Instituciones que hicieron posible mi estancia: **Campus France, UNAM, Institut de Biochimie et Génétique Cellulaires, Université de Bordeaux**.

A los integrantes del Comité Tutor:

**Dr. Edmundo Chávez Cossío**  
**Dra. María Soledad Funes Argüello**

A los integrantes del Jurado de Examen:

Presidente: **Dr. Antonio Peña Díaz**  
Vocal: **Dra. Marietta Tuena Sangri**  
Vocal: **Dr. Horacio Reyes Vivas**  
Vocal: **Dr. José Salud Rodríguez Zavala**  
Secretario: **Dr. Ismael Bustos Jaimes**

A las asistentes de procesos del Programa de Maestría y Doctorado en Ciencias Bioquímicas: **Leticia García Gutiérrez, Adelina González Pérez, Sara Méndez Ibáñez**.

A la **Dra. Natalia Chiquete Félix**, Técnico Académico del lab. 305-Ote, IFC, UNAM.

A **Teresa Castillo**, secretaria de la Sociedad Mexicana de Bioquímica, oficina IFC, UNAM.

A **Gabriela Valdés**, secretaria del Departamento de Genética Molecular, IFC, UNAM.

## Índice

<b>1. Antecedentes</b>	<b>1</b>
1.1 El metabolismo y la bioenergética	1
1.2 La glucólisis en <i>Saccharomyces cerevisiae</i>	2
1.3 La fosforilación oxidativa en <i>S. cerevisiae</i>	6
1.4 El canal mitocondrial inespecífico de <i>S. cerevisiae</i> ( <i>ScMUC</i> )	13
1.5 El efecto Crabtree	17
1.6 El 1,4-bisfosfobutano, análogo de la fructosa-1,6-bisfosfato	20
<b>2. Planteamiento del problema</b>	<b>21</b>
<b>3. Hipótesis</b>	<b>21</b>
<b>4. Objetivos</b>	<b>21</b>
4.1. Objetivo general	
4.2. Objetivos particulares	
<b>5. Materiales y métodos</b>	<b>22</b>
5.1. Cultivo de la levadura	22
5.2. Obtención de las mitocondrias	22
5.3. Cuantificación de proteína	23
5.4. Consumo de oxígeno	23
5.5. Hinchamiento mitocondrial	23
5.6. Potencial transmembranal	24
5.7. Síntesis del 1,4-bisfosfobutano	24
5.8. Actividad de la aldolasa	26
<b>6. Resultados</b>	<b>27</b>
6.1. Efecto de las hexosas fosfato sobre el consumo de oxígeno	27
6.2. Efecto de las hexosas fosfato sobre el potencial transmembranal	30
6.3. Efecto de las hexosas fosfato sobre el hinchamiento mitocondrial	33
6.4. Efectos de la F1,6BP sobre la respiración en mitocondrias de <i>S. cerevisiae</i> y <i>K. lactis</i>	36
6.5. Resonancia Magnética Nuclear (RMN) de la síntesis del 1,4- bisfosfobutano	38
6.6. Efecto del 1,4-bisfosfobutano sobre la actividad de la aldolasa	45
6.7. Efecto del 1,4-bisfosfobutano sobre el hinchamiento mitocondrial	46
6.8. Efecto del 1,4-bisfosfobutano sobre el potencial transmembranal	47

<b>7.</b>	<b>Discusión</b>	<b>49</b>
<b>8.</b>	<b>Conclusiones</b>	<b>52</b>
<b>9.</b>	<b>Perspectivas</b>	<b>52</b>
<b>10.</b>	<b>Referencias</b>	<b>53</b>
<b>11.</b>	<b>Anexos</b>	

11.1 Informe de estancia en cotutela con la Universidad de Bordeaux, Francia.

11.2 Artículos publicados.

### Tabla de abreviaturas

<b>ANT</b>	Translocador de nucleótidos de adenina
<b>BSA</b>	Albúmina sérica bobina
<b>CsA</b>	Ciclosporina A
<b>CypD</b>	Ciclofilina D
<b>Cyt c</b>	Citocromo c
<b>CCCP</b>	Cianocarbonil- <i>m</i> -clorofenilhidrazona
<b>F1,6BP</b>	Fructosa 1,6-bisfosfato
<b>G6P</b>	Glucosa-6-fosfato
<b>GAPDH</b>	Gliceraldehido-3-fosfato deshidrogenasa
<b>MIM</b>	Membrana interna mitocondrial
<b>MEM</b>	Membrana externa mitocondrial
<b>MUC</b>	Canal mitocondrial inespecífico
<b>Prot.</b>	Proteína
<b>PGK</b>	3-Fosfo glicerato cinasa
<b>Pic</b>	Acarreador de fosfato
<b>Pi</b>	Fosfato inorgánico
<b>PTP</b>	Poro de transición de la permeabilidad
<b>ROS</b>	Especies reactivas de oxígeno
<b>RMN</b>	Resonancia magnética nuclear
<b>scMUC</b>	Canal mitocondrial inespecífico
<b>VDAC</b>	Canal aniónico dependiente de voltaje
<b>ΔG</b>	Cambio en la energía libre de Gibbs
<b>1,4bpb</b>	1,4-bisfosfobutano

## Resumen

En *Saccharomyces cerevisiae*, la adición de glucosa al medio de cultivo inhibe la respiración. Este fenómeno se denomina efecto Crabtree, el cual es resultado de diversas condiciones metabólicas reversibles y rápidas, como la competencia entre la glucólisis y la fosforilación oxidativa por el ADP y el Pi. Previamente se demostró que la glucosa-6-fosfato (G6P) acelera la respiración y la fructosa-1,6-bisfosfato (F1,6BP) inhibe la actividad de los complejos mitocondriales III y IV. Sin embargo, no se sabe qué otros mecanismos podrían estar involucrados en dicho fenómeno. El <sub>Sc</sub>MUC regula la fosforilación oxidativa dependiendo de su estado de apertura; es a su vez modulado por Pi, Ca<sup>2+</sup>, Mg<sup>2+</sup>, ATP y la actividad de la cadena respiratoria. El objetivo de este trabajo consistió en estudiar los efectos de las hexosas fosfato de la glucólisis sobre el canal inespecífico mitocondrial de *S. cerevisiae* y determinar si el <sub>Sc</sub>MUC podría estar implicado en la inducción del efecto Crabtree. Se observó que la G6P abre parcialmente el <sub>Sc</sub>MUC, sin embargo su efecto es inhibido por la F1,6BP, la cual cierra el <sub>Sc</sub>MUC, causando una disminución en el consumo de oxígeno. Además la F1,6BP no tiene efectos sobre la respiración en la levadura Crabtree negativa *K. lactis*, lo cual sugiere que el <sub>Sc</sub>MUC participa en la inducción del efecto Crabtree. Para poder estudiar los efectos de la F1,6BP sobre el <sub>Sc</sub>MUC en la levadura completa se sintetizó un análogo estructural de la F1,6BP, el cual había sido previamente reportado como un inhibidor competitivo de la aldolasa (1,4-bisfosfobutano). El compuesto sintetizado es un buen análogo no metabolizable de la F1,6BP, ya que es un inhibidor competitivo de la aldolasa, cierra al <sub>Sc</sub>MUC y evita los efectos de la G6P en la mitocondria aislada.

## **Abstract**

In *Saccharomyces cerevisiae* addition of glucose inhibits oxygen consumption, i.e. *S. cerevisiae* is Crabtree-positive. During active glycolysis hexoses-phosphate accumulate, and probably interact with mitochondria. In an effort to understand the mechanism underlying the Crabtree effect, the effect of two glycolysis-derived hexoses-phosphate was tested on the *S. cerevisiae* mitochondrial unspecific channel ( $_{Sc}MUC$ ). Glucose-6-phosphate (G6P) promoted partial opening of  $_{Sc}MUC$ , which led to proton leakage and uncoupling which in turn resulted in accelerated oxygen consumption. In contrast, fructose-1,6-bisphosphate (F1,6BP) closed  $_{Sc}MUC$  and thus inhibited the rate of oxygen consumption. When added together, F1,6BP reverted the mild G6P-induced effects. F1,6BP is proposed to be an important modulator of  $_{Sc}MUC$ . This inhibition of  $_{Sc}MUC$  is exclusive for *S. cerevisiae*, because in isolated mitochondria of *K. lactis* a Crabtree negative yeast, any effects of F1,6BP was observed. In order to determinate if F1,6BP modulates the  $_{Sc}MUC$  in the whole cell, a F1,6BP analog was synthetized (1,4-bisphosphobutane). This molecule is a competitive inhibitor of the aldolase previously reported. In isolated mitochondria 1,4BPPB closes the  $_{Sc}MUC$  and protects against the effects of G6P. Then the 1,4-bisphosphobutane is a good non metabolizable analog of F1,6BP.

## 1. Antecedentes

### 1.1 El metabolismo y la bioenergética.

El metabolismo es el conjunto de reacciones bioquímicas que ocurren en la célula; se divide en catabolismo y anabolismo: El catabolismo es la transformación de moléculas más grandes a moléculas más pequeñas, con el objetivo de producir energía y obtener moléculas necesarias para una gran diversidad de funciones. El anabolismo es la generación de moléculas más complejas a partir de moléculas más simples utilizando energía. La mayoría de estas reacciones no son espontáneas, se trata de reacciones que se favorecen por la participación de las enzimas y dependen de la concentración de sustratos, productos, coenzimas y la energía disponible; la cual se conserva a través de la generación de moléculas como el ATP o la producción de calor (Leverve, 2007; Mazat y col., 2013). La bioenergética se encarga de estudiar estos procesos a través de la termodinámica, considerando a la célula como un sistema abierto, irreversible y fuera del equilibrio, donde el progreso de las reacciones bioquímicas está regulado por los cambios en la energía libre de las reacciones de oxidorreducción (Nicholls y Ferguson, 2003):

$$\Delta G_{\text{ox/red}} = \Delta G^\circ + \ln [\text{NADH}]/[\text{NAD}^+]$$

y el potencial de fosfato de la célula:

$$\Delta G_P = \Delta G^\circ + \ln [\text{ATP}]/[\text{ADP}][\text{Pi}]$$

Tomando a *Saccharomyces cerevisiae* como ejemplo para explicar los potenciales de oxidorreducción y fosfato durante la glucólisis, se ha observado que para que haya un flujo eficiente en la vía, debe haber disponibilidad de fosfato inorgánico (Pi) y de NAD<sup>+</sup>, para oxidar al gliceraldehído-3-fosfato a 1,3-bifosfoglicerato, y ADP y fosfato para que la fosfoglicerato cinasa y la

piruvato cinasa, sinteticen ATP a nivel de sustrato. Si la concentración de ATP supera la concentración de ADP y Pi, quiere decir que la célula tiene suficiente energía y no es necesario sintetizar más del primero por la vía glucolítica. La producción de etanol es una estrategia para regenerar al NAD<sup>+</sup> y permitir que la glucólisis continúe, porque la alcohol deshidrogenasa tiene una constante de equilibrio fuertemente desplazada hacia la producción de alcohol, que además se diluye porque éste es expulsado al exterior. Es así que tanto el potencial de fosfato como el de oxidorreducción permiten la homeostasis celular. Otro ejemplo del acoplamiento entre el potencial de oxidorreducción y el potencial de fosfato, es la fosforilación oxidativa. Donde el NADH se oxida a NAD<sup>+</sup>, mediante las enzimas de la cadena respiratoria, transformando su potencial de oxidorreducción en un potencial electroquímico de protones, el cual es utilizado por la ATP sintasa para la fosforilación del ADP y obtención del ATP (Devin y Rigoulet, 2007). En este caso, la energía obtenida de las reacciones de oxidorreducción se acopla a la síntesis de ATP.

## 1.2 La glucólisis en *Scharomyces cerevisiae*.

La glucólisis es probablemente la vía metabólica más conservada; puede observarse en bacterias, plantas, levaduras y animales. En *S. cerevisiae*, glucólisis comienza por la fosforilación de la glucosa mediante la hexocinasa, ésta se transforma en fructosa-6-fosfato y posteriormente se transforma en fructosa-1,6-bisfosfato mediante la fosfofructocinasa (PFK). Este es el primer punto de regulación irreversible para esta vía, ya que depende de los niveles de ATP y de la concentración de fructosa-2,6-bisfosfato. Si la concentración de ATP es baja, el flujo glucolítico continúa y los niveles de fructosa-2,6-bisfosfato aumentan, activando a la PFK. Posteriormente la fructosa-1,6-bisfosfato se transforma en gliceraldehído-3-fosfato y dihidroxiacetona-3-fosfato gracias a la aldolasa. Estos

productos pueden continuar hacia la producción de etanol o bien, ser utilizados para la producción de glicerol.

La mayor parte de la dihidroxiacetonafosfato es transformada por la triosa fosfato isomerasa en gliceraldehído-3-fosfato y continúa hacia la producción de etanol. La gliceraldehído-3-fosfato deshidrogenasa lo oxida a 1,3-bisfosfoglicerato; luego la fosfoglicerato cinasa genera el 3-fosfoglicerato y el primer ATP de la glucólisis. Posteriormente, la fosfoglicerato mutasa transforma el 3-fosfoglicerato en 2-fosfoglicerato, que la enolasa transforma a su vez en fosfoenolpiruvato, el cual sirve como sustrato para la producción del segundo ATP de la glucólisis, a cargo de la piruvato cinasa. Esta enzima es el segundo punto de control importante, regulado por la concentración de ADP, Pi y ATP. El piruvato se transforma en acetaldehído mediante la piruvato descarboxilasa, y la alcohol deshidrogenasa reduce el acetaldehído a etanol, (Lehninger y col., 2005). Finalmente el etanol sale de la célula (Fig. 1), y cuando la glucosa se termina, éste puede ser utilizado por la alcohol deshidrogenasa y generar NADH, el cual es utilizado por las NADH deshidrogenasas mitocondriales para la obtención de ATP mediante la fosforilación oxidativa. A éste fenómeno se le denomina cambio diáuxico (Schweizer, 1999) y no sucede en otras levaduras como *Kluyveromyces lactis* (Piskur y col., 2006).

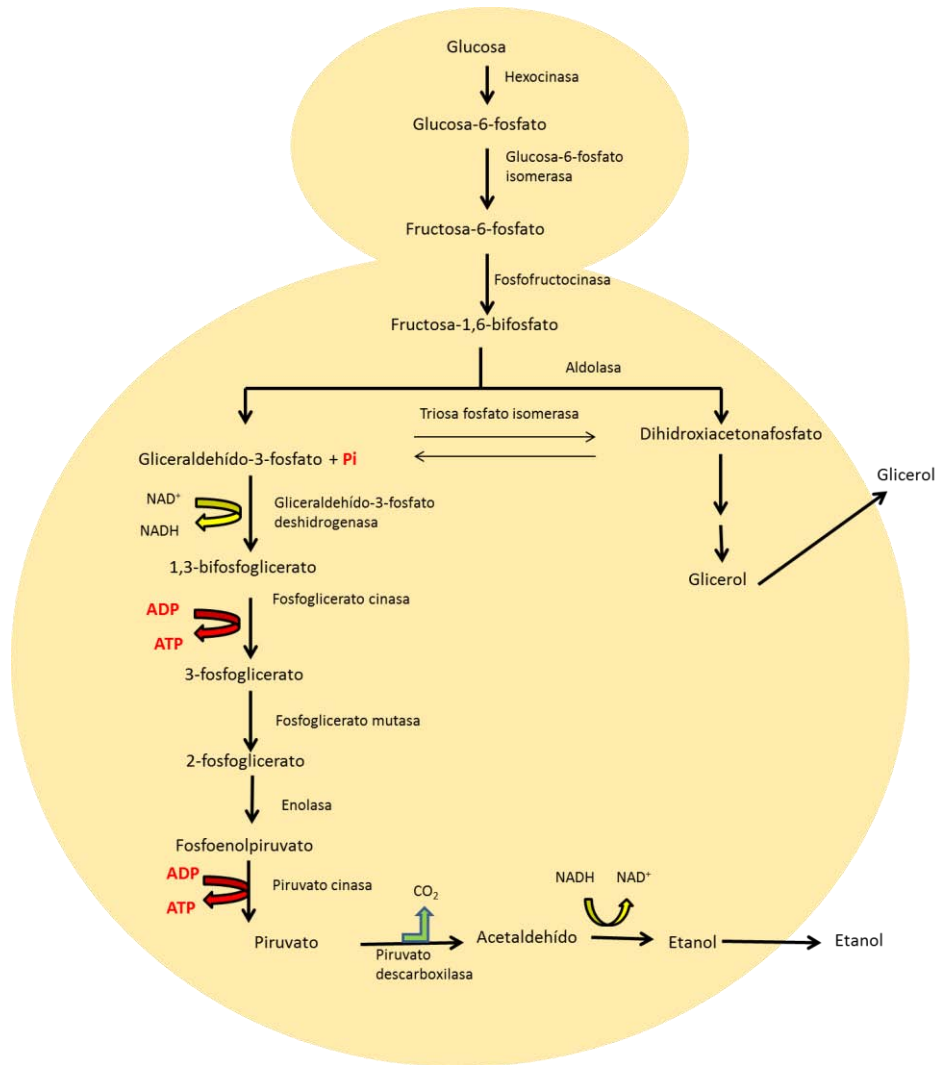


**Fig. 1. La glucólisis en *Saccharomyces cerevisiae*.**

La regulación de la glucólisis depende de la expresión de proteínas, coenzimas y disponibilidad de sustratos. Se sabe que la regulación más importante para la glucólisis en *S. cerevisiae* es a nivel postranscripcional. La PFK y la PK son las enzimas más importantes en la regulación del flujo de la vía y se regulan principalmente por el ADP disponible y la cantidad de ATP en el medio (Daran-Lapujade y col., 2007). Sin embargo, para poder analizar la regulación de estas vías, también debe tomarse en cuenta la formación de metabolones, previamente sugerida (Clegg, 1984). Se propone que la saturación de sustratos y proteínas en el citoplasma, promueve la asociación de proteínas de la misma vía metabólica, lo cual favorece la canalización y compartimentalización de sustratos (Ovadi y Saks, 2004). En *S. cerevisiae*, las enzimas contiguas de la glucólisis interaccionan unas con otras (Araiza-Olivera y col., 2010) y su asociación es estabilizada por la actina filamentosa. Estas asociaciones también pueden servir para proteger a las enzimas de posibles inhibidores o la presencia de solutos compatibles que aumentan la viscosidad del medio y podrían afectar su actividad (Araiza-Olivera y col., 2013). Los metabolones no son estáticos, obedecen a las necesidades energéticas de la célula; además el citoesqueleto parece funcionar como un sensor metabólico para favorecer o disminuir la formación de metabolones, ya que tanto la actina como la tubulina requieren de nucleótidos trifosfato para polimerizar (Cassimeris y col., 2012). Recientemente, se demostró que la actina cambia su estructura dependiendo de la fase de crecimiento y probablemente de la presencia de glucosa en el medio (Oláh y col., 2013).

Se sugiere la existencia de un metabolón que comunica la glucólisis, el ciclo de Krebs y la fosforilación oxidativa para hacer más eficiente la producción de ATP. En mamíferos y plantas se reportó la interacción directa de enzimas de la glucólisis (principalmente hexocinasa) (Xie y Wilson, 1988; Pastorino y Hoek, 2008), el citoesqueleto (actina y tubulina) y la mitocondria a través del canal aniónico dependiente de voltaje (VDAC) (Ahmadzadeh y col., 1996; Colombini, 2004; Balasubramanian y col., 2007; Rostovtseva y col., 2008; Kuznetsov y col., 2013). En *S. cerevisiae*

algunas enzimas de la glucólisis interaccionan con la mitocondria (Brandina y col., 2006). Además *in vivo*, el NADH generado en el citoplasma mediante la adición de Fructosa-1,6-bisfosfato, es canalizado hacia la mitocondria a través del VDAC, lo cual vuelve más eficiente la respiración que cuando el NADH proviene de la oxidación del etanol (Avéret y col., 2002). Es así evidente que en *S. cerevisiae*, existe una estrecha comunicación entre la glucólisis y la fosforilación oxidativa de una manera diferente a las células aerobias, pero sí comparable con las células tumorales, ya que su alto potencial fermentativo, inhibe el consumo de oxígeno en presencia de glucosa (Díaz-Ruiz y col., 2009).

### 1.3. La fosforilación oxidativa en *S. cerevisiae*.

Los organismos eucariontes poseen organelos delimitados por membranas con funciones específicas. La mitocondria es el organelo que se encarga principalmente de la síntesis del ATP. Es una red dinámica de dos membranas que da lugar a dos compartimentos: la matriz mitocondrial delimitada por la membrana interna mitocondrial, y el espacio intermembranal, situado entre la membrana interna mitocondrial (MIM) y la membrana externa mitocondrial. La MIM, es altamente selectiva e impermeable, tiene múltiples invaginaciones a causa de la estructura de los dímeros de la ATP sintasa, lo cual aumenta su extensión. La dinámica de las crestas mitocondriales cambia según el estado energético de la célula, el estrés oxidante, la apoptosis o procesos patológicos. La membrana externa mitocondrial tiene más lípidos, es menos selectiva y no tiene invaginaciones (Mannella, 2006). En la Fig. 2 se observa la red mitocondrial de una célula en gemación de *S. cerevisiae* (A) y un corte transversal de la mitocondria (B), donde se observan: la membrana externa, las crestas mitocondriales de la membrana interna y los sitios de contacto entre ambas membranas.

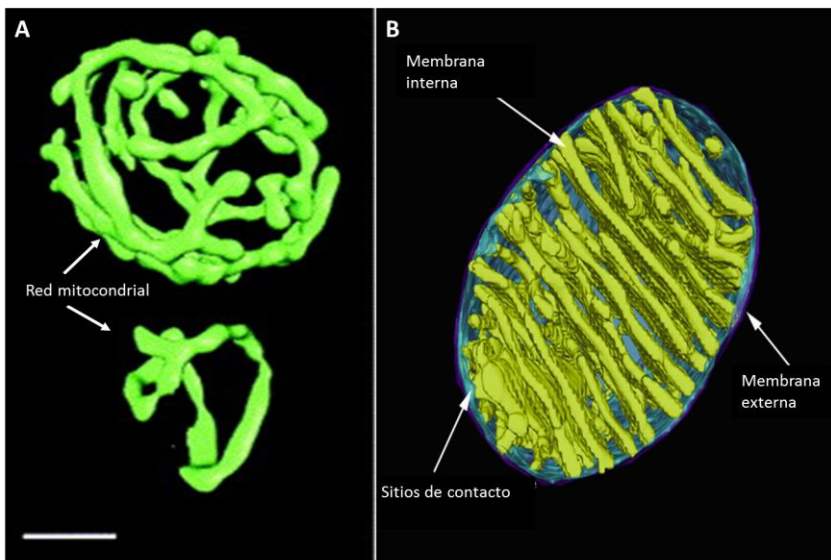


**Fig. 2. La estructura de la mitocondria** **A**, Reconstrucción tridimensional de microscopía electrónica de fluorescencia de alta resolución. En verde se observa la proteína verde fluorescente (GFP), que marca la matriz mitocondrial en una célula de *S. cerevisiae* en gemación (Egner y Hell, 2005). **B**, reconstrucción tridimensional de una microscopía electrónica de células dendríticas del cerebelo (modificado de (Perkins y col., 1997). Se muestran la membrana externa en morado, la membrana interna en amarillo y los sitios de contacto en azul claro.

De acuerdo con la teoría quimiosmótica, la fosforilación oxidativa es el proceso mediante el cual las proteínas de la cadena respiratoria oxidan a los productos del ciclo de Krebs (NADH y  $\text{FADH}_2$ ), transfieren los electrones desde oxidases de mayor a menor potencial electroquímico, a la vez que bombean protones desde la matriz mitocondrial, hacia espacio intermembranal. Esta diferencia de concentración de protones entre el espacio intermembranal y la matriz mitocondrial, genera un potencial electroquímico, el cual es transformado en trabajo por la ATP sintasa para la producción de ATP (Mitchell, 1966). Recordando que la progresión de una reacción bioquímica está dada por el cambio en la energía libre de la reacción, en el caso del bombeo de los protones se puede expresar de la siguiente manera:

$$\Delta G = 2.3 RT \log ([H^+]_A/[H^+]_B) \dots \dots \dots (1)$$

Donde  $[H_A]$  y  $[H_B]$  representan la concentración de protones en la matriz mitocondrial y el espacio intermembranal,  $R$  ( $J \text{ mol}^{-1} \text{ K}^{-1}$ ) es la constante de los gases y  $T$  ( $K$ ) es la temperatura. Debido a que los protones son átomos con carga, se establece una diferencia de potencial electroquímico que se expresa como:

$$\Delta G = -mF\Delta\Psi \dots \dots \dots \text{(Marty y col.)}$$

Siendo  $m$  el número de moles (1),  $F$  la constante de Faraday ( $96485,309 \text{ C mol}^{-1}$ ) y  $\Delta\Psi$ , la diferencia de cargas entre la matriz mitocondrial y el espacio intermembranal. Dado que el  $\Delta G$  de la reacción, se compone tanto de la concentración de protones como de la carga eléctrica de éstos, entonces se suman las ecuaciones 1 y 2, de lo cual resulta:

$$\Delta G (\text{kJmol}^{-1}) = 2.3 RT \log ([H^+]_A/[H^+]_B) - F\Delta\Psi \dots \dots \dots (3)$$

Debido a que el  $\Delta G$ , en realidad es un potencial de protones y  $\log ([H^+]_A/[H^+]_B)$  es un  $\Delta pH$ , la ecuación (3) puede expresarse también de la siguiente manera:

$$\Delta\mu_{H^+} = 2.3 RT \Delta pH - F\Delta\Psi \dots \dots \dots (4)$$

Para ilustrar el término de la fuerza protón motriz o  $\Delta p$ , que relaciona el potencial de oxidorreducción con la acumulación de  $H^+$ , puede tomarse la ecuación (4) y dividirla por la constante de Faraday, para obtener (5), y al sustituir los valores de R ( $8.3 \text{ kJmol}^{-1} \text{ K}^{-1}$ ) y T (298.15 K), se obtiene (6). Entonces esta ecuación representa el potencial electroquímico que es necesario para la síntesis del ATP, mediante la ATP sintasa (Nicholls y col., 2003).

Debido a que el acoplamiento de la fosforilación oxidativa depende tanto de las reacciones de oxidorreducción y el potencial electroquímico generados por la cadena respiratoria, es importante que no existan transportes inespecíficos que alteren la homeostasis electroquímica; es por ello que el transporte de los metabolitos que entran y salen de la mitocondria, son procesos altamente regulados. Es posible conocer la integridad de la mitocondria y el acoplamiento de la fosforilación oxidativa midiendo el consumo de oxígeno, el establecimiento del potencial transmembranal y el hinchamiento mitocondrial. Los estados clásicos descritos para la respiración son 4; el estado I corresponde al consumo de oxígeno por la mitocondria sola en presencia de fosfato, el estado II se produce al adicionar un sustrato de la cadena respiratoria, el estado III se induce al agregar una cantidad definida de ADP, lo cual incrementa el consumo de oxígeno debido a que el potencial transmembranal generado se utiliza para la síntesis de ATP y la cadena respiratoria aumenta su actividad. El estado IV, se obtiene una vez que el ADP adicionado se terminó y el consumo de oxígeno sólo es debido a la presencia del sustrato, algunos autores sugieren que el estado 2 y 4 son equivalentes (Nicholls y col., 2003). Adicionalmente pueden compararse estos estados con el estado desacoplado (U), el cual se produce en presencia de sustrato y un desacoplante como el CCCP o

FCCP, éstas moléculas son ácidos débiles hidrofóbicos que se protonan en el espacio intermembranal y se desprotonan en la matriz mitocondrial, lo cual causa una disminución del potencial transmembranal y acelera el consumo de oxígeno. Al realizar el cociente del consumo de oxígeno en estado 3 y 4, puede conocerse el CR o control respiratorio. El cociente U/4, también puede decir que tan acopladas están las mitocondrias ya que compara la respiración máxima de la cadena respiratoria y la respiración en presencia de sustrato. En la levadura un CR o U/4 cercano a 2 o más, implica que las mitocondrias están acopladas

El potencial transmembranal puede medirse mediante el cambio de absorbancia o fluorescencia de colorantes catiónicos como la O-safranina, la cual es atraída hacia la matriz mitocondrial mientras la mitocondria pueda establecer potencial, esto provoca una disminución en su absorbancia o fluorescencia, la cual se recupera al adicionar un desacoplante, ya que se abate el potencial, la safranina nuevamente es liberada y se recupera su absorbancia.

Las mitocondrias responden a cambios en la osmolaridad, si existe un transporte inespecífico de solutos y agua, la membrana interna pierde su estructura plegada y la mitocondria se hincha. Si se siguen estos cambios en un espectrofotómetro, se observará un descenso en la absorbancia de la suspensión mitocondrial. El hinchamiento descontrolado, puede causar la ruptura de la membrana externa. Se ha observado por ejemplo, que la alteración mitocondrial está involucrada en procesos patológicos, principalmente muerte celular descontrolada, cáncer y diabetes.

La cadena respiratoria de las mitocondrias cambia dependiendo el organismo; en los mamíferos se compone de: la NADH deshidrogenasa (complejo I) que dona los electrones del NADH a la quinona, la reduce a quinol y a la vez bombea 4 protones hacia el espacio intermembranal. La succinato deshidrogenasa (complejo II), que reduce al FAD a FADH<sub>2</sub> y también dona los electrones a

la quinona, pero no bombea protones. Posteriormente, la quinol oxidasa (complejo III) recibe los electrones del ubiqinol, uno a uno a la vez que bombea 2 protones por cada electrón. Posteriormente, el complejo III transfiere los electrones al citocromo *c*, que a su vez los transfiere a la citocromo *c* oxidasa; este complejo bombea 2 protones por cada electrón (complejo IV). Finalmente la citocromo *c* oxidasa reduce al oxígeno para producir H<sub>2</sub>O. La cadena respiratoria de *S. cerevisiae* no tiene complejo I; se cree que éste es sustituido por las NADH deshidrogenasas, una en la matriz mitocondrial y las otras dos en el espacio intermembranal; ambas son periféricas y ninguna bombea protones. También tiene complejo II, complejo III, citocromo *c* y complejo IV. Además de estos componentes clásicos, también posee una glicerol fosfato deshidrogenasa y una lactato deshidrogenasa. La primera dona sus electrones directo a la quinona y produce dihidroxiacetona fosfato, mientras que la segunda, dona sus electrones directo al citocromo *c* (Pallotta y col., 2004) y produce piruvato. La composición de la cadena respiratoria de *S. cerevisiae* se muestra en la Fig. 3. Donde se muestra que las únicas bombas de protones que posee son el complejo III y IV.

### Espacio intermembranal

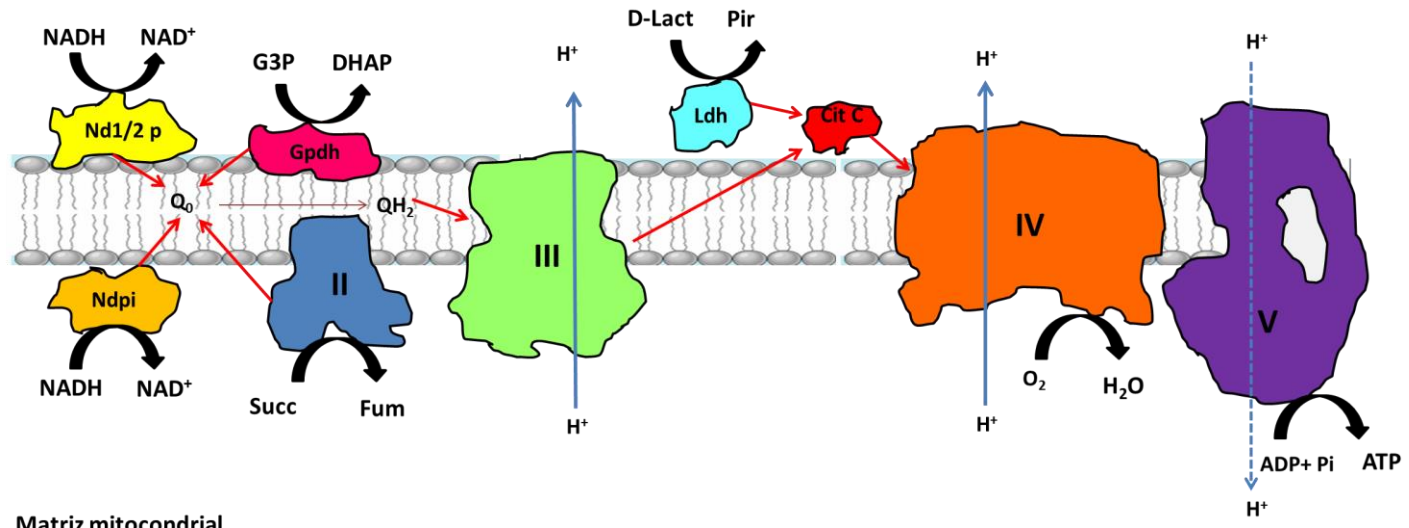


**Fig. 3. La cadena respiratoria de *S.Cerevisiae*.** Se muestran en amarillo las NADH deshidrogenasas externas (Nd1/2 p) y la NADH deshidrogenasa interna (Ndpi). En rosa, la glicerol-3-fosfato deshidrogenasa (Gpdh), que oxida el glicerol-3-fosfato a dihidroxiacetona fosfato. En azul el complejo II que oxida el succinato a fumarato. Todas estas enzimas donan los electrones a la quinona ( $Q_o$ ) para convertirla en ubiquinol ( $QH_2$ ). En verde, el complejo II, y en azul agua, la lactato deshidrogenasa que oxida el lactato (D-Lact) a piruvato (Pir). Ambas enzimas donan sus electrones al citocromo c (cit c), en rojo. En naranja, el complejo IV y el morado el complejo V. Las flechas rojas indican el camino de los electrones, las azules el bombeo de los protones desde la matriz mitocondrial al espacio intermembranal. La flecha azul discontinua, señala el retorno de los protones a través de la ATP sintasa.

Se ha planteado que los complejos de la cadena respiratoria no están dispersos en la membrana interna mitocondrial, sino que fluctúan entre dos estados: la formación de supercomplejos y un estado libre con diferentes pozas de quinonas; ésto principalmente para el complejo II, lo cual mejora la canalización de los electrones y podría evitar el estrés oxidante. En *S. cerevisiae*, se ha observado la asociación de los complejos III y IV, la cual es estabilizada por la cardiolipina (Zhang y col., 2005).

#### 1.4. El canal inespecífico mitocondrial de *S. cerevisiae* (*ScMUC*)

En la mitocondria se realiza la fosforilación oxidativa; en el proceso participan las proteínas localizadas en la membrana interna mitocondrial; las de la cadena respiratoria y la ATP sintasa. Se plantea que este proceso tuvo lugar una vez que la atmósfera primitiva aumentó la concentración de oxígeno durante el evento de la gran oxigenación (GOE) (Mentel y Martin, 2008) y que los organismos que habitaban la tierra evolucionaron para aprovechar el alto potencial electronegativo de éste y con ello hacer más eficiente la síntesis del ATP (Lang y col., 1999; Tielens y col., 2002). Algunos autores sugieren que este proceso también originó a la mitocondria, ya que la mayoría de los organismos de vida libre que no se adaptaron al nuevo entorno se extinguieron (Castresana y Saraste, 1995).

La concentración de oxígeno en la atmósfera es mucho mayor que la necesaria para realizar la fosforilación oxidativa (Wilson y col., 1988); es por ello que también es un potente agente tóxico, ya que la presencia de los electrones desapareados de las moléculas puede reaccionar fácilmente con él y producir especies reactivas de oxígeno, (Abele, 2002). Las ROS sirven como moléculas señalizadoras, pero si se producen en exceso causan daño a las membranas, las proteínas y el ADN (D'Autreaux y Toledano, 2007). Los organismos han desarrollado diversos mecanismos para lidiar con esto. Los multicelulares son en su mayoría oxirreguladores y tienen sistemas sofisticados como branquias o sistemas circulatorios que disminuyen la concentración del oxígeno dentro del organismo (Popel, 1989; Hill, 2004; Konigsberg y col., 2013; Galli y Richards, 2014). Los organismos de vida libre son en su mayoría oxiconfórmeros (Ingledew y Poole, 1984; Tschischka y col., 2000; Guerrero-Castillo y col., 2011); éstos adaptan su metabolismo a la concentración del oxígeno del ambiente. Algunas de estas adaptaciones sirven para reducir al oxígeno sin formar ATP, a la vez que abaten el potencial transmembranal y permiten que el flujo de electrones de la cadena respiratoria permanezca

constante, evitando así la saturación del complejo III, la acumulación de semiquinonas y formación de ROS (Kadenbach, 2003). Tanto oxiconfórmberos como oxirreguladores comparten algunos mecanismos para detoxificar al oxígeno: las proteínas desacoplantes, oxidases alternas y los canales mitocondriales inespecíficos, lo cual respalda la teoría de una conservación evolutiva (Guerrero-Castillo y col., 2011). En este trabajo nos interesa estudiar el papel del canal inespecífico mitocondrial de *S. cerevisiae* y su participación en el efecto Crabtree como mecanismo de desacoplamiento fisiológico.

Los canales inespecíficos mitocondriales han sido observados en levaduras (*Debaryomyces hansenii* y *S. cerevisiae*), plantas y mamíferos. Estos canales promueven la *transición de la permeabilidad mitocondrial* (TP), la cual se define como: la alteración de la permeabilidad de la membrana interna, que permite el paso de moléculas hasta de 1.5 kDa. La TP desacopla la fosforilación oxidativa e incrementa el volumen de la matriz mitocondrial; cuando no se controla, se rompe la membrana externa mitocondrial (Bernardi y col., 2006), lo cual puede causar la muerte celular. Sin embargo, algunos estudios sugieren que la TP es fisiológica y reversible, que sirve para purgar cationes y regular la actividad respiratoria, disminuyendo la producción de especies reactivas de oxígeno (Petronilli y col., 1999; Halestrap, 2004; Uribe-Carvajal y col., 2011).

Se ha propuesto que el canal mitocondrial inespecífico de los mamíferos ( $_m$ MUC), también denominado PTP (poro de transición de la permeabilidad) está formado por la ANT (translocasa de adenin nucleótidos), Pic (acarreador de fosfato), VDAC (canal aniónico dependiente de voltaje) y CypD (ciclofilina D) (Halestrap, 2004; Bernardi y Forte, 2007). Estudios recientes proponen que el PTP está formado por el dímero del complejo V mitocondrial o ATP sintasa (Bonora y col., 2013) (Bernardi, 2013; Giorgio y col., 2013). El  $_m$ MUC se abre en presencia de  $\text{Ca}^{2+}$  (Haworth y Hunter, 1979), Pi, alto pH,  $\text{NAD(P)}^+$ , atractilato, la reducción de enlaces disulfuro (Bernardi, 1999), el flujo rápido de electrones en la cadena respiratoria y algunos análogos de las quinonas (Fontaine y

Bernardi, 1999). Se cierra con Mg<sup>2+</sup>, NAD(P)H, CsA, GSH, ADP, bonkrekato, y por la disminución del pH.

En *S. cerevisiae* se demostró la existencia de un equivalente del <sub>m</sub>MUC (Prieto y col., 1992; Guerin y col., 1994; Manon y col., 1998), denominado <sub>Sc</sub>MUC (canal mitocondrial inespecífico de *S. cerevisiae*), el cual responde de manera similar a algunos de los reguladores del PTP y de manera contraria a otros. Se propone que el <sub>Sc</sub>MUC podría estar conformado por las proteínas VDAC, Pic y ANT (Gutiérrez-Aguilar y col., 2007; Gutiérrez-Aguilar y col., 2010). Este canal se abre en presencia de ATP, bajo Pi y el flujo rápido de electrones de la cadena respiratoria (Guerin y Napias, 1978; Guerin y col., 1994; Manon y Guerin, 1998). Lo cierran el Pi, Ca<sup>2+</sup> y Mg<sup>2+</sup> (Cortés y col., 2000; Perez-Vazquez y col., 2003). Actualmente se han identificado los blancos de algunos de estos reguladores del <sub>Sc</sub>MUC; sin embargo, la estructura del canal y la participación de otros metabolitos en su regulación, continúa siendo tema de debate. En la tabla 1, se muestran los efectores y algunos blancos identificados del canal mitocondrial inespecífico de *S. cerevisiae*, y el MUC de otras especies.

**Tabla 1. Efectores y blancos identificados del MUC de diferentes especies.**

Modulador	Possible blanco	Efecto	MUC
Ácido bonkreiko, ADP	ANT	Cierra	<i>m</i> MUC, <i>L</i> MUC, <i>pea</i> MUC
Carboxiatractilósido y Ácido agárico	ANT	Abre	<i>m</i> MUC
Carboxiatractilósido	ANT	Cierra parcialmente	<i>Sc</i> MUC
Rojo de rutenio	MCU, VDAC	Cierra	<i>m</i> MUC, <i>Zf</i> MUC
Ciclosporina A Sangliferina A	CypD	Cierra	<i>m</i> MUC, <i>Zf</i> MUC, <i>Om</i> MUC, <i>L</i> MUC, <i>Ze</i> MUC, <i>Pt</i> MUC, <i>At</i> MUC, <i>Nt</i> MUC y <i>pea</i> MUC
Hydroxy- decilubiquinona	Desconocido	Abre	<i>m</i> MUC
Ubiquinona 0, decilubiquinona	Desconocido	Cierra	<i>Zf</i> MUC and <i>m</i> MUC
Ca <sup>2+</sup> , Cu <sup>2+</sup> , Cd <sup>2+</sup> , Pb <sup>2+</sup> y Hg <sup>2+</sup>	Desconocido	Abre	<i>m</i> MUC, <i>Sc</i> MUC, <i>Zf</i> MUC, <i>Om</i> MUC, <i>Gs</i> MUCZeMUC, <i>Pt</i> MUC, <i>oa</i> MUC, <i>wheat</i> MUC y <i>At</i> MUC
Me <sup>2+</sup> y La <sup>3+</sup>	Desconocido	Cierra	<i>m</i> MUC, <i>Sc</i> MUC, <i>L</i> MUC, <i>At</i> MUC y <i>Dh</i> MUC
Aquilaminas	Desconocido/VDAC	Cierra	<i>m</i> MUC y <i>Sc</i> MUC
Agentes oxidantes de tioles	ANT y PiC	Cierra	<i>m</i> MUC, <i>Sc</i> MUC and <i>Zf</i> MUC
Maleimidas	ANT y PiC	Cierra	<i>m</i> MUC y <i>Zf</i> MUC
dVO <sub>4</sub>	VDAC	Cierra	<i>Sc</i> MUC
As <sub>2</sub> O <sub>3</sub>	VDAC	Abre	<i>m</i> MUC y <i>Sc</i> MUC
Péptidos con señal mitocondrial y mastoparán	desconocido (PIM?)	Abre	<i>m</i> MUC y <i>oa</i> MUC
Especies reactivas de oxígeno	Tioles específicos	Abre	<i>m</i> MUC, <i>Sc</i> MUC and <i>At</i> MUC
Fosfato	Desconocido	Abre	<i>m</i> MUC, <i>Sc</i> MUC, <i>Zf</i> MUC y <i>Dh</i> MUC
Fosfato	Desconocido	Abre (en presencia de Ca <sup>2+</sup> )	<i>m</i> MUC

Modificado de Uribe-Carvajal y col., 2011. MUC, canal mitocondrial inespecífico; MCU, uniportador mitocondrial de Ca<sup>2+</sup>; PIM, maquinaria mitocondrial de importación de proteínas; *m*, mamífero; *Sc*, *Saccharomyces cerevisiae*; *Zf*, pez cebra; *Om*, *Oncorhynchus mykiss*; *Gs*, camarón fantasma; *Ze*, *Zinnia elegans*, *Pt*, papa; *Dh*, *Debaryomyces hansenii*; *At*, *Arabidopsis thaliana*; *Nt*, *Nicotiana tabacum*; *pea*, *Pisum sativum* y *At*, *Artemia franciscana*.

### 1.5. El efecto Crabtree

El efecto Crabtree consiste en la inhibición en el consumo de oxígeno en presencia de glucosa; es un proceso rápido y reversible que ha sido observado principalmente en células tumorales (Crabtree, 1929) y algunos tipos de levadura (Merico y col., 2007). También lo presentan células no tumorales con alta tasa de proliferación (Greiner y col., 1994) y algunas bacterias (Mustea y Muresian, 1967). Se ha planteado que el metabolismo de las células tumorales es muy similar al de *S. cerevisiae* (Díaz-Ruiz y col., 2009), ya que cuando ésta crece en medios no fermentables (glicerol, lactato, acetato o etanol) utiliza la fosforilación oxidativa para producir ATP (Rolland y col., 2002), mientras que con glucosa o fructosa, su metabolismo es fermentativo y se reprime el consumo de O<sub>2</sub>. Las causas de este fenómeno no son muy claras, pero se plantea que intervienen varias condiciones metabólicas tanto a corto como a largo plazo. Algunos estudios sugieren que predominan las condiciones a corto plazo y permiten que este fenómeno sea reversible (Díaz-Ruiz y col., 2011).

Se ha planteado que el estado redox de la célula, la disponibilidad de sustratos para la mitocondria y el potencial termodinámico del fosfato son determinantes en esta condición. En un principio se pensaba que un alto flujo glucolítico promueve la competencia por sustratos como el ADP y Pi entre la glucólisis y la fosforilación oxidativa. Sin embargo, esta explicación no tiene mucho sentido en condiciones fisiológicas ya que la Km por el ADP para la translocasa de adenín nucleótidos (ANT) es al menos 100 veces más baja que la Km de la piruvato cinasa y la 3-fosfoglicerato cinasa (Veech y col., 1979). También se observó en células tumorales que durante la adición de glucosa hay una caída abrupta en la concentración de fosfato, lo cual disminuye la respiración y este efecto se revierte al adicionar fosfato (Rodríguez-Enriquez y col., 2001). La participación del calcio en este fenómeno ha sido poco aceptada ya que en la mayoría de las células que presentan efecto Crabtree los niveles de calcio se mantienen constantes y sólo pasa en células

de ascitis de Ehrlich (Wojtczak y col., 1999). El efecto de la disponibilidad de sustratos para la mitocondria y el balance NADH/NAD<sup>+</sup>, requieren estudios más profundos, pero son factores limitantes para la fosforilación oxidativa (Mazat y col., 2013).

La sobreactivación de enzimas glucolíticas también se ha vinculado al efecto Crabtree, pues se observó que la PFK (fosfofructocinasa) y la PDC (piruvato descarboxilasa) incrementan su actividad durante la adición de glucosa al medio, lo cual es de vital importancia, ya que la PFK es una enzima reguladora de la glucólisis (Gatt y Racker, 1959). La piruvato descarboxilasa juega un papel muy importante en la formación del acetaldehído para luego transformarlo en etanol, producto final de la glucólisis, lo cual permite la regeneración de NAD<sup>+</sup> para que la glucólisis continúe. Otros estudios sugieren que los fenómenos que promueven el efecto Crabtree a corto plazo, tienen que ver con el flujo glucolítico y la acumulación de metabolitos señalizadores, los cuales conducen el metabolismo ya sea hacia la fermentación o la fosforilación oxidativa. Se ha observado que la relación NADH/NAD<sup>+</sup> y la glucosa-6-fosfato tienen oscilaciones importantes durante la glucólisis (Richard y col., 1993), mientras que la fructosa-1,6-bisfosfato se acumula de manera lineal con el consumo de glucosa y la producción de etanol (Huberts y col., 2012). En este contexto, el potencial termodinámico del fosfato no se modifica en función del flujo metabólico. Además, la acumulación de la fructosa-1,6-bisfosfato sólo sucede en levaduras Crabtree positivas (Stefan y Sauer, 2011). La relación entre el flujo metabólico, la acumulación de metabolitos señalizadores y el efecto Crabtree se demostró en 2008 (Díaz-Ruiz y col., 2008). Tanto la glucosa-6-fosfato como la fructosa-1,6-bisfosfato afectan la respiración. En condiciones no fosforilantes (Estado IV), la G6P estimula la actividad del complejo III, pero no afecta la respiración en condiciones fosforilantes (Estado III). Esto sugiere que la G6P podría funcionar como un desacoplante. Sin embargo, la F1,6BP inhibe la respiración en Estado 4 y no afecta el Estado 3. Se observó que la F1,6BP afecta directamente la actividad del complejo III, lo cual causa que el complejo IV también disminuya su actividad, y ello explica la disminución en el consumo de oxígeno. Además la F1,6BP elimina los efectos de la G6P y

F6P sobre el complejo III sin causar desacoplamiento, lo cual explica por qué las mitocondrias permanecen acopladas durante la inducción del efecto Crabtree, y la represión del consumo de oxígeno es reversible. Los efectos de la F1,6BP sobre la cadena respiratoria no se observan en células Crabtree negativas como *Candida utilis* o *Kluyveromyces lactis*, pero puede observarse la inducción del efecto Crabtree en hepatocitos al adicionar F1,6BP (Díaz-Ruiz y col., 2008). Por otra parte, es necesario evaluar otros posibles blancos que afecten el acoplamiento de la fosforilación oxidativa como el canal mitocondrial inespecífico de *S. cerevisiae*.

## 1.6. El 1,4-bisfosfobutano, análogo de la fructosa-1,6-bisfosfato.

Previamente se demostró que la F1,6BP disminuye la respiración en esferoplastos permeabilizados de *S. cerevisiae* y promueve el efecto Crabtree en el hepatocito (Díaz-Ruiz y col., 2008). Sin embargo, fue necesario adicionar yodoacetato, éste es un inhibidor irreversible de la GAPDH, lo cual evita la transformación de F1,6BP (Meyerhof y Kiessling, 1935). Tomando en cuenta este fenómeno y para evaluar de manera más cuantitativa los efectos de la F1,6BP en la célula completa, es necesario utilizar moléculas no metabolizables, pero que generen los mismos efectos que el sustrato sobre las enzimas (Uribe-Carvajal y cols., 1981). Se ha descrito que el 1,4-bisfosfobutano es un inhibidor competitivo de la aldolasa (Hartman y Barker, 1965) debido a su conformación lineal y la distancia que existen entre los grupos fosfato en las posiciones 1 y 4. Por lo tanto se decidió probar sus efectos en la mitocondria aislada. Dado que este compuesto no existe en el mercado, fue sintetizado. La Fig. 4 muestra la estructura del 1,4-bisfosfobutano (A) y la Fructosa-1,6-bisfosfato (B).

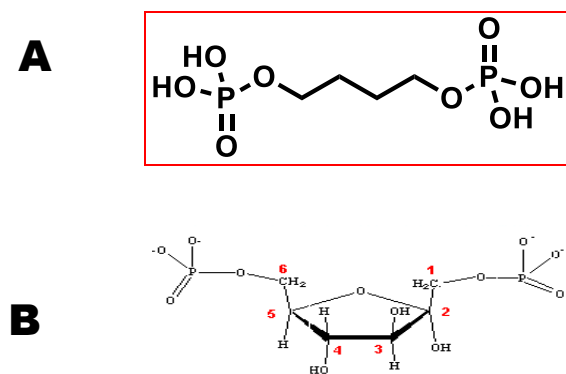


Fig. 4. Estructura del 1,4 bisfosfobutano (A) y la Fructosa-1,6-bisfosfato (B).

## **2. Planteamiento del problema**

En *S. cerevisiae* la glucólisis y la fosforilación oxidativa se regulan mutuamente. La participación del *ScMUC* en el efecto Crabtree no ha sido estudiada, y probablemente éste sea regulado por las hexosas fosfato de la glucólisis.

## **3. Hipótesis**

Si la G6P, F6P y F1,6BP inducen el efecto Crabtree, deben modular el estado de apertura del *ScMUC*.

## **4. Objetivos**

### **4.4. Objetivo general**

Determinar el efecto de la glucosa-6-fosfato, la fructosa-6-fosfato y la fructosa-1,6-bisfosfato sobre el *ScMUC*.

### **4.2. Objetivos particulares**

**4.2.1.** Evaluar el acoplamiento mitocondrial en presencia de G6P, F6P y F16BP.

**4.2.2.** Caracterizar los efectos de la G6P, F6P y F1,6BP sobre el hinchamiento mitocondrial.

**4.2.3.** Determinar si la G6P y la F1,6BP compiten en el *ScMUC*.

**4.2.4.** Evaluar el efecto del 1,4-bisfosfobutano sobre el *ScMUC*.

## **5. Material y métodos**

### **5.1. Cultivo de la levadura**

Las levaduras *S. cerevisiae* “yeast foam” (YF) y *K. lactis* (levadura Crabtree negativa) se resembraron cada mes en medio sólido YPD (Extracto de levadura 1%, peptona de gelatina 2%, dextrosa 2% y agar 2%). Se realizaron precultivos tomando una asada de levadura que se inoculó en 75 mL de medio YPD (Extracto de levadura 1%, peptona de gelatina 2% y dextrosa 2%), y se incubó a 30 °C en agitación a 250 rpm durante 8 h. El precultivo se agregó a 1 L de medio YPlac (Extracto de levadura 1%, peptona de gelatina 1%,  $(\text{NH}_4)_2\text{SO}_4$  0.12%,  $\text{KH}_2\text{PO}_4$  0.1%, ácido láctico 2% y pH = 5.5) y se incubó en las mismas condiciones durante 15 h. Una vez obtenidas las levaduras se lavaron con agua destilada mediante centrifugación a 3,800 x g durante 5 min.

### **5.2. Obtención de las mitocondrias**

Las levaduras se resuspendieron en amortiguador de aislamiento (manitol 0.6 M, MES 5 mM pH 6.8 TEA, 0.1% BSA) y se homogeneizaron en un Bead Beater con perlas de vidrio de 0.45 mm de diámetro en cámara de hielo 3 veces, utilizando 20 s de agitación y 40 s de descanso (Uribe y col., 1985). Las mitocondrias se obtuvieron mediante centrifugación diferencial (Peña y col., 1977) a 4 °C, utilizando una centrífuga Sorvall R5B en un rotor GSA. Las fracciones más pesadas se separaron centrifugando el homogeneizado a 1,017 x g durante 5 min. El sobrenadante se recuperó y se centrifugó a 10,700 x g durante 10 min. El botón se resuspendió cuidadosamente con un pincel, se llevó a un volumen final de 30 mL y se centrifugó a 3,600 x g durante 5 min. El sobrenadante se recuperó y se centrifugó a 17,000 x g durante 10 min. El botón de aspecto marrón se resuspendió con un pincel en aproximadamente 300  $\mu\text{L}$  de medio sin albúmina y se cuantificó la proteína.

### **5.3. Cuantificación de la proteína**

La proteína se midió mediante el método de Biuret (Gornall y col., 1949), leyendo la absorbancia de la muestra en un espectrofotómetro Beckman DU-50 a 540 nm, utilizando BSA como estándar. Se utilizaron 2 mL del reactivo de Biuret, 125 µL de desoxicolato de sodio 1%, 350 µL de agua destilada y 25 µL de la suspensión de mitocondrias.

### **5.4. Consumo de oxígeno**

Se utilizó un oxímetro Strathkelvin modelo 782 (Warner/Strathkelvin Instruments) con un electrodo tipo Clark inmerso en una cámara de 1 mL, T= 30°C con un baño PolyScience (Model 9000, USA). El consumo de oxígeno se midió utilizando medio de la reacción se llevó a cabo en medio de aislamiento (manitol 0.6 mM, MES 5 mM pH 6.8 TEA, 0.1% BSA), 250 µg/mL de mitocondrias. Se agregaron agregando 2 µL/mL de etanol absoluto como sustrato respiratorio para inducir el estado 4, el estado desacoplado (U) se indujo con CCCP 0.3 µM y se calculó el cociente U/4 (Gutiérrez-Aguilar y col., 2007).

### **5.5. Hinchamiento mitocondrial**

Es conocido que la apertura del <sub>sc</sub>MUC, permite la entrada masiva de K<sup>+</sup> hacia la matriz mitocondrial, lo cual induce un aumento en el volumen de ésta y la densidad óptica disminuye. El hinchamiento mitocondrial se determinó mediante el cambio en la absorbencia a 540 nm, inducido por la adición de 20 mM de KCl (Castrejón y col., 1997). Se utilizó un espectrofotómetro (AMINCO DW 2000, Olis, Inc., Bogart, GA, EUA) en modo “split”. La reacción se llevó a cabo en medio de aislamiento con etanol absoluto 2 µL/mL, 250 µg/mL de mitocondrias y diferentes concentraciones

finales de Pi: 0.1, 0.4, 1 y 4 mM; y KCl 20 mM donde se indica. La mezcla de reacción se mantuvo en agitación constante.

## **5.6. Potencial transmembranal**

Se utilizó un espectrofotómetro (AMINCO DW 2000, Olis, Inc., Bogart, GA, EUA) en modo dual a 511-533 nm. La reacción se llevó a cabo utilizando medio de homogenización con KCl 10 mM, etanol 2 µL/mL, O-safranina 15 µM y Pi a 0.1, 0.4, 1 ó 4 mM. La mezcla se mantuvo en agitación constante. Posteriormente se agregaron 250 µg/mL de las mitocondrias, y para abatir el potencial transmembranal se utilizó CCCP 1.2 µM (Akerman y Wikstrom, 1976).

## **5.7. Síntesis del 1,4-bisfosfobutano**

Se realizó de acuerdo con lo reportado por Hartman y cols., 1965, con algunas modificaciones. Se sintetizó el donador de fosfatos dibencilfosfonato (DBPH) (Atherton y Todd, 1947). Posteriormente se realizó la activación del DBPH mediante cloración con N-Clorosuccinimida (Gao y col., 2006), y se obtuvo un aceite amarillo pálido, el cloruro de dibencilfosfonato (Cl-DBP). Este producto inestable se agregó sin purificar a una solución de 1,4-butanodiol en piridina. Se obtuvo el 1,4-dibencilfosforilbutano (1,4-DBPB). Para desplazar los grupos bencilo se hidrogenó con paladio sobre carbón activado en metanol; se obtuvo así una solución metanólica de 1,4-bisfosfobutano, y se agregó ciclohexilamina para obtener la sal. Se evaporó el metanol y se obtuvo un sólido blanco, que se lavó con diclorometano. La pureza de todos los intermediarios (DBPH, 1,4-DBPB) y el producto final (1,4BPP), se comprobaron mediante RMN de protón ( $H^1$ ) y carbono ( $^{13}C$ ). El diagrama de la síntesis se muestra en la Fig. 5.

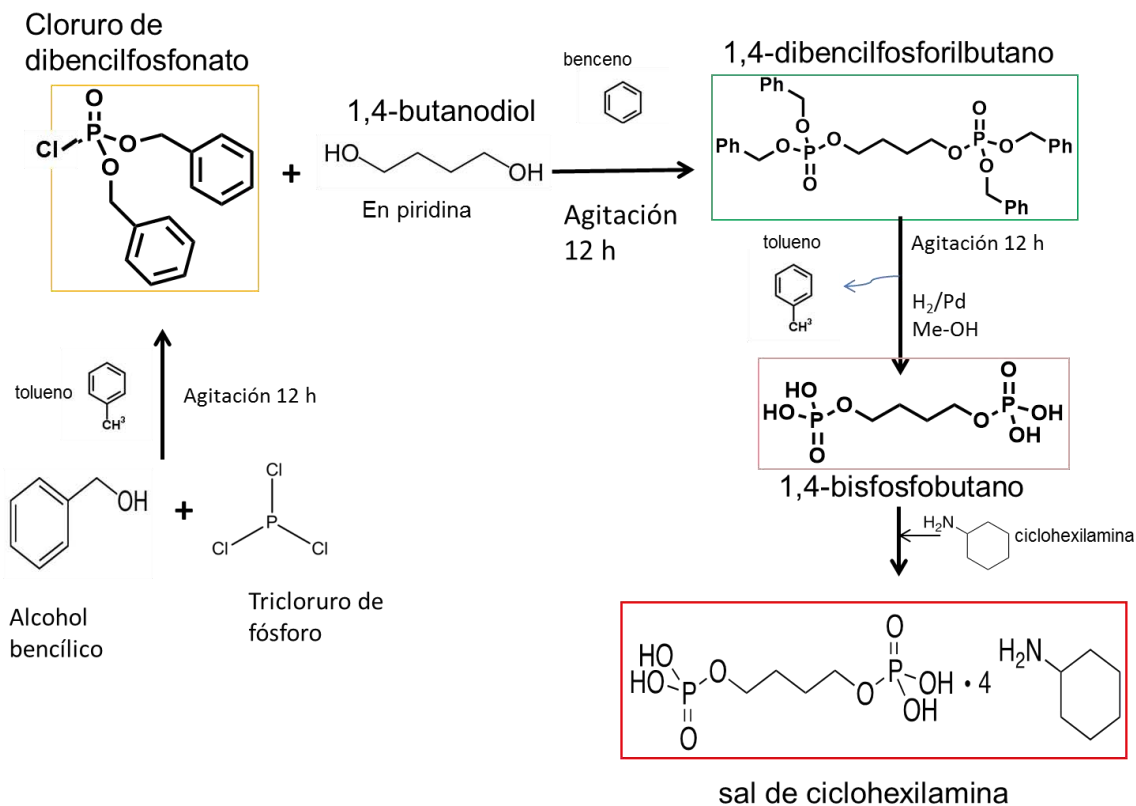


**Fig. 5.** Esquema de la síntesis del 1,4-bisfosfobutano. Los compuestos en recuadros fueron analizados mediante RMN H<sup>1</sup> y <sup>13</sup>C. En amarillo la molécula donadora del grupo fosfato, en verde el éster-fosfato protegido y en rojo el 1,4-bisfosfobutano y la sal de ciclohexilamina.

### **5.8. Actividad de la aldolasa.**

La actividad de la aldolasa se midió mediante la determinación de hidrazona a 240 nm en un espectrofotómetro Aminco DW-2000 (Olis Inc., Bogart, GA, USA), utilizando como coeficiente de extinción molar  $2.7 \times 10^3 \text{ M}^{-1} \text{ cm}^{-1}$ . Medio de reacción:  $\text{NaH}_2\text{PO}_4$  10 mM, pH= 7.6, hidrazina 350 mM y EDTA 10 mM. Se utilizaron 2  $\mu\text{g}/\text{mL}$  de enzima por cada ensayo y se realizó una curva de actividad de aldolasa a diferentes concentraciones de fructosa-1,6-bisfosfato: 10, 20, 40, 80, 100 y 200  $\mu\text{M}$ , en presencia o en ausencia de 1,4-bisfosfobutano 2 mM. Se graficó la actividad de la aldolasa en función de la concentración de sustrato (Fig. 16 A) y posteriormente se realizó el regráfigo de los dobles recíprocos (Fig. 16 B), para obtener la  $K_m$  y  $V_{max}$ .

## 6. Resultados

### 6.1. Efecto de las hexosas fosfato sobre el consumo de oxígeno.

Previamente se demostró que la apertura del  $\text{scMUC}$  acelera la respiración y desacopla la fosforilación oxidativa (Crompton, 1999; Azoulay-Zohar y col., 2004). La apertura y cierre de este canal puede modularse mediante la concentración de fosfato en el medio. Se evaluaron los efectos de la F16BP y G6P sobre el consumo de oxígeno en estado IV y desacoplado (U) inducido con CCCP. En Pi 1 mM, el  $\text{scMUC}$  está semicerrado; la G6P acelera el consumo de oxígeno en estado IV y U a partir de 6 mM, disminuyendo el cociente U/IV de 1.6 sin G6P hasta 1.2 a 20 mM de G6P. En Pi 4 mM la G6P aumenta el consumo de oxígeno en estado 4 y mantiene constante el U; el desacoplamiento es significativo sólo con 20 mM de G6P. La G6P no produce desacoplamiento en Pi 4 mM, cuando el  $\text{scMUC}$  se encuentra totalmente cerrado (Tabla 2).

En Pi 0.1 mM, la F16BP disminuye el consumo de oxígeno en estado IV a partir de 2 mM, sin afectar significativamente el estado U, lo cual indica un acoplamiento. En Pi 4 mM la F1,6BP disminuye el consumo de oxígeno en estado IV a 10 y 20 mM. En estas mismas condiciones también disminuye el estado U y se observa un ligero desacoplamiento (Tabla 3). Estos resultados sugieren que la G6P desacopla parcialmente, mientras que la F1,6BP acopla. La fructosa-6-fosfato (F6P) no produjo efectos importantes sobre la respiración.

**Tabla 2. Efecto de la G6P sobre el consumo de oxígeno.** Medio de reacción: 0.6 M Manitol, 5 mM MES, pH 6.8 (TEA), 2 µL/mL de etanol, 10 mM KCl, Pi y Glucosa-6-fosfato (G6P) como se indica, mitocondrias (250 µg/mL). El estado U se indujo agregando CCCP 1.5 µM.

Pi	G6P (mM)	Estado IV	Estado U	U/IV
		(natgO/min/mgprot)	(natgO/min/mgprot)	
<b>1 mM</b>	0	132.0 ± 17.0	210 ± 19.8	1.6
	2	138.0 ± 19.8	198 ± 36.8	1.4
	4	150.0 ± 31.1	212 ± 39.6	1.4
	6	160.0 ± 11.3	214 ± 14.1	1.3
	10	194.0 ± 19.8	262 ± 14.1	1.3
	20	234.0 ± 14.1	280 ± 11.3	1.2
<b>4 mM</b>	0	162.9 ± 28.8	310.0 ± 45.4	1.9
	2	170.8 ± 5.25	278.8 ± 32.9	1.6
	4	196.7 ± 23.5	318.2 ± 23.6	1.6
	6	212.0 ± 18.3	333.9 ± 21.6	1.6
	10	208.7 ± 7.8	326.6 ± 11.0	1.6
	20	231.2 ± 16.5	332.8 ± 40.7	1.4

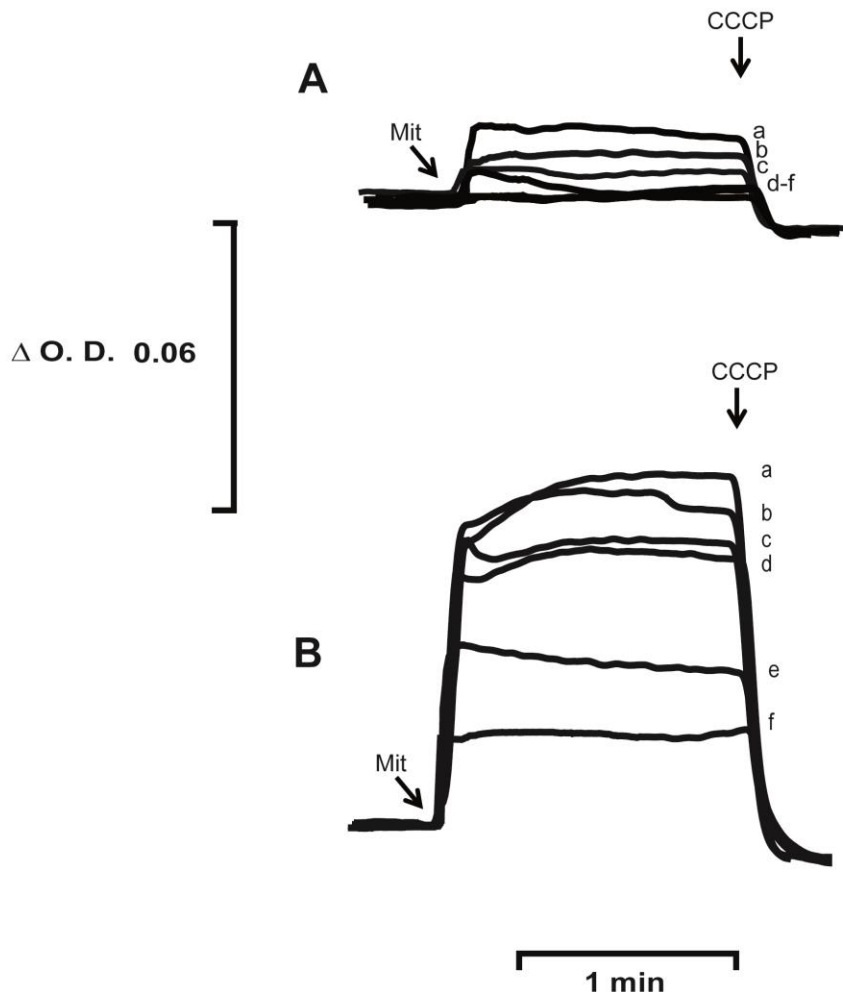
**Tabla 3. Efecto de la F1,6BP sobre el consumo de oxígeno.** Medio de reacción: 0.6 M Manitol, 5 mM MES, pH 6.8 (TEA), 2 µL/mL de etanol, 10 mM KCl, Pi y Fructosa 1,6-bisfosfato (F1,6BP) como se indica, mitocondrias (250 µg/mL). El estado U se indujo con CCCP 1.5 µM.

	Pi (mM)	F1,6BP (mM)	Estado IV (natgO/min/mg prot)	Estado U (natgO/min/mg prot)	U/IV
<b>0.1 mM</b>	0	328.4 ± 29.0	339.2 ± 24.0	1.0	
	2	167.6 ± 21.3	257.9 ± 46.0	1.5	
	4	143.3 ± 27.3	263.2 ± 25.0	1.8	
	6	129.4 ± 4.9	254.0 ± 43.0	2.0	
	10	142.2 ± 12.5	276.7 ± 66.0	1.9	
	20	140.6 ± 21.7	250.4 ± 46.0	1.8	
<b>4 mM</b>	0	240.7 ± 21.1	452.5 ± 40.3	1.9	
	2	214.2 ± 5.1	408.0 ± 48.5	1.9	
	4	229.0 ± 19.4	422.2 ± 57.9	1.8	
	6	208.3 ± 24.6	385.9 ± 8.8	1.8	
	10	194.1 ± 24.4	357.3 ± 56.0	1.8	
	20	192.7 ± 27.6	334.7 ± 28.3	1.7	

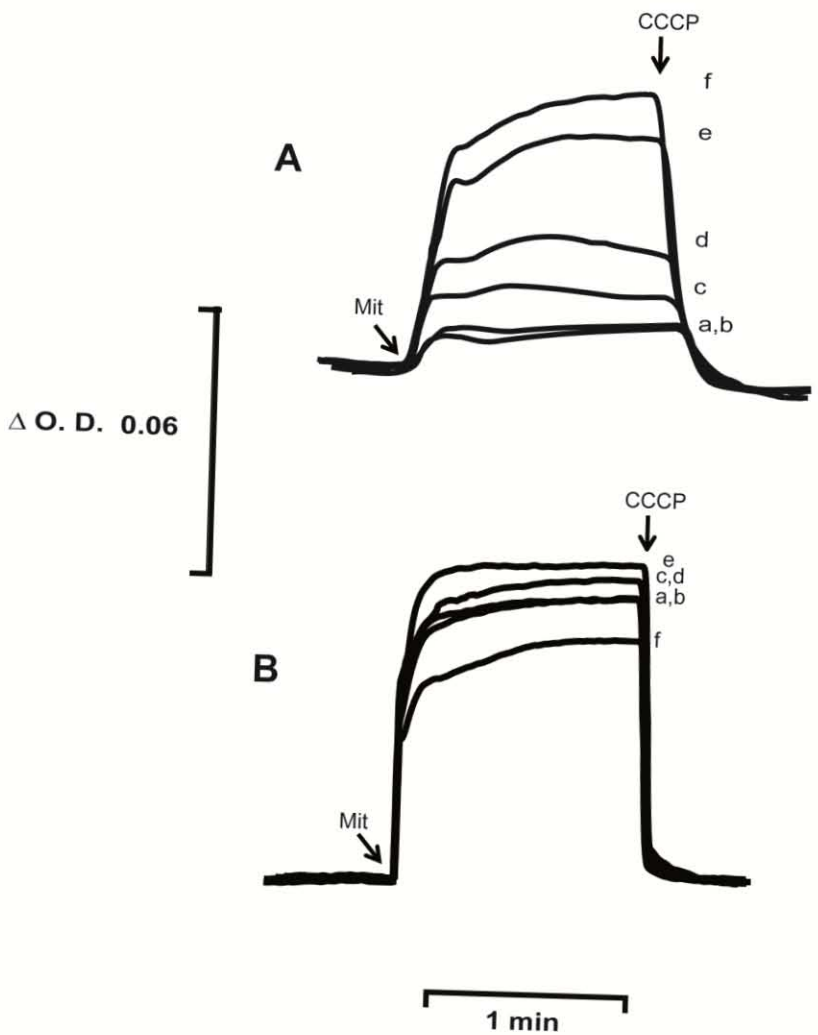
## **6.2. Efecto de las hexosas fosfato sobre el potencial transmembranal.**

Los resultados obtenidos del consumo de oxígeno sugieren que la G6P desacopla y la F1,6BP acopla, ya que la G6P acelera el consumo de oxígeno en el estado IV, mientras que la F1,6BP lo disminuye. En ambos casos el estado desacoplado no se modifica. Para investigar los efectos de estas hexosas sobre el  $s_c$ MUC, se evaluaron los efectos de las hexosas fosfato sobre el potencial transmembranal. Cuando el  $s_c$ MUC está semiabierto ( $P_i$  1 mM), se observa un potencial transmembranal bajo, pero estable, que se abate al adicionar G6P (Fig. 6, A), mientras que en  $P_i$  4 mM, cuando el  $s_c$ MUC está cerrado, el potencial transmembranal es más alto que en  $P_i$  1 mM y se abate totalmente a 10 y 20 mM de G6P (Fig. 6, B trazos e y f).

En  $P_i$  0.1 mM, donde el  $s_c$ MUC está abierto, no se observa potencial transmembranal, y al agregar F16BP, éste se mantiene desde 6 mM (Fig. 7, A trazo d). En  $P_i$  4 mM, cuando el  $s_c$ MUC está cerrado, la F16BP muestra un efecto bifásico en el cual aumenta ligeramente el potencial transmembranal de 6 a 10 mM (Fig. 7, B trazos c-e), y promueve una ligera baja en 20 mM (Fig. 7, B trazo f). Estos resultados correlacionan con el consumo de oxígeno y sugieren que la F16BP y la G6P actúan sobre el  $s_c$ MUC, ya que además de modular el consumo de oxígeno, también modifican el potencial transmembranal. La F6P no tuvo efectos sobre el potencial transmembranal (no se muestran los datos).



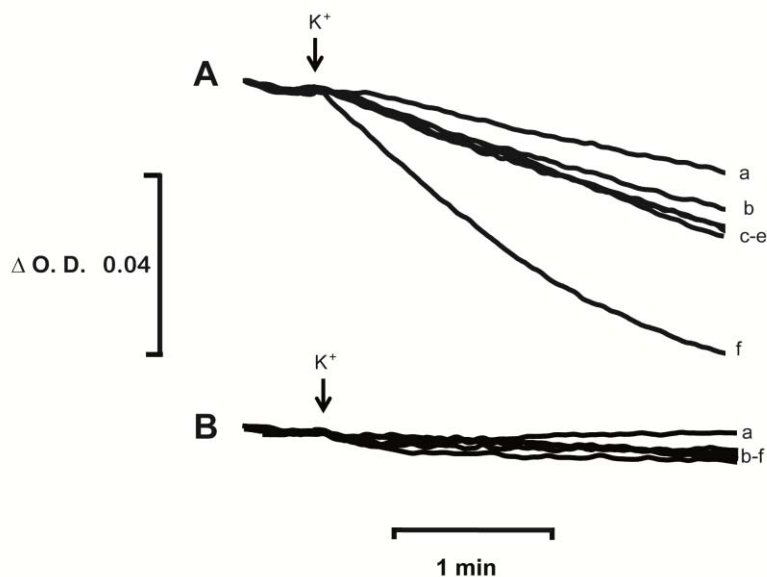
**Fig. 6. Efecto de la G6P sobre potencial transmembranal.** Mezcla de reacción: Manitol 0.6 M, MES 5 mM TEA pH= 6.8, KCl 10 mM, 0-safranina 15  $\mu\text{M}$ , etanol 2  $\mu\text{L/mL}$ , mitocondrias (Mit) 250  $\mu\text{g/mL}$  y CCCP, se indica con la flecha. A, Pi 1 mM y B, Pi 4 mM. G6P (mM): a, 0; b, 2; c, 4; d, 6; e, 10; f, 20.



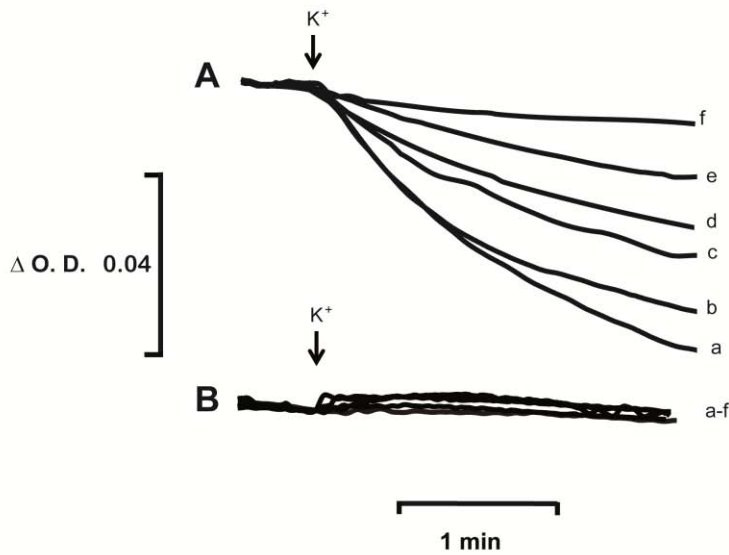
**Fig. 7. Efecto de la F16BP sobre potencial transmembranal.** Mezcla de reacción: Manitol 0.6 M, MES 5 mM TEA pH=6.8, KCl 10 mM, O-safranina 15  $\mu$ M, etanol 2  $\mu$ L/mL. Adiciones de mitocondrias, Mit (250  $\mu$ g/mL) y CCCP, se indican con la flecha. A, Pi 0.1 mM, y B, Pi 4 mM. F1,6BP (mM): a, 0; b, 2; c, 4; d, 6; e, 10; f, 20.

### 6.3. Efecto de las hexosas fosfato sobre el hinchamiento mitocondrial

Estudios previos han demostrado que cuando el  $_{Sc}$ MUC se encuentra abierto, se favorece el transporte de potasio hacia la matriz mitocondrial, lo cual promueve hinchamiento, mientras que cuando el  $_{Sc}$ MUC está cerrado, el  $K^+$  no lo afecta (Castrejón y col., 2002). Se evaluó el efecto de las hexosas fosfato sobre el hinchamiento mitocondrial inducido por  $K^+$  en diferentes estados de apertura del  $_{Sc}$ MUC modulados por Pi. En Pi 1 mM, se observó un ligero hinchamiento promovido por el  $K^+$ , el cual aumenta significativamente a 20 mM de G6P (Fig. 8 A, trazo f). En Pi 4 mM no se observa hinchamiento mitocondrial a ninguna concentración de G6P (Fig. 8 B). En Pi 0.1 mM se observa un hinchamiento importante, el cual se inhibe totalmente a 4 mM de F1,6BP (Fig. 9, A). La F1,6BP no muestra ningún efecto sobre el hinchamiento en Pi 4 mM (Fig. 9, B). La F6P no mostró efectos sobre el hinchamiento mitocondrial (no se muestran los datos).

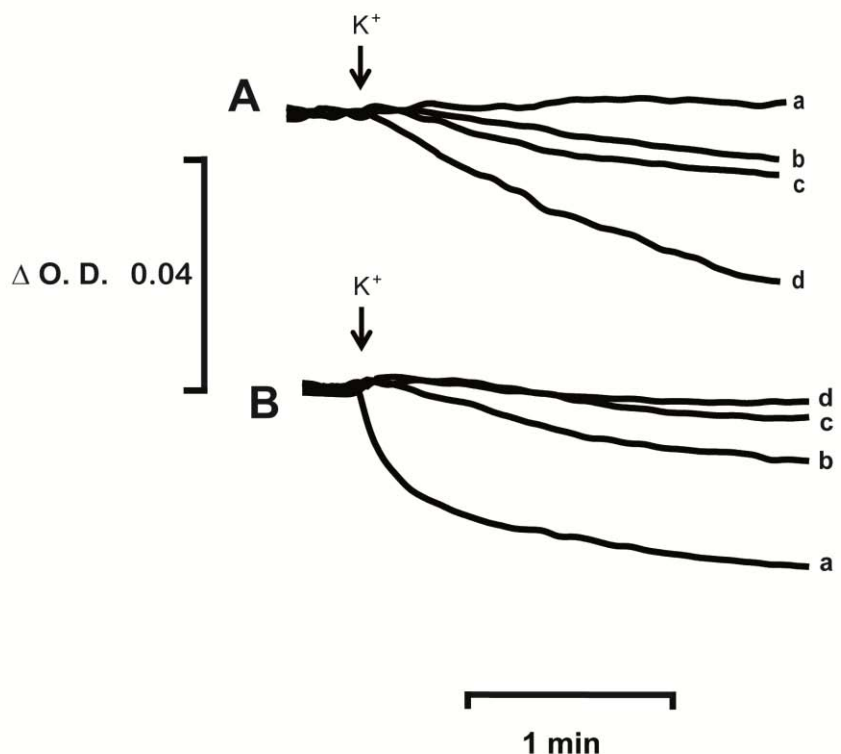


**Fig. 8. Efecto de la G6P sobre el hinchamiento mitocondrial.** Mezcla de reacción: Manitol 0.3 M, MES 5 mM, TEA pH 6.8, etanol 2  $\mu$ L/mL, mitocondrias (250  $\mu$ g/mL). La adición de KCl 20 mM, se indica con la flecha. A, Pi 1 mM y B, Pi 4 mM. G6P (mM): a, 0; b, 2; c, 4; d, 6; e, 10; f, 20.



**Fig. 9. Efecto de la F1,6BP sobre el hinchamiento mitocondrial.** Mezcla de reacción: Manitol 0.3 M, MES 5 mM, TEA pH=6.8, etanol 2  $\mu$ L/mL, mitocondrias (250  $\mu$ g/mL). La adición de KCl 20 mM, se indica con la flecha. A, Pi 0.1 mM y B, Pi 4 mM. F1,6BP (mM): a, 0; b, 0.25; c, 0.5; d, 0.75; e, 2; f, 4.

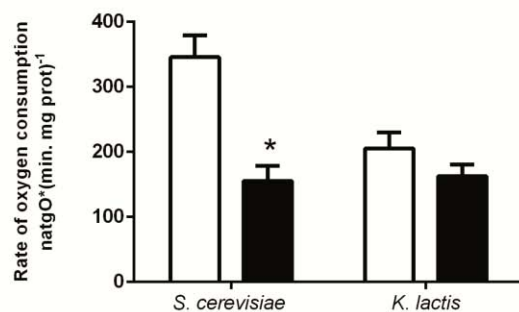
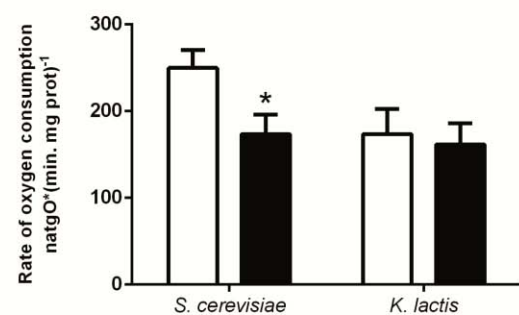
Estos resultados sugieren que la G6P abre del  $_{Sc}$ MUC, y que la F1,6BP lo cierra. Durante la glucólisis se producen ambas hexosas fosfato; por lo tanto, se decidió estudiar el efecto de la competencia de ambas sobre el hinchamiento mitocondrial. En Pi 0.1 mM, cuando el  $_{Sc}$ MUC está abierto, la adición de 2 mM de F1,6BP inhibe el hinchamiento, el cual se promueve al agregar G6P 10 mM (Fig. 10 A, trazo d). En Pi 1 mM la G6P promueve hinchamiento mitocondrial, el cual es inhibido con 0.5 mM de F1,6BP (Fig. 10 B, trazo b). Estos resultados confirman que la F16BP cierra el  $_{Sc}$ MUC y su efecto predomina sobre el de la G6P.



**Fig. 10. Competencia entre la F1,6BP y G6P sobre el hinchamiento mitocondrial.** Mezcla de reacción: Manitol 0.3 M, MES 5 mM TEA pH= 6.8, etanol 2  $\mu$ L/mL, mitocondrias (250 $\mu$ g/mL). La adición de KCl 20 mM, se indica con la flecha. A, Pi 0.1 mM + 2 mM F1,6BP y diferentes concentraciones de G6P (mM): a, 0; b, 4; c, 10; d, 20. B, Pi 1 mM + G6P 10 mM y diferentes concentraciones de F1,6BP (mM): a, 0; b, 0.5; c, 4; d, 10.

#### **6.4. Efectos de la Fructosa-1,6-bisfosfato sobre la respiración en *S. cerevisiae* y *K. lactis*.**

Los resultados obtenidos demuestran que la F1,6BP cierra el  $_{Sc}MUC$  y que compite con los efectos de la G6P. Se ha propuesto que la F1,6BP es un mensajero metabólico común en las levaduras Crabtree positivas ya que se acumula hasta 10 mM (Stefan y col., 2011). Por lo tanto, se decidió estudiar el efecto de la F16BP sobre la respiración en mitocondrias aisladas de *K. lactis* (levadura Crabtree negativa), para comparar con *S. cerevisiae*. La F1,6BP inhibe la respiración en *S. cerevisiae* tanto en Pi 0.1 mM como en Pi 1 mM, mientras que en *K. lactis* no tiene efectos significativos (Fig. 11). Estos datos sugieren que la F1,6BP es importante para la inducción del efecto Crabtree.

**A****B**

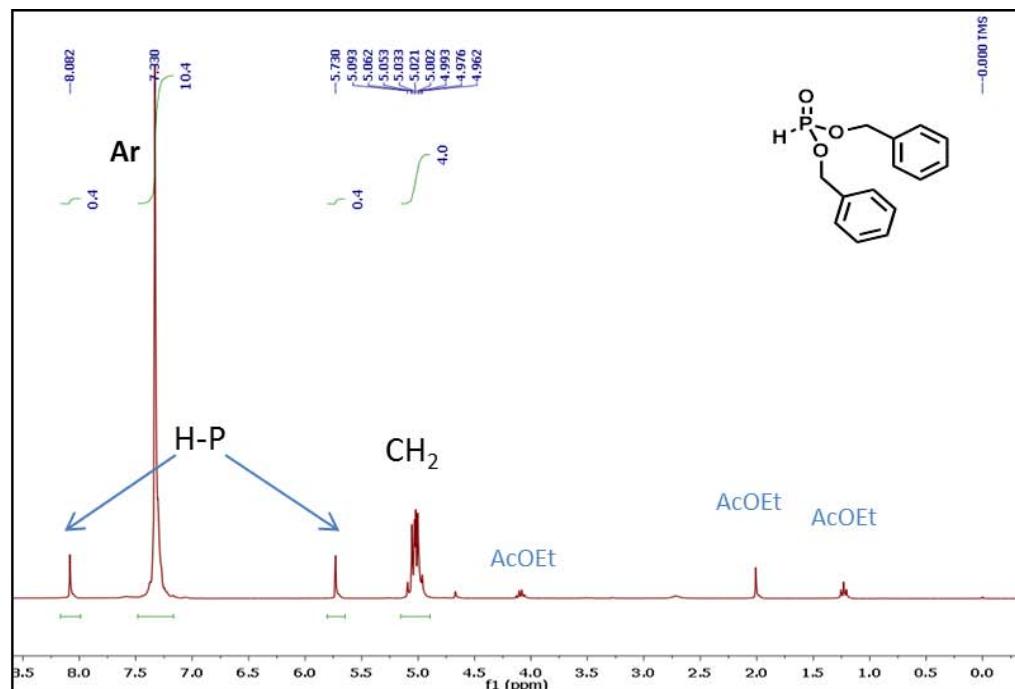
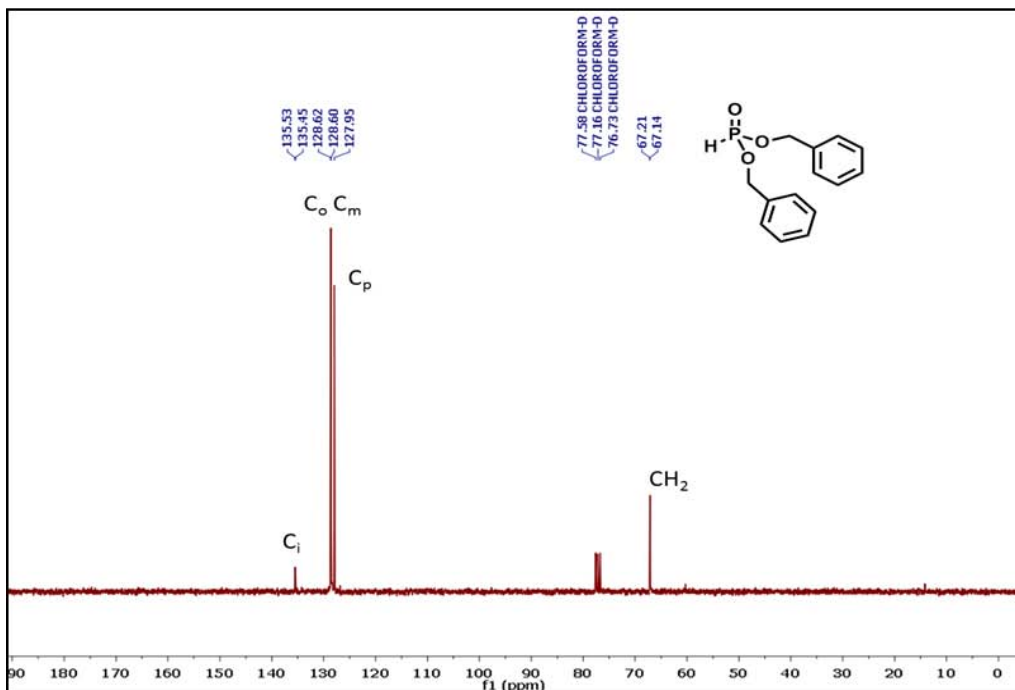
**Fig. 11. Efecto de la F1,6BP sobre el consumo de oxígeno en *S. cerevisiae* o *K. lactis*.** Las barras blancas sin F1,6BP y en las negras 10 mM F1,6BP. Mezcla de reacción como en la tabla 2, excepto que en A, Pi 0.1 mM y B Pi 1 mM.

\*Diferencia significativa basada en ANOVA y comparación múltiple de tukey. P < 0.01.

## **6.5. Síntesis del 1,4-bisfosfobutano**

La caracterización de cada compuesto se realizó mediante espectros de resonancia magnética nuclear (RMN) de hidrógeno ( $H^1$ ) y carbono ( $^{13}C$ ), buscando señales características de cada compuesto según sus grupos funcionales, dentro de una escala determinada por un solvente deuterado. Cada señal tiene dos componentes: el desplazamiento y la integral y el área bajo la curva. El desplazamiento es la zona de la escala en la que aparecen las señales, depende del grupo funcional y los grupos vecinos que modifiquen su respuesta. La integral es el número de átomos que contribuyen a una misma señal por encontrarse dentro del mismo grupo.

La síntesis del 1,4-bisfosfobutano descrita por Hartman y cols., 1965, utilizaba una molécula donadora de fosfatos que ya no se ofrece comercialmente. Por lo tanto se realizó la síntesis del dibencifosfonato (DBP) de acuerdo con Atherton y cols., 1945. En la Fig. 12 se muestran los espectros para el DBP. En A ( $H^1$ ). Se observa una señal característica de los hidrógenos (H) de los bencilos en la zona de 7.3 ppm (desplazamiento químico) que integra (área bajo la curva de la señal) para 10 H, por cada fenilo (4 en posición orto, 4 en posición meta y 2 en posición para de cada anillo). En 8.08 y 5.7 ppm, se observa la señal del protón ácido del compuesto que integran para 1. En 5.0 ppm, se observa la señal del metileno que une al fosfato con el anillo y estas señales integran para 4 H (2 por cada grupo).

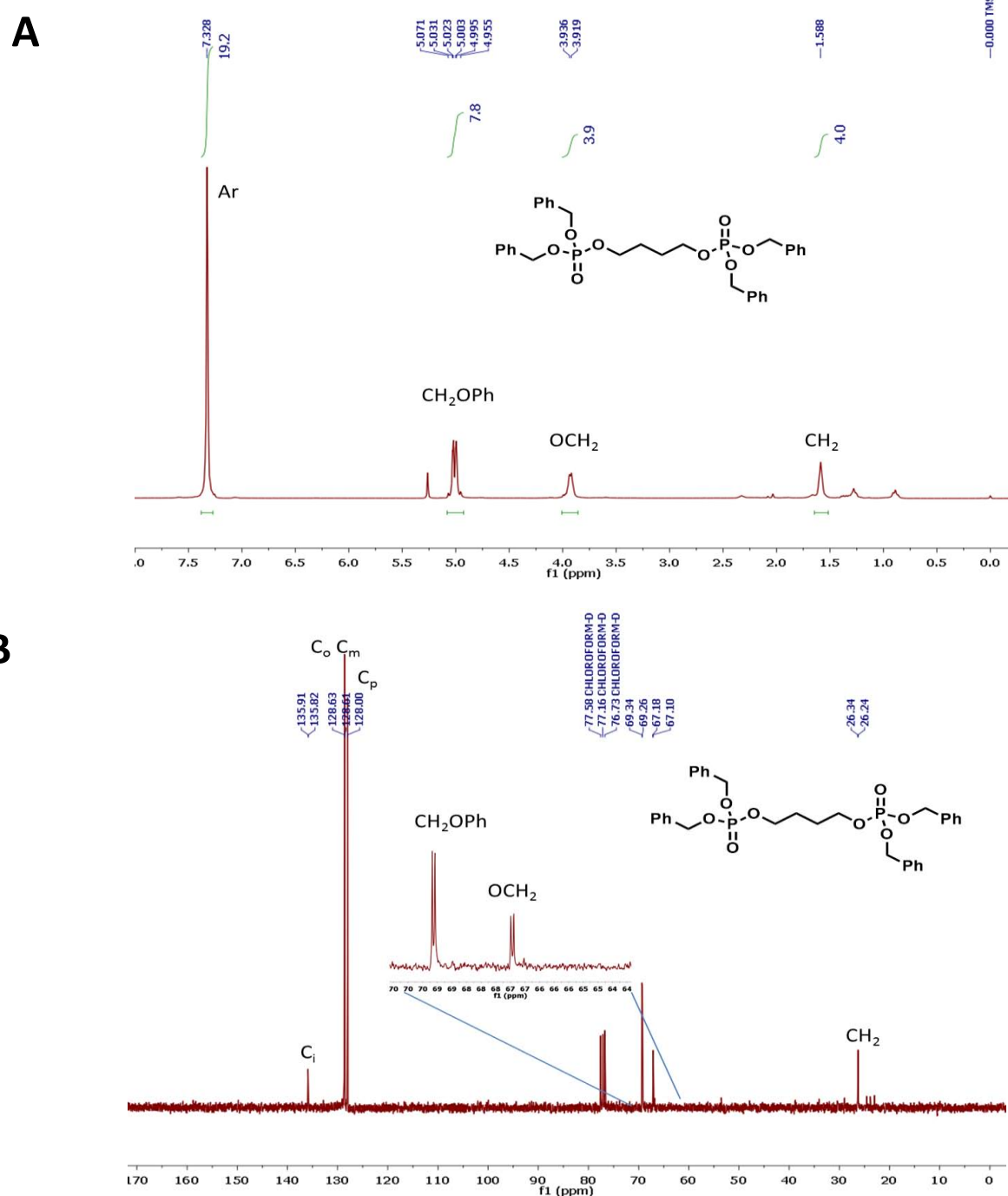
**A****B**

**Fig. 12.** Espectros de RMN a 300 MHz. en cloroformo deuterado. **A**, RMN de  $^1\text{H}$  para el dibencifosfonato. Ar, hidrógenos del anillo aromático; H-P, hidrógeno unido al fosfato; CH<sub>2</sub>, metíleno alifático; AcOEt, acetato de etilo. **B**, RMN de  $^{13}\text{C}$ . C<sub>i</sub>, carbono interior; C<sub>o</sub> carbono en orto; C<sub>m</sub>, carbono en meta y C<sub>p</sub>, carbono en para.

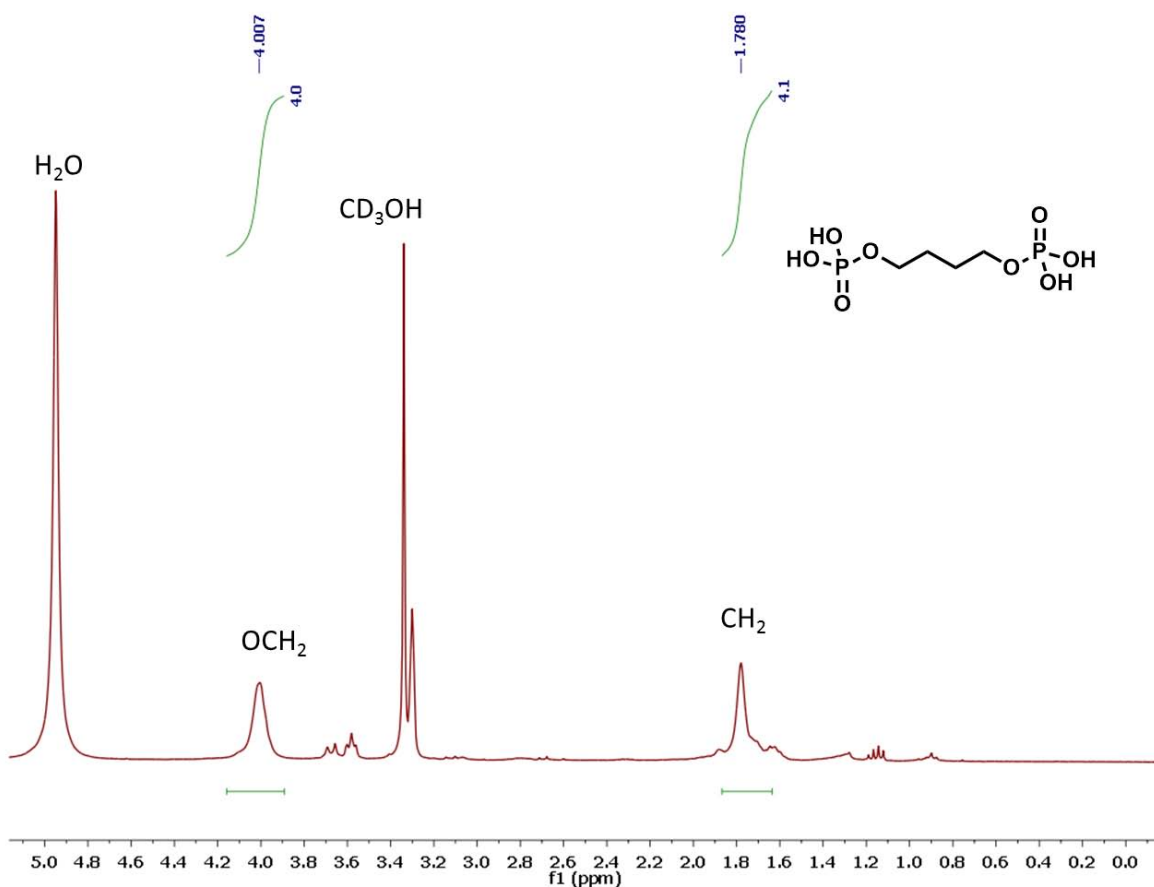
En B ( $^{13}\text{C}$ ) se observan 4 especies diferentes de carbono (C). En 135.5 ppm se observa la señal del carbono que une al anillo aromático con el fosfato ( $\text{C}_i$ ) y los componentes del anillo aromático: en 135.4 ppm C orto ( $\text{C}_o$ ), en 128.6, C en meta ( $\text{C}_m$ ) y en 127.95, C en para ( $\text{C}_p$ ). En 67.2 se encuentra el C del metileno ( $\text{CH}_2$ ). En conclusión, las señales de RMN corresponden con la estructura del compuesto esperado.

El cloruro de dibencilfosfonato adicionado (2:1 meq.) al 1,4-butanodiol forma el 1,4-dibencilfosforilbutano. En la Fig. 13, se muestran los espectros de RMN para este compuesto. En A ( $\text{H}^1$ ) se observa la señal los hidrógenos aromáticos en 7.3 ppm; en este caso, la integral es para 20, ya que hay 4 anillos aromáticos. En 5.0-4.9 ppm se encuentran los hidrógenos del  $\text{CH}_2\text{OP}$  e integran para 7.8 (casi 8 H, 2 hidrógenos por cada bencilo). En 4.0 ppm se observan las señales del grupo  $\text{OCH}_2$  que integran para 4 y en 1.5 ppm, los metilenos alifáticos que integran para 4. En la fig. 9 B se observan las señales correspondientes al  $\text{C}_i$  en 135.9 ppm. Los carbonos aromáticos en 128.6-128 ppm ( $\text{C}_o$ ,  $\text{C}_m$  y  $\text{C}_p$ ). En 69 y 70 ppm se observan el  $\text{CH}_2\text{OP}$  y en 67 ppm  $\text{OCH}_2$ . En 26.34 ppm se observa el  $\text{CH}_2$  alifático que integra para 4. Los datos concuerdan con que el grupo fosfato se adicionó al 1,4-butanodiol en las posiciones adecuadas, por lo tanto se procedió a desplazar a los grupos bencilo mediante hidrogenación y así obtener el 1,4-bisfosfobutano.

La caracterización por RMN  $\text{H}^1$  del 1,4-bisfosfobutano se realizó en metanol deuterado y el espectro se muestra en la Fig. 14. En 4.0 ppm, se observa la señal del  $\text{OCH}_2$  (el metileno que se encuentra unido al oxígeno del fosfato) e integra para 4 H. También se observa el  $\text{CH}_2$  (metileno de la cadena alifática) que integra para 4 H. Las señales del RMN corresponden a la molécula esperada.



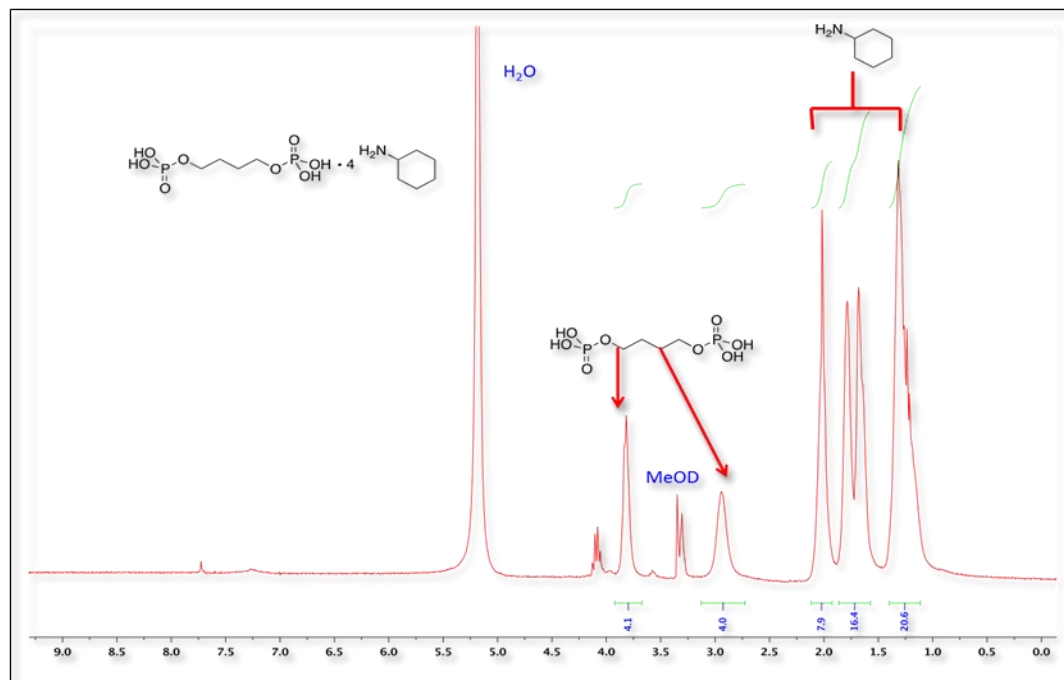
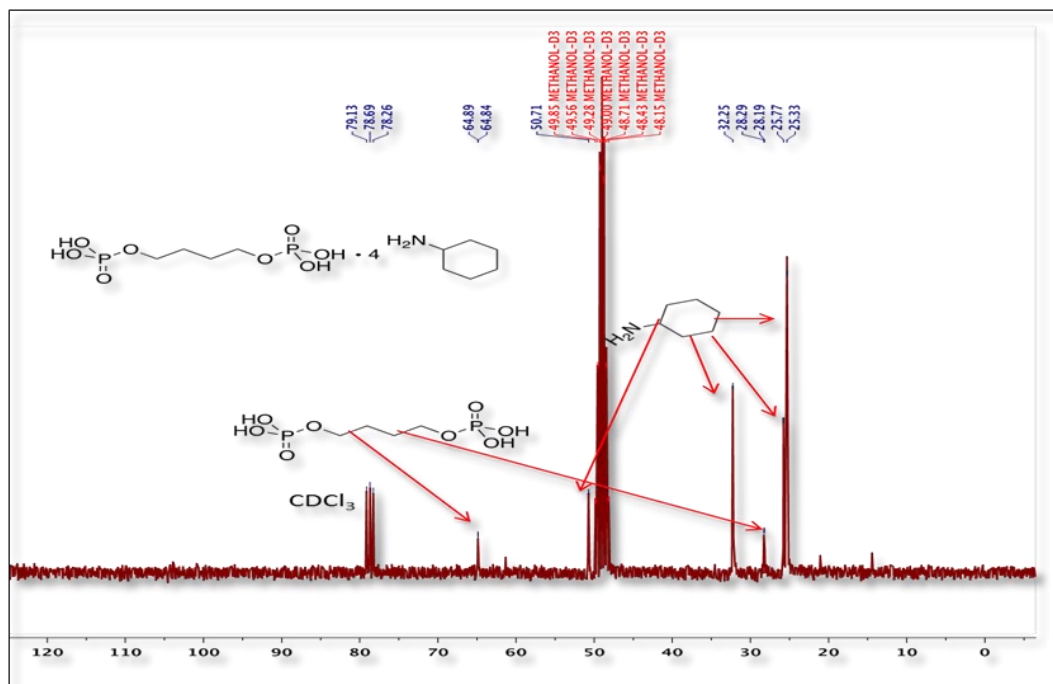
**Fig.13. Espectros de RMN a 300 MHz. en cloroformo deuterado.** A, RMN de  $H^1$  para el dibencilfosfonato 1,4-dibenciforilbutano. Ar, hidrógenos del anillo aromático;  $CH_2OPh$ , etileno del fenilo unido al fosfato;  $OCH_2$ , metileno de la cadena del butano; unido al oxígeno,  $CH_2$ ; metileno alifático. B, RMN de  $^{13}C$ .  $C_i$ , carbono interior;  $C_o$  carbono en orto;  $C_m$ , carbono en meta y  $C_p$ , carbono en para.



**Fig. 14. Espectro de RMN en metanol deuterado de  $\text{H}^1$  para el 1,4-bisfosfobutano.**  $\text{H}_2\text{O}$ , agua;  $\text{OCH}_2$ , primer metíleno unido al oxígeno del fosfato;  $\text{CD}_3\text{OH}$ , metanol deuterado (disolvente);  $\text{CH}_2$ , metíleno alifático.

Para comprobar que se obtuvo la sal pura del 1,4-bisfosfobutano, se realizó el análisis de  $\text{H}^1$  y  $^{13}\text{C}$  por RMN de la sal de ciclohexilamina 1,4-bisfosfobutano (1,4BPB). En la Fig. 15 A se muestra el espectro de RMN de  $\text{H}^1$  en cloroformo-metanol deuterado. Se observan las señales de los hidrógenos correspondientes al anillo de la ciclohexilamina (cuatro picos) de 1 a 2, con una integral de 44 (suma de los hidrógenos del anillo de la ciclohexilamina multiplicada por 4 equivalentes de ésta presentes en la molécula). La señal de la amina no se observa, porque se superpone con la del agua en 5.25. Los metilenos centrales del 1,4-bisfosfobutano se observan en 3, con una integral de 4 y los

metilenos unidos al fosfato en 3.75, con integral de 4. Las señales de metanol y cloroformo corresponden al solvente. También se observó agua, ya que el compuesto es higroscópico. En la Fig. 15 B se observa el espectro de RMN de C<sup>13</sup>, las señales del anillo de ciclohexilamina se observan en 25, 31 (ciclo) y 51 (carbono unido a la amina). En 27 y 65 se observan las señales del 1,4-bisfosfobutano y nuevamente la presencia de cloroformo. No se observan otras señales importantes que sugieran contaminación. El rendimiento de la síntesis fue de 88 %.

**A****B**

**Fig. 15. Espectros de RMN de  $\text{H}^1$  y  $\text{C}^{13}$ , de la sal de ciclohexilamina del 1,4-bisfosfobutano.** Se observan las señales correspondientes a los anillos y la cadena alifática del 1,4-bisfosfobutano. Me-OD, metanol y  $\text{CDCl}_3$ , cloroformo. Las flechas indican la correspondencia de los grupos funcionales de cada molécula con su señal en el espectro.

## 6.6. Efecto del 1,4-bisfosfobutano sobre la actividad de la aldolasa

Para comprobar que el 1,4-bisfosfobutano es un análogo de la fructosa-1,6-bisfosfato y un inhibidor competitivo de la aldolasa, se probaron los efectos del compuesto sobre la actividad de esta enzima. En la Fig. 16 se muestra el gráfico de actividad de la aldolasa (A) y el regráfico de los dobles recíprocos (B). Se observó que es un inhibidor competitivo: aumenta la  $K_m$  de la aldolasa de 173.1  $\mu\text{M}$  sin inhibidor a 335.1  $\mu\text{M}$  en presencia del inhibidor, mientras que la velocidad máxima se mantiene en 15  $\mu\text{mol/min/mg prot}$  en ambos casos.

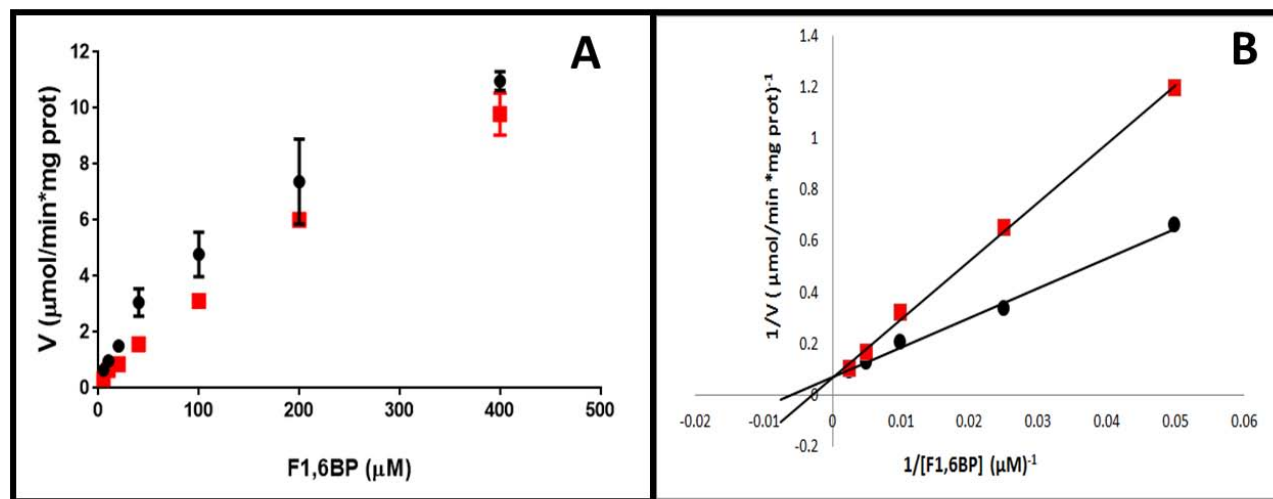


**Fig. 16. Efecto del 1,4-bisfosfobutano sobre la actividad de la aldolasa.** A, actividad de la aldolasa sin inhibidor (cuadros negros) y en presencia de 1,4-bisfosfobutano 2 mM (círculos rojos). B, gráfico de dobles recíprocos de la actividad de la aldolasa en presencia y ausencia del 1,4-bisfosfobutano.

## 6.7. Efecto del 1,4-bisfosfobutano sobre el hinchamiento mitocondrial

Para evaluar los efectos del 1,4-bisfosfobutano en la célula completa se probaron primero sus efectos sobre la mitocondria aislada, comenzando por el hinchamiento mitocondrial. Se observó que cuando el  $\text{ScMUC}$  se encuentra abierto ( $\text{Pi} 0.1 \text{ mM}$ ), el 1,4BPB inhibe el hinchamiento desde 1 mM (Fig. 17, trazo d). Además el 1,4BPB compite con la G6P en  $\text{Pi} 0.1 \text{ mM}$ , pues la G6P inhibe totalmente el efecto del 1,4BPB a 40 mM (Fig. 18, trazo e). En  $\text{Pi} 4 \text{ mM}$  el 1,4 BPB no tiene efecto sobre el hinchamiento.

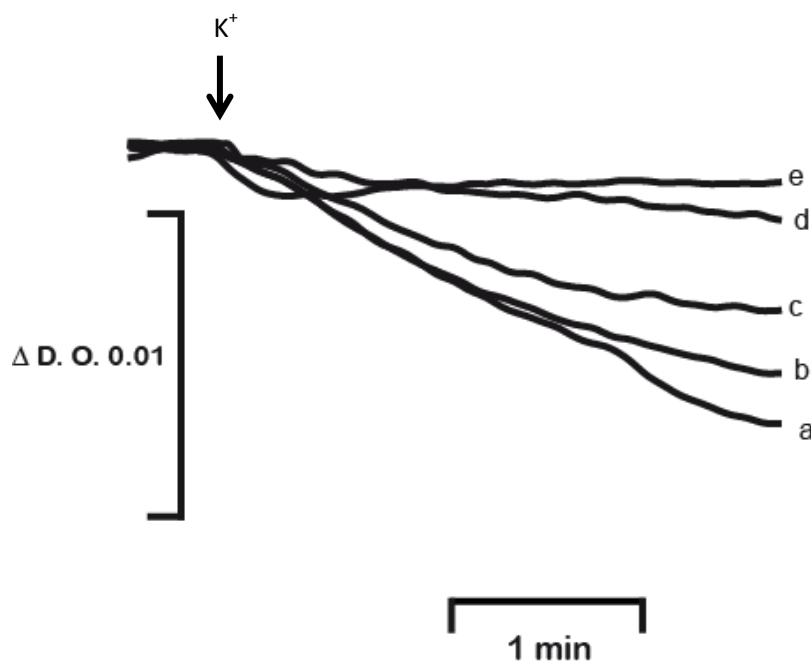


**Fig. 17. Efecto del 1,4-bisfosfobutano sobre el hinchamiento mitocondrial.** Mezcla de reacción: Manitol 0.3 M, MES 5 mM, TEA pH=6.8, Pi 0.1 mM, etanol 2  $\mu\text{L}/\text{mL}$ , mitocondrias (250  $\mu\text{g}/\text{mL}$ ). La adición de KCl 20 mM, se indica con la flecha. 1,4BPB: a, 0, b, 0.1, c, 0.5, d, 1, e, Pi 4 mM.

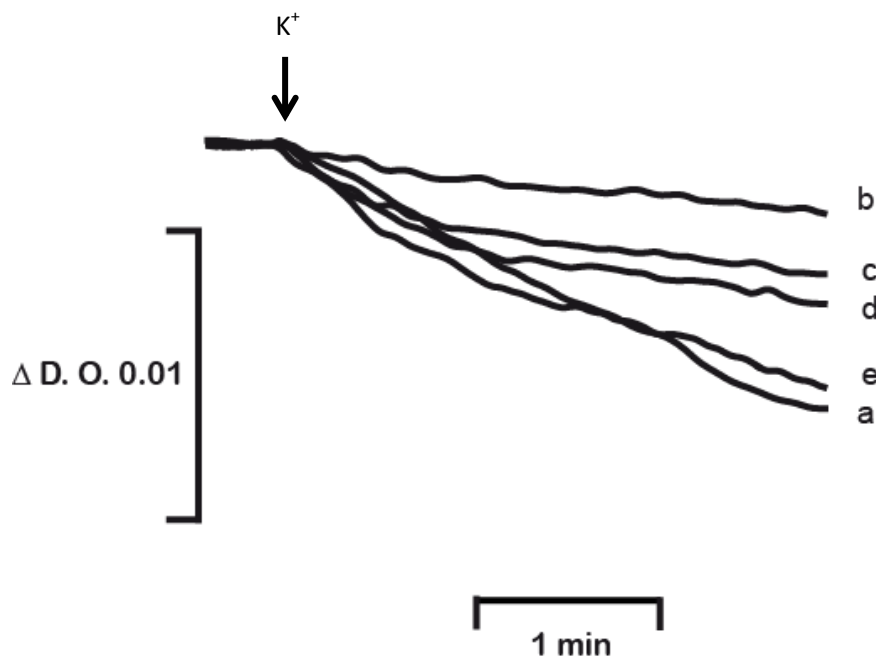


**Fig. 18. Competencia entre el 1,4-bisfosfobutano y la G6P sobre el hinchamiento mitocondrial.** Mezcla de reacción: Manitol 0.3 M, MES 5 mM, TEA pH=6.8, Pi 0.1 mM, etanol 2  $\mu$ L/mL mitocondrias (250  $\mu$ g/mL). La adición de KCl 20 mM, se indica con la flecha. 1,4BPB (mM): a, 0, b-e, 0.1. G6P (mM): c, 10, d, 20, e, 40.

#### 6.8. Efectos del 1,4-bisfosfobutano sobre el potencial transmembranal.

Debido a que el 1,4-bisfosfobutano inhibe el hinchamiento cuando el  $_{sc}$ MUC se encuentra abierto, y sólo se contrarresta su efecto al adicionar 40 mM de G6P, se decidió evaluar los efectos del 1,4-BPB sobre el potencial transmembranal. Se observó que mantiene el potencial transmembranal en Pi 0.1 mM y este efecto desaparece al adicionar G6P 40 mM (Fig. 19).

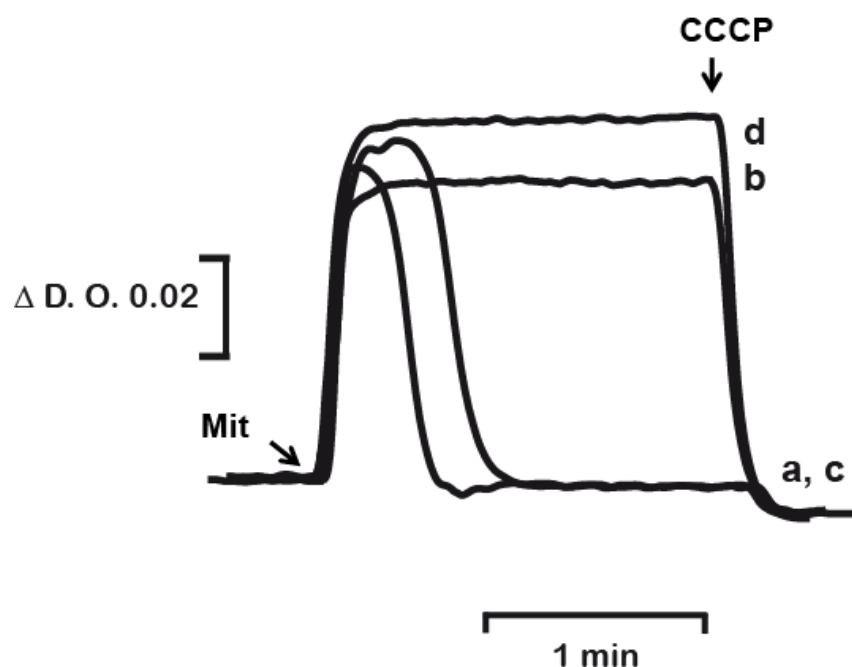


**Fig. 19. Efecto del 1,4-BPB sobre el potencial transmembranal.** Mezcla de reacción: Manitol 0.6 M, MES 5 mM TEA pH=6.8, KCl 10 mM, O-safranina 15  $\mu$ M, etanol 2  $\mu$ L/mL. Adiciones de mitocondrias, Mit (250  $\mu$ g/mL) y CCCP, se indican con la flecha. Pi 0.1 mM, a-c. Se adicionó 1,4BPB 1 mM en b y c. Sólo en c se adicionó G6P 40 mM. Pi 4 mM, d.

## 7. Discusión

### 7.1 Los efectos de la G6P sobre el $S_c$ MUC

Previamente se demostró que la adición de glucosa al medio de cultivo promueve una acumulación cíclica de G6P. Las concentraciones de G6P varían entre 2 y 8 mM y cuando aumentan, el NADH disminuye, y viceversa (Richard y col., 1993). La G6P es un metabolito que puede utilizarse tanto para la síntesis de pentosas fosfato o bien para la producción de trehalosa o glucógeno, y es probable que estas oscilaciones se deban a que la G6P se acumule y posteriormente sea utilizada en alguna de estas vías. Los estudios de Díaz-Ruiz (Díaz-Ruiz y col., 2008) mostraron que la G6P acelera la respiración debido a que estimula la actividad del complejo III de la cadena respiratoria de *S. cerevisiae*, pero esta estimulación es inhibida cuando el cociente G6P/F1,6BP <1. En este estudio se observó que la G6P acelera la respiración, tanto en estado III como en estado U sólo cuando el  $S_c$ MUC está semi-aberto (Pi 1 mM) y es significativo a partir de 10 mM; estas concentraciones se salen de los límites fisiológicos y concuerdan con lo reportado por Díaz-Ruiz y col., (2008), lo cual sugiere que la G6P no participa en la inducción del efecto Crabtree y sólo abre parcialmente el  $S_c$ MUC.

### 7.2 Los efectos de la Fructosa-1,6-bisfosfato sobre la mitocondria.

El efecto Crabtree se caracteriza por la inhibición de la respiración en presencia de glucosa. Se ha propuesto que resulta de diversas condiciones metabólicas rápidas y reversibles, tales como la sobreactivación de algunas enzimas glucolíticas, la competencia entre la glucólisis y la fosforilación oxidativa por el ADP y Pi, así como la participación de señales activadas por cAMP (Díaz-Ruiz y col., 2011). Estudios recientes demostraron que al agregar glucosa al medio de cultivo, las levaduras Crabtree positivas acumulan F1,6BP (Stefan y col., 2011) y ésta inhibe los complejos mitocondriales III y IV, lo cual causa que disminuya el consumo de oxígeno sin promover desacoplamiento (Díaz-

Ruiz y col., 2008). En este estudio se observó que cuando el  $s_c$ MUC está cerrado, la F1,6BP inhibe la respiración, se promueve una ligera caída de potencial y no afecta el hinchamiento mitocondrial, lo cual prueba que no abre el  $s_c$ MUC, pero sí afecta la cadena respiratoria. Sin embargo, cuando el  $s_c$ MUC se encuentra abierto, la F1,6BP inhibe el hinchamiento, mantiene el potencial transmembranal e inhibe la respiración en el estado 4, y todo ello promueve el acoplamiento. Además suprime los efectos de la G6P y no tiene efectos importantes sobre la respiración en mitocondrias aisladas de *K. lactis*. Estos resultados sugieren que la F1,6BP participa en la inducción del efecto Crabtree y mantiene el  $s_c$ MUC cerrado, lo cual inhibe la transición de la permeabilidad.

La transición de la permeabilidad descontrolada está implicada en la muerte celular de la levadura y en otros tipos celulares (Lemasters y col., 1998; Manon y col., 1998; Halestrap y col., 2000; Azoulay-Zohar y col., 2004). Sin embargo, los efectos de la F1,6BP sobre la transición de la permeabilidad y su relación con la muerte celular requiere otro tipo de estudios.

### **7.3. El 1,4-bisfosfobutano, la F1,6BP y el $s_c$ MUC.**

Actualmente se conocen pocos inhibidores de las enzimas glucolíticas, los más conocidos son la 2-deoxiglucosa, un inhibidor de la hexocinasa y el yodoacetato, un potente inhibidor un irreversible no competitivo de las deshidrogenasas, principalmente GAPDH. El interés de encontrar un análogo no metabolizable de la F1,6BP, condujo este trabajo hacia la síntesis de un inhibidor competitivo de la aldolasa: 1,4-bisfosfobutano. Se logró sintetizar el compuesto con algunas modificaciones importantes al protocolo previamente reportado, sobre todo la reacción de adición de fosfatos, ya que se modificó el compuesto donador de fosfatos de la síntesis original y se sustituyó por el cloruro de dibencilfosfonato (Atherton y col., 1947). Estas modificaciones requieren de un ambiente anhidro y es necesario cuidar la proporción de butanodiol y cloruro de dibencilfosfonato, para generar la mayor cantidad de 1,4-dibencilfosforil butano y no generar

monobencilfosforilbutoanodiol, ya que no es posible separarlos posteriormente y ninguno de estos factores se encuentra reportado por Hartman y cols. (1965).

Una vez obtenido el compuesto, se corroboró su efecto inhibidor sobre la actividad de la aldolasa. Los efectos del 1,4bpb sobre el <sub>Sc</sub>MUC, demuestran que la estructura de la F1,6BP es importante para su actividad, ya que ambos lo cierran y compiten con los efectos de la G6P, tanto en el hinchamiento como en potencial transmembranal, lo cual sugiere un sitio de interacción específico para las hexosas fosfato de la glucólisis en la mitocondria. Sin embargo, para probar la existencia de este sitio y la importancia de la F1,6BP como un mensajero metabólico, es necesario estudiar sus efectos sobre el consumo de oxígeno en la célula completa.

Es probable que el 1,4-bisfosfobutano pueda ser empleado para identificar las proteínas que conforman el <sub>Sc</sub>MUC y sería de interés estudiar sus efectos inhibitorios sobre la glucólisis.

## **8. Conclusiones**

- 8.1. La Fructosa-1,6-bisfosfato cierra el  $ScMUC$  y participa en la inducción del efecto Crabtree.
- 8.2. La Glucosa-6-fosfato abre parcialmente el  $ScMUC$ .
- 8.3. La Fructosa-6-fosfato no tiene efectos sobre el  $ScMUC$ .
- 8.4. El 1,4-bisfosfobutano es un análogo de la F1,6BP y cierra el  $ScMUC$ .

## **9. Perspectivas**

- 9.1. Evaluar el efecto del 1,4-bisfosfobutano sobre el consumo de oxígeno en la mitocondria aislada y en el esferoplasto permeabilizado.
- 9.2. Evaluar los efectos del 1,4-bisfosfobutano sobre la glucólisis.
- 9.3. Encontrar posibles blancos del 1,4-bisfosfobutano que permitan encontrar las proteínas que conforman el  $ScMUC$ .

## 10. Referencias

- Abele, D., **2002**, Toxic oxygen: the radical life-giver, *Nature*, 420: 6911, 27.
- Ahmadzadeh, M., Horng, A. and Colombini, M., **1996**, The control of mitochondrial respiration in yeast: a possible role of the outer mitochondrial membrane, *Cell Biochem Funct*, 14: 3, 201-8.
- Akerman, K. E. and Wikstrom, M. K., **1976**, Safranine as a probe of the mitochondrial membrane potential, *FEBS Lett*, 68: 2, 191-7.
- Araiza-Olivera, D., Chiquete-Félix, N., Rosas-Lemus, M., Sampedro, J. G., Peña, A., Mujica, A. and Uribe-Carvajal, S., **2013**, A glycolytic metabolon in *Saccharomyces cerevisiae* is stabilized by F-actin, *FEBS J*, 280: 16, 3887-905.
- Araiza-Olivera, D., Sampedro, J. G., Mujica, A., Pena, A. and Uribe-Carvajal, S., **2010**, The association of glycolytic enzymes from yeast confers resistance against inhibition by trehalose, *FEMS Yeast Res*, 10: 3, 282-9.
- Atherton, F. R. and Todd, A. R., **1947**, Studies on phosphorylation; further observations on the reaction of phosphites with polyhalogen compounds in presence of bases and its application to the phosphorylation of alcohols, *J Chem Soc*, 674-8.
- Avéret, N., Aguilaniu, H., Bunoust, O., Gustafsson, L. and Rigoulet, M., **2002**, NADH is specifically channeled through the mitochondrial porin channel in *Saccharomyces cerevisiae*, *J Bioenerg Biomembr*, 34: 6, 499-506.
- Azoulay-Zohar, H., Israelson, A., Abu-Hamad, S. and Shoshan-Barmatz, V., **2004**, In self-defence: hexokinase promotes voltage-dependent anion channel closure and prevents mitochondria-mediated apoptotic cell death, *Biochem. J.*, 377: 2, 347-355.
- Balasubramanian, R., Karve, A., Kandasamy, M., Meagher, R. B. and Moore, B., **2007**, A role for F-actin in hexokinase-mediated glucose signaling, *Plant Physiol*, 145: 4, 1423-34.
- Bernardi, P., **1999**, Mitochondrial transport of cations: channels, exchangers, and permeability transition, *Physiol Rev*, 79: 4, 1127-55.
- Bernardi, P., **2013**, The mitochondrial permeability transition pore: a mystery solved? , *Front Physiol*, 4: 95.
- Bernardi, P. and Forte, M., **2007**, The mitochondrial permeability transition pore, *Novartis Found Symp*, 287: 157-64; discussion 164-9.

Bernardi, P., Krauskopf, A., Basso, E., Petronilli, V., Blachly-Dyson, E., Di Lisa, F. and Forte, M. A., **2006**, The mitochondrial permeability transition from in vitro artifact to disease target, *FEBS J.*, 273: 10, 2077-99.

Bonora, M., Bononi, A., De Marchi, E., Giorgi, C., Lebiedzinska, M., Marchi, S., Paternani, S., Rimessi, A., Suski, J. M., Wojtala, A., Wieckowski, M. R., Kroemer, G., Galluzzi, L. and Pinton, P., **2013**, Role of the c subunit of the FO ATP synthase in mitochondrial permeability transition, *Cell Cycle*, 12: 4, 674-83.

Brandina, I., Graham, J., Lemaitre-Guillier, C., Entelis, N., Krasheninnikov, I., Sweetlove, L., Tarassov, I. and Martin, R. P., **2006**, Enolase takes part in a macromolecular complex associated to mitochondria in yeast, *Biochim Biophys Acta*, 1757: 9-10, 1217-28.

Cassimeris, L., Silva, V. C., Miller, E., Ton, Q., Molnar, C. and Fong, J., **2012**, Fueled by microtubules: does tubulin dimer/polymer partitioning regulate intracellular metabolism?, *Cytoskeleton (Hoboken)*, 69: 3, 133-43.

Castrejón, V., Parra, C., Moreno, R., Peña, A. and Uribe, S., **1997**, Potassium collapses the deltaP in yeast mitochondria while the rate of ATP synthesis is inhibited only partially: modulation by phosphate, *Arch Biochem Biophys*, 346: 1, 37-44.

Castrejón, V., Peña, A. and Uribe, S., **2002**, Closure of the yeast mitochondria unspecific channel (YMUC) unmasks a Mg<sup>2+</sup> and quinine sensitive K<sup>+</sup> uptake pathway in *Saccharomyces cerevisiae*, *J Bioenerg Biomembr*, 34: 4, 299-306.

Castresana, J. and Saraste, M., **1995**, Evolution of energetic metabolism: the respiration-early hypothesis, *Trends Biochem Sci*, 20: 11, 443-8.

Clegg, J. S., **1984**, Properties and metabolism of the aqueous cytoplasm and its boundaries, *Am J Physiol*, 246: 2 Pt 2, R133-51.

Colombini, M., **2004**, VDAC: the channel at the interface between mitochondria and the cytosol, *Mol Cell Biochem*, 256-257: 1-2, 107-15.

Cortés, P., Castrejón, V., Sampedro, J. G. and Uribe, S., **2000**, Interactions of arsenate, sulfate and phosphate with yeast mitochondria, *Biochim Biophys Acta*, 1456: 2-3, 67-76.

Crabtree, H. G., **1929**, Observations on the carbohydrate metabolism of tumours, *Biochem J*, 23: 3, 536-45.

Crompton, M., **1999**, The mitochondrial permeability transition pore and its role in cell death, *Biochem. J.*, 341: 2, 233-249.

D'Autreux, B. and Toledano, M. B., **2007**, ROS as signalling molecules: mechanisms that generate specificity in ROS homeostasis, *Nat Rev Mol Cell Biol*, 8: 10, 813-24.

Daran-Lapujade, P., Rossell, S., van Gulik, W. M., Luttik, M. A. H., de Groot, M. J. L., Slijper, M., Heck, A. J. R., Daran, J.-M., de Winde, J. H., Westerhoff, H. V., Pronk, J. T. and Bakker, B. M., **2007**, The fluxes through glycolytic enzymes in *Saccharomyces cerevisiae* are predominantly regulated at posttranscriptional levels, *Proceedings of the National Academy of Sciences*, 104: 40, 15753-15758.

Devin, A. and Rigoulet, M., **2007**, Mechanisms of mitochondrial response to variations in energy demand in eukaryotic cells, *Am J Physiol Cell Physiol*, 292: 1, C52-8.

Díaz-Ruiz, R., Avéret, N., Araiza, D., Pinson, B., Uribe-Carvajal, S., Devin, A. and Rigoulet, M., **2008**, Mitochondrial oxidative phosphorylation is regulated by fructose 1,6-bisphosphate. A possible role in Crabtree effect induction? , *J Biol Chem*, 283: 40, 26948-55.

Díaz-Ruiz, R., Rigoulet, M. and Devin, A., **2011**, The Warburg and Crabtree effects: On the origin of cancer cell energy metabolism and of yeast glucose repression, *Biochim Biophys Acta*, 1807: 6, 568-76.

Díaz-Ruiz, R., Uribe-Carvajal, S., Devin, A. and Rigoulet, M., **2009**, Tumor cell energy metabolism and its common features with yeast metabolism, *Biochim Biophys Acta*, 1796: 2, 252-65.

Egner, A. and Hell, S. W., **2005**, Fluorescence microscopy with super-resolved optical sections, *Trends Cell Biol*, 15: 4, 207-15.

Fontaine, E. and Bernardi, P., **1999**, Progress on the mitochondrial permeability transition pore: regulation by complex I and ubiquinone analogs, *J Bioenerg Biomembr*, 31: 4, 335-45.

Galli, G. J. and Richards, J., **2014**, Mitochondria from anoxia-tolerant animals reveal common strategies to survive without oxygen, *Journal of Comparative Physiology B*, 184: 3, 285-302.

Gao, F., Yan, X., Shakya, T., Baettig, O. M., Ait-Mohand-Brunet, S., Berghuis, A. M., Wright, G. D. and Auclair, K., **2006**, Synthesis and Structure-Activity Relationships of Truncated Bisubstrate Inhibitors of Aminoglycoside 6'-N-Acetyltransferases, *Journal of Medicinal Chemistry*, 49: 17, 5273-5281.

Gatt, S. and Racker, E., **1959**, Regulatory mechanisms in carbohydrate metabolism. I. Crabtree effect in reconstructed systems, *J Biol Chem*, 234: 5, 1015-23.

Giorgio, V., von Stockum, S., Antoniel, M., Fabbro, A., Fogolari, F., Forte, M., Glick, G. D., Petronilli, V., Zoratti, M., Szabo, I., Lippe, G. and Bernardi, P., **2013**, Dimers of mitochondrial ATP synthase form the permeability transition pore, *Proc Natl Acad Sci U S A*, 110: 15, 5887-92.

Gornall, A. G., Bardawill, C. J. and David, M. M., **1949**, Determination of serum proteins by means of the biuret reaction, *J Biol Chem*, 177: 2, 751-66.

Greiner, E. F., Guppy, M. and Brand, K., **1994**, Glucose is essential for proliferation and the glycolytic enzyme induction that provokes a transition to glycolytic energy production, *J Biol Chem*, 269: 50, 31484-90.

Guerin, B., Bunoust, O., Rouqueys, V. and Rigoulet, M., **1994**, ATP-induced unspecific channel in yeast mitochondria, *J Biol Chem*, 269: 41, 25406-10.

Guerin, M. and Napias, C., **1978**, Phosphate transport in yeast mitochondria: purification and characterization of a mitoribosomal synthesis dependent proteolipid showing a high affinity for phosphate, *Biochemistry*, 17: 13, 2510-6.

Guerrero-Castillo, S., Araiza-Olivera, D., Cabrera-Orefice, A., Espinasa-Jaramillo, J., Gutierrez-Aguilar, M., Luevano-Martinez, L. A., Zepeda-Bastida, A. and Uribe-Carvajal, S., **2011**, Physiological uncoupling of mitochondrial oxidative phosphorylation. Studies in different yeast species, *J Bioenerg Biomembr*, 43: 3, 323-31.

Gutiérrez-Aguilar, M., Pérez-Martínez, X., Chavez, E. and Uribe-Carvajal, S., **2010**, In *Saccharomyces cerevisiae*, the phosphate carrier is a component of the mitochondrial unselective channel, *Arch Biochem Biophys*, 494: 2, 184-91.

Gutiérrez-Aguilar, M., Pérez-Vazquez, V., Bunoust, O., Manon, S., Rigoulet, M. and Uribe, S., **2007**, In yeast, Ca<sup>2+</sup> and octylguanidine interact with porin (VDAC) preventing the mitochondrial permeability transition, *Biochim Biophys Acta*, 1767: 10, 1245-51.

Halestrap, A. P., **2004**, Does the mitochondrial permeability transition have a role in preconditioning? , *Circulation*, 110: 11, e303; author reply e303.

Halestrap, A. P., **2004**, Mitochondrial permeability: dual role for the ADP/ATP translocator? , *Nature*, 430: 7003, 1 p following 983.

Halestrap, A. P., Gillespie, J. P., O'Toole, A. and Doran, E., **2000**, Mitochondria and cell death: a pore way to die? , *Symp Soc Exp Biol*, 52: 65-80.

Hartman, F. C. and Barker, R., **1965**, An exploration of the active site of aldolase using structural analogs of fructose diphosphate, *Biochemistry*, 4: 6, 1068-75.

Haworth, R. A. and Hunter, D. R., **1979**, The Ca<sup>2+</sup>-induced membrane transition in mitochondria. II. Nature of the Ca<sup>2+</sup> trigger site, *Arch Biochem Biophys*, 195: 2, 460-7.

Huberts, D. H., Niebel, B. and Heinemann, M., **2012**, A flux-sensing mechanism could regulate the switch between respiration and fermentation, *FEMS Yeast Res*, 12: 2, 118-28.

Ingledew, W. J. and Poole, R. K., **1984**, The respiratory chains of Escherichia coli, *Microbiol Rev*, 48: 3, 222-71.

Kadenbach, B., **2003**, Intrinsic and extrinsic uncoupling of oxidative phosphorylation, *Biochim Biophys Acta*, 1604: 2, 77-94.

Konigsberg, M., Perez, V. I., Rios, C., Liu, Y., Lee, S., Shi, Y. and Van Remmen, H., **2013**, Effect of oxygen tension on bioenergetics and proteostasis in young and old myoblast precursor cells, *Redox Biol*, 1: 1, 475-82.

Kuznetsov, A. V., Javadov, S., Guzun, R., Grimm, M. and Saks, V., **2013**, Cytoskeleton and regulation of mitochondrial function: the role of beta-tubulin II, *Front Physiol*, 4: 82.

Lang, B. F., Gray, M. W. and Burger, G., **1999**, Mitochondrial genome evolution and the origin of eukaryotes, *Annu Rev Genet*, 33: 351-97.

Lemasters, J. J., Nieminen, A. L., Qian, T., Trost, L. C., Elmore, S. P., Nishimura, Y., Crowe, R. A., Cascio, W. E., Bradham, C. A., Brenner, D. A. and Herman, B., **1998**, The mitochondrial permeability transition in cell death: a common mechanism in necrosis, apoptosis and autophagy, *Biochim Biophys Acta*, 1366: 1-2, 177-96.

Leverve, X. M., **2007**, Mitochondrial function and substrate availability, *Crit Care Med*, 35: 9 Suppl, S454-60.

Mannella, C. A., **2006**, Structure and dynamics of the mitochondrial inner membrane cristae, *Biochim Biophys Acta*, 1763: 5-6, 542-8.

Manon, S. and Guerin, M., **1998**, Investigation of the yeast mitochondrial unselective channel in intact and permeabilized spheroplasts, *Biochem Mol Biol Int*, 44: 3, 565-75.

Manon, S., Roucou, X., Guerin, M., Rigoulet, M. and Guerin, B., **1998**, Characterization of the yeast mitochondria unselective channel: a counterpart to the mammalian permeability transition pore? , *J Bioenerg Biomembr*, 30: 5, 419-29.

Marty, G. D., Saksida, S. M. and Quinn, T. J., 2nd, **2010**, Relationship of farm salmon, sea lice, and wild salmon populations, *Proc Natl Acad Sci U S A*, 107: 52, 22599-604.

Mazat, J. P., Ransac, S., Heiske, M., Devin, A. and Rigoulet, M., **2013**, Mitochondrial energetic metabolism-some general principles, *IUBMB Life*, 65: 3, 171-9.

Mentel, M. and Martin, W., **2008**, Energy metabolism among eukaryotic anaerobes in light of Proterozoic ocean chemistry, *Philos Trans R Soc Lond B Biol Sci*, 363: 1504, 2717-29.

Merico, A., Sulo, P., Piškur, J. and Compagno, C., **2007**, Fermentative lifestyle in yeasts belonging to the Saccharomyces complex, *FEBS Journal*, 274: 4, 976-989.

Meyerhof, O. and Kiessling, W., **1935**, Über die enzymatische Umwandlung von Glycerinaldehydphosphorsäure in Dioxyacetophosphorsäure, *Biochem. Z.*, 279: 40-48.

Mitchell, P., **1966**, Chemiosmotic coupling in oxidative and photosynthetic phosphorylation, *Biol Rev Camb Philos Soc*, 41: 3, 445-502.

Mustea, I. and Muresian, T., **1967**, Crabtree effect in some bacterial cultures, *Cancer*, 20: 9, 1499-501.

Oláh, J., Tőkési, N., Lehotzky, A., Orosz, F. and Ovádi, J., **2013**, Moonlighting microtubule-associated proteins: Regulatory functions by day and pathological functions at night, *Cytoskeleton (Hoboken)*, 70: 11, 677-685.

Ovadi, J. and Saks, V., **2004**, On the origin of intracellular compartmentation and organized metabolic systems, *Mol Cell Biochem*, 256-257: 1-2, 5-12.

Pallotta, M. L., Valenti, D., Iacobino, M. and Passarella, S., **2004**, Two separate pathways for d-lactate oxidation by Saccharomyces cerevisiae mitochondria which differ in energy production and carrier involvement, *Biochimica et Biophysica Acta (BBA) - Bioenergetics*, 1608: 2-3, 104-113.

Pastorino, J. G. and Hoek, J. B., **2008**, Regulation of hexokinase binding to VDAC, *J Bioenerg Biomembr*, 40: 3, 171-82.

Peña, A., Piña, M. Z., Escamilla, E. and Piña, E., **1977**, A novel method for the rapid preparation of coupled yeast mitochondria, *FEBS Lett*, 80: 1, 209-13.

Perez-Vazquez, V., Saavedra-Molina, A. and Uribe, S., **2003**, In *Saccharomyces cerevisiae*, cations control the fate of the energy derived from oxidative metabolism through the opening and closing of the yeast mitochondrial unselective channel, *J Bioenerg Biomembr*, 35: 3, 231-41.

Perkins, G., Renken, C., Martone, M. E., Young, S. J., Ellisman, M. and Frey, T., **1997**, Electron Tomography of Neuronal Mitochondria: Three-Dimensional Structure and Organization of Cristae and Membrane Contacts, *J Struct Biol*, 119: 3, 260-272.

Petronilli, V., Miotto, G., Canton, M., Brini, M., Colonna, R., Bernardi, P. and Di Lisa, F., **1999**, Transient and long-lasting openings of the mitochondrial permeability transition pore can be monitored directly in intact cells by changes in mitochondrial calcein fluorescence, *Biophys J*, 76: 2, 725-34.

Piskur, J., Rozpedowska, E., Polakova, S., Merico, A. and Compagno, C., **2006**, How did *Saccharomyces* evolve to become a good brewer? , *Trends Genet*, 22: 4, 183-6.

Popel, A. S., **1989**, Theory of oxygen transport to tissue, *Crit Rev Biomed Eng*, 17: 3, 257-321.

Prieto, S., Bouillaud, F., Ricquier, D. and Rial, E., **1992**, Activation by ATP of a proton-conducting pathway in yeast mitochondria, *Eur J Biochem*, 208: 2, 487-91.

Richard, P., Teusink, B., Westerhoff, H. V. and van Dam, K., **1993**, Around the growth phase transition *S. cerevisiae*'s make-up favours sustained oscillations of intracellular metabolites, *FEBS Lett*, 318: 1, 80-2.

Rodríguez-Enriquez, S., Juarez, O., Rodriguez-Zavala, J. S. and Moreno-Sánchez, R., **2001**, Multisite control of the Crabtree effect in ascites hepatoma cells, *Eur J Biochem*, 268: 8, 2512-9.

Rolland, F., Winderickx, J. and Thevelein, J. M., **2002**, Glucose-sensing and -signalling mechanisms in yeast, *FEMS Yeast Res*, 2: 2, 183-201.

Rostovtseva, T. K., Sheldon, K. L., Hassanzadeh, E., Monge, C., Saks, V., Bezrukov, S. M. and Sackett, D. L., **2008**, Tubulin binding blocks mitochondrial voltage-dependent anion channel and regulates respiration, *Proc Natl Acad Sci U S A*, 105: 48, 18746-51.

Stefan, C. and Sauer, U., **2011**, Intracellular characterization of aerobic glucose metabolism in seven yeast species by <sup>13</sup>C flux analysis and metabolomics, *FEMS Yeast Res*, 11: 3, 263-272.

Tielens, A. G., Rotte, C., van Hellemond, J. J. and Martin, W., **2002**, Mitochondria as we don't know them, *Trends Biochem Sci*, 27: 11, 564-72.

Tschischka, K., Abele, D. and Portner, H. O., **2000**, Mitochondrial oxyconformity and cold adaptation in the polychaete *Nereis pelagica* and the bivalve *Arctica islandica* from the Baltic and White Seas, *J Exp Biol*, 203: Pt 21, 3355-68.

Uribe-Carvajal, S., Luevano-Martinez, L. A., Guerrero-Castillo, S., Cabrera-Orefice, A., Corona-de-la-Pena, N. A. and Gutierrez-Aguilar, M., **2011**, Mitochondrial Unselective Channels throughout the eukaryotic domain, *Mitochondrion*, 11: 3, 382-90.

Uribe, S., Ramirez, J. and Pena, A., **1985**, Effects of beta-pinene on yeast membrane functions, *J Bacteriol*, 161: 3, 1195-1200.

Veech, R. L., Lawson, J. W., Cornell, N. W. and Krebs, H. A., **1979**, Cytosolic phosphorylation potential, *J Biol Chem*, 254: 14, 6538-47.

Wilson, D. F., Rumsey, W. L., Green, T. J. and Vanderkooi, J. M., **1988**, The oxygen dependence of mitochondrial oxidative phosphorylation measured by a new optical method for measuring oxygen concentration, *J Biol Chem*, 263: 6, 2712-8.

Wojtczak, L., Teplova, V. V., Bogucka, K., Czyz, A., Makowska, A., Wieckowski, M. R., Duszynski, J. and Evtodienko, Y. V., **1999**, Effect of glucose and deoxyglucose on the redistribution of calcium in ehrlich ascites tumour and Zajdela hepatoma cells and its consequences for mitochondrial energetics. Further arguments for the role of Ca(2+) in the mechanism of the crabtree effect, *Eur J Biochem*, 263: 2, 495-501.

Xie, G. C. and Wilson, J. E., **1988**, Rat brain hexokinase: the hydrophobic N-terminus of the mitochondrially bound enzyme is inserted in the lipid bilayer, *Arch Biochem Biophys*, 267: 2, 803-10.

Zhang, M., Mileykovskaya, E. and Dowhan, W., **2005**, Cardiolipin is essential for organization of complexes III and IV into a supercomplex in intact yeast mitochondria, *J Biol Chem*, 280: 33, 29403-8.

## **11. Anexos**

**11.1 Informe de estancia en cotutela con la Universidad de Bordeaux, Francia.**



## UNIVERSIDAD NACIONAL AUTÓNOMA DE MÉXICO

**Programa de Maestría y Doctorado en Ciencias Bioquímicas**

**Informe de estancia en cotutela con la:**

**Université de Bordeaux, France, Institut de Biochimie et Génétique cellulaires.**

**Programa de movilidad estudiantil: Campus France,**

**bourse d'excellence Eiffel.**

### **El esferoplasto permeabilizado como modelo de estudio para la integración del metabolismo glucolítico y la fosforilación oxidativa en *Saccharomyces cerevisiae*.**

1. Efecto de la Fructosa 1,6-bisfosfato sobre el canal mitocondrial inespecífico de *Saccharomyces cerevisiae*.
2. Estudio de la canalización de la Fructosa-1,6-bifosfato hacia la mitocondria y el efecto Crabtree.

M. en C. Mónica Rosas Lemus

Comité tutorial UNAM: Dr. Edmundo Chávez Cosío  
Dra. Soledad Funes Argüello  
Dr. Salvador Uribe Carvajal

Tutor Université de Bordeaux: Dra. Anne Devin  
Con la participación de: Dr. Michel Rigoulet y Mtr. de conf. Nicole Avéret

3 de octubre de 2014- 31 de julio de 2015

## **1. Antecedentes.**

Los organismos eucariontes no fotosintéticos obtienen su energía mediante la producción de ATP a través de la glucólisis y la fosforilación oxidativa. En *Saccharomyces cerevisiae* la glucólisis es predominante cuando se cultiva en fuentes de carbono fermentables y conduce a la producción de etanol. Las enzimas de la glucólisis: aldolasa y gliceraldehido-3-fosfato deshidrogenasa interaccionan, y esta interacción es estabilizada por el citoesqueleto de actina, lo cual favorece la canalización de sustratos y hace más eficiente la vía (Araiza-Olivera y col., 2013). La fosforilación oxidativa se observa en presencia de sustratos no fermentables (lactato, glicerol, etanol), y también se ha observado la formación de supercomplejos mediante la asociación de los complejos 3 y 4 de la cadena respiratoria (Schägger y Pfeiffer, 2000), lo cual permitiría la canalización de electrones y probablemente la disminución de ROS. En mamíferos se ha demostrado la interacción de proteínas glucolíticas y el citoesqueleto de actina con la mitocondria (Ovadi y col., 2004). Sin embargo, en *S. cerevisiae* existen muy pocos estudios acerca de la interacción o posible canalización de sustratos entre estas dos vías metabólicas (Clemençon, 2012).

La evidencia más importante de la interacción de la glucólisis con la fosforilación oxidativa en *S. cerevisiae* es el efecto Crabtree. Este fenómeno fue reportado por primera vez al estudiar un modelo de células tumorales (Crabtree, 1929). Se produce al añadir glucosa al medio, lo cual disminuye la respiración; éste es un fenómeno a corto plazo y reversible; lo presentan algunos tipos de levadura, células tumorales, células no tumorales con alta tasa de proliferación y algunas bacterias (Díaz-Ruiz y col., 2011). El efecto Crabtree está relacionado con diversas condiciones metabólicas: la competencia entre la glucólisis y la fosforilación oxidativa por el ATP y el Pi, así como la acumulación de fructosa-1,6-bifosfato (F1,6BP). En

*S. cerevisiae* la F1,6BP disminuye la actividad del complejo III de la cadena respiratoria. Por otra parte, la G6P estimula la respiración en mitocondrias aisladas; sin embargo, sus efectos no son importantes mientras el cociente  $[G6P]/[F1,6BP] < 1$ . Además, se observó que el esferoplasto permeabilizado es más sensible a la disminución de la respiración causado por la F1,6BP (Díaz-Ruiz y col., 2008). Estudios recientes sugieren que el efecto Crabtree podría ser inducido por un alto flujo glucolítico, el cual probablemente genere concentraciones locales de F1,6BP que sean canalizadas a la mitocondria e inhiban el complejo III de la cadena respiratoria.

La fosforilación oxidativa en *S. cerevisiae* también es regulada por el canal mitocondrial inespecífico. En la mitocondria aislada, cuando este canal se abre, disminuye la fosforilación oxidativa, se acelera la respiración en el estado IV, el potencial de membrana disminuye y la mitocondria se hincha. Cuando el canal se cierra, la respiración disminuye, aumenta el potencial transmembranal, se acopla la fosforilación oxidativa y se inhibe el hinchamiento. La estructura de este canal aún está en controversia, pero se propone que podría estar formado por: El VDAC (canal aniónico dependiente de voltaje), Pic (acarreador de fosfato), ANT (translocasa de adenin nucleótidos (Gutiérrez-Aguilar y col., 2007) o bien la ATP sintasa (Giorgio y col., 2013). Se sabe que el Pi,  $Ca^{2+}$ ,  $Mg^{2+}$  y ADP lo cierran, pero el ATP y NADH lo abren (Gutiérrez-Aguilar y col., 2007). Se propone que la apertura y cierre del ScMUC, es un evento fisiológico y que depende del estado energético de la célula (Gutierrez-Aguilar y Uribe-Carvajal, 2015), por lo cual es importante estudiar su regulación en presencia de otros metabolitos.

Debido a que los efectos de la inhibición de la respiración de la F1,6BP son más importantes durante el estado IV que durante el estado III, se estudió su efecto sobre el

$_{Sc}MUC$ . Se observó que la F1,6BP mantiene el  $_{Sc}MUC$  cerrado aun cuando el fosfato sea bajo y en presencia de G6P. Además, las concentraciones necesarias para estos efectos son mucho menores que para inhibir la respiración cuando el  $_{Sc}MUC$  se encuentra cerrado. Los efectos de la F1,6BP sobre la respiración no se observan en la levadura Crabtree negativa *Kluyveromyces lactis*, aún en condiciones donde el Pi es bajo, lo cual demuestra que esta regulación es exclusiva de *S. cerevisiae*. Estos estudios sugieren que la F1,6BP podría contribuir a la inducción del efecto Crabtree, al cerrar el  $_{Sc}MUC$  (Rosas-Lemus y col., 2014). Para tener una visión más general de la regulación glucólisis-fosforilación oxidativa, es importante estudiar los efectos de la F1,6BP sobre el canal inespecífico mitocondrial en el esferoplasto permeabilizado, ya que es un modelo que conserva la estructura celular con la ventaja de que al permeabilizar la membrana citoplásmica es posible adicionar sustratos y estudiar sus efectos *in situ*. La regulación del canal inespecífico mitocondrial en el esferoplasto ha sido muy poco estudiada (Manon y col., 1998) y la F1,6BP es un sustrato glucolítico; por lo tanto es necesario realizar estudios preliminares que permitan estudiar el modelo y adaptarlo a nuestras interrogantes.

Se demostró que en presencia de yodoacetato (inhibidor irreversible de la gliceraldehído-3-fosfatodeshidrogenasa), la F1,6BP disminuye la respiración en el estado IV. Para evitar el uso de yodoacetato, se sintetizó el 1,4-bifosfobutano (1,4bpb); este compuesto es un análogo no metabolizable de la F16BP y un inhibidor competitivo de la aldolasa (Hartman y col., 1965). Se estudiaron sus efectos sobre el  $_{Sc}MUC$  en la mitocondria aislada y sobre la aldolasa. Se observó que el 1,4bpb es un inhibidor competitivo de la aldolasa y que mantiene el  $_{Sc}MUC$  cerrado; queda por evaluar la actividad del compuesto en el esferoplasto permeabilizado (Rosas-Lemus y cols., en preparación).

En el laboratorio de bioenergética y metabolismo celular del Instituto de biología y genética celular, Universidad de Bordeaux Francia, la Dra. Anne Devin estudia el metabolismo energético de *S. cerevisiae* en la mitocondria aislada, la célula entera y el esferoplasto permeabilizado. Actualmente su investigación se centra en el papel de la glucólisis en la inducción del efecto Crabtree en *S. cerevisiae*, para lo cual ha empleado diversas mutantes de las enzimas glucolíticas, entre ellas una delección en el gen que codifica para la hexocinasa ( $\Delta$ hXk2). Esta delección confiere un fenotipo Crabtree negativo a la levadura, lo cual podría deberse a que esta isoforma es la que más se expresa en presencia de glucosa y participa en la represión catabólica. Resultados preliminares de este estudio muestran que en células enteras la cepa,  $\Delta$ hXk2 y su cepa silvestre mantienen el mismo cociente G6P/F16BP, que no existe una competencia por el fosfato a nivel de la ATP sintasa y la glucólisis; además, tampoco hay diferencias significativas en la cantidad de citocromos mitocondriales. Con lo anterior, no ha sido posible explicar por qué la cepa mutante no presenta efecto Crabtree. De acuerdo con las hipótesis acerca de éste fenómeno, quedan por probar el flujo glucolítico y la posible canalización de las hexosas fosfato hacia la mitocondria. Se reportó previamente que en la levadura, la hexocinasa, enolasa (ENO), piruvato cinasa (PK) y gliceraldehído-3-fosfatodeshidrogenasa (GAPDH) pueden asociarse a la mitocondria; esta asociación podría permitir crear un microambiente propicio para generar concentraciones locales de las hexosas fosfato más elevadas que en el resto del citoplasma y la falta de la Hxk2 podría perturbar la formación de este microambiente. Para comprobar esta hipótesis es necesario recurrir al esferoplasto permeabilizado.

## **2. Objetivos**

2.1 Aprender la técnica de preparación y utilización de esferoplastos permeabilizados de *S.*

*cerevisiae*.

2.2 Evaluar el efecto de la fructosa-1,6-bifosfato y el 1,4-bifosfobutano sobre el ScMUC.

2.3 Estudiar el efecto de la canalización de la Fructosa-1,6-bifosfato y Glucosa-6-fosfato sobre la mitocondria y la posible inducción del efecto Crabtree.

### **3. Material y métodos.**

#### 3.1 Cultivo de la levadura y cepas utilizadas.

Cepa industrial “Yeast Foam”

BY4742 de *S. cerevisiae* (MAT $\alpha$  ; his3Δ1 ; leu2Δ0 ; lys2Δ0 ; ura3Δ0).

BY4742 Δhxk2 de *S.cerevisiae* (MAT $\alpha$  ; his3Δ1 ; leu2Δ0 ; lys2Δ0 ; ura3Δ0 ; Hxk2 :: kan MX4).

Para el estudio del  $_{Sc}$ MUC se utilizó la cepa industrial de *S. cerevisiae* “Yeast foam”. Se cultivaron en medio YPlac (1% Extracto de levadura, 1% peptona de gelatina, 0.12%  $(NH_4)_2SO_4$ , 0.1%  $KH_2PO_4$  y 2% ácido láctico, pH 5.5) hasta obtener 500 mL con una D.O. de 4. Posteriormente se lavaron mediante centrifugación y se realizó la preparación de esferoplastos.

El estudio de la canalización de las hexosas fosfato hacia la mitocondria y su relación con el efecto Crabtree, se realizó utilizando las cepas: BY4742 y BY4742 Δhxk2. Ambas cepas se cultivaron en medio sintético completo (Sc) (1,75 g/L de yeast nitrogen base, 5 g/L de  $NH_4SO_4$ , 1 g/L de  $KH_2PO_4$  y 4 g/L de hidrolizado de caseína y 2% de lactato, pH 5,5 (NaOH), suplementado con 2 g/L de uracilo, 4 g/L adenina y triptofano), hasta obtener 500 mL de cultivo a 1 U.D.O (600 nm). Las células se lavaron con agua desionizada 3 veces mediante centrifugación (5000 rpmx 5 min) y se realizó la preparación de esferoplastos.

### 3.2 Preparación de esferoplastos.

Los esferoplastos son células que han perdido la pared celular y son un buen modelo de estudio, ya que pueden permeabilizarse y facilitar la entrada de sustratos (Averet y col., 1998). En 20 mL de buffer-  $\beta$ -mercaptoetanol (0.1 M tris, 0.5 M  $\beta$ -mercaptoetanol pH 9.3 (NaOH)), se incuba 1 g de peso seco de levadura, durante 15 min a 30°C. Posteriormente se lavan 4 veces con buffer de lavado (0.5 M KCl, 10 mM tris-HCl pH 7) mediante centrifugación (5,000 rpm x 5 min.) y se resuspenden en 10 mL de buffer de digestión (1,35 M sorbitol, 1 mM EGTA, ácido cítrico 10 mM, fosfato monosódico pH 5.8) con la citohelicasa (0.17g citohelicasa/g peso seco). La suspensión se incuba a 30 °C en agitación (250 rpm) durante 30 min. La digestión se interrumpe al 90% adicionando buffer de esferoplastos frío (1 M sorbitol, 10 mM KH<sub>2</sub>PO<sub>4</sub>, 1.7 mM NaCl, 2 mM MgSO<sub>4</sub>, 0.5 mM EGTA) y se lava mediante centrifugación 3 veces ((3, 800 x g, 10 min). En el último lavado, se descarta el sobrenadante y el precipitado se resuspendió en 6mL de buffer de esferoplastos. La cantidad de proteína se cuantifica por el método de biuret (Gornall y col., 1949).

### 3.3 Oximetría.

Se utiliza un oxímetro de la marca Hito acoplado a un graficador, con una celda de 1 mL con agitación constante a 28 °C. Para permeabilizar los esferoplastos, primero se agrega el medio a la celda del oxímetro: A, (0.25 M KCl, 0.5 M sorbitol, 0.5 mM EGTA, 10 mM Tris-HCl, pH 6.8, 6 mM iodoacetato, 0.1% ABS), B (50 mM KCl, 0.9 M sorbitol, 0.5 mM EGTA, 10 mM Tris-HCl, pH 6.8, 6 mM iodoacetato, 0.1% ABS) para el estudio del <sub>Sc</sub>MUC o C (Sorbitol 1 M, MgSO<sub>4</sub> 2 mM, EGTA 0.5 mM, NaCl 1.7 mM, NH<sub>4</sub>Cl 10 mM, KH<sub>2</sub>PO<sub>4</sub> 10 mM pH 6.8, ABS 0.1%) para estudiar la glucólisis. Posteriormente se agregan los esferoplastos (1 mg/mL) y la nistatina (20  $\mu$ g/mL), y por medio de una cánula se oxigena la celda durante 10 min en agitación constante. Cuando los esferoplastos ya no consumen oxígeno por sí solos y la respiración es constante, se agregan los sustratos: NADH 10 mM

para generar el estado IV, posteriormente el ADP (2 mM) para generar el estado III y/o CCCP (10  $\mu$ M) para generar el estado desacoplado.

### 3.4 Gel azul nativo (BN-PAGE).

Se utilizan geles nativos en gradiente de acrilamida de 4-16% (Native PAGE NOVEX Bis-trisGels, invitrogen). Se utilizan 2 mg de esferoplastos y se resuspenden en buffer de muestra (ácido aminocaproico 750 mM, 25 mM de imidazol pH 7.0, (HCl)), posteriormente se agrega la digitonina (3mg/mg prot) y se incuba en hielo durante 30 min, agitando por inversión cada 5 min. Se centrifuga el homogenizado en una microultracentrifuga (100,000 g x 20 min a 4°C). Posteriormente se descarta el precipitado y el sobrenadante se mezcla con azul de coomassie (Serva blue G-250) al 5% en amortiguador de muestra. En el cuarto frío (4°C) se prepara la cámara de electroforesis montando el gel y añadiendo tanto el amortiguador del cátodo 1 (Tricina 50 mM, imidazol 7.5 mM, azul de Coomassie de Serva 0.02 %) como del ánodo (Tricina 50 mM, imidazol 7.5 mM); se cargan las muestras. Se realiza la electroforesis a 15 mA con un voltaje máximo de 300 V. Una vez que las proteínas migraron a 1/3 del gel, se cambia el amortiguador del cátodo 2 (Tricina 50 mM, imidazol 7.5 mM), azul de Coomassie de Serva 0.002 %) y se añade el amortiguador del cátodo B-100 (Schägger y col., 2000). Las proteínas terminan de migrar aproximadamente en 3 h.

### 3.5

#### Western blot

Una vez terminada la electroforesis, se transfieren las proteínas a una membrana de PVDF en amortiguador y se realiza el western blot. En todos los casos la membrana se bloquea durante 30 min con 0.1% de BSA en PBS-tween 0.1% en agitación constante. El anticuerpo primario se incuba toda la noche a 4ºC: aldolasa (1:2500), GAPDH (1:20000), VDAC (1:20000) y hexocinasa (1:100000), posteriormente se lava la membrana 4 x 5 min. Se agrega el anticuerpo secundario acoplado a peroxidasa de rábano ( $\alpha$ -ratón 1:20,000;  $\alpha$ -conejo 1:100,000;  $\alpha$ -cabra 1:20,000) y se incuba durante 1 h a temperatura ambiente. Finalmente se lava la membrana (4 x5 min) y se revela utilizando el kit de Amersham (ECL) y soluciones de revelado de Kodak.

### 3.6 Cuantificación de F16BP y G6P en el esferoplasto permeabilizado.

Se utiliza 1 mg prot/mL de esferoplastos y se permeabilizan como en 3.3. Se agrega NADH 10 mM y posteriormente ADP 2 mM para inducir el estado III y generar ATP mitocondrial. Se realizan las adiciones de glucosa hasta 30 mM. Una vez que se observa la inhibición de la respiración, se interrumpe la reacción adicionando a la cámara del oxímetro formaldehído (3.7%) y se deja incubar 10 min. Posteriormente se centrifuga la muestra (2,500 rpm x 5 min), se descarta el sobrenadante y los esferoplastos se resuspenden en 5 mL finales de buffer de extracción (Hepes 10 mM y Et-OH 70%). Se incuba durante 3 min a 80ºC y se evapora todo el líquido en un rota evaporador 10 min a 60ºC. El sólido restante en el tubo se conserva a -20ºC hasta el día de su utilización. Para cuantificar la cantidad de G6P, F6p y F1,6BP se resuspende el sólido obtenido anteriormente en 550  $\mu$ L de agua desionizada, se centrifuga a velocidad máxima en una microfuga durante 5 min y se descarta el precipitado. Se toman 200  $\mu$ L de muestra y se adicionan a una celda de espectrofotómetro para UV con 800  $\mu$ L de buffer ETRAM (0,2 M trietanolamina, 30 mM MgCl<sub>2</sub>, 15 mM EDTA, pH 7,4).

Para la cuantificación de G6P: Se añade a la celda con el buffer y la muestra NAD<sup>+</sup> 0.1 mM y se inicia el registro de la absorbencia de la línea base a 340 nm. Posteriormente se agregan: 0.3

U/ml de glucosa-6-fosfato deshidrogenasa (G6PDH) y se deja la reacción aproximadamente 15 min. Para comprobar la estequiometría de la reacción, se agregó una cantidad conocida de NADH y G6P. Así la cantidad de G6P es estequiométricamente igual a la cantidad de NADH medida al adicionar G6PDH. Las diferentes concentraciones se calculan utilizando la ley de Lambert-Beer utilizando un coeficiente de extinción para  $\epsilon_{\text{NADH}} = 6220 \text{ M}^{-1}$ .

La cuantificación de la F1,6BP se realizó mediante la reacción enzimática acoplada entre la aldolasa (ALD), la gliceraldehído 3-fosfato deshidrogenasa (GAPDH) y fosfoglicerato cinasa (PGK). Se añaden 200  $\mu\text{L}$  de muestra en una celda para UV con 800  $\mu\text{L}$  de buffer ETRAM. Se agregan, 0,1 mM de  $\text{NAD}^+$ , 0.1 mM Pi, 0.1 mM ADP, 0.6 U/mL de PGK y 0.3 U/mL de ALD. Se inicia el registro en el espectrofotómetro a 340 nm durante 15 min y se añaden 0.6 U/ mL GAPDH, y la reacción se deja durante 15 min. Dado que la reacción es estequiométrica, la cantidad de NADH producido equivale a la cantidad de F1,6BP presente en la muestra.

#### **4. Resultados.**

##### **4.1. Efecto del 1,4-bifosfobutano sobre el $s_c$ MUC en el esferoplasto permeabilizado.**

El  $s_c$ MUC, se ha estudiado principalmente en la mitocondria aislada, pero se demostró que puede inducirse su transición de la permeabilidad en el esferoplasto permeabilizado en presencia de KCl y ATP (Manon y col., 1998). Sin embargo en estas condiciones se pierde la sensibilidad al fosfato; por lo tanto, se buscó un sistema en el cual el  $s_c$ MUC respondiera a la modulación por Pi. En la tabla 1 se muestra que en 10 mM de Pi, el  $s_c$ MUC se encuentra semicerrado, aunque el acoplamiento es inferior a 2 y la adición de F1,6BP no mejora el CR. En Pi 0.1 mM se observa una aceleración del estado IV y un acoplamiento de 1.1; sin embargo, la adición de F1,6BP no tiene ningún efecto. Esto puede deberse a que el KCl podría aumentar la fuerza iónica del medio y con ello favorece la separación de algunas proteínas que permiten el acceso de la F1,6BP a la mitocondria; Por ello se realizó un experimento para determinar si el NADH pierde su canalización en estas condiciones y se observó que al generar 0.5 mM de NADH mediante la GAPDH, en presencia de 0.25 M de KCl , se pierde la estimulación de la respiración (datos no mostrados), mientras que sin KCl, la misma cantidad de NADH producido estimula la respiración. Por lo tanto, se buscó un buffer con el KCl necesario para inducir la transición de la permeabilidad, modular el  $s_c$ MUC en función del Pi y donde se observaran los efectos de la F16BP.

**Tabla 1. Efecto del KCl y la Fructosa-1,6-bifosfato sobre el  $s_c$ MUC en el esferoplasto permeabilizado.** Medio de reacción: B (KCl 0.25 M, sorbitol 0.5 M, EGTA 0.5 mM, Tris-HCl 10 mM pH 6.8, 6 mM de iodoacetato), esferoplastos 1 mg prot/mL, nistatina 20  $\mu$ L/mL, NADH 10 mM, ADP 2 mM.

Condición	Estado IV (natgO/min*mg prot)	Estado III (natgO/min*mg prot)	CR
Pi 10 mM + ATP 4mM	201.6	327.6	1.6
Pi 0.1 mM + 4 mM	340.2	340.2	1
Pi 10 mM+ ATP 4mM + F1,6BP 8 mM	235.2	361.2	1.5
Pi 0.1 mM + ATP 4 mM + F1,6 BP 8mM	289.8	315	1.1

En la tabla 2 se muestra que en Pi 0.1 mM el CR es cercano a 1, el estado III y IV son similares y mucho menores que el estado III en Pi 10 mM, donde se observa un acoplamiento (CR 2.5). Al agregar F1,6BP en presencia de yodoacetato, no se observa ningún efecto sobre la respiración o el acoplamiento. El 1,4BPB, tampoco tiene efectos sobre la respiración; sin embargo, al adicionar F1,6BP 10mM y 1,4BPB 2 mM juntos, se observó disminución de la respiración tanto en el estado IV como en el estado III con un CR cercano a 2, lo cual podría indicar un acoplamiento. Probablemente se encontró la condición adecuada para estudiar el  $s_c$ MUC en el esferoplasto permeabilizado, y la razón por la cual no se observa la aceleración de la respiración en el estado IV al abrir el  $s_c$ MUC como en la mitocondria aislada, puede ser que la regulación es diferente en el esferoplasto permeabilizado o no se logra un desacoplamiento verdadero como se reportó en el trabajo de Manon y cols. (1998). Anteriormente se demostró que el VDAC se encuentra cerrado en el esferoplasto permeabilizado, mientras que en la mitocondria aislada está abierto, lo cual facilita la entrada de NADH en la mitocondria aislada. Sin embargo, en el esferoplasto permeabilizado, la Km por el NADH adicionado es 10 veces mayor que el NADH producido por la gliceraldehído-3-fosfato

deshidrogenasa, lo cual sugiere que en este sistema los metabolitos son canalizados desde el citoplasma hacia la mitocondria (Avéret y col., 2002) .Es necesario estudiar la Regulación del *ScMUC* en estas condiciones para determinar si su regulación es similar a la mitocondria aislada y poder reproducir los efectos de la F1,6BP y el 14-bifosfobutano.

**Tabla 2. Efecto de la F1,6BP y el 1,4 bifosfobutano sobre el *ScMUC* en el esferoplasto permeabilizado en presencia de 50 mM de KCl. Medio de reacción:** 50 mM KCl, 0.9 M sorbitol, 0.5 mM EGTA, 10 mM Tris-HCl, pH 6.8, 6 mM iodoacetato, 0.1% BSA.

Condición	Estado IV (natgO/min*mg prot)	Estado III (natgO/min*mg prot)	CR
Pi 10 mM	84	205.8	2.5
Pi 0.1 mM	138.6	159.6	1.1
Pi 0.1 mM + F1,6BP 10 mM	92.4	113.4	1.2
Pi 0.1 mM + 1,4 BPB 10mM	100.8	130.2	1.3
Pi 0.1 mM + F1,6BP 10 mM + 1,4BPB 2 mM	50.4	113.4	2.3

## **4.2. Estudio de la canalización de la Fructosa-1,6-bisfosfato hacia la mitocondria y el efecto Crabtree en el esferoplasto permeabilizado.**

### **4.2.1 Efecto de la G6P y F1,6BP en el esferoplasto permeabilizado**

Para determinar si la proporción  $\frac{G6P}{F1,6BP} < 1$  es un factor importante para la inducción del efecto Crabtree, se cuantificó la cantidad de G6P y F1,6BP generados al añadir glucosa al medio de cultivo (resultados del laboratorio, en proceso de publicación). Sin embargo, tanto para la cepa silvestre como para la  $\Delta hck2$ , se encontró el mismo cociente, siendo que la mutante es Crabtree negativa y la silvestre Crabtree positiva. Dado que este cociente fue reportado en la cepa industrial (yeast foam) de *S. cerevisiae* (Díaz-Ruiz y col., 2008), se decidió estudiar diferentes concentraciones de F1,6BP y G6P en esferoplastos permeabilizados de las cepas BY4742 y BY4742  $\Delta hck2$ . Para evitar el metabolismo de la F1,6BP se utilizó iodoacetato (inhibidor de la GAPDH).

Se estudió el efecto de la G6P sobre la respiración en estado III y IV utilizando NADH como sustrato respiratorio, y se observó que en el estado IV la cepa silvestre muestra una inhibición con 2 a 10 mM de G6P y a partir de 20 mM se recupera la respiración, mientras que en la cepa mutante  $\Delta hck2$ , no se observan cambios significativos. Por otra parte en el estado III, la G6P inhibe la respiración de 2-10 mM en ambas cepas, pero sólo la mutante recupera la respiración a partir de 10 mM y la silvestre continúa inhibida (Fig.1). Esto sugiere que la adición de 2-10mM de G6P podría generar F1,6BP, y como esta no puede ser metabolizada debido al yodoacetato; es probable que se acumule e inhiba la respiración. Al continuar las adiciones de G6P el cociente G6P/F1,6BP podría aumentar y estimular la respiración en el estado IV, mientras que en el estado 3 la producción de ATP podría favorecer la producción de G6P al desfosforilar la F1,6BP en la mutante y tal vez se favorezca la formación de F1,6BP en la silvestre. También es probable que el fosfato disponible sea cada vez menor al ser utilizado en la formación de F16BP en el caso de la silvestre, y no así en la mutante, lo cual favorecería la inhibición en el estado III. Para corroborar esta hipótesis se decidió

estudiar los efectos de la F1,6BP en el esferoplasto permeabilizado. Se observó que tiende a inhibir la respiración en ambas cepas, tanto en estado III como en estado IV; sin embargo, no se observan diferencias significativas en la respiración (Fig. 2). Esto podría deberse a que la F1,6BP necesita ser conducida del citoplasma hacia la mitocondria y al ser el esferoplasto un sistema abierto, no se favorece su interacción. Previamente se reportó que existe una canalización importante entre la mitocondria y la glucólisis para el NADH, lo cual sugiere que estas dos vías se encuentran comunicadas (Averet y col., 1998). Para comprobar si la generación de F1,6BP en el esferoplasto mejoraría sus efectos, sobre la respiración se decidió evaluar el efecto de la glucosa sobre la respiración en el esferoplasto permeabilizado.

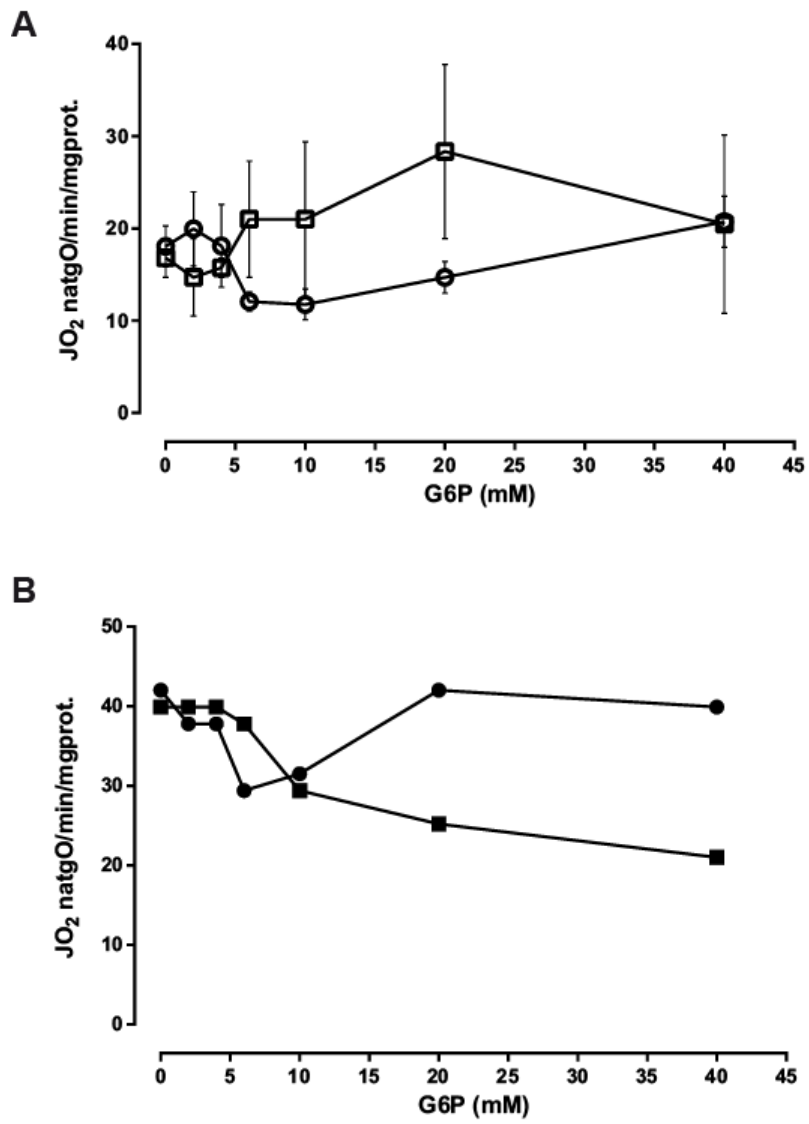


**Fig. 1. Efecto de la G6P sobre la respiración en el esferoplasto permeabilizado.** A, estado IV y B, estado III. Las cepas: BY4742 (wt) en cuadros y BY4742  $\Delta$ hxk2 ( $\Delta$ hxk2) en círculos. Medio de reacción: Sorbitol 1 M, MgSO<sub>4</sub> 2 mM, EGTA 0.5 mM, NaCl 1.7 mM, NH<sub>4</sub>Cl 10 mM, KH<sub>2</sub>PO<sub>4</sub> 10 mM pH 6.8, ABS 0.1%. Esferoplastos 1 mg prot/ mL, NADH 1 0mM como sustrato respiratorio, ADP 2 mM y 20  $\mu$ g/mL de nistatina. G6P como se indica.

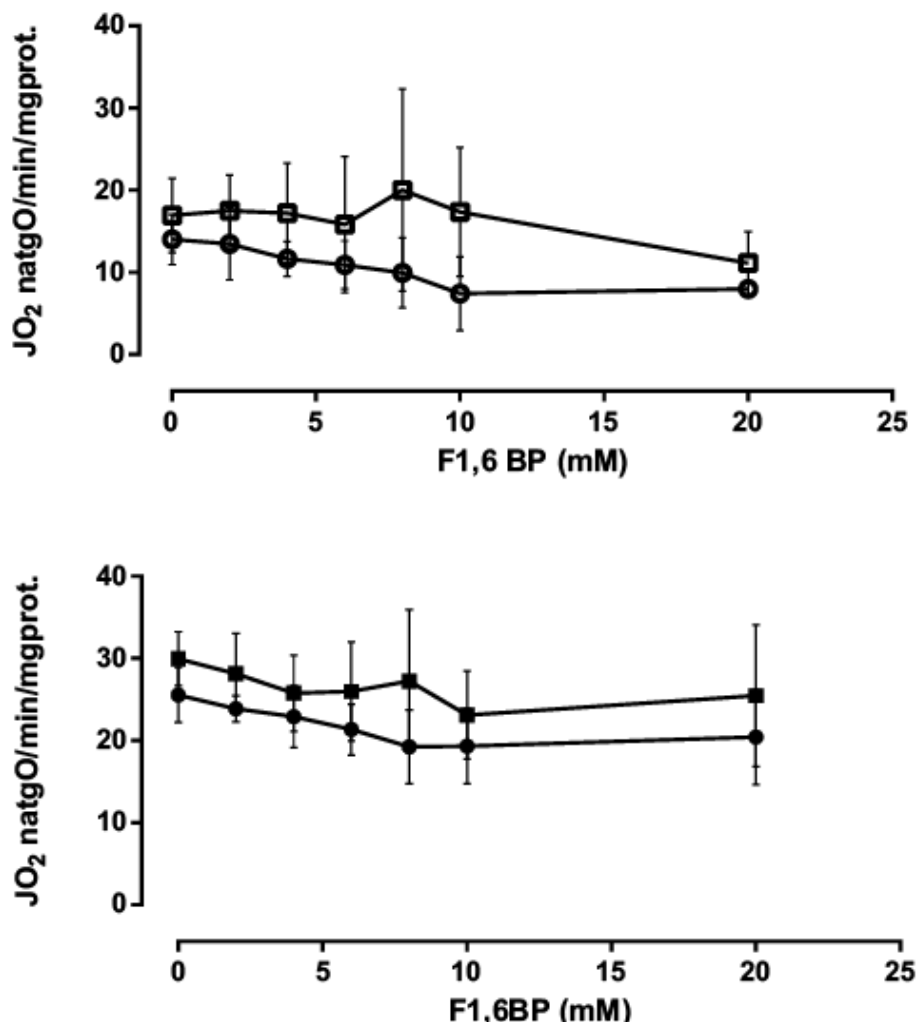


**Fig. 2. Efecto de la F1,6BP sobre la respiración del esferoplasto permeabilizado.** A, en estado IV y B, en estado III. Las cepas: BY4742 (wt) en círculos y BY4742  $\Delta$ hxk2 ( $\Delta$ hxk2) en cuadros. Medio de reacción: Sorbitol 1 M, MgSO<sub>4</sub> 2 mM, EGTA 0.5 mM, NaCl 1.7 mM, NH<sub>4</sub>Cl 10 mM, KH<sub>2</sub>PO<sub>4</sub> 10 mM pH 6.8, ABS 0.1%. Esferoplastos 1mg prot/ mL, NADH 10mM como sustrato respiratorio y 20  $\mu$ g/mL de nistatina. F1,6BP como se indica y 2 mM de ADP para inducir el estado III.

#### **4.2.2 Generación de G6P y F1,6BP en el esferoplasto.**

En estudios previos se demostró que durante la permeabilización, moléculas como el NAD<sup>+</sup>, ADP y ATP salen del esferoplasto, lo cual permite manipular la respiración mitocondrial agregando concentraciones conocidas de estos metabolitos, y es posible reconstituir la glucólisis agregando estas moléculas y NH<sub>4</sub>Cl para activar a la fructosa-6-fosfatocinasa (PFK) (Averet y col., 1998).

Para determinar si la posible canalización de las hexosas fosfato podría explicar el fenotipo Crabtree negativo de la mutante  $\Delta$ hXk2, se utilizó el esferoplasto permeabilizado en presencia de yodoacetato para inhibir la GAPDH, y de NH<sub>4</sub>Cl para activar la PFK. Debido a que el esferoplasto presenta una gran actividad de las ATPasas (membrana plasmática, vacuolar, adenilato ciclase ATP sintasa), no se adicionó ATP, sino ADP para generar ATP mitocondrial y evitar la hidrólisis del ATP añadido. Además, ésto permite saber si existe o no una comunicación entre la glucólisis y la mitocondria, ya que la hexocinasa tomaría el ATP proveniente de la mitocondria para iniciar la glucólisis como se reportó previamente en el mamífero (Xie y col., 1988; Pastorino y col., 2008) y probablemente también la PFK tenga acceso a este ATP mitocondrial, lo cual representaría una mejor producción de hexosas fosfato. En la Fig. 3 A se muestra el efecto de la adición de glucosa al medio sobre el consumo de oxígeno en estado IV. Se observó que tanto en la cepa silvestre como en la cepa mutante existe una tendencia a la inhibición de la respiración que sólo es significativa en la cepa silvestre a 30 mM. Sin embargo, en el estado III, la inhibición de la respiración en la cepa silvestre se observa a partir de 10 mM y es mucho mayor que en el estado IV. Por otra parte, la tendencia a la inhibición de la cepa mutante también es más grande que en el estado IV, pero no es significativa. Estos resultados podrían sugerir que la generación de ATP al adicionar ADP es importante para la inhibición de la respiración, probablemente porque el ATP sirva para fosforilar a las hexosas, favorecer la acumulación de F1,6BP y este fenómeno sea más eficiente en la cepa silvestre y no en la mutante, debido a la deficiencia de la hexocinasa 2. Para comprobar que estos

resultados se deben a la formación de F1,6BP *in situ* y a su posible canalización, es necesario conocer las concentraciones de hexosas fosfato generadas en estas condiciones. Sin embargo, el esferoplasto permeabilizado en suspensión no permite la cuantificación de las hexosas fosfato, debido a la presencia de sorbitol en el medio. Con el objetivo de recuperar en mayor medida la estructura del esferoplasto y los posibles microambientes formados por las interacciones de proteínas, los esferoplastos fueron fijados con paraformaldehído y se procedió a la extracción de metabolitos como se indica en material y métodos.

Se observó que sin glucosa, la cepa silvestre acumula más G6P que la mutante, mientras que al adicionar glucosa la cepa mutante produce más G6P. Por otra parte, la F1,6BP es similar entre ambas cepas; cuando no hay glucosa, los niveles de F1,6BP son muy bajos o no detectables, y al adicionar glucosa se alcanzan niveles similares. Sin embargo el cociente G6P/F1,6BP en presencia de glucosa es similar en ambos casos. Es importante señalar que una acumulación mayor de G6P en la cepa silvestre podría estar relacionada con una conexión favorable entre la mitocondria y la hexocinasa. Estos resultados son similares a los observados en la célula entera, salvo que esta vez se favoreció la acumulación de F1,6BP en ambas cepas al adicionar yodoacetato (Tabla 3). Al comparar este cociente con la respiración, puede observarse que a partir de 20 mM de glucosa, la cepa mutante tiende a disminuir la respiración en estado III. Además la adición de 20 mM de F1,6BP en el estado III, no tiene efectos sobre la respiración en la cepa mutante, lo cual indica que la formación local de F1,6BP es mejor que la adición (Fig. 4).

Actualmente se están realizando los controles necesarios para asegurar que la cantidad de las hexosas fosfato obtenidas son representativas de lo que se genera en la célula y no se perturban al momento de la extracción. También se está desarrollando la técnica para cuantificar el volumen del esferoplasto y poder conocer las concentraciones generadas de hexosas fosfato por célula.

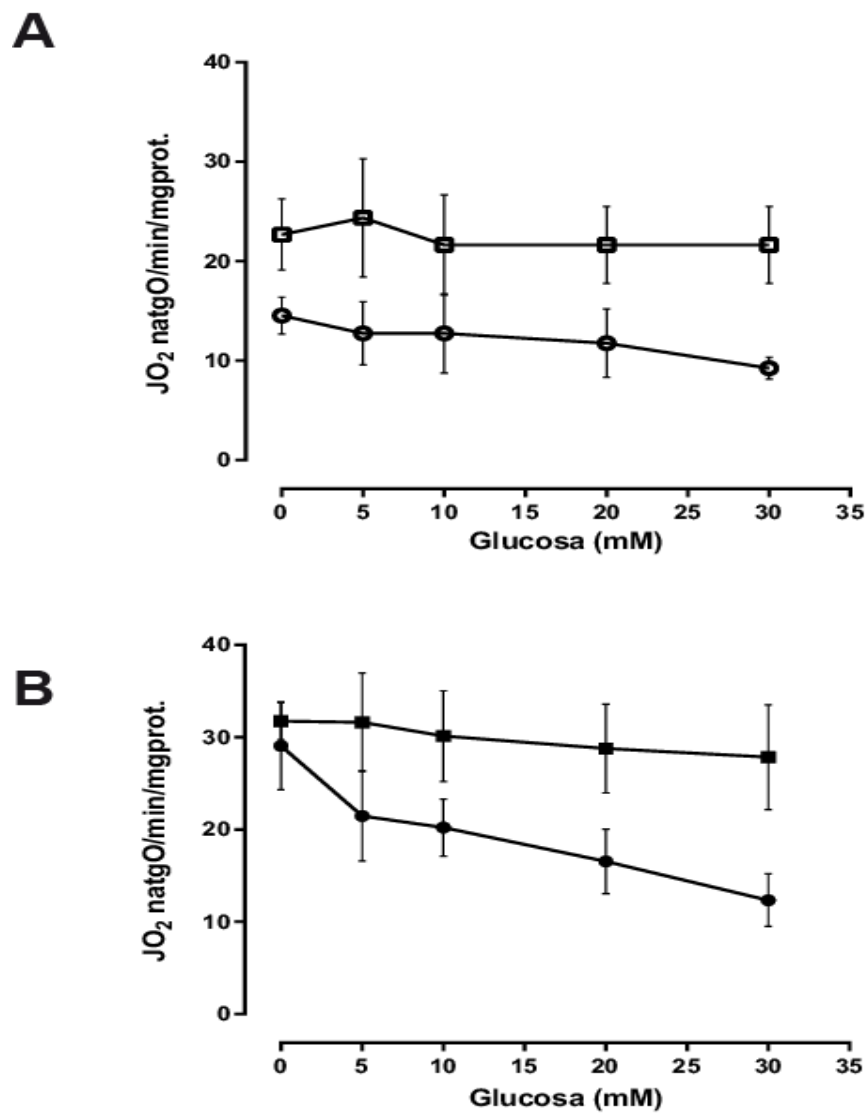


**Fig. 3 Efecto de la glucosa sobre la respiración del esferoplasto permeabilizado.** A, en estado IV y B en estado III. Las cepas: BY4742 (wt) en círculos y BY4742  $\Delta$ hxk2 ( $\Delta$ hxk2) en cuadros. Medio de reacción: Sorbitol 1 M, MgSO<sub>4</sub> 2 mM, EGTA 0.5 mM, NaCl 1.7 mM, NH<sub>4</sub>Cl 10 mM, KH<sub>2</sub>PO<sub>4</sub> 10 mM pH 6.8, ABS 0.1%. Esferoplastos 1 mg prot/ mL, NADH 10 mM como sustrato respiratorio, 20  $\mu$ g/mL de nistatina y 2 mM ADP para inducir el estado III. Glucosa como se indica.

**Tabla 3. Cuantificación de G6P y F1,6BP en el esferoplasto permeabilizado.** Medio de reacción como se indica en 3.6.

Cepa	[G6P] (nmol/mg prot)	[F1,6BP] (nmol/mgprot)	G6P/F1,6BP
<b>Δhxr2</b>	7.9	0.5	18.8
<b>Δhxr2 + Gluc 30mM</b>	65.8	11.0	6.1
<b>Wt</b>	43.8	n.d.	n.d.
<b>Wt + Gluc 30mM</b>	45.9	14.1	5.7

Finalmente, para determinar si existe o no una canalización de la F1,6BP hacia la mitocondria, es necesario estudiar las interacciones proteína-proteína tanto de la glucólisis como de la glucólisis- mitocondria.

#### **4.2.3. Estudio de la interacción de las proteínas de la glucólisis con la mitocondria.**

Previamente se reportó que las proteínas de la glucólisis interaccionan, y que esta interacción es estabilizada por el citoesqueleto de actina. Respecto a la interacción de proteínas de la glucólisis con la mitocondria, hay varios estudios que han encontrado enzimas glucolíticas en fracciones mitocondriales. Previamente en el laboratorio se demostró que la hexocinasa y el VDAC coimmunoprecipitan, aunque no hay evidencia de que esta interacción sea directa como la reportada en el mamífero (De Cerqueira Cesar y Wilson, 1998). Además, otros estudios han reportado la presencia de la piruvato cinasa, gliceraldehído-3-fosfato deshidrogenasa y enolasa en extractos mitocondriales de *S. cerevisiae* (Brandina y col., 2006). Por lo tanto, se decidió estudiar los complejos proteínicos que podrían formarse en el esferoplasto, buscando proteínas de la glucólisis (ALD, GAPDH, HXK) y el VDAC, mediante geles azules nativos. En la Fig.5, se muestra el western blot para cada proteína tanto en la cepa mutante como en la silvestre. A partir de estos resultados puede decirse que la ALD y GAPDH migran a la misma altura, lo que sugiere que ambas proteínas interaccionan, lo cual coincide con los estudios de Araiza-Olivera, 2011, donde se demuestra la

interacción de la ALD y GAPD. La hexocinasa y el VDAC migran a una masa molecular diferente a la de GAPDH y ALD, lo cual descartaría una interacción directa de estas proteínas. Sin embargo, a partir de estos resultados no puede decirse que los metabolones no existan, y es probable que la extracción de la muestra y manipulación para la preparación de geles azules nativos no sea la adecuada. Además es posible que estos metabolones sean dinámicos y sólo se formen en presencia de glucosa.

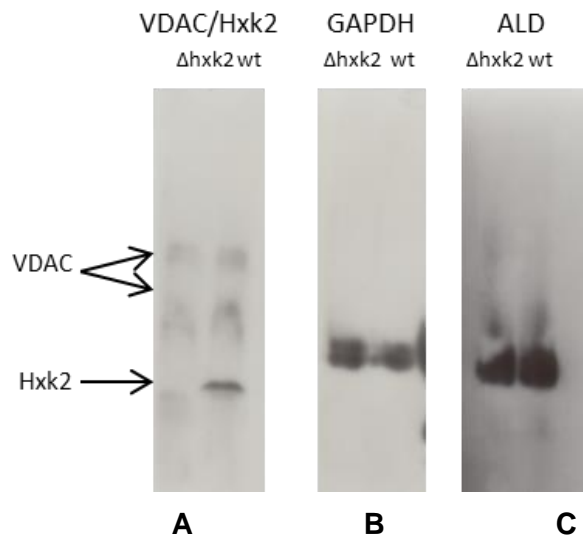


**Fig. 4 Western blot del gel nativo azul.** En el panel A se observan las bandas correspondientes al VDAC y la hexocinasa (indicado con las flechas) tanto para la cepa mutante como para la silvestre. B, muestra las bandas correspondientes a la gliceraldehído-3-fosfato-deshidrogenasa (GAPDH) tanto para la mutante como para la silvestre. C, muestra las bandas que corresponden a la aldolasa (ALD). Figura representativa de 3 experimentos independientes.

Por otra parte, el gel nativo utilizado (4-16 %) es útil para estudiar complejos proteínicos de hasta 10 MDa (Wittig y col., 2006). Dadas las interacciones de la actina con las proteínas de la glucólisis y la mitocondria, es probable, que estos complejos sean más grandes y en este caso sólo se observen las proteínas que se encuentren libres o los complejos más pequeños, ya que se observan en la zona de bajo peso molecular del gel en el caso de las proteínas de la glucólisis, mientras que el VDAC presenta 2 bandas más arriba. Ésto indica que el VDAC se encuentra asociado a otras proteínas y/o se encuentra como oligómero, como ya se ha reportado (Colombini, 2004). Probablemente se realicen estudios utilizando geles large pore, en los que se pueden separar megacomplejos de proteínas de más de 10 MDa (Strecker y col., 2010) o se realicen coinmunoprecipitaciones.



## **5. Conclusiones.**

- 5.1 La regulación del  $_{Sc}MUC$  en el esferoplasto permeabilizado requiere de estudios más profundos.
- 5.2 Es probable que las hexosas fosfato de la glucólisis sea canalizada hacia la mitocondria para contribuir a la inducción del efecto Crabtree en *Saccharomyces cerevisiae*.

## **6. Perspectivas.**

- 6.1 Realizar los estudios correspondientes a la regulación del  $_{Sc}MUC$  en *S. cerevisiae*.
- 6.2 Concluir los estudios sobre las interacciones de las proteínas glucolíticas con la mitocondria en el esferoplasto, al adicionar glucosa tanto en la cepa silvestre como en la mutante  $\Delta hxk2$ .

## **7. Actividades complementarias durante la estancia.**

- 7.1 Participación en el curso: Regulation du metabolisme cellulaire. Master 2 del programa: Master Biochimie-Chimie-Biologie de la université de Bordeaux, a cargo del Dr. Michel Rigoulet, con el tema: La canalisation des substrats.
- 7.2 Seminario del Instituto de genética y biología celular con el tema: L'effet Crabtree Chez *Saccharomyces cerevisiae*: Le fructose 1,6-bisphosphate et ses effets sur la mitochondrie.

7.3 Participación en el congreso: 8<sup>eme</sup> colloque meetochondrie 10-13 mai, 2015 Gidel-plages (Morbihan), Francia con el poster: L'effet Crabtree chez *S. cerevisiae* : rôle du MUC et des hexoses phosphate de la glycolyse.

7.4. Participación en la instrucción de Leo Vivant, estudiante de BTS (Brevet de technicien supérieur) durante su estancia de formación en investigación científica (18 mayo-19 de junio, 2015).

## 8. Referencias

Abele, D., **2002**, Toxic oxygen: the radical life-giver, *Nature*, 420: 6911, 27.

Ahmazadeh, M., Horng, A. and Colombini, M., **1996**, The control of mitochondrial respiration in yeast: a possible role of the outer mitochondrial membrane, *Cell Biochem Funct*, 14: 3, 201-8.

Akerman, K. E. and Wikstrom, M. K., **1976**, Safranine as a probe of the mitochondrial membrane potential, *FEBS Lett*, 68: 2, 191-7.

Araiza-Olivera, D., Chiquete-Félix, N., Rosas-Lemus, M., Sampedro, J. G., Peña, A., Mujica, A. and Uribe-Carvajal, S., **2013**, A glycolytic metabolon in *Saccharomyces cerevisiae* is stabilized by F-actin, *FEBS J*, 280: 16, 3887-905.

Araiza-Olivera, D., Sampedro, J. G., Mujica, A., Pena, A. and Uribe-Carvajal, S., **2010**, The association of glycolytic enzymes from yeast confers resistance against inhibition by trehalose, *FEMS Yeast Res*, 10: 3, 282-9.

Atherton, F. R. and Todd, A. R., **1947**, Studies on phosphorylation; further observations on the reaction of phosphites with polyhalogen compounds in presence of bases and its application to the phosphorylation of alcohols, *J Chem Soc*, 674-8.

Avéret, N., Aguilaniu, H., Bunoust, O., Gustafsson, L. and Rigoulet, M., **2002**, NADH is specifically channeled through the mitochondrial porin channel in *Saccharomyces cerevisiae*, *J Bioenerg Biomembr*, 34: 6, 499-506.

Averet, N., Fitton, V., Bunoust, O., Rigoulet, M. and Guerin, B., **1998**, Yeast mitochondrial metabolism: from in vitro to in situ quantitative study, *Mol Cell Biochem*, 184: 1-2, 67-79.

Azoulay-Zohar, H., Israelson, A., Abu-Hamad, S. and Shoshan-Barmatz, V., **2004**, In self-defence: hexokinase promotes voltage-dependent anion channel closure and prevents mitochondria-mediated apoptotic cell death, *Biochem. J.*, 377: 2, 347-355.

Balasubramanian, R., Karve, A., Kandasamy, M., Meagher, R. B. and Moore, B., **2007**, A role for F-actin in hexokinase-mediated glucose signaling, *Plant Physiol*, 145: 4, 1423-34.

Bernardi, P., **1999**, Mitochondrial transport of cations: channels, exchangers, and permeability transition, *Physiol Rev*, 79: 4, 1127-55.

Bernardi, P., **2013**, The mitochondrial permeability transition pore: a mystery solved? , *Front Physiol*,4: 95.

Bernardi, P. and Forte, M., **2007**, The mitochondrial permeability transition pore, *Novartis Found Symp*,287: 157-64; discussion 164-9.

Bernardi, P., Krauskopf, A., Basso, E., Petronilli, V., Blachly-Dyson, E., Di Lisa, F. and Forte, M. A., **2006**, The mitochondrial permeability transition from in vitro artifact to disease target, *FEBS J*,273: 10, 2077-99.

Bonora, M., Bononi, A., De Marchi, E., Giorgi, C., Lebiedzinska, M., Marchi, S., Paterniani, S., Rimessi, A., Suski, J. M., Wojtala, A., Wieckowski, M. R., Kroemer, G., Galluzzi, L. and Pinton, P., **2013**, Role of the c subunit of the FO ATP synthase in mitochondrial permeability transition, *Cell Cycle*,12: 4, 674-83.

Brandina, I., Graham, J., Lemaitre-Guillier, C., Entelis, N., Krasheninnikov, I., Sweetlove, L., Tarassov, I. and Martin, R. P., **2006**, Enolase takes part in a macromolecular complex associated to mitochondria in yeast, *Biochim Biophys Acta*,1757: 9-10, 1217-28.

Cassimeris, L., Silva, V. C., Miller, E., Ton, Q., Molnar, C. and Fong, J., **2012**, Fueled by microtubules: does tubulin dimer/polymer partitioning regulate intracellular metabolism? , *Cytoskeleton (Hoboken)*,69: 3, 133-43.

Castrejón, V., Parra, C., Moreno, R., Peña, A. and Uribe, S., **1997**, Potassium collapses the deltaP in yeast mitochondria while the rate of ATP synthesis is inhibited only partially: modulation by phosphate, *Arch Biochem Biophys*,346: 1, 37-44.

Castrejón, V., Peña, A. and Uribe, S., **2002**, Closure of the yeast mitochondria unspecific channel (YMUC) unmasks a Mg<sup>2+</sup> and quinine sensitive K<sup>+</sup> uptake pathway in *Saccharomyces cerevisiae*, *J Bioenerg Biomembr*,34: 4, 299-306.

Castresana, J. and Saraste, M., **1995**, Evolution of energetic metabolism: the respiration-early hypothesis, *Trends Biochem Sci*,20: 11, 443-8.

Clegg, J. S., **1984**, Properties and metabolism of the aqueous cytoplasm and its boundaries, *Am J Physiol*,246: 2 Pt 2, R133-51.

Clemençon, B., **2012**, Yeast mitochondrial interactosome model: metabolon membrane proteins complex involved in the channeling of ADP/ATP, *Int J Mol Sci*,13: 2, 1858-85.

Colombini, M., **2004**, VDAC: the channel at the interface between mitochondria and the cytosol, *Mol Cell Biochem*,256-257: 1-2, 107-15.

Cortés, P., Castrejón, V., Sampedro, J. G. and Uribe, S., **2000**, Interactions of arsenate, sulfate and phosphate with yeast mitochondria, *Biochim Biophys Acta*, 1456: 2-3, 67-76.

Crabtree, H. G., **1929**, Observations on the carbohydrate metabolism of tumours, *Biochem J*, 23: 3, 536-45.

Crompton, M., **1999**, The mitochondrial permeability transition pore and its role in cell death, *Biochem. J.*, 341: 2, 233-249.

D'Autreaux, B. and Toledano, M. B., **2007**, ROS as signalling molecules: mechanisms that generate specificity in ROS homeostasis, *Nat Rev Mol Cell Biol*, 8: 10, 813-24.

Daran-Lapujade, P., Rossell, S., van Gulik, W. M., Luttik, M. A. H., de Groot, M. J. L., Slijper, M., Heck, A. J. R., Daran, J.-M., de Winde, J. H., Westerhoff, H. V., Pronk, J. T. and Bakker, B. M., **2007**, The fluxes through glycolytic enzymes in *Saccharomyces cerevisiae* are predominantly regulated at posttranscriptional levels, *Proceedings of the National Academy of Sciences*, 104: 40, 15753-15758.

De Cerqueira Cesar, M. and Wilson, J. E., **1998**, Further Studies on the Coupling of Mitochondrially Bound Hexokinase to Intramitochondrially Compartmented ATP, Generated by Oxidative Phosphorylation, *Arch Biochem Biophys*, 350: 1, 109-117.

Devin, A. and Rigoulet, M., **2007**, Mechanisms of mitochondrial response to variations in energy demand in eukaryotic cells, *Am J Physiol Cell Physiol*, 292: 1, C52-8.

Díaz-Ruiz, R., Avéret, N., Araiza, D., Pinson, B., Uribe-Carvajal, S., Devin, A. and Rigoulet, M., **2008**, Mitochondrial oxidative phosphorylation is regulated by fructose 1,6-bisphosphate. A possible role in Crabtree effect induction? , *J Biol Chem*, 283: 40, 26948-55.

Díaz-Ruiz, R., Rigoulet, M. and Devin, A., **2011**, The Warburg and Crabtree effects: On the origin of cancer cell energy metabolism and of yeast glucose repression, *Biochim Biophys Acta*, 1807: 6, 568-76.

Díaz-Ruiz, R., Rigoulet, M. and Devin, A., **2011**, The Warburg and Crabtree effects: On the origin of cancer cell energy metabolism and of yeast glucose repression, *Biochim Biophys Acta*, 1807: 6, 568-76.

Díaz-Ruiz, R., Uribe-Carvajal, S., Devin, A. and Rigoulet, M., **2009**, Tumor cell energy metabolism and its common features with yeast metabolism, *Biochim Biophys Acta*, 1796: 2, 252-65.

Egner, A. and Hell, S. W., **2005**, Fluorescence microscopy with super-resolved optical sections, *Trends Cell Biol*, 15: 4, 207-15.

Fontaine, E. and Bernardi, P., **1999**, Progress on the mitochondrial permeability transition pore: regulation by complex I and ubiquinone analogs, *J Bioenerg Biomembr*, 31: 4, 335-45.

Galli, G. J. and Richards, J., **2014**, Mitochondria from anoxia-tolerant animals reveal common strategies to survive without oxygen, *Journal of Comparative Physiology B*, 184: 3, 285-302.

Gao, F., Yan, X., Shakya, T., Baettig, O. M., Ait-Mohand-Brunet, S., Berghuis, A. M., Wright, G. D. and Auclair, K., **2006**, Synthesis and Structure-Activity Relationships of Truncated Bisubstrate Inhibitors of Aminoglycoside 6'-N-Acetyltransferases, *Journal of Medicinal Chemistry*, 49: 17, 5273-5281.

Gatt, S. and Racker, E., **1959**, Regulatory mechanisms in carbohydrate metabolism. I. Crabtree effect in reconstructed systems, *J Biol Chem*, 234: 5, 1015-23.

Giorgio, V., von Stockum, S., Antoniel, M., Fabbro, A., Fogolari, F., Forte, M., Glick, G. D., Petronilli, V., Zoratti, M., Szabo, I., Lippe, G. and Bernardi, P., **2013**, Dimers of mitochondrial ATP synthase form the permeability transition pore, *Proc Natl Acad Sci U S A*, 110: 15, 5887-92.

Gornall, A. G., Bardawill, C. J. and David, M. M., **1949**, Determination of serum proteins by means of the biuret reaction, *J Biol Chem*, 177: 2, 751-66.

Greiner, E. F., Guppy, M. and Brand, K., **1994**, Glucose is essential for proliferation and the glycolytic enzyme induction that provokes a transition to glycolytic energy production, *J Biol Chem*, 269: 50, 31484-90.

Guerin, B., Bunoust, O., Rouqueys, V. and Rigoulet, M., **1994**, ATP-induced unspecific channel in yeast mitochondria, *J Biol Chem*, 269: 41, 25406-10.

Guerin, M. and Napias, C., **1978**, Phosphate transport in yeast mitochondria: purification and characterization of a mitoribosomal synthesis dependent proteolipid showing a high affinity for phosphate, *Biochemistry*, 17: 13, 2510-6.

Guerrero-Castillo, S., Araiza-Olivera, D., Cabrera-Orefice, A., Espinasa-Jaramillo, J., Gutierrez-Aguilar, M., Luevano-Martinez, L. A., Zepeda-Bastida, A. and Uribe-Carvajal, S., **2011**, Physiological uncoupling of mitochondrial oxidative phosphorylation. Studies in different yeast species, *J Bioenerg Biomembr*, 43: 3, 323-31.

Gutiérrez-Aguilar, M., Pérez-Martínez, X., Chavez, E. and Uribe-Carvajal, S., **2010**, In *Saccharomyces cerevisiae*, the phosphate carrier is a component of the mitochondrial unselective channel, *Arch Biochem Biophys*, 494: 2, 184-91.

Gutiérrez-Aguilar, M., Pérez-Vazquez, V., Bunoust, O., Manon, S., Rigoulet, M. and Uribe, S., **2007**, In yeast, Ca<sup>2+</sup> and octylguanidine interact with porin (VDAC) preventing the mitochondrial permeability transition, *Biochim Biophys Acta*, 1767: 10, 1245-51.

Gutierrez-Aguilar, M. and Uribe-Carvajal, S., **2015**, The mitochondrial unselective channel in *Saccharomyces cerevisiae*, *Mitochondrion*, 22: 85-90.

Halestrap, A. P., **2004**, Does the mitochondrial permeability transition have a role in preconditioning? , *Circulation*, 110: 11, e303; author reply e303.

Halestrap, A. P., **2004**, Mitochondrial permeability: dual role for the ADP/ATP translocator? , *Nature*, 430: 7003, 1 p following 983.

Halestrap, A. P., Gillespie, J. P., O'Toole, A. and Doran, E., **2000**, Mitochondria and cell death: a pore way to die? , *Symp Soc Exp Biol*, 52: 65-80.

Hartman, F. C. and Barker, R., **1965**, An exploration of the active site of aldolase using structural analogs of fructose diphosphate, *Biochemistry*, 4: 6, 1068-75.

Haworth, R. A. and Hunter, D. R., **1979**, The Ca<sup>2+</sup>-induced membrane transition in mitochondria. II. Nature of the Ca<sup>2+</sup> trigger site, *Arch Biochem Biophys*, 195: 2, 460-7.

Huberts, D. H., Niebel, B. and Heinemann, M., **2012**, A flux-sensing mechanism could regulate the switch between respiration and fermentation, *FEMS Yeast Res*, 12: 2, 118-28.

Ingledew, W. J. and Poole, R. K., **1984**, The respiratory chains of *Escherichia coli*, *Microbiol Rev*, 48: 3, 222-71.

Kadenbach, B., **2003**, Intrinsic and extrinsic uncoupling of oxidative phosphorylation, *Biochim Biophys Acta*, 1604: 2, 77-94.

Konigsberg, M., Perez, V. I., Rios, C., Liu, Y., Lee, S., Shi, Y. and Van Remmen, H., **2013**, Effect of oxygen tension on bioenergetics and proteostasis in young and old myoblast precursor cells, *Redox Biol*, 1: 1, 475-82.

Kuznetsov, A. V., Javadov, S., Guzun, R., Grimm, M. and Saks, V., **2013**, Cytoskeleton and regulation of mitochondrial function: the role of beta-tubulin II, *Front Physiol*, 4: 82.

Lang, B. F., Gray, M. W. and Burger, G., **1999**, Mitochondrial genome evolution and the origin of eukaryotes, *Annu Rev Genet*, 33: 351-97.

Lemasters, J. J., Nieminen, A. L., Qian, T., Trost, L. C., Elmore, S. P., Nishimura, Y., Crowe, R. A., Cascio, W. E., Bradham, C. A., Brenner, D. A. and Herman, B., **1998**, The mitochondrial permeability transition in cell death: a common mechanism in necrosis, apoptosis and autophagy, *Biochim Biophys Acta*, 1366: 1-2, 177-96.

Leverve, X. M., **2007**, Mitochondrial function and substrate availability, *Crit Care Med*, 35: 9 Suppl, S454-60.

Mannella, C. A., **2006**, Structure and dynamics of the mitochondrial inner membrane cristae, *Biochim Biophys Acta*, 1763: 5-6, 542-8.

Manon, S. and Guerin, M., **1998**, Investigation of the yeast mitochondrial unselective channel in intact and permeabilized spheroplasts, *Biochem Mol Biol Int*, 44: 3, 565-75.

Manon, S., Roucou, X., Guerin, M., Rigoulet, M. and Guerin, B., **1998**, Characterization of the yeast mitochondria unselective channel: a counterpart to the mammalian permeability transition pore? , *J Bioenerg Biomembr*, 30: 5, 419-29.

Marty, G. D., Saksida, S. M. and Quinn, T. J., 2nd, **2010**, Relationship of farm salmon, sea lice, and wild salmon populations, *Proc Natl Acad Sci U S A*, 107: 52, 22599-604.

Mazat, J. P., Ransac, S., Heiske, M., Devin, A. and Rigoulet, M., **2013**, Mitochondrial energetic metabolism-some general principles, *IUBMB Life*, 65: 3, 171-9.

Mentel, M. and Martin, W., **2008**, Energy metabolism among eukaryotic anaerobes in light of Proterozoic ocean chemistry, *Philos Trans R Soc Lond B Biol Sci*, 363: 1504, 2717-29.

Merico, A., Sulo, P., Piškur, J. and Compagno, C., **2007**, Fermentative lifestyle in yeasts belonging to the *Saccharomyces* complex, *FEBS Journal*, 274: 4, 976-989.

Meyerhof, O. and Kiessling, W., **1935**, Über die enzymatische Umwandlung von Glycerinaldehydphosphorsäure in Dioxyacetophosphorsäure, *Biochem. Z*, 279: 40-48.

Mitchell, P., **1966**, Chemiosmotic coupling in oxidative and photosynthetic phosphorylation, *Biol Rev Camb Philos Soc*, 41: 3, 445-502.

Mustea, I. and Muresian, T., **1967**, Crabtree effect in some bacterial cultures, *Cancer*, 20: 9, 1499-501.

Oláh, J., Tőkési, N., Lehotzky, A., Orosz, F. and Ovádi, J., **2013**, Moonlighting microtubule-associated proteins: Regulatory functions by day and pathological functions at night, *Cytoskeleton (Hoboken)*, 70: 11, 677-685.

Ovadi, J. and Saks, V., **2004**, On the origin of intracellular compartmentation and organized metabolic systems, *Mol Cell Biochem*, 256-257: 1-2, 5-12.

Pallotta, M. L., Valenti, D., Iacovino, M. and Passarella, S., **2004**, Two separate pathways for d-lactate oxidation by *Saccharomyces cerevisiae* mitochondria which differ in energy production and carrier involvement, *Biochimica et Biophysica Acta (BBA) - Bioenergetics*, 1608: 2-3, 104-113.

Pastorino, J. G. and Hoek, J. B., **2008**, Regulation of hexokinase binding to VDAC, *J Bioenerg Biomembr*, 40: 3, 171-82.

Peña, A., Piña, M. Z., Escamilla, E. and Piña, E., **1977**, A novel method for the rapid preparation of coupled yeast mitochondria, *FEBS Lett*, 80: 1, 209-13.

Perez-Vazquez, V., Saavedra-Molina, A. and Uribe, S., **2003**, In *Saccharomyces cerevisiae*, cations control the fate of the energy derived from oxidative metabolism through the opening and closing of the yeast mitochondrial unselective channel, *J Bioenerg Biomembr*, 35: 3, 231-41.

Perkins, G., Renken, C., Martone, M. E., Young, S. J., Ellisman, M. and Frey, T., **1997**, Electron Tomography of Neuronal Mitochondria: Three-Dimensional Structure and Organization of Cristae and Membrane Contacts, *J Struct Biol*, 119: 3, 260-272.

Petronilli, V., Miotto, G., Canton, M., Brini, M., Colonna, R., Bernardi, P. and Di Lisa, F., **1999**, Transient and long-lasting openings of the mitochondrial permeability transition pore can be monitored directly in intact cells by changes in mitochondrial calcein fluorescence, *Biophys J*, 76: 2, 725-34.

Piskur, J., Rozpedowska, E., Polakova, S., Merico, A. and Compagno, C., **2006**, How did *Saccharomyces* evolve to become a good brewer? , *Trends Genet*, 22: 4, 183-6.

Popel, A. S., **1989**, Theory of oxygen transport to tissue, *Crit Rev Biomed Eng*, 17: 3, 257-321.

Prieto, S., Bouillaud, F., Ricquier, D. and Rial, E., **1992**, Activation by ATP of a proton-conducting pathway in yeast mitochondria, *Eur J Biochem*, 208: 2, 487-91.

Richard, P., Teusink, B., Westerhoff, H. V. and van Dam, K., **1993**, Around the growth phase transition *S. cerevisiae*'s make-up favours sustained oscillations of intracellular metabolites, *FEBS Lett*, 318: 1, 80-2.

Rodríguez-Enriquez, S., Juarez, O., Rodriguez-Zavala, J. S. and Moreno-Sanchez, R., **2001**, Multisite control of the Crabtree effect in ascites hepatoma cells, *Eur J Biochem*, 268: 8, 2512-9.

Rolland, F., Winderickx, J. and Thevelein, J. M., **2002**, Glucose-sensing and -signalling mechanisms in yeast, *FEMS Yeast Res*, 2: 2, 183-201.

Rosas-Lemus, M., Uribe-Alvarez, C., Chiquete-Felix, N. and Uribe-Carvajal, S., **2014**, In *Saccharomyces cerevisiae* fructose-1,6-bisphosphate contributes to the Crabtree effect through closure of the mitochondrial unspecific channel, *Arch Biochem Biophys*, 555-556: 66-70.

Rostovtseva, T. K., Sheldon, K. L., Hassanzadeh, E., Monge, C., Saks, V., Bezrukov, S. M. and Sackett, D. L., **2008**, Tubulin binding blocks mitochondrial voltage-dependent anion channel and regulates respiration, *Proc Natl Acad Sci U S A*, 105: 48, 18746-51.

Schägger, H. and Pfeiffer, K., **2000**, Supercomplexes in the respiratory chains of yeast and mammalian mitochondria, *EMBO J*, 19: 8, 1777-83.

Stefan, C. and Sauer, U., **2011**, Intracellular characterization of aerobic glucose metabolism in seven yeast species by <sup>13</sup>C flux analysis and metabolomics, *FEMS Yeast Res*, 11: 3, 263-272.

Strecker, V., Wumaier, Z., Wittig, I. and Schägger, H., **2010**, Large pore gels to separate mega protein complexes larger than 10 MDa by blue native electrophoresis: Isolation of putative respiratory strings or patches, *Proteomics*, 10: 18, 3379-3387.

Tielens, A. G., Rotte, C., van Hellemond, J. J. and Martin, W., **2002**, Mitochondria as we don't know them, *Trends Biochem Sci*, 27: 11, 564-72.

Tschischka, K., Abele, D. and Portner, H. O., **2000**, Mitochondrial oxyconformity and cold adaptation in the polychaete *Nereis pelagica* and the bivalve *Arctica islandica* from the Baltic and White Seas, *J Exp Biol*, 203: Pt 21, 3355-68.

Uribe-Carvajal, S., Luevano-Martinez, L. A., Guerrero-Castillo, S., Cabrera-Orefice, A., Corona-de-la-Pena, N. A. and Gutierrez-Aguilar, M., **2011**, Mitochondrial Unselective Channels throughout the eukaryotic domain, *Mitochondrion*, 11: 3, 382-90.

Uribe, S., Ramirez, J. and Pena, A., **1985**, Effects of beta-pinene on yeast membrane functions, *J Bacteriol*, 161: 3, 1195-1200.

Veech, R. L., Lawson, J. W., Cornell, N. W. and Krebs, H. A., **1979**, Cytosolic phosphorylation potential, *J Biol Chem*, 254: 14, 6538-47.

Wilson, D. F., Rumsey, W. L., Green, T. J. and Vanderkooi, J. M., **1988**, The oxygen dependence of mitochondrial oxidative phosphorylation measured by a new optical method for measuring oxygen concentration, *J Biol Chem*, 263: 6, 2712-8.

Wittig, I., Braun, H. P. and Schagger, H., **2006**, Blue native PAGE, *Nat Protoc*, 1: 1, 418-28.

Wojtczak, L., Teplova, V. V., Bogucka, K., Czyz, A., Makowska, A., Wieckowski, M. R., Duszynski, J. and Evtodienko, Y. V., **1999**, Effect of glucose and deoxyglucose on the redistribution of calcium in ehrlich ascites tumour and Zajdela hepatoma cells and its consequences for mitochondrial energetics. Further arguments for the role of Ca(2+) in the mechanism of the crabtree effect, *Eur J Biochem*, 263: 2, 495-501.

Xie, G. C. and Wilson, J. E., **1988**, Rat brain hexokinase: the hydrophobic N-terminus of the mitochondrially bound enzyme is inserted in the lipid bilayer, *Arch Biochem Biophys*, 267: 2, 803-10.

Zhang, M., Mileykovskaya, E. and Dowhan, W., **2005**, Cardiolipin is essential for organization of complexes III and IV into a supercomplex in intact yeast mitochondria, *J Biol Chem*, 280: 33, 29403-8.

## **11.2 Publicaciones asociadas:**

- A glycolytic metabolon in *Saccharomyces cerevisiae* is stabilized by F-actin (2013).
- The branched mitochondrial respiratory chain from *Debaryomyces hansenii*: components and supramolecular organization (2014).
- In *Saccharomyces cerevisiae* fructose-1,6-bisphosphate contributes to the Crabtree effect through closure of the mitochondrial unspecific channel (2014).
- Effects of ubiquinone derivatives on the mitochondrial unselective channel of *Saccharomyces cerevisiae* (2015).
- OXYGEN: from toxic waste to optimal (toxic) fuel of life (enviado, 2015).

# A glycolytic metabolon in *Saccharomyces cerevisiae* is stabilized by F-actin

Daniela Araiza-Olivera<sup>1</sup>, Natalia Chiquete-Felix<sup>1</sup>, Mónica Rosas-Lemus<sup>1</sup>, José G. Sampedro<sup>2</sup>, Antonio Peña<sup>1</sup>, Adela Mujica<sup>3</sup> and Salvador Uribe-Carvajal<sup>1</sup>

<sup>1</sup> Department of Molecular Genetics, Instituto de Fisiología Celular, Universidad Nacional Autónoma de México, Mexico City, Mexico

<sup>2</sup> Instituto de Física, Universidad Autónoma de San Luis Potosí, Mexico

<sup>3</sup> Department of Cellular Biology, Centro de Investigaciones y Estudios Avanzados, Instituto Politécnico Nacional, Mexico City, Mexico

## Keywords

actin; cytoskeleton; enzyme association; glycolytic metabolon; yeast metabolism

## Correspondence

S. Uribe-Carvajal, Department of Molecular Genetics, Instituto de Fisiología Celular, Universidad Nacional Autónoma de México, Apartado Postal 70-214, Circuito Exterior, Coyoacán, 04510 Mexico DF, Mexico  
 Fax: +52 55 56225630  
 Tel: +52 55 56225632  
 E-mail: suribe@ifc.unam.mx

(Received 19 October 2012, revised 9 May 2013, accepted 7 June 2013)

doi:10.1111/febs.12387

In the *Saccharomyces cerevisiae* glycolytic pathway, 11 enzymes catalyze the stepwise conversion of glucose to two molecules of ethanol plus two CO<sub>2</sub> molecules. In the highly crowded cytoplasm, this pathway would be very inefficient if it were dependent on substrate/enzyme diffusion. Therefore, the existence of a multi-enzymatic glycolytic complex has been suggested. This complex probably uses the cytoskeleton to stabilize the interaction of the various enzymes. Here, the role of filamentous actin (F-actin) in stabilization of a putative glycolytic metabolon is reported. Experiments were performed in isolated enzyme/actin mixtures, cytoplasmic extracts and permeabilized yeast cells. Polymerization of actin was promoted using phalloidin or inhibited using cytochalasin D or latrunculin. The polymeric filamentous F-actin, but not the monomeric globular G-actin, stabilized both the interaction of isolated glycolytic pathway enzyme mixtures and the whole fermentation pathway, leading to higher fermentation activity. The associated complexes were resistant against inhibition as a result of viscosity (promoted by the disaccharide trehalose) or inactivation (using specific enzyme antibodies). In *S. cerevisiae*, a glycolytic metabolon appears to assemble in association with F-actin. In this complex, fermentation activity is enhanced and enzymes are partially protected against inhibition by trehalose or by antibodies.

## Structured digital abstract

- ALD physically interacts with PGK and GAPDH by anti bait coimmunoprecipitation ([View interaction](#))
- ALD physically interacts with GAPDH and PGK by affinity chromatography technology ([View interaction](#))

## Introduction

The cytoplasm is a highly concentrated suspension of proteins, polysaccharides, nucleic acids and small solutes [1,2]. It has been proposed that saturation promotes specific protein–protein interactions [1,3], and, once associated, enzymes in a given pathway team up to catalyze several consecutive reactions; these enzyme complexes are called metabolons [4,5]. In metabolons,

intermediaries are channeled, i.e. enzymes that catalyze consecutive reactions transfer intermediaries directly to each other [2,6,7]. Substrate channeling confers a number of benefits, including altered reaction kinetics, preservation of cellular solvation capacity [8] or sequestration of toxic intermediaries [9]. The highly dynamic nature of enzyme–enzyme interactions

## Abbreviations

ADH, alcohol dehydrogenase; ALD, aldolase; ENO, enolase; F-actin, filamentous actin; G-actin, globular (monomeric) actin; GAPDH, glyceraldehyde-3-phosphate dehydrogenase; GPI, glucose-6-phosphate isomerase; HKX, hexokinase; PFK, phosphofructokinase; PGAM, phosphoglyceromutase; PGK, phosphoglycerate kinase; PK, pyruvate kinase; TPI, triosephosphate isomerase.

[10] probably regulates their reaction rate, and channels substrates through specific pathway(s) [2,6,11]. Various groups have described metabolons in the cysteine synthase complex, the Calvin cycle, cyanogenic glucoside synthesis and the phenylpropanoid pathway of plants [12], the urea cycle of rat hepatocytes [13], the citrate cycle of porcine liver [14] and the glycolytic pathway of rabbit skeletal muscle and mouse fibroblasts [15,16]. Each enzyme may associate with other specific enzymes as described for mouse fibroblasts and plants [16,17], and thus channeling may be ‘leaky’ [18]. Association/dissociation has been observed in the ribosomes of rabbit reticulocytes [19] and in mitochondrial voltage-dependent anion channels of mouse brain neurons [20].

Eukaryotic cell morphology is supported by a cytoplasmic fibrous protein network known as the cytoskeleton, which comprises microtubules (tubulin), microfilaments (actin) and intermediate filaments (keratin, vimentin, desmin, laminins, etc.) [21]. Fibers are highly dynamic, as proteins switch between globular monomeric (G) and filamentous polymeric (F) states [22,23]. The cytoskeleton undergoes constant and rapid remodeling during cellular processes such as morphogenesis, cytokinesis [24], endocytosis [25], vesicle trafficking [26], polarization [23], motility, adhesion [27] or the cell cycle [28]. In yeast, glycolytic enzyme associations with the cytoskeleton have also been described [29,30]. Various elements of the cytoskeleton of red blood cells or fibroblasts associate with glycolytic enzymes in mammals such as mice [4,16,31,32] or humans [33]. The association of the cytoskeleton with diverse proteins is highly dynamic and responds to various stimuli and metabolic conditions [22,23].

Cytoskeleton/enzyme association may modify kinetics [34–36]. F-actin stimulates the rabbit skeletal muscle enzymes aldolase (ALD) [37], phosphofructokinase (PFK) [38] and phosphorylase kinase [39]. F-actin increases glyceraldehyde-3-phosphate dehydrogenase (GAPDH) activity but G-actin has no effect [34,40]. Most mammalian glycolytic enzymes bind actin, both *in vivo* and *in vitro* [36,41,42]. Brownian dynamics predict the interaction of actin filaments with ALD [43] and GAPDH [44]. Actin from rabbit skeletal muscle binds tightly to ALD and GAPDH [34,45], and loosely to other glycolytic pathway enzymes [46].

Yeast is an ideal system to study the role of the cytoskeleton in the regulation of metabolism [26]. In *Saccharomyces cerevisiae*, it has been shown that GAPDH and hexokinase (Hxk), which are highly sensitive to viscosity, become resistant when mixed with ALD or phosphoglycerate kinase (PGK),

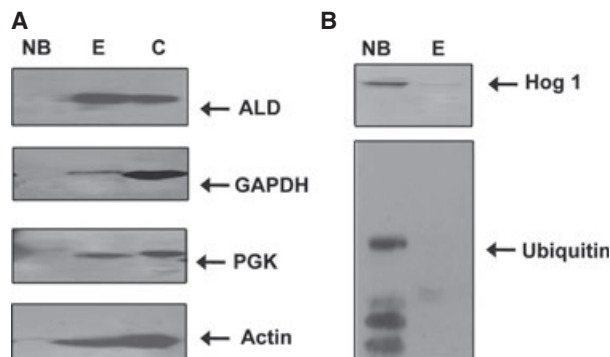
although a stable complex has not been detected [47]. Here, it is reported that, in the *S. cerevisiae* glycolytic pathway, enzyme interactions were stabilized by F-actin, but not by G-actin. F-actin/enzyme complexes catalyzing the whole fermentation pathway exhibited high efficiency and were resistant against inhibition promoted by an increase in viscosity or by specific antibodies. In *S. cerevisiae*, F-actin protected the activity of the fermentation pathway, which exhibited the kinetic behavior predicted for a multi-enzyme complex [48,49], suggesting the existence of a functional glycolytic metabolon.

## Results

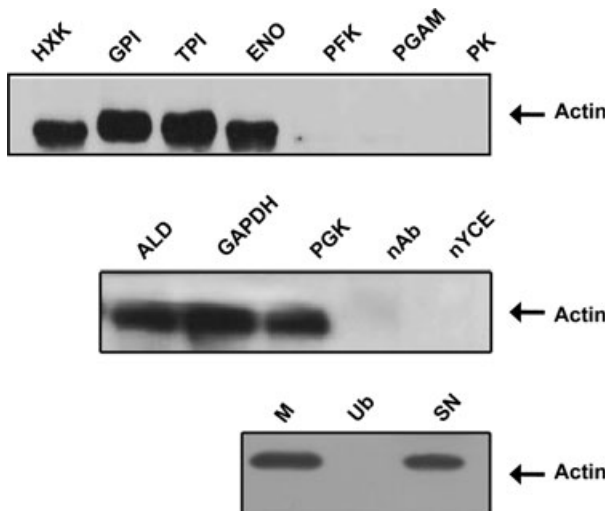
### In cytoplasmic extracts from *Saccharomyces cerevisiae*, glycolytic pathway enzymes associate among themselves and with actin

Enzyme association appears to control metabolism [50] and protect against stress [47]. In mice muscle extracts, enzyme–enzyme and enzyme–microtubule associations stabilize enzyme activities [51,52]. In *S. cerevisiae*, associated glycolytic pathway enzymes are protected against inhibition by viscosity promoted by compatible solutes, which are defined as small molecules produced by the cell to protect itself against stress situations that do not interfere (are compatible) with metabolism [47]. Identifying the factors that stabilize enzyme interactions would be highly desirable in order to better understand metabolism and enhance biotechnological applications.

In mammals and other species, ALD binds to various glycolytic pathway enzymes [47,53]. Thus, it was decided to determine which glycolytic pathway enzymes bind ALD in *S. cerevisiae* and whether a putative metabolon is assembled. A cytoplasmic extract was added to a Sepharose 4B/ALD column, and the eluted fractions were collected and analyzed by western blotting. GAPDH, PGK, ALD and actin were detected in the bound fraction (Fig. 1A), while the proteins that we used as negative controls, ubiquitin and Hog1 [53a], were present in the free fraction (Fig. 1B). Thus, the column containing immobilized *S. cerevisiae* ALD retained actin and several yeast glycolytic enzymes, suggesting the existence of an actin-bound glycolytic complex. As a control, to test whether the association of glycolytic enzymes was a specific property, the cytoplasmic extract was passed through a column containing bound DNase, a protein chosen randomly, and it was observed that the DNase column did not retain ALD (Fig. S1), i.e. glycolytic pathway enzymes specifically bind ALD.



To further explore the interactions between actin and glycolytic pathway enzymes, a co-immunoprecipitation assay was performed in which binding of actin to each of the yeast glycolytic enzymes was evaluated. Each enzyme was precipitated using a specific antibody, and co-immunoprecipitation was evaluated by immunoblotting with an actin antibody (Fig. 2). Actin co-immunoprecipitated with HXK, glucose-6-phosphate isomerase (GPI), ALD, triosephosphate isomerase (TPI), GAPDH, PGK and enolase (ENO), but did not precipitate with PFK, phosphoglyceromutase (PGAM) or pyruvate kinase (PK) (Fig. 2), i.e. most yeast glycolytic enzymes interacted with actin. The slight differences in molecular mass of the various actin co-immunoprecipitates are probably due to the differences in complex stoichiometries and expression levels of each glycolytic enzyme tested. As a positive control for each enzyme, we included a sample of striated rabbit muscle extract (M). Negative controls comprised a sample in the absence of precipitating antibody (nAb) and a sample to which no cytoplasmic extract was added (nYCE). In addition, when we precipitated ubiquitin (Ub), no co-immunoprecipitated actin was detected. To show that actin was always present, its presence was revealed in the supernatant of samples where no precipitating antibody had been added (SN) (Fig. 2). Thus, the co-immunoprecipitation results indicate that a large number of glycolytic pathway enzymes specifically interact with actin, constituting a multi-enzyme complex. As a next step, we



decided to test whether the polymerization state of actin has an effect on enzyme binding.

#### Only the polymeric form of actin (F-actin) binds glycolytic enzymes

Actin alternates between the monomeric (G-actin) and polymeric filamentous (F-actin) states. Previous studies in mammals have suggested that these forms of actin exhibit different affinities for glycolytic enzymes [29,54]. The different oligomerization states were promoted using either phalloidin, which promotes polymerization, or the depolymerizing agent cytochalasin D [55]. In our experiment, yeast cytoplasmic extracts pre-incubated in the absence (NT) or presence of either phalloidin (P) or cytochalasin D (CD) were immunoprecipitated with actin antibody (Fig. 3). The precipitates were immunoblotted using specific antibodies against each glycolytic enzyme. As expected from the previous experiment, HXK, GPI, ALD, TPI, GAPDH, PGK and ENO (Fig. 3A) precipitated with actin. Treatment with actin-targeting drugs modified the associations as follows: phalloidin promoted stronger binding, while cytochalasin weakened binding (Table 1). PFK, PGAM and PK did not bind actin

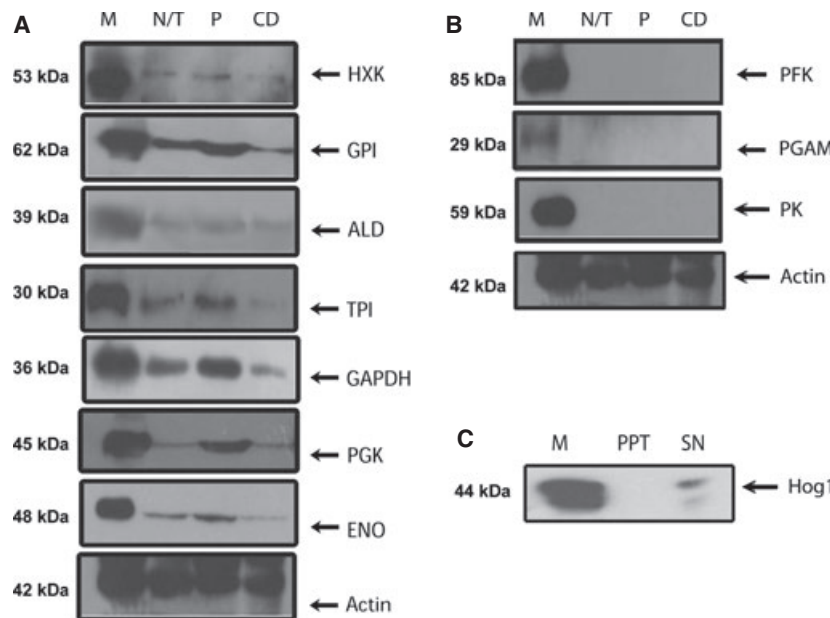


**Fig. 3.** Effect of actin-targeting drugs on actin/glycolytic-enzyme association. Yeast cytoplasmic extracts were assayed for interactions between actin and glycolytic enzymes. As indicated, samples were either not treated (N/T) or pre-treated with phalloidin (P) or cytochalasin D (CD). Each sample was immunoprecipitated with anti-actin. Muscle extract was used as a positive control (M). Anti-actin precipitates were immunoblotted against (A) glycolytic enzymes that exhibited an interaction with actin (HXK, GPI, ALD, TPI, GAPDH, PGK and ENO) and (B) glycolytic enzymes that did not precipitate with actin (PFK, PGAM and PK). Actin was used as a loading control. (C) Hog1 was used as a negative control and was not detected in the precipitate (PPT), although it was detected in the supernatant (SN).

**Table 1.** Effect of actin-targeting drugs on enzyme/actin association. The band intensity of the co-immunoprecipitation bands shown in Fig. 3 [non-treated (N/T) and pre-treated with phalloidin (P) or cytochalasin D (CD)] was measured by densitometry. Values are means  $\pm$  SEM of three independent experiments each performed in triplicate. Asterisks indicate statistically significant differences compared with untreated extracts (one-way ANOVA, Dunnett's multiple comparison test; \* $P < 0.05$ , \*\* $P < 0.01$ ). Data are given in percentages relative to the untreated samples.

	HXK	GPI	ALD	TPI	GAPDH	PGK	ENO
Untreated (N/T)	100	100	100	100	100	100	100
Phalloidin (P)	136.4 $\pm$ 23**	259.4 $\pm$ 76**	209.0 $\pm$ 80	155.1 $\pm$ 22**	227.2 $\pm$ 20*	230.7 $\pm$ 56*	149.0 $\pm$ 33*
Cytochalasin D (CD)	47.0 $\pm$ 14*	25.3 $\pm$ 9	52.6 $\pm$ 32	74.5 $\pm$ 4*	58.7 $\pm$ 6**	92.7 $\pm$ 53	44.3 $\pm$ 20*

under any conditions (Fig. 3B). As a positive control, an extract of rabbit striated muscle (M) was added in all cases. As a negative control, we precipitated a cytoplasmic sample with actin antibody and revealed against Hog1 using a Hog1 antibody, which did not precipitate (PPT) but instead remained in the supernatant (SN) (Fig. 3C). These results strongly suggest that a glycolytic complex dynamically assembles or dissociates following the interconversions between F-actin and G-actin.

#### Enzyme association is enhanced by F-actin

Once it had been demonstrated that actin interacts with most glycolytic pathway enzymes, it was decided

to evaluate whether the oligomeric state of actin modifies enzyme/enzyme interactions (Fig. 4). This was assayed in yeast cytoplasmic extracts incubated alone (NT) or with either phalloidin (P) or cytochalasin D (CD). After incubation, ALD was immunoprecipitated, and co-immunoprecipitation with GAPDH and PGK was evaluated. The precipitates were subjected to western blotting for GAPDH, PGK or ALD, and co-immunoprecipitation was observed in all cases. When compared with the samples in the absence of additions (NT), precipitation was higher in the phalloidin samples (P) and lower in cytochalasin samples (CD) (Fig. 4A). In all cases, a rabbit striated muscle sample was included as a positive control (M). In addition, it was observed that neither ubiquitin (Ub)

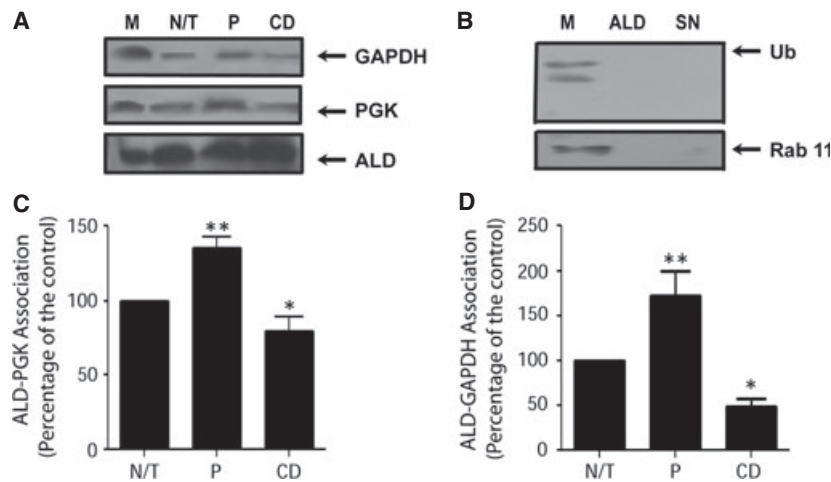


**Fig. 4.** Association of glycolytic enzymes in the presence of actin-targeting drugs. Yeast cytoplasmic extracts were incubated alone (N/T), in the presence of phalloidin (P) or in the presence of cytochalasin D (CD). Then the samples were immunoprecipitated with anti-ALD. Muscle extracts were used as a positive control (M). Precipitates were immunoblotted against (A) GAPDH or PGK, with ALD as a loading control, and (B) the non-related proteins ubiquitin (Ub) and Rab11 as negative controls. Densitometry was performed to estimate the degree of association between (C) ALD and PGK or (D) ALD and GAPDH. Values are means  $\pm$  SEM of three independent experiments, each performed in triplicate. Asterisks indicate statistically significant differences compared with untreated extracts (one-way ANOVA, Dunnett's multiple comparison test; \* $P$  < 0.05, \*\* $P$  < 0.01).

nor Rab 11 (a nuclear protein from the RAS family [55a]) precipitated with aldolase (Fig. 4B). The bands in Fig. 4A were subjected to densitometry, and it was observed that immunoprecipitation increases in the presence of phalloidin and decreases in the presence of cytochalasin for both PGK (Fig. 4C) and GAPDH (Fig. 4D). The results suggest that the polymeric state of actin stabilizes the association observed for the tested glycolytic pathway enzymes.

#### F-actin enhances the protective effect of PGK and ALD against trehalose-mediated inhibition of GAPDH

In mixtures, some glycolytic pathway enzymes show enhanced resistance to the viscosity-mediated inhibition promoted by accumulation of compatible solutes such as glycerol or trehalose [47]. Therefore, it was decided to analyze whether the presence of actin further increased resistance to trehalose-mediated inhibition of highly sensitive GAPDH, mildly resistant PGK or highly resistant ALD, and mixtures of GAPDH with either PGK or ALD (Fig. 5). The activity of the isolated enzymes in the presence of F-actin and various concentrations of trehalose was assayed. The GAPDH activity was  $0.059 \mu\text{mol}\cdot\text{min}^{-1}\cdot\text{mg protein}^{-1}$ , but decreased to  $0.016 \mu\text{mol}\cdot\text{min}^{-1}\cdot\text{mg protein}^{-1}$  in the presence of the highest concentration of trehalose (1 M) (Fig. 5A,B). The

PGK activity was  $0.081 \mu\text{mol}\cdot\text{min}^{-1}\cdot\text{mg protein}^{-1}$ , and this increased to  $0.12 \mu\text{mol}\cdot\text{min}^{-1}\cdot\text{mg protein}^{-1}$  in the presence of 0.6 M trehalose, and decreased to  $0.052 \mu\text{mol}\cdot\text{min}^{-1}\cdot\text{mg protein}^{-1}$  in the presence of 1 M trehalose (Fig. 5A). ALD was not inhibited by viscosity, as its activity remained constant at approximately  $1.5 \mu\text{mol}\cdot\text{min}^{-1}\cdot\text{mg protein}^{-1}$  regardless of the presence of trehalose (Fig. 5B). When the mixture GAPDH/PGK/actin was assayed (Fig. 5A), the activity of both enzymes became resistant to inhibition. GAPDH activity was always approximately  $0.25 \mu\text{mol}\cdot\text{min}^{-1}\cdot\text{mg protein}^{-1}$  regardless of the trehalose concentration. This is 1.6 times the activity reported for GAPDH/PGK without actin [47]. The activity of PGK in the same GAPDH/PGK/actin mixture was  $0.24 \mu\text{mol}\cdot\text{min}^{-1}\cdot\text{mg protein}^{-1}$ , and it was also resistant to inhibition (Fig. 5A). In the case of the GAPDH/ALD/actin mixture, GAPDH also became resistant to inhibition, remaining constant at  $1.4 \mu\text{mol}\cdot\text{min}^{-1}\cdot\text{mg protein}^{-1}$  at all concentrations of trehalose tested (Fig. 5B), i.e. in the mixture with ALD and actin, GAPDH increased its activity 20-fold, and, in addition, became totally resistant to viscosity-mediated inhibition, while the activity of ALD remained constant under all conditions (Fig. 5B). The results in Fig. 5 demonstrate that, in the presence of actin, the enzyme mixtures GAPDH/PGK or GAPDH/ALD, exhibit enhanced enzymatic activity of both GAPDH and PGK, which is resistant to viscosity-mediated inhibition. These results suggest that

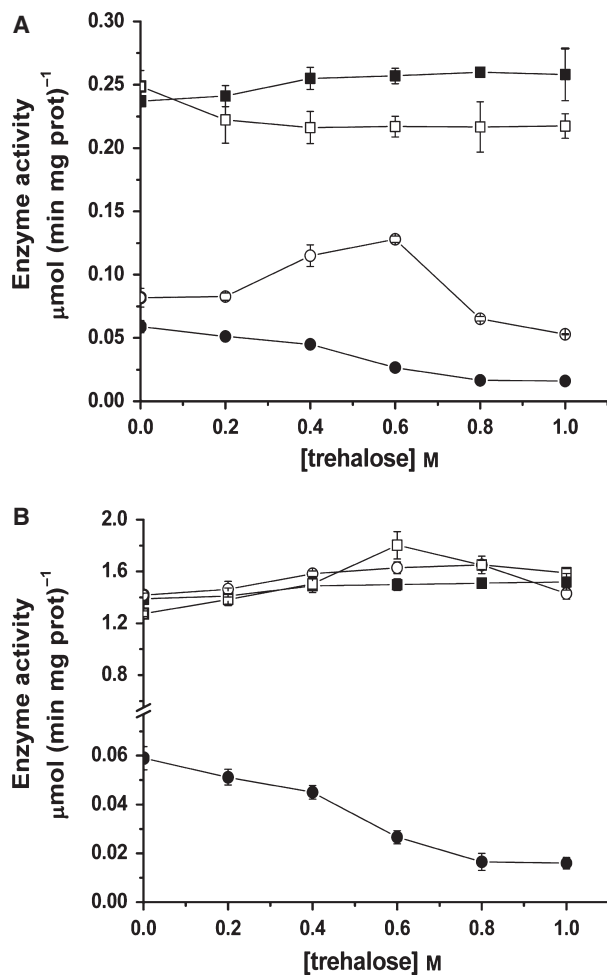


**Fig. 5.** Effect of various concentrations of trehalose on the activity of various isolated and mixed glycolytic pathway enzymes in the presence of actin. Each isolated enzyme or mixture was incubated with 5 mM F-actin, and the indicated enzyme activity was measured in the presence of 0, 0.2, 0.4, 0.6, 0.8 or 1 M trehalose. The reaction conditions for each assay are described in Experimental procedures. (A) Closed circle, GAPDH/actin; open circle, PGK/actin; open square, GAPDH activity in the GAPDH/PGK/actin mixture; closed square, PGK activity in the GAPDH/PGK/actin mixture. (B) Closed circle, GAPDH/actin; open circle, ALD/actin; open square, GAPDH activity in the GAPDH/ALD/actin mixture; closed square, ALD activity in the GAPDH/ALD/actin mixture.

the actin/enzyme associations observed in a glycolytic metabolon may protect enzymes from inhibition by various agents and increase the rate of the whole pathway.

#### F-actin protects the whole glycolytic pathway against trehalose-mediated inhibition

Having observed that actin protects some glycolytic enzymes against inhibition, it was decided to measure

the effect of different actin polymerization states on the whole fermentation pathway (Figs 6 and 7). In addition, the inhibitory effect of various concentrations of trehalose was measured. Experiments were performed in SLO-permeabilized cells (Fig. 6) and cytoplasmic extracts (Fig. 7), and were subjected to kinetic analysis assuming that the alcohol dehydrogenase reaction is the limiting step in glycolysis (Eqn 3) [56–58]. The effects of actin or trehalose were determined under each condition. Kinetic analysis of the data led to the curves illustrated in Figs 6 and 7. In addition, the kinetic parameters are reported in Table S1 for SLO-permeabilized cells and in Table S2 for cytoplasmic extracts. The initial burst in activity was interpreted as production of ethanol using available NADH, while the second, slower rate of ethanol production reflects the requirement for NAD<sup>+</sup> to be released by alcohol dehydrogenase (ADH) in addition to its reduction at other levels of the pathway (GAPDH) [56,57]. In SLO-permeabilized cells, ethanol production was approximately 20 μmol·mg cells<sup>-1</sup> (wet weight, ww, the units we used in all experiments) over 16 min. Only the highest concentration of trehalose (1 M) decreased production of ethanol, to 18 μmol·mg cells<sup>-1</sup> (ww) over 16 min (Fig. 6A). When the ethanol production data from permeabilized cells were fitted to Eqn 3, kinetic analysis indicated that the rapid initial rate of ethanol production ( $k_b$ ) in the control decreased only at 0.8 and 1.0 M trehalose. In the absence of trehalose,  $k_b$  was 2.74 min<sup>-1</sup>, while  $k_b$  was 1.23 min<sup>-1</sup> at 1 M trehalose (Fig. 6A and Table S1). In addition, the slow (steady-state) rate in absence of trehalose,  $k_{ss} = 0.083$  min<sup>-1</sup>, decreased to 0.011 min<sup>-1</sup> in 1 M trehalose (Fig. 6A and Table S1).

In order to determine the effect of the polymerization state of actin on its ability to protect the activity of the glycolytic pathway, phalloidin (Fig. 6B), cytochalasin D (Fig. 6C) or latrunculin B, a strong depolymerizing agent (Fig. 6D), were added. In the presence of phalloidin, the production of ethanol was 40 μmol·mg cells<sup>-1</sup> (ww) over 16 min; twice as much as in the control, probably due to tighter association of the glycolytic pathway enzymes. In addition, phalloidin prevented the trehalose-mediated inhibition of fermentation (Fig. 6B). The kinetics in the presence of phalloidin (Fig. 6B and Table S1) indicated a more pronounced initial burst in ethanol production plus higher steady-state production of ethanol. The rate constants were not affected by trehalose. In contrast to phalloidin, cytochalasin D decreased ethanol production to <10 μmol·mg cells<sup>-1</sup> (ww) over 16 min, i.e. half that of the control and four times less than with phalloidin (Fig. 6C). In the presence of cytochala-

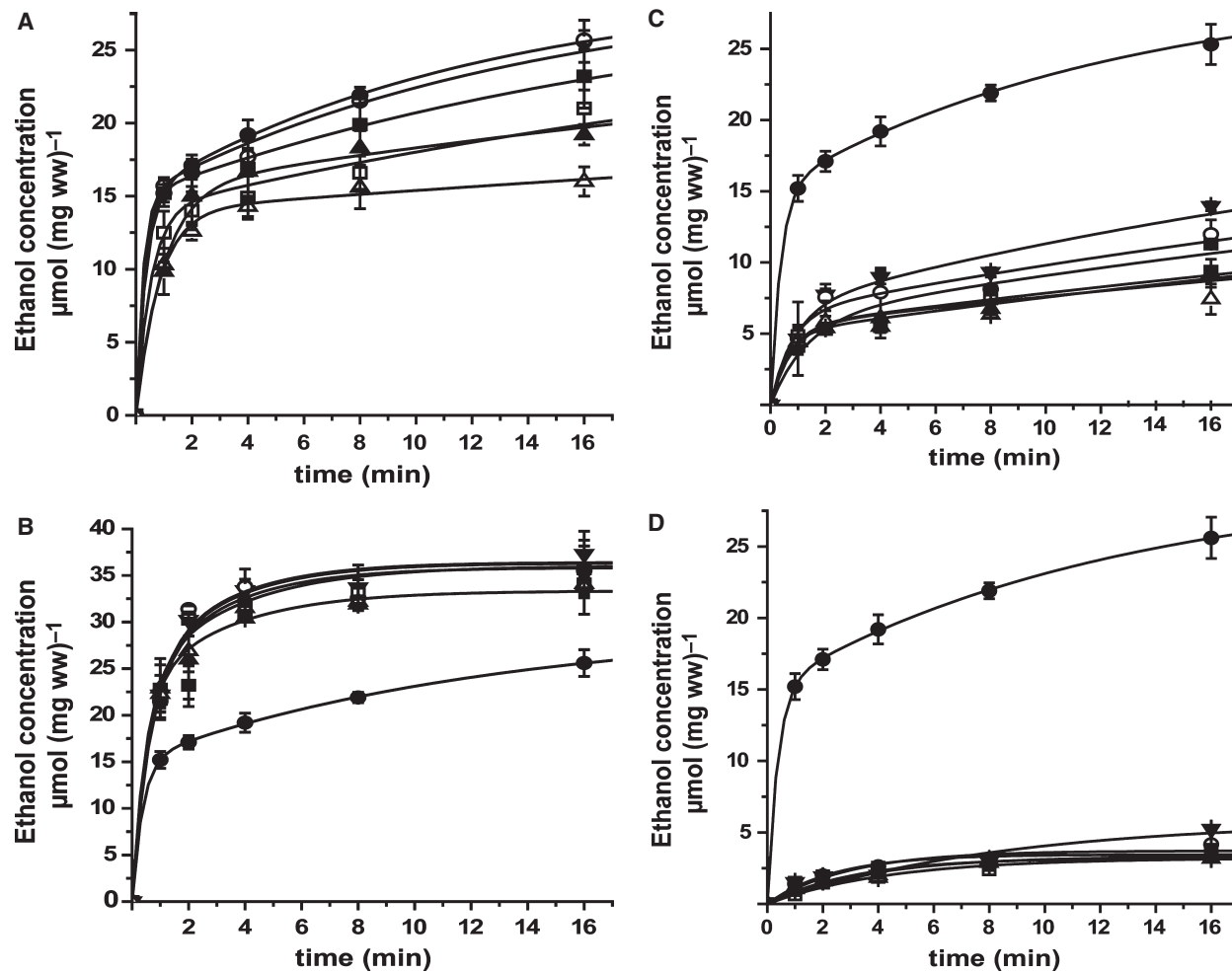


**Fig. 6.** Production of ethanol by SLO-permeabilized cells incubated with phalloidin, cytochalasin D or latrunculin B in the presence of various concentrations of trehalose. The results show the fermentation activity of SLO-permeabilized yeast cells (5 mg ww per mL). In all cases, non-treated controls with 0 M trehalose were included (closed circle). Cells were pre-incubated in the absence of additions (A), in the presence of 59  $\mu$ M phalloidin (B), in the presence of 400  $\mu$ M cytochalasin D (C) or in the presence of 200  $\mu$ M latrunculin B (D). The closed inverted triangle indicates phalloidin plus 0 M trehalose in (B), cytochalasin D plus 0 M trehalose in (C) and latrunculin B plus 0 M trehalose in (D). In (A–D), open circles indicate 0.2 M trehalose; closed squares indicate 0.4 M trehalose; open squares indicate 0.6 M trehalose; closed upright triangles indicate 0.8 M trehalose and open upright triangles indicate 1 M trehalose. The scale in (B) was modified due to higher ethanol production.

sin D, trehalose inhibited fermentation further, with an activity of 5  $\mu$ mol·mg cells<sup>-1</sup> (ww) at 1 M trehalose (Fig. 6C). Kinetic analysis in the presence of cytochalasin indicated that  $k_b$  was constant while  $k_{ss}$  decreased drastically, all at very low levels of ethanol production (Fig. 6C and Table S1). Using latrunculin B, the production of ethanol was <5  $\mu$ mol·mg cells<sup>-1</sup> (ww), and 1 M trehalose inhibited fermentation to 3  $\mu$ mol·mg cells<sup>-1</sup> (ww) (Fig. 6D). The kinetic analysis in the presence of latrunculin indicates that the initial burst activity was minimal, and a very low steady-state production of ethanol was observed, which increased marginally upon trehalose addition (Table S1). Hence

it appears that F-actin but not G-actin increases fermentation and prevents inhibition by trehalose.

The results in permeabilized cells suggest that the cytoskeleton supports a glycolytic metabolon. To further explore this possibility, we removed the plasmatic membrane to create cytoplasmic extracts. In these extracts, fermentation was measured in samples containing actin in various polymeric states, allowing molecules that became detached from the cytoskeleton to diffuse into the medium (Fig. 7). Fermentation was evaluated at various trehalose concentrations. The untreated extracts produced approximately 12  $\mu$ mol ethanol per mg protein in 8 min, and addition of

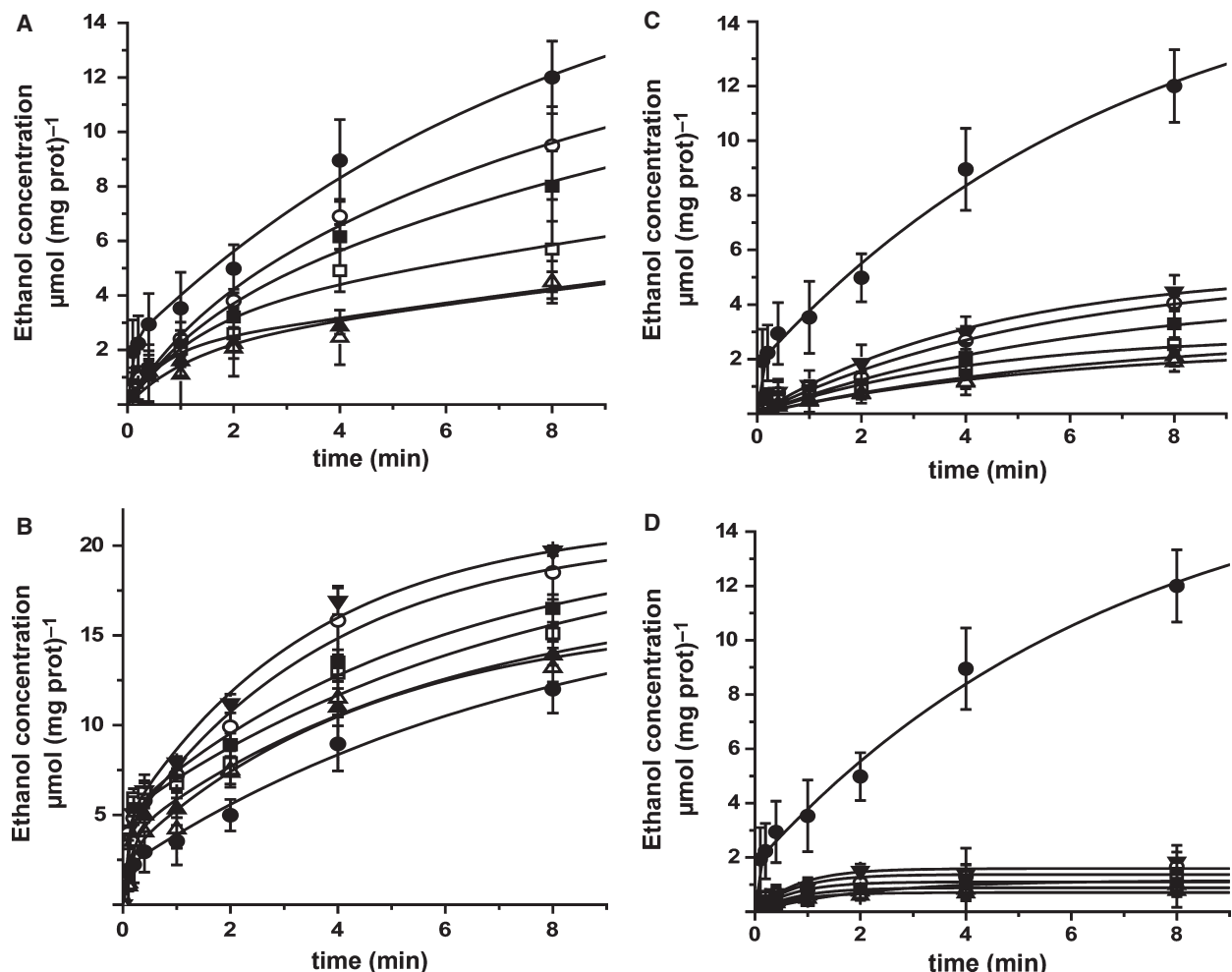


**Fig. 7.** Fermentation of yeast cytoplasmic extracts ( $1 \text{ mg protein} \cdot \text{mL}^{-1}$ ) incubated with phalloidin, cytochalasin or latrunculin in the presence or absence of various trehalose concentrations. In all cases, non-treated controls with  $0 \text{ M}$  trehalose were included (closed circle). Cytoplasmic extracts were pre-incubated in the absence of additions (A), in the presence of  $59 \mu\text{M}$  phalloidin (B), in the presence of  $400 \mu\text{M}$  cytochalasin D (C) or in the presence of  $200 \mu\text{M}$  latrunculin B (D), and activity was measured in the presence of various trehalose concentrations. The closed inverted triangle indicates phalloidin plus  $0 \text{ M}$  trehalose in (B), cytochalasin D plus  $0 \text{ M}$  trehalose in (C) and latrunculin B plus  $0 \text{ M}$  trehalose in (D). In (A–D), open circles indicate  $0.2 \text{ M}$  trehalose; closed squares indicate  $0.4 \text{ M}$  trehalose; open squares indicate  $0.6 \text{ M}$  trehalose; closed upright triangles indicate  $0.8 \text{ M}$  trehalose and open upright triangles indicate  $1 \text{ M}$  trehalose. The scale in (B) was modified due to higher ethanol production.

increasing concentrations of trehalose up to  $1 \text{ M}$  decreased the fermentation to  $4 \mu\text{mol}$  ethanol per mg protein (Fig. 7A). Accordingly, the rapid rate of ethanol production ( $k_b$ ), which was much lower than in the permeabilized cells, decreased by almost 45%, while the steady-state rate of ethanol production ( $k_{ss}$ ) was inhibited by 80% (Table S2). Phalloidin increased fermentation to almost  $19 \mu\text{mol}$  ethanol per mg protein over 8 min. In the presence of phalloidin,  $1 \text{ M}$  trehalose decreased ethanol production to  $12 \mu\text{mol} \cdot \text{mg protein}^{-1}$  over 8 min (Fig. 7B). The rapid rate of ethanol production ( $k_b$ ) was similar to that of

the control, although now ethanol production became resistant to trehalose, while the slow rate of ethanol production ( $k_{ss}$ ) was higher than in the control and was inhibited by trehalose by 35% only (Fig. 7B and Table S2). Cytochalasin D-treated samples produced  $4 \mu\text{mol}$  ethanol per mg protein over 8 min, and  $1 \text{ M}$  trehalose inhibited ethanol production to  $1 \mu\text{mol} \cdot \text{mg protein}^{-1}$  (Fig. 7C). Kinetic analysis indicated that fermentation was very low even in the absence of trehalose, and the rapid burst in activity disappeared (Fig. 7C and Table S2). Latrunculin B-treated samples produced very little ethanol, approx-

imately  $2 \mu\text{mol}\cdot\text{mg protein}^{-1}$ , and trehalose ( $0.2\text{--}1 \text{ M}$ ) inhibited fermentation completely (Fig. 7D). This is reflected in the kinetic data (Fig. 7D and Table S2). Thus, in cytoplasmic extracts, the production of ethanol was much lower than in permeabilized cells, and the initial rapid burst of activity was lost in the presence of each actin-depolymerizing agent.

Comparison of the data obtained for the SLO-permeabilized cells and for the cytoplasmic extracts indicates that ethanol production was higher *in situ*, probably due to better preservation of pathway architecture, strongly suggesting that a glycolytic metabolon does exist in yeast. In contrast, the cytoplasmic extracts were more sensitive to the cytoskeleton-acting drugs, probably due to higher accessibility and component diffusion after detachment from their anchoring site.

### In complex with F-actin, enzymes are protected from inhibition by their antibodies

The above results suggest that, in yeast, F-actin but not G-actin promotes organization of the glycolytic pathway, increasing the efficiency of fermentation. In addition, within the complex, enzymes are protected against inhibition by compatible solutes. In order to further characterize the glycolytic complex, we tested specific antibodies for GAPDH, PGK and ALD. When tested against each isolated enzyme, these antibodies inhibited activity by at least 80% (Fig. 8A). In contrast, when the ALD antibody was added to SLO-permeabilized cells, the activity of ALD (Fig. 8B) and the other enzymes (data not shown) were resistant to the antibody. Furthermore, protection varied when the polymerization of actin was modified by incubating the cells with phalloidin, cytochalasin D or latrunculin B. In the control, fermentation was  $20 \mu\text{mol}$  ethanol per mg cells (ww) over 16 min, compared with  $40 \mu\text{mol}$  ethanol per mg cells in the phalloidin-treated samples; addition of the ALD antibody did not inhibit fermentation either in the control or in the phalloidin-treated sample (Fig. 8B). In contrast, in the cells treated with cytochalasin D, the ALD antibody partially inhibited fermentation to  $6 \mu\text{mol}$  ethanol per mg cells (ww) over 16 min, while fermentation in the presence of latrunculin B was  $2 \mu\text{mol}$  ethanol per mg cells (ww) over 16 min, i.e. half the activity of their respective controls (Fig. 8B). Similar effects were observed with the GAPDH and PGK antibodies (data not shown). The data support the idea that F-actin promotes formation of a multi-enzymatic glycolytic complex in which the individual enzymes are shielded from their specific antibodies. Also, it is possible that the intact

cytoskeleton forms a tight mesh that precludes antibodies from reaching their targets: this mesh may become permeable to large molecules such as antibodies upon monomerization of the actin filaments. In contrast, the monomeric G-actin does not support this association, and in this case individual enzymes are partially exposed. This is not the only possible interpretation of our data in Fig. 8, e.g. the permeability of

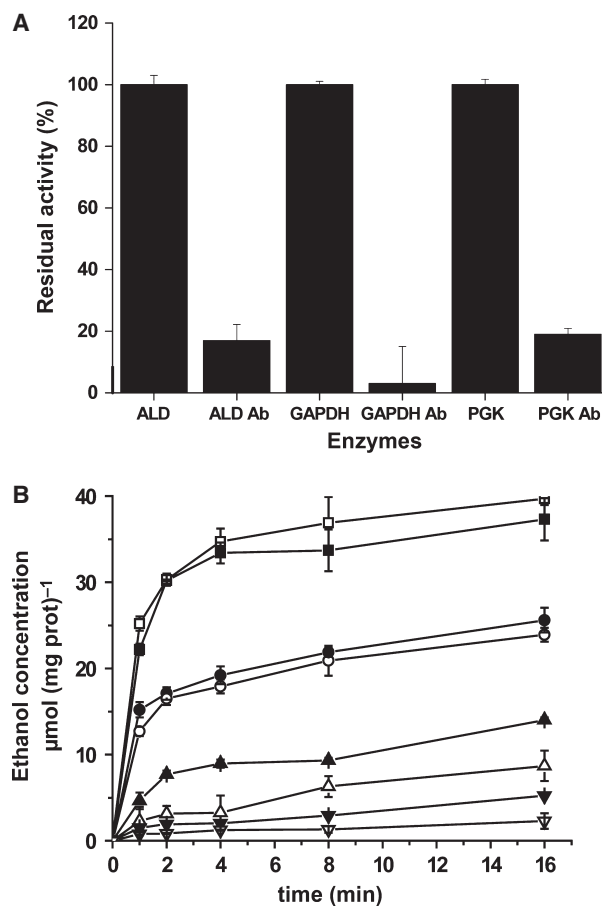


**Fig. 8.** Effect of specific antibodies on the activity of ALD and other glycolytic pathway enzymes. (A) The activity of ALD, GAPDH and PGK was measured as described in Experimental procedures in the absence and the presence of  $48 \mu\text{g}\cdot\text{mL}^{-1}$  anti-ALD, anti-GAPDH and anti-PGK. (B) Effect of ALD antibody on ALD activity in permeabilized cells alone or treated with phalloidin, cytochalasin D or latrunculin. Conditions used were the same as in Fig. 6. Closed circles indicate permeabilized cells alone; open circles indicate permeabilized cells with anti-ALD; closed circles indicate permeabilized cells pre-treated with phalloidin; open squares indicate permeabilized cells with phalloidin and anti-ALD; closed upright triangles indicate permeabilized cells pre-treated with cytochalasin D; open upright triangles indicate permeabilized cells with cytochalasin D and anti-ALD; closed inverted triangles indicate permeabilized cells pre-treated with latrunculin B; open inverted triangles indicate permeabilized cells with latrunculin B and anti-ALD. Ethanol was quantified with ADH.

the SLO-permeabilized cells to the antibodies may have been modified by the cytoskeleton effectors. Therefore, we tested *in vitro* whether actin shielded some glycolytic enzymes against their specific antibodies. We assayed ALD/antibody binding in the absence and the presence of GAPDH, actin or both, evaluating in each case the disappearance of ALD by SDS/PAGE (Fig. 9A). ALD and the mixture of ALD and GAPDH reacted with the ALD antibody to a greater extent

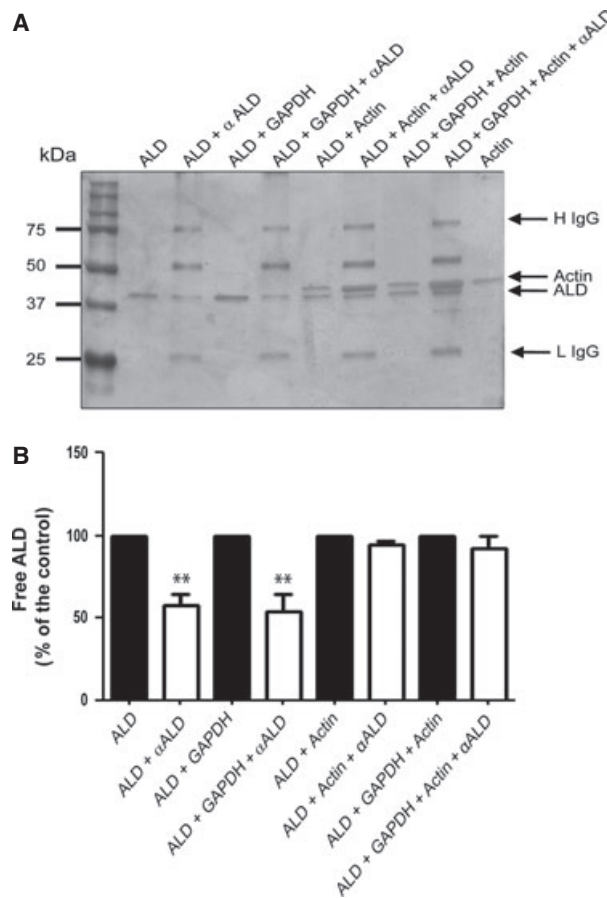


**Fig. 9.** Effect of actin and GAPDH on the binding of an ALD antibody to ALD. Aldolase was exposed to its specific antibody in the absence and the presence of GAPDH, actin and a GAPDH/actin mixture. (A) The reaction mixture was the same as described for determination of ALD activity (Fig. 5). Lane 2, 9  $\mu\text{g}\cdot\text{mL}^{-1}$  aldolase (ALD); lanes 3, 5, 7 and 9, addition of 9  $\mu\text{g}\cdot\text{mL}^{-1}$  ALD antibody ( $\alpha$ ALD); lanes 4, 5, 8 and 9, addition of 9  $\mu\text{g}\cdot\text{mL}^{-1}$  GAPDH; lanes 6–10, addition of 8.5  $\mu\text{g}\cdot\text{mL}^{-1}$  actin. After 30 min incubation, SDS/PAGE was performed for all samples. Bands for heavy (H IgG) and light (L IgG) antibody chains and for ALD are indicated by arrows. (B) Densitometry was performed to estimate the difference between the untreated and antibody-treated samples. Values are mean  $\pm$  SEM of three independent experiments, each performed in triplicate. Asterisks indicate statistically significant differences compared with untreated samples (one-way ANOVA, Dunnett's multiple comparison test; \*\* $P < 0.01$ ).

than the mixtures containing actin (Fig. 9A). To further evaluate this, the intensity of ALD bands in each case was quantified by gel scanning (Fig. 9B). Thus, even in the absence of membrane barriers, actin appears to prevent reactivity of the antibody with ALD (Fig. 9), suggesting that at least part of the enzyme is shielded from the medium by actin.

The results presented here suggest that F-actin functions as a scaffold for glycolytic pathway enzymes. The glycolytic metabolon thus formed is more efficient than the non-associated enzymes at producing ethanol from glucose. Also, in the metabolic complex, glycolytic enzymes are protected against various inhibiting conditions.

## Discussion

Metabolons are complexes of enzymes participating in sequence within a metabolic pathway. Metabolons have been proposed to enhance metabolic efficiency through direct passage of intermediaries between enzymes, thus avoiding diffusion into the medium. In addition, in these complexes, individual active sites may be protected from competitive inhibitors (Fig. 10). Recently, it has been proposed that enzymes within metabolons are protected against other adverse conditions, such as the increase in viscosity that results from accumulation of compatible solutes in response to stress. It has not been established whether the glycolytic pathway is organized into a metabolon. In mammals, many glycolytic enzymes interact with the cytoskeleton [29,42,51,59], sometimes through known, specific binding domains found in tubulin [60] and actin [54,59]. Detailed studies with isolated F-actin revealed that ALD and GAPDH bind firmly to F-actin, PFK and PK bind quite tightly F-actin, and GPI, TPI, PGAM and ENO do not interact with actin or at least are bound less firmly [29,34,40,46,61]. Consecutive enzymes in the pathway such as ALD, GAPDH and PGK associate and interact directly with actin [40]. Although four glycolytic pathway enzymes did not associate with actin directly, it is suggested that, if a glycolytic pathway enzyme complex exists, these non-adsorbing enzymes interact with one or more of the enzymes that do bind actin [40]. This is called 'piggy backing' [30,40,61], and has been observed for PGAM, which interacts with lactate dehydrogenase, which in turn binds F-actin [30,40]. In mammals, ALD and GAPDH appear to anchor the glycolytic complex to actin [43,62]. In yeast, it has been shown that many glycolytic enzymes bind to each other and to actin. The role of actin as a scaffold for the glycolytic metabolon appears to be dynamic, as the

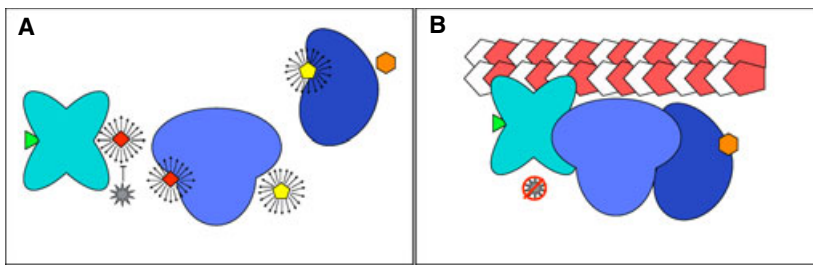


**Fig. 10.** Advantages of metabolons. (A) In isolated enzymes, the substrate (green), intermediaries (red and yellow) and product (orange) diffuse into the aqueous phase (small arrows). Toxic intermediaries and inhibitors (grey) are free to exit/enter the active site in each enzyme. (B) In metabolons, channeling allows transfer of the substrate (green) from the active site of an enzyme directly to the next to obtain a final product (orange) without diffusion to the cytoplasm of intermediaries (not shown), while inhibitors (grey) are excluded from the active site. Filamentous actin is shown in red and white.

oligomeric actin filaments but not the monomers support binding.

Glycolytic pathway enzyme/actin interactions have been described in higher eukaryotes [30]. *S. cerevisiae* cells exhibit the same electrostatic forces as higher eukaryotes [30]. Indeed, our results indicate that F-actin/enzyme interactions occur in yeast (Figs 1–4). As observed in mammals, most of the yeast glycolytic enzymes bind to actin. However, in yeast, there are some important enzymes that did not bind actin, such as PFK and PK (Figs 2 and 3). These observations indicate that, in yeast, the interactions are of low affinity, as predicted by Brownian dynamic studies [30]. The lower affinity is probably due, at least in part, to the fact that yeast actin has two fewer negatively charged amino acid residues at the N-terminus [30]. The difference in structure may be one of the reasons for the lack of association, as the surfaces of enzymes possess strikingly different capacities for actin binding [41,63]. ALD and GAPDH displayed strong affinity for actin, both in rabbit striated muscle [41] and in yeast (Figs 2 and 3). In contrast, in yeast, PFK, PGAM and PK did not bind actin (Figs 2 and 3); a reason for this difference may be the variation in enzyme structure. In mammals, PFK is a homo-tetramer, while in the yeast species *S. cerevisiae* and *Kluyveromyces lactis*, PFK is a hetero-octamer [59]. PFK interactions with F-actin have not been detected [59]. Actin/enzyme interactions probably play an important role in compartmentation and substrate channeling [30]. Therefore, the weak interaction of some yeast enzymes with actin does not mean that there is no metabolon. Thus, it is possible that the yeast enzymes may be ‘piggy-backing’ and in this manner interact with the cytoskeleton [30].

The glycolytic pathway probably uses the cytoskeleton as a scaffold [6,41]. Actin/enzyme interactions are electrostatic [40], so pH, ionic strength [45] and cations

[61] modulate binding [45] and consequently enzyme kinetics, interactions among enzymes and the structure of actin filaments [64]. Association with the cytoskeleton stabilizes the enzyme structure [2,65,66], e.g. PFK inactivation by dilution is prevented but not reversed by ALD addition, whereas, in the presence of microtubules, ALD reactivates PFK [51,52].

In response to stress, compatible solutes accumulate in the cytoplasm and protect membranes and proteins [67]. Stabilization results from decreased vibration of the protein due to increased viscosity [68,69]. Indeed, Kramer’s theory proposes that the viscosity of the medium inhibits the structural movements of proteins and thus catalysis [69a]. Viscosity is probably the reason why compatible solutes are rapidly eliminated [70], as it appears to inhibit growth [71]. During lyophilization the isolated plasma membrane H<sup>+</sup>-ATPase from *K. lactis* was protected by trehalose but its activity was transiently inhibited [69]. It was proposed that compatible solutes inhibit metabolic fluxes through an increase in viscosity [72].

Many factors control the binding of glycolytic enzymes among themselves and with the cytoskeleton, which is an important modulator of metabolic functions [45]. Apparently association and dissociation of enzymes regulate metabolic activity [50], as indicated by the protection of several glycolytic pathway enzymes from viscosity-mediated inhibition [47]. Here, it is reported that the glycolytic pathway enzymes constitute a complex with F-actin (Figs 2–7). In addition, it is demonstrated that enzymes in association with actin retain activity even at high compatible solute concentrations (Figs 5–7). The enzymes in this complex were resistant against trehalose-mediated inhibition (Figs 5–7) and against inactivation by antibodies (Figs 8 and 9). Enzymatic complexes appear to favor stable folding, eliminating some non-productive conformations [73]. This explains the more efficient

catalysis and improved resistance against viscosity-mediated inhibition [69].

Glycolysis has been very well described as a collection of individual steps, but understanding it as a whole appears to be more difficult. Many groups have studied the behavior of the glycolytic pathway using numerous experimental and modeling approaches [74]. Hynne *et al.* [75] proposed a method of fitting a biochemical pathway into a model using experimental substrate concentrations and dynamic properties when the mechanism of the individual enzymatic steps is known. Accordingly, rate constants and maximum velocities of the glycolytic pathway may be calculated from experimental data by simple algebra without integration of kinetic equations [72].

Interestingly, under specific conditions, the behavior of the glycolytic pathway shows a rapid increase in activity followed by oscillations in the concentrations of various intermediates, co-enzymes and extracellular species. The biological significance of this behavior has long been debated [74]. *S. cerevisiae* intact cells fit to a model of glycolysis and glycolytic oscillations [76–79] that has led to proposal of a model that involves rapid initial metabolic fluxes followed by slower kinetics [72,75]. Our own data indicate that, when the cytoskeleton is intact, an initial burst of activity occurs, probably as a result of the activity of alcohol dehydrogenase, which is saturated with  $\text{NADH} + \text{H}^+$ , and then a second phase of steady-state kinetics ensues. The reduction of  $\text{NAD}^+$  required in this second stage appears to be more efficient in the presence of an intact cytoskeleton, which probably channels  $\text{NADH}/\text{NAD}$  back and forth between the reducing and oxidizing enzymes (Figs 6 and 7). In cytoplasmic extracts, the inhibition of glycolysis due to cytoskeleton disruption is more pronounced, probably because enzymes detached from the broken filaments diffuse into the medium instead of being contained within the cell.

It has been reported that cells harvested at the point of glucose depletion or later exhibit a constant mean glycolytic flux, which agrees with the second, steady-state rate in our fermentation experiments (Figs 6 and 7). A constant flux results from the ‘supercritical Hopf bifurcation’ [72,75] proposed for glucose metabolism, i.e. as saturation occurs close to the glucose bifurcation point, leading to stable metabolite concentrations. In consequence, glucose-depleted cells may be used to estimate the metabolic fluxes of the system [75]. The stoichiometry and identity of the metabolites, as well as the branching connectivity of the network, are required to analyze the kinetic behavior of a complex of enzymes working together [74]. It appears that

network stoichiometry induces dynamic constraints on the concentration changes arising from mass conservation [72].

Our data add support to the concept that the cytoskeleton is a dynamic network where various proteins interact. This barely explored phenomenon modulates whole metabolic pathways, as observed when using actin-targeting drugs during fermentation (Figs 6 and 7). In addition to the glycolytic pathway, the cytoskeleton also associates with organelles. During cell division, actin and tubulin direct mitochondria to specific sites in the cell. Tubulin controls oxidative phosphorylation coupling with mitochondrial voltage-dependent anion channels [80]. In short, in the cytoplasm, glycolytic enzymes appear to be highly organized [81], using the cytoskeleton as a scaffold [65] (Fig. 10). Thus, the cytoskeleton is required for association, stability and protection of enzymes in the glycolytic pathway and most probably other pathways. It appears that the association of actin with glycolytic pathway enzymes may regulate catalysis and enhance resistance to inactivation during stress. Resistance to inactivation during stress had not been described before and yet, it may be the *raison d'être* of metabolons.

## Experimental procedures

### Materials

All reagents were of analytical quality. Glucose, trehalose, HEPES, EDTA, MES, TEA, SDS,  $\text{MgCl}_2$ , glycerol, hydrazine hemisulfate, ammonium molybdate, L-ascorbic acid, D,L-dithiothreitol, actin, the *Saccharomyces cerevisiae* enzymes ALD, PGK, GAPDH and ADH, D-fructose 1,6-biphosphate, D-glucose 6-phosphate, D-(–)-3-phosphoglyceric acid, D,L-glyceraldehyde 3-phosphate, cytochalasin D, phalloidin,  $\text{NADP}^+$ , NADH, ATP and ADP were obtained from Sigma (St Louis, MO, USA). KOH, magnesium and potassium acetate, sodium phosphate salt, trichloroacetic acid and  $\text{K}_2\text{HPO}_4$  were obtained from J.T. Baker (Houston, TX, USA). Sodium acetate was obtained from Merck (Darmstadt, Germany). Yeast extract was obtained from DIFCO (Detroit, MI, USA) and peptone was obtained from Bioxon (Cuautitlán, Mexico). Pro-albumin was obtained from Celliance (San Francisco, CA, USA). Complete protease inhibitor cocktail and protein A agarose were obtained from Roche (Basel, Switzerland). The enhanced chemiluminescence reagent kit (ECL) was purchased from Amersham Biosciences (Arlington Heights, IL, USA). Acrylamide/bisacrylamide, N,N,N',N'-tetramethyl-ethylene-diamine (TEMED) ammonium persulfate, the protein assay kit and molecular weight markers were obtained from Bio-Rad (Richmond, CA, USA).

## Antibodies

Goat polyclonal anti-ALD, anti-PGAM, anti-ENO and anti-PK and rabbit polyclonal anti-HXK, anti-GPI, anti-PFK, anti-GAPDH, anti-TPI and anti-PGK were obtained from Santa Cruz Biotechnology (Santa Cruz, CA, USA). The monoclonal antibody against actin was provided by J.M. Hernández (Department of Cell Biology, Centro de Investigaciones y Estudios Avanzados del Instituto Politécnico Nacional, Mexico) [82]. The secondary antibodies (horseradish peroxidase-labeled anti-rabbit, anti-goat and anti-mouse) were purchased from Jackson ImmunoResearch Laboratories Inc. (West Grove, PA, USA).

## Yeast cells and cytoplasmic extracts

An industrial strain of *S. cerevisiae* ('yeast foam') was used. Cells were incubated for 16 h in 500 mL YPD (1% yeast extract, 5% gelatin peptone and 5% dextrose), and washed twice at 676 g for 5 min. The pellet was resuspended to 50% in lysis buffer (100 mM HEPES/KOH pH 7.5, 600 mM potassium acetate, 10 mM magnesium acetate, 1 mM EDTA, 20% glycerol, 8 mM 2-mercaptoethanol and one tablet of Complete protease inhibitor cocktail. SLO cells (50 mg ww in 1 mL) were permeabilized by incubation for 30 min with 1 mg SLO. In all experiments, cells were added to a final concentration of 5 mg ww per mL. To obtain cytoplasmic extracts, cells were disrupted using a 'Bead-Beater' (BIOSPEC Products, Southern Pines, NC, USA) containing 0.5 mm diameter glass beads, three times for 20 s each. Finally, the homogenate was centrifuged at 24 500 g for 1 h at 4 °C (Beckman ultracentrifuge, Beckman Coulter, Brea, CA, USA) and the supernatant was kept at -80 °C [83]. The protein concentration of the yeast cytoplasmic extract was measured by the biuret method [84].

## Purification of actin from *Saccharomyces cerevisiae* using affinity chromatography

Yeast actin is not available commercially. Thus, we obtained it using the protocol described by Zechel [85]. Briefly, 5 mg of DNase I, which exhibits a high affinity for actin, was covalently bound to a Sepharose 4B column activated using 1 g cyanogen bromide (Sigma). The resin was washed and swollen in cold 1 mM HCl for at least 30 min. Then it was washed with distilled water at 676 g for 5 min and with 0.1 M NaHCO<sub>3</sub>/0.5 M NaCl coupling buffer (pH 8.3–8.5). The protein was mixed with Sepharose 4B (5–10 mg per mL of resin) overnight at 4 °C. Unreacted ligand was washed away using NaHCO<sub>3</sub>/NaCl coupling buffer. Unreacted groups were blocked with 0.2 M glycine, pH 8.0, for 2 h at room temperature. To remove the blocking solution from the resin, it was washed extensively, first with basic coupling buffer, pH of approximately 8.5, then with 0.1 M acetate buffer, pH 4, containing 0.5 M NaCl. This wash cycle was completed four or five times with the high- and low-pH buffer solutions. The washed resin was equilibrated in a column using 10 mM Tris pH 7.4 (equilibrium buffer). Yeast cytoplasmic extracts were ultracentrifuged at 12 000 rpm for 30 min. Then the yeast cytoplasmic extracts were added to the column and extensively washed with equilibrium buffer, until no protein was detected by Bradford assay [86]. Bound material was eluted by stepwise addition of increasing concentrations of Tris, pH 7.4 (50, 100, 150, 200, 250, 300, 350, 400, 450 and 500 mM) in 3 mL aliquots, and protein was measured by the Bradford assay [86]. Peaks

with basic coupling buffer, pH of approximately 8.5, then with 0.1 M acetate buffer, pH 4, containing 0.5 M NaCl. This wash cycle was completed five times each with the high- and low-pH buffer solutions. Yeast cytoplasmic extracts were sonicated three times for 60 s each in buffer G containing 2 mM Tris pH 7.9, 0.2 mM CaCl<sub>2</sub>, 0.2 mM ATP, 0.2 mM dithiothreitol, 10% formamide, and centrifuged at 35 000 rpm for 1 h. The extracts were then added to an immobilized DNase I column previously washed with buffer G, incubated overnight and extensively washed with the same buffer by centrifugation at 12 000 rpm for 15 min. The DNase I/cytoplasmic extract column was equilibrated and extensively washed with buffer G, until no protein was detected by Bradford assay [86]. Then it was eluted again using buffer G + 0.2 M NH<sub>4</sub>Cl until no protein was detected by Bradford assay. Finally G-actin was eluted using buffer G with 40% formamide and 20% glycerol, the protein was concentrated in Amicon Ultra Centrifugal Filter Units (Millipore, Billerica, MA, USA) and measured using the Bradford assay [86]. Purity was evaluated by PAGE and immunoblotting. Polymerization of 5 mM actin was performed in 2 mM Tris/HCl pH 8, 1.2 mM ATP, 200 mM CaCl<sub>2</sub>, 50 mM KCl, 1 mM MgCl<sub>2</sub> and 0.5 mM dithiothreitol by incubation for 1 h at room temperature.

## Isolation of aldolase- and DNase I-associated proteins by affinity chromatography

Ten milligrams of ALD or DNase I were covalently bound to a cyanogen bromide-activated Sepharose 4B column (Sigma). To achieve binding, 1 g cyanogen-bromide activated resin was washed and swollen in cold 1 mM HCl for at least 30 min. The resin was washed with distilled water, 5–10 column volumes, then washed with 0.1 M NaHCO<sub>3</sub>/0.5 M NaCl coupling buffer (pH 8.3–8.5). The protein was mixed with Sepharose 4B (5–10 mg per mL of resin) overnight at 4 °C. Unreacted ligand was washed away using NaHCO<sub>3</sub>/NaCl coupling buffer. Unreacted groups were blocked with 0.2 M glycine, pH 8.0, for 2 h at room temperature. To remove the blocking solution from the resin, it was washed extensively, first with basic coupling buffer, pH of approximately 8.5, then with 0.1 M acetate buffer, pH 4, containing 0.5 M NaCl. This wash cycle was completed four or five times with the high- and low-pH buffer solutions. The washed resin was equilibrated in a column using 10 mM Tris pH 7.4 (equilibrium buffer). Yeast cytoplasmic extracts were ultracentrifuged at 12 000 rpm for 30 min. Then the yeast cytoplasmic extracts were added to the column and extensively washed with equilibrium buffer, until no protein was detected by Bradford assay [86]. Bound material was eluted by stepwise addition of increasing concentrations of Tris, pH 7.4 (50, 100, 150, 200, 250, 300, 350, 400, 450 and 500 mM) in 3 mL aliquots, and protein was measured by the Bradford assay [86]. Peaks

collected between 50 and 150 were pooled obtaining 10 mg protein which were concentrated using an Amicon Ultra Centrifugal Filter Unit. Aldolase- or DNase I-associated proteins were detected by western blotting.

### Immunoprecipitation

Each antibody ( $3 \mu\text{g}\cdot\text{mL}^{-1}$ ), as indicated in the legend to each figure, was incubated with 7  $\mu\text{L}$  protein A agarose at 4 °C for 5 min, mixed with 3  $\text{mg}\cdot\text{mL}^{-1}$  protein of yeast cytoplasmic extract, and stirred overnight at 4 °C in a final volume of 100  $\mu\text{L}$ . Samples were collected by centrifugation at 5000  $\text{g}$  for 10 min, and washed extensively using RIPA buffer (20 mM Tris/HCl, 316 mM NaCl, 2 mM EDTA, 20 mM sodium orthovanadate, 20 mM sodium molybdate, 50 mM sodium fluoride and 1% Triton X-100, pH 7.5). The pellet was resuspended in 50 mM Tris/HCl, pH 7.5, 0.1% Tween 20 and protease inhibitors. Precipitates were subjected to western blotting. Rabbit striated muscle was used as a positive control [87].

### Electrophoresis and western blotting

All samples were diluted in 0.5 mL sample buffer (500 mM Tris, pH 6.8, 10% glycerol, 10% SDS, 0.05%  $\beta$ -mercaptoethanol and 0.01% bromophenol blue) and boiled for 5 min [88]. SDS/PAGE was performed in 10% polyacrylamide. Proteins were electrotransferred to poly(vinylidene difluoride) membranes for immunoblotting using 25 mM potassium phosphate, 25 mM sodium phosphate, 12 mM Tris, 192 mM glycine and 20% methanol, pH 7.0 [89]. Membranes were blocked with 0.5% albumin in TBS/T (50 mM Tris, 104 mM NaCl, pH 7.6, 0.1% Tween 20) for 1 h, and incubated overnight at 4 °C with the primary antibody, washed with TBS/T and incubated at 37 °C for 1 h with horseradish peroxidase-conjugated secondary antibody. Antibodies were diluted in TBS/T. Once the membranes were washed, the bands were developed by chemiluminescence using an ECL kit [87].

### Silver staining of gels

The SDS/PAGE gel was incubated in buffer I (30% ethanol and 10% acetic acid) for 8 min. Then buffer II (30% ethanol, 10% sodium acetate, 0.3% acetic acid and 0.1% sodium thiosulfate) was added and incubated for 15 min. The gel was extensively washed with distilled water, first three times for 5 min each, then twice for 8 min each. Buffer III was added [0.1% silver nitrate ( $\text{AgNO}_3$ ), 3% ethanol and 0.024% formaldehyde], and incubated for 20 min. The gel was washed again using distilled water. Finally, the gel was incubated with buffer IV (2.5% sodium carbonate and 0.4% formaldehyde) until bands appear, changing the solution when it became oxidized. The reaction was stopped with 5% acetic acid.

### Densitometry

The band intensity of non-treated samples (N/T) and samples pre-treated with phalloidin (P) or cytochalasin D (CD) for each co-immunoprecipitation was measured using a scanner, and IMAGEJ version 1.46 (NIH, Bethesda, MD, USA). One-way ANOVA (Dunnett's multiple comparison test) was performed to compare the differences between the N/T band and the P or CD bands, respectively, using GRAPHPAD PRISM version 5 (GraphPad Software, Inc., La Jolla, CA, USA).

### Activity of glyceraldehyde-3-phosphate dehydrogenase

GAPDH activity was measured in 20 mM HEPES, 1 mM  $\text{MgCl}_2$ , 1 mM dithiothreitol and 1 mM EDTA, pH 7.5, in the presence of various concentrations of trehalose (0, 0.2, 0.4, 0.6, 0.8 and 1 M), 0.1 mM  $\text{NAD}^+$ , 8 mM phosphate-HEPES 7.5 and 9  $\mu\text{g}\cdot\text{mL}^{-1}$  GAPDH. After 15 s, 600  $\mu\text{M}$  glyceraldehyde 3-phosphate was added. NADH production was measured spectrophotometrically at 340 nm in an Aminco-Olis DW2000 spectrophotometer (Olis Inc., Bogart, GA, USA) [90].

### Activity of aldolase

The aldolase activity was measured in 10 mM sodium phosphate, 0.1 mM EDTA, pH 7.6, trehalose as indicated in the legend to each figure, 3.5 mM hydrazine hemisulfate, 0.1 mM fructose 1,6-bisphosphate and 9  $\mu\text{g}\cdot\text{mL}^{-1}$  ALD. Activity was quantified in an Aminco-Olis DW2000 spectrophotometer. Hydrazone was measured at 240 nm in an Aminco-Olis DW2000 spectrophotometer using an extinction coefficient of  $2.73 \times 10^3 \text{ M}^{-1}\cdot\text{cm}^{-1}$  [91].

### Activity of 3-phosphoglycerate phosphokinase

The 3-phosphoglycerate phosphokinase activity was measured in 20 mM HEPES, 1 mM  $\text{MgCl}_2$ , 1 mM dithiothreitol and 1 mM EDTA, pH 7.5, trehalose as indicated, 0.2 mM ATP, 1 mM PGK and 6 mM D-(–)-3-phosphoglyceric acid. Each test tube was incubated for 10 min at 30 °C, and 30% trichloroacetic acid was added. Then the samples were centrifuged at 5000  $\text{g}$  for 20 min, and neutralized using NaOH. Finally, 0.16 mM NADH and 9  $\mu\text{g}\cdot\text{mL}^{-1}$  GAPDH were added. Samples were incubated in a shaker bath (New Brunswick Scientific, Edison, NJ, USA) for 1 h at 20 °C. The reaction was stopped using 5% SDS. Pi was measured [92].

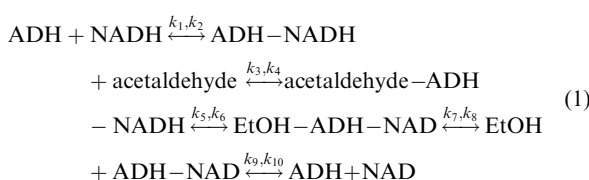
### Rate of fermentation

Ethanol production was measured by incubating permeabilized cells (5 mg ww per mL) or yeast cytoplasmic extract (1 mg protein·mL<sup>-1</sup>) in the presence of actin-targeting drugs such as 59  $\mu\text{M}$  phalloidin, 400  $\mu\text{M}$  cytochalasin D or

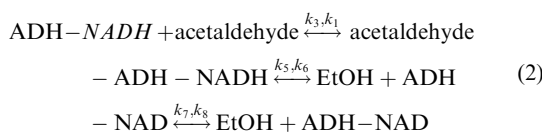
200  $\mu\text{M}$  latrunculin B, and in figure 8 48  $\text{mg}\cdot\text{mL}^{-1}$  antibodies against GAPDH, ALD or PGK [93]. The incubation buffer was 0.1 M MES/TEA, pH 7.0, 20 mM glucose; trehalose was added as indicated in the legend for each figure. The final volume was 2 mL. The reaction was stopped with 0.1 mL 30% trichloroacetic acid, and the sample was centrifuged at 676 g for 15 min at 20 °C. The supernatant was neutralized using NaOH, and ethanol was measured using an aliquot of 0.05 mL of the supernatant in 2 mL of 114 mM K<sub>2</sub>HPO<sub>4</sub>, pH 7.6, and 1.8 mM NAD<sup>+</sup>. After 10 s, 30  $\mu\text{g}\cdot\text{mL}^{-1}$  ADH was added, and absorbance was determined at 340 nm. The results are reported as  $\mu\text{mol}$  ethanol per mg cells (ww) for the permeabilized cells, or as  $\mu\text{mol}$  ethanol per mg protein for cytoplasmic extracts.

### Kinetic analysis for fermentation data

The enzyme kinetics for *S. cerevisiae* ADH display an ordered bi bi mechanism whereby NADH is bound first and then acetaldehyde, catalysis is performed, and ethanol is released followed by NAD [57] (Eqn 1); NAD release has been identified as the rate-limiting step for ADH [56]:



In our experiments, we measured the rate of ethanol production (Figs 6 and 7); the first product in the ADH catalytic cycle. Ethanol production kinetics exhibited an initial ‘burst’ that represents a rapid pre-steady state reaction of acetaldehyde with ADH-NADH to generate ethanol and the ADH-NAD complex. Then NAD is released in order to allow ADH to begin a new catalytic cycle [56,57]. The initial ‘burst’ originates when ADH is completely saturated with NADH, i.e. ADH-NADH is already present at the beginning of the reaction (Eqn 2). This reaction was observed mainly in permeabilized cells when the NADH concentration is high (Fig. 6A–C and Table S1) as a result of active glycolysis. In *S. cerevisiae*, Hald and Sørensen showed recently that the NADH concentration is increased immediately when glucose is added [72]; therefore, the first substrate for ADH is provided immediately and before acetaldehyde builds up at the end of the glycolytic pathway. Under these conditions, ADH behaves with an ordered uni bi mechanism (or uni uni mechanism for our experimental conditions) as shown in Eqn 2:



Thus, when glycolysis is not fully active under certain experimental conditions, the initial ‘burst’ is absent. Ethanol production data were fitted by non-linear regression to Eqn 3 using ORIGIN 6.0 software (OriginLab Corporation, Northampton, MA, USA):

$$[\text{EtOH}] = [\text{EtOH}]_0 + [\text{EtOH}]_b \cdot (1 - \exp(-k_b \cdot t)) + [\text{EtOH}]_{ss} \cdot (1 - \exp(-k_{ss} \cdot t)) \quad (3)$$

The reaction rate constant for the ‘burst’ is represented by  $k_b$ , which provides information about rate constants  $k_3$ ,  $k_4$ ,  $k_5$  and  $k_6$ , and the amount of ethanol synthesized is represented by its amplitude value,  $[\text{EtOH}]_b$ . After a few seconds, a steady-state reaction for ADH is established ( $k_{ss}$ ), and the amplitude  $[\text{EtOH}]_{ss}$  indicates the ethanol concentration reached. Therefore, the ‘burst’ amplitude shows the amount of ADH initially complexed to NADH before the ADH reaction attains the steady-state condition [58].

### Acknowledgements

This study was partially funded by grants Consejo Nacional de Ciencia y Tecnología 79989 and Dirección General de Asuntos de Personal Académico/Universidad Nacional Autónoma de México IN202612 to S.U.C., and Consejo Nacional de Ciencia y Tecnología 0156497 and Programa para el Mejoramiento del Profesorado Universidad Autónoma de San Luis Potosí-Folio-301 to J.G.S. D.A.O. is a Consejo Nacional de Ciencia y Tecnología fellow enrolled in the Biochemistry Graduate Program at the Universidad Nacional Autónoma de México. Armando Zepeda-Bastida participated in the discussion and design of experiments. We thank Ramón Méndez-Franco for technical assistance.

### References

- Ellis RJ & Minton AP (2003) Cell biology: join the crowd. *Nature* **425**, 27–28.
- Ovadi J & Saks V (2004) On the origin of intracellular compartmentation and organized metabolic systems. *Mol Cell Biochem* **256–257**, 5–12.
- Chebotareva NA (2007) Effect of molecular crowding on the enzymes of glycogenolysis. *Biochemistry (Mosc)* **72**, 1478–1490.
- Green DE, Murer E, Hultin HO, Richardson SH, Salmon B, Brierley GP & Baum H (1965) Association of integrated metabolic pathways with membranes. I. Glycolytic enzymes of the red blood corpuscle and yeast. *Arch Biochem Biophys* **112**, 635–647.

- 5 Clegg JS (1984) Properties and metabolism of the aqueous cytoplasm and its boundaries. *Am J Physiol* **246**, R133–R151.
- 6 Srere PA (1987) Complexes of sequential metabolic enzymes. *Annu Rev Biochem* **56**, 89–124.
- 7 Graham JW, Williams TC, Morgan M, Fernie AR, Ratcliffe RG & Sweetlove LJ (2007) Glycolytic enzymes associate dynamically with mitochondria in response to respiratory demand and support substrate channeling. *Plant Cell* **19**, 3723–3738.
- 8 Ovadi J & Srere PA (2000) Macromolecular compartmentation and channeling. *Int Rev Cytol* **192**, 255–280.
- 9 Møller BL & Conn EE (1980) The biosynthesis of cyanogenic glucosides in higher plants. Channeling of intermediates in dhurrin biosynthesis by a microsomal system from *Sorghum bicolor* (Linn) Moench. *J Biol Chem* **255**, 3049–3056.
- 10 Han JW, Thieleczek R, Varsanyi M & Heilmeyer LM Jr (1992) Compartmentalized ATP synthesis in skeletal muscle triads. *Biochemistry* **31**, 377–384.
- 11 Srere PA & Ovadi J (1990) Enzyme–enzyme interactions and their metabolic role. *FEBS Lett* **268**, 360–364.
- 12 Jorgensen K, Rasmussen AV, Morant M, Nielsen AH, Bjarnholt N, Zagrobelny M, Bak S & Møller BL (2005) Metabolon formation and metabolic channeling in the biosynthesis of plant natural products. *Curr Opin Plant Biol* **8**, 280–291.
- 13 Cheung CW, Cohen NS & Rajzman L (1989) Channeling of urea cycle intermediates *in situ* in permeabilized hepatocytes. *J Biol Chem* **264**, 4038–4044.
- 14 Shatalin K, Lebreton S, Rault-Leonardon M, Velot C & Srere PA (1999) Electrostatic channeling of oxaloacetate in a fusion protein of porcine citrate synthase and porcine mitochondrial malate dehydrogenase. *Biochemistry* **38**, 881–889.
- 15 Vértesy B & Ovádi J (1987) A simple approach to detect active-site-directed enzyme–enzyme interactions. The aldolase/glycerol-phosphate-dehydrogenase enzyme system. *Eur J Biochem* **164**, 655–659.
- 16 Clegg JS & Jackson SA (1990) Glucose metabolism and the channeling of glycolytic intermediates in permeabilized L-929 cells. *Arch Biochem Biophys* **278**, 452–460.
- 17 Uhrig JF (2006) Protein interaction networks in plants. *Planta* **224**, 771–781.
- 18 Keleti T & Ovadi J (1988) Control of metabolism by dynamic macromolecular interactions. *Curr Top Cell Regul* **29**, 1–33.
- 19 Ryazanov AG, Ashmarina LI & Muronetz VI (1988) Association of glyceraldehyde-3-phosphate dehydrogenase with mono- and polyribosomes of rabbit reticulocytes. *Eur J Biochem* **171**, 301–305.
- 20 Martin LJ, Adams NA, Pan Y, Price A & Wong M (2011) The mitochondrial permeability transition pore regulates nitric oxide-mediated apoptosis of neurons induced by target deprivation. *J Neurosci* **31**, 359–370.
- 21 Botstein D (1988) Why study the cytoskeleton in yeast? *Harvey Lect* **82**, 157–167.
- 22 Michelot A & Drubin DG (2011) Building distinct actin filament networks in a common cytoplasm. *Curr Biol* **21**, R560–R569.
- 23 Moseley JB & Goode BL (2006) The yeast actin cytoskeleton: from cellular function to biochemical mechanism. *Microbiol Mol Biol Rev* **70**, 605–645.
- 24 Balasubramanian MK, Bi E & Glotzer M (2004) Comparative analysis of cytokinesis in budding yeast, fission yeast and animal cells. *Curr Biol* **14**, R806–R818.
- 25 Engqvist-Goldstein AE & Drubin DG (2003) Actin assembly and endocytosis: from yeast to mammals. *Annu Rev Cell Dev Biol* **19**, 287–332.
- 26 Ayscough KR & Drubin DG (1996) Actin: general principles from studies in yeast. *Annu Rev Cell Dev Biol* **12**, 129–160.
- 27 Pollard TD & Borisy GG (2003) Cellular motility driven by assembly and disassembly of actin filaments. *Cell* **112**, 453–465.
- 28 Kovar DR, Sirotkin V & Lord M (2010) Three's company: the fission yeast actin cytoskeleton. *Trends Cell Biol* **21**, 177–187.
- 29 Arnold H, Henning R & Pette D (1971) Quantitative comparison of the binding of various glycolytic enzymes to F-actin and the interaction of aldolase with G-actin. *Eur J Biochem* **22**, 121–126.
- 30 Waingeh VF, Gustafson CD, Kozliak EI, Lowe SL, Knull HR & Thomasson KA (2006) Glycolytic enzyme interactions with yeast and skeletal muscle F-actin. *Biophys J* **90**, 1371–1384.
- 31 Knull HR (1985) Extraction of glycolytic enzymes: myo-inositol as a marker of membrane porosity. *J Neurochem* **45**, 1433–1440.
- 32 Al-Habori M (1995) Microcompartmentation, metabolic channelling and carbohydrate metabolism. *Int J Biochem Cell Biol* **27**, 123–132.
- 33 Puchulu-Campanella E, Chu H, Anstee DJ, Galan JA, Tao WA & Low PS (2013) Identification of the components of a glycolytic enzyme metabolon on the human red blood cell membrane. *J Biol Chem* **288**, 848–858.
- 34 Poglavov BF & Livanova NB (1986) Interaction of actin with the enzymes of carbohydrate metabolism. *Adv Enzyme Regul* **25**, 297–305.
- 35 Walsh JL, Keith TJ & Knull HR (1989) Glycolytic enzyme interactions with tubulin and microtubules. *Biochim Biophys Acta* **999**, 64–70.
- 36 Knull HR & Walsh JL (1992) Association of glycolytic enzymes with the cytoskeleton. *Curr Top Cell Regul* **33**, 15–30.

- 37 Walsh TP, Clarke FM & Masters CJ (1977) Modification of the kinetic parameters of aldolase on binding to the actin-containing filaments of skeletal muscle. *Biochem J* **165**, 165–167.
- 38 Pette D (1975) Some aspects of supramolecular organization of glycogenolytic and glycolytic enzymes in muscle. *Acta Histochem Suppl* **14**, 47–68.
- 39 Poglavov BF, Livanova NB & Ostrovskaia MV (1982) Actin interaction with phosphorylase kinase. *Dokl Akad Nauk SSSR* **263**, 221–224 (article in Russian).
- 40 Bronstein WW & Knull HR (1981) Interaction of muscle glycolytic enzymes with thin filament proteins. *Can J Biochem* **59**, 494–499.
- 41 Masters CJ (1981) Interactions between soluble enzymes and subcellular structure. *CRC Crit Rev Biochem* **11**, 105–143.
- 42 Lehotzky A, Telegi M, Liliom K & Ovadi J (1993) Interaction of phosphofructokinase with tubulin and microtubules. Quantitative evaluation of the mutual effects. *J Biol Chem* **268**, 10888–10894.
- 43 Ouporov IV, Knull HR & Thomasson KA (1999) Brownian dynamics simulations of interactions between aldolase and G- or F-actin. *Biophys J* **76**, 17–27.
- 44 Ouporov IV, Knull HR, Lowe SL & Thomasson KA (2001) Interactions of glyceraldehyde-3-phosphate dehydrogenase with G- and F-actin predicted by Brownian dynamics. *J Mol Recognit* **14**, 29–41.
- 45 Clarke FM & Masters CJ (1975) On the association of glycolytic enzymes with structural proteins of skeletal muscle. *Biochim Biophys Acta* **381**, 37–46.
- 46 Kurganova BI, Sugrobova NP & Mil'man LS (1985) Supramolecular organization of glycolytic enzymes. *J Theor Biol* **116**, 509–526.
- 47 Araiza-Olivera D, Sampedro JG, Mujica A, Pena A & Uribe-Carvajal S (2010) The association of glycolytic enzymes from yeast confers resistance against inhibition by trehalose. *FEMS Yeast Res* **10**, 282–289.
- 48 van Eunen K, Kiewiet JA, Westerhoff HV & Bakker BM (2012) Testing biochemistry revisited: how *in vivo* metabolism can be understood from *in vitro* enzyme kinetics. *PLoS Comput Biol* **8**, e1002483.
- 49 Mendes P & Kell DB (2001) MEG (Model Extender for Gepasi): a program for the modelling of complex, heterogeneous, cellular systems. *Bioinformatics* **17**, 288–289.
- 50 Ovadi J & Srere PA (1996) Metabolic consequences of enzyme interactions. *Cell Biochem Funct* **14**, 249–258.
- 51 Vertessy BG, Orosz F, Kovacs J & Ovadi J (1997) Alternative binding of two sequential glycolytic enzymes to microtubules. Molecular studies in the phosphofructokinase/aldolase/microtubule system. *J Biol Chem* **272**, 25542–25546.
- 52 Rais B, Ortega F, Puigjaner J, Comin B, Orosz F, Ovadi J & Cascante M (2000) Quantitative characterization of homo- and heteroassociations of muscle phosphofructokinase with aldolase. *Biochim Biophys Acta* **1479**, 303–314.
- 53 Ouporov IV, Knull HR, Huber A & Thomasson KA (2001) Brownian dynamics simulations of aldolase binding glyceraldehyde 3-phosphate dehydrogenase and the possibility of substrate channeling. *Biophys J* **80**, 2527–2535.
- 53a Konte T & Plemenitas A (2013) The HOG signal pathway in the halophilic fungus *Wallemia ichtyophaga*: identification and characterization of MAP kinases WiHog1A and WiHog1B. *Extremophiles* **17**, 623–636.
- 54 Mejean C, Pons F, Benyamin Y & Roustan C (1989) Antigenic probes locate binding sites for the glycolytic enzymes glyceraldehyde-3-phosphate dehydrogenase, aldolase and phosphofructokinase on the actin monomer in microfilaments. *Biochem J* **264**, 671–677.
- 55 Kustermans G, Piette J & Legrand-Poels S (2008) Actin-targeting natural compounds as tools to study the role of actin cytoskeleton in signal transduction. *Biochem Pharmacol* **76**, 1310–1322.
- 55a Kahn AR (2013) Oligomerization of rab/effectors complexes in the regulation of vesicular trafficking. *Prog Mol Biol Transl Sci* **117**, 579–614.
- 56 Dickinson FM & Monger GP (1973) A study of the kinetics and mechanism of yeast alcohol dehydrogenase with a variety of substrates. *Biochem J* **131**, 261–270.
- 57 Ganzhorn AJ, Green DW, Hershey AD, Gould RM & Plapp BV (1987) Kinetic characterization of yeast alcohol dehydrogenases. Amino acid residue 294 and substrate specificity. *J Biol Chem* **262**, 3754–3761.
- 58 Segel IH (1993) Enzyme Kinetics. Wiley, New York.
- 59 Schwock J, Kirchberger J, Edelmann A, Kriegel TM & Kopperschlager G (2004) Interaction of 6-phosphofructokinase with cytosolic proteins of *Saccharomyces cerevisiae*. *Yeast* **21**, 483–494.
- 60 Volker KW & Knull H (1997) A glycolytic enzyme binding domain on tubulin. *Arch Biochem Biophys* **338**, 237–243.
- 61 Walsh JL & Knull HR (1988) Heteromeric interactions among glycolytic enzymes and of glycolytic enzymes with F-actin: effects of poly(ethylene glycol). *Biochim Biophys Acta* **952**, 83–91.
- 62 Lowe SL, Atkinson DM, Waingeh VF & Thomasson KA (2002) Brownian dynamics of interactions between aldolase mutants and F-actin. *J Mol Recognit* **15**, 423–431.
- 63 Lowe SL, Adrian C, Ouporov IV, Waingeh VF & Thomasson KA (2003) Brownian dynamics simulations of glycolytic enzyme subsets with F-actin. *Biopolymers* **70**, 456–470.

- 64 O'Reilly G & Clarke F (1993) Identification of an actin binding region in aldolase. *FEBS Lett* **321**, 69–72.
- 65 Keleti T, Ovadi J & Batke J (1989) Kinetic and physico-chemical analysis of enzyme complexes and their possible role in the control of metabolism. *Prog Biophys Mol Biol* **53**, 105–152.
- 66 Keller A, Peltzer J, Carpentier G, Horvath I, Olah J, Duchesnay A, Orosz F & Ovadi J (2007) Interactions of enolase isoforms with tubulin and microtubules during myogenesis. *Biochim Biophys Acta* **1770**, 919–926.
- 67 Ocon A, Hampp R & Requena N (2007) Trehalose turnover during abiotic stress in arbuscular mycorrhizal fungi. *New Phytol* **174**, 879–891.
- 68 Kaushik JK & Bhat R (2003) Why is trehalose an exceptional protein stabilizer? An analysis of the thermal stability of proteins in the presence of the compatible osmolyte trehalose. *J Biol Chem* **278**, 26458–26465.
- 69 Sampedro JG & Uribe S (2004) Trehalose–enzyme interactions result in structure stabilization and activity inhibition. The role of viscosity. *Mol Cell Biochem* **256–257**, 319–327.
- 69a Kramers HA (1940) Brownian motion in a field of force and the diffusion model of chemical reactions. *Physica*, **7**, 284–304.
- 70 Attfield PV (1987) Trehalose accumulates in *Saccharomyces cerevisiae* during exposure to agents that induce heat shock response. *FEBS Lett* **225**, 259–263.
- 71 Wera S, De Schrijver E, Geuskens I, Nwaka S & Thevelein JM (1999) Opposite roles of trehalase activity in heat-shock recovery and heat-shock survival in *Saccharomyces cerevisiae*. *Biochem J* **343**, 621–626.
- 72 Hald BO & Sørensen PG (2010) Modeling diauxic glycolytic oscillations in yeast. *Biophys J* **99**, 3191–3199.
- 73 Villali J & Kern D (2010) Choreographing an enzyme's dance. *Curr Opin Chem Biol* **14**, 636–643.
- 74 Henson MA, Muller D & Reuss M (2002) Cell population modelling of yeast glycolytic oscillations. *Biochem J* **368**, 433–446.
- 75 Hynne F, Danø S & Sørensen PG (2001) Full-scale model of glycolysis in *Saccharomyces cerevisiae*. *Biophys Chem* **94**, 121–163.
- 76 Danø S, Hynne F, De Monte S, d'Ovidio F, Sørensen PG & Westerhoff H (2001) Synchronization of glycolytic oscillations in a yeast cell population. *Faraday Discuss*, 261–276; discussion 325–351.
- 77 Richard P, Diderich JA, Bakker BM, Teusink B, van Dam K & Westerhoff HV (1994) Yeast cells with a specific cellular make-up and an environment that removes acetaldehyde are prone to sustained glycolytic oscillations. *FEBS Lett* **341**, 223–226.
- 78 Richard P, Teusink B, Hemker MB, Van Dam K & Westerhoff HV (1996) Sustained oscillations in free-energy state and hexose phosphates in yeast. *Yeast* **12**, 731–740.
- 79 Teusink B, Passarge J, Reijenga CA, Esgalhado E, van der Weijden CC, Schepper M, Walsh MC, Bakker BM, van Dam K, Westerhoff HV *et al.* (2000) Can yeast glycolysis be understood in terms of *in vitro* kinetics of the constituent enzymes? Testing biochemistry. *Eur J Biochem* **267**, 5313–5329.
- 80 Lemasters JJ & Holmuhamedov E (2006) Voltage-dependent anion channel (VDAC) as mitochondrial governor – thinking outside the box. *Biochim Biophys Acta* **1762**, 181–190.
- 81 Clegg JS & Jackson SA (1989) Evidence for intermediate channelling in the glycolytic pathway of permeabilized L-929 cells. *Biochem Biophys Res Commun* **160**, 1409–1414.
- 82 Pasten-Hidalgo K, Hernandez-Rivas R, Roa-Espitia AL, Sanchez-Gutierrez M, Martinez-Perez F, Monrroy AO, Hernandez-Gonzalez EO & Mujica A (2008) Presence, processing, and localization of mouse ADAM15 during sperm maturation and the role of its disintegrin domain during sperm–egg binding. *Reproduction* **136**, 41–51.
- 83 Lebedeva N, Auffret Vander Kemp P, Bjornsti MA, Lavrik O & Boiteux S (2006) Trapping of DNA topoisomerase I on nick-containing DNA in cell free extracts of *Saccharomyces cerevisiae*. *DNA Repair (Amst)* **5**, 799–809.
- 84 Gornall AG, Bardawill CJ & David MM (1949) Determination of serum proteins by means of the biuret reaction. *J Biol Chem* **177**, 751–766.
- 85 Zechel K (1980) Isolation of polymerization-competent cytoplasmic actin by affinity chromatography on immobilized DNase I using formamide as eluant. *Eur J Biochem* **110**, 343–348.
- 86 Bradford MM (1976) A rapid and sensitive method for the quantitation of microgram quantities of protein utilizing the principle of protein–dye binding. *Anal Biochem* **72**, 248–254.
- 87 Chiquete-Felix N, Hernandez JM, Mendez JA, Zepeda-Bastida A, Chagolla-Lopez A & Mujica A (2009) In guinea pig sperm, aldolase A forms a complex with actin, WAS, and Arp2/3 that plays a role in actin polymerization. *Reproduction* **137**, 669–678.
- 88 Laemmli UK (1970) Cleavage of structural proteins during the assembly of the head of bacteriophage T4. *Nature* **227**, 680–685.
- 89 Towbin H, Staehelin T & Gordon J (1979) Electrophoretic transfer of proteins from polyacrylamide gels to nitrocellulose sheets: procedure and some applications. *Proc Natl Acad Sci USA* **76**, 4350–4354.
- 90 Bergmeyer HU (1983) *Methods of Enzymatic Analysis*, pp. 202–203. John Wiley and Sons, New York, USA.

- 91 Sygusch J & Beaudry D (1984) Catalytic activity of rabbit skeletal muscle aldolase in the crystalline state. *J Biol Chem* **259**, 10222–10227.
- 92 Katewa SD & Katyare SS (2003) A simplified method for inorganic phosphate determination and its application for phosphate analysis in enzyme assays. *Anal Biochem* **323**, 180–187.
- 93 Zepeda-Bastida A, Chiquete-Felix N, Uribe-Carvajal S & Mujica A (2010) The acrosomal matrix from guinea pig sperm contains structural proteins, suggesting the presence of an actin skeleton. *J Androl* **32**, 411–419.

## Supporting information

Additional supporting information may be found in the online version of this article at the publisher's web site:

**Fig. S1.** Lack of ALD association with DNase I.

**Table S1.** Kinetic parameters for fermentation by permeabilized cells (experimental data in Fig. 7).

**Table S2.** Kinetic parameters for fermentation by cytoplasmic extracts (experimental data in Fig. 8).



# The branched mitochondrial respiratory chain from *Debaryomyces hansenii*: Components and supramolecular organization

Alfredo Cabrera-Orefice, Natalia Chiquete-Félix, Juan Espinasa-Jaramillo, Mónica Rosas-Lemus, Sergio Guerrero-Castillo, Antonio Peña, Salvador Uribe-Carvajal \*

Dept. of Molecular Genetics, Instituto de Fisiología Celular, Universidad Nacional Autónoma de México, Mexico City, Mexico



## ARTICLE INFO

### Article history:

Received 12 June 2013

Received in revised form 23 July 2013

Accepted 25 July 2013

Available online 7 August 2013

### Keywords:

Respiratory chain

*Debaryomyces hansenii*

Alternative oxidase

Alternative NADH dehydrogenase

Glycerol-phosphate dehydrogenase

Supercomplexes

## ABSTRACT

The branched respiratory chain in mitochondria from the halotolerant yeast *Debaryomyces hansenii* contains the classical complexes I, II, III and IV plus a cyanide-insensitive, AMP-activated, alternative-oxidase (AOX). Two additional alternative oxidoreductases were found in this organism: an alternative NADH dehydrogenase (NDH2e) and a mitochondrial isoform of glycerol-phosphate dehydrogenase (<sub>Mit</sub>GPDH). These monomeric enzymes lack proton pump activity. They are located on the outer face of the inner mitochondrial membrane. NDH2e oxidizes exogenous NADH in a rotenone-insensitive, flavone-sensitive, process. AOX seems to be constitutive; nonetheless, most electrons are transferred to the cytochrome pathway. Respiratory supercomplexes containing complexes I, III and IV in different stoichiometries were detected. Dimeric complex V was also detected. In-gel activity of NADH dehydrogenase, mass spectrometry, and cytochrome c oxidase and ATPase activities led to determine the composition of the putative supercomplexes. Molecular weights were estimated by comparison with those from the yeast *Y. lipolytica* and they were IV<sub>2</sub>, I–IV, III<sub>2</sub>–IV<sub>4</sub>, V<sub>2</sub>, I–III<sub>2</sub>, I–III<sub>2</sub>–IV, I–III<sub>2</sub>–IV<sub>2</sub>, I–III<sub>2</sub>–IV<sub>3</sub> and I–III<sub>2</sub>–IV<sub>4</sub>. Binding of the alternative enzymes to supercomplexes was not detected. This is the first report on the structure and organization of the mitochondrial respiratory chain from *D. hansenii*.

© 2013 Elsevier B.V. All rights reserved.

## 1. Introduction

The halotolerant, non-pathogenic, oleaginous yeast *Debaryomyces hansenii* is found in the sea and other hyperosmotic habitats [1,2]. *D. hansenii* grows in various environmental conditions including different salt concentrations [3–5], low temperatures [3] and different pHs [3,6]. In addition, *D. hansenii* assimilates many different carbon sources [7–9]. The ability of this yeast to synthesize and store lipids is used in biotechnology to make products of commercial interest, such as cheese [2,10].

*D. hansenii* has high aerobic metabolism and low fermentative activity which are enhanced by high extracellular NaCl or KCl [11–13]. Isolated *D. hansenii* mitochondria undergo permeability transition due to the opening of a mitochondrial unspecific channel (MUC) [14]. Both, the MUCs from *D. hansenii* (<sub>Dh</sub>MUC) and *S. cerevisiae* (<sub>Sc</sub>MUC) are

regulated by effectors such as phosphate, Mg<sup>2+</sup> or Ca<sup>2+</sup> [14–19]. The <sub>Dh</sub>MUC is the only MUC reported to date that is closed by Na<sup>+</sup> or K<sup>+</sup> [14] probably accounting for the monovalent cation coupling effects observed in whole yeast [12,13].

The mammalian oxidative phosphorylation system contains the four “orthodox” respiratory complexes (I, II, III and IV) plus the F<sub>1</sub>F<sub>0</sub>-ATP synthase (complex V) [20]. In addition to the above, mitochondria from plants, fungi, protozoa and some animals may contain “alternative” redox enzymes that substitute or coexist with the classical complexes; e.g. alternative NADH dehydrogenases and oxidases [21–25]. In fungi a mammalian-like respiratory complex may be substituted by an alternative enzyme, e.g. in *S. cerevisiae* complex I the oxidoreductase activity was substituted by an internal alternative NADH dehydrogenase [26,27].

The fungal alternative oxidases (AOXs) are single subunit proteins bound to the matrix side of the inner mitochondrial membrane (IMM) [28–31]. The cyanide-resistant AOX transfers electrons from ubiquinol to oxygen. AOX is inhibited by hydroxamic acids and by n-alkyl-gallates [29,32]. The presence of AOX constitutes an uncoupled branch of the respiratory chain probably designed to prevent substrate overload and overproduction of reactive oxygen species (ROS) [25,28,33–36].

Alternative type II NADH dehydrogenases (NDH2s) transfer electrons from NADH to ubiquinone without pumping protons [37]. NDH2s are monomeric proteins bound to the inner (NDH2i) or the outer (NDH2e) face of IMM [21,37]. NDH2s are not sensitive to rotenone, but instead are specifically inhibited by flavone [38].

**Abbreviations:** ADP, adenosine diphosphate; AMP, adenosine monophosphate; AOX, alternative oxidase; BN, blue-native; COX, cytochrome c oxidase; CRR, cyanide-resistant respiration; Dig, digitonin; IMM, inner mitochondrial membrane; LC-MS, liquid chromatography mass spectrometry; LM, laurylmaltoside; <sub>Mit</sub>GPDH, glycerol-phosphate dehydrogenase (mitochondrial isoform); MUC, mitochondrial unspecific channel; MW, molecular weight; NDH, NADH dehydrogenase activity; NDH2e, alternative external NADH dehydrogenase; PAGE, polyacrylamide-gel electrophoresis; PG, propyl-gallate; ROS, reactive oxygen species; SDS, sodium dodecyl sulfate; 2D, second dimension

\* Corresponding author at: Departamento de Genética Molecular, Instituto de Fisiología Celular, Universidad Nacional Autónoma de México, Ciudad Universitaria, Apdo. Postal 70-242, Mexico City, Mexico. Tel.: +52 55 5622 5632; fax: +52 55 5622 5630.

E-mail address: [suribe@ifc.unam.mx](mailto:suribe@ifc.unam.mx) (S. Uribe-Carvajal).

The mitochondrial isoform of glycerol-phosphate dehydrogenase ( $M_{\text{Mit}}\text{GPDH}$ ) is another component of branched respiratory chains [39,40].  $M_{\text{Mit}}\text{GPDH}$  oxidizes glycerol-phosphate to dihydroxyacetone-phosphate and reduces ubiquinone. Also, this protein is located on the outer face of the IMM [41]. The peripheral proteins NDH2s,  $M_{\text{Mit}}\text{GPDH}$  and AOX are not proton pumps [21,29,40].

Two major models describe the structure/function relationship of the respiratory chain. The *fluid* or *random collision* model proposes that respiratory complexes float freely within the IMM and electron transport occurs through the diffusible carriers ubiquinone and cytochrome c [42]. On the other hand, the *solid* model proposes that respiratory complexes are organized into stable hetero-oligomers (supercomplexes or “respirasomes”) that channel electrons between them [43–46]. There are data that support each model [47]. Kinetic studies show that each respiratory complex can be purified individually, retaining activity [42]. By contrast, blue native gel polyacrylamide electrophoresis (BN-PAGE) reveals the existence of supercomplexes composed of several respiratory complexes [48]. Respiratory supercomplexes can be observed when solubilizing mitochondrial membranes with small amounts of mild detergents such as digitonin [44]. The presence of respiratory supercomplexes has been well documented in mammals [48,49], plants [43,46,50] and different yeast species [51–54]. Additionally, a third model has been proposed: the *plasticity* model, where respiratory complexes undergo a dynamic association-dissociation process and isolated supercomplexes transfer electrons from NADH to oxygen [55]. The plasticity model suggests that complex association/dissociation regulates oxidative phosphorylation [55,56].

Here, the mitochondrial respiratory chain of *D. hansenii*, which has been reported to contain all four mammalian-like respiratory complexes [57] plus a putative stationary-phase-inducible AOX, was characterized [58,59]. This branched respiratory chain contains all the complexes reported [59] plus an external NDH2 and a glycerol-phosphate dehydrogenase. In addition, association of these complexes in different supercomplexes was observed.

## 2. Materials and methods

### 2.1. Chemicals

All chemicals were reagent grade. D-sorbitol, D-mannitol, D-glucose, D-galactose, glycerol, Trizma® base (Tris), malic acid, pyruvic acid, citric acid, maleic acid, DL- $\alpha$ -glycerophosphate, NADH, ATP, ADP, rotenone, flavone, antimycin A, propyl-gallate, digitonin, *n*-dodecyl  $\beta$ -D-maltoside (laurylmaltoside), Nitrotetrazolium blue chloride and antifoam A were from Sigma Chem Co. (St Louis, MO). Bovine serum albumin (Probulmin™) was from Millipore. Yeast extract and bacto-peptone were from BD Bioxon. DL-lactic acid,  $H_3PO_4$ , NaCN, KCl,  $MgCl_2$  and ethanol were from J.T. Baker. 3,3'-Diaminobenzidine tetrahydrochloride hydrate was from Fluka. Coomassie Blue G was from SERVA (Heidelberg, Germany). Coomassie® brilliant blue G-250 and electrophoresis reagents were from BIO-RAD (Richmond, CA).

### 2.2. Biologicals

*D. hansenii* Y7426 strain (US Dept. of Agriculture) was used throughout this work. The strain was maintained in YPGal-NaCl (1% yeast extract, 2% bacto-peptone, 2% D-galactose, 1 M NaCl and 2% bacto agar) plate cultures. *Yarrowia lipolytica* E150 strain was also used. This strain was maintained in YD (1% yeast extract and 2% D-glucose and 2% bacto agar) plate cultures.

### 2.3. Yeast culture and isolation of coupled mitochondria

*D. hansenii* cells were grown as follows: pre-cultures were prepared inoculating 100 mL of YPLac-NaCl medium (1% yeast extract, 2% bacto-peptone, 2% lactic acid, pH 5.5 adjusted with NaOH and adding NaCl to

reach 0.6 M  $Na^+$ ) containing antifoam A emulsion 50  $\mu$ L/L. Pre-cultures were grown for 36 h under continuous agitation in an orbital shaker at 250 rpm at 29 °C. Then, each pre-culture was used to inoculate a 750 mL flask with the same medium. Incubation was continued for 24 h (i.e. medium to late logarithmic phase). *D. hansenii* mitochondria were isolated as reported previously [14]. Mitochondria from *Y. lipolytica* were isolated as in [51].

### 2.4. Protein quantification

Mitochondrial protein was measured by the Biuret method [60]. Absorbance was determined at 540 nm in a Beckman DU-50 spectrophotometer. Bovine serum albumin was used as a standard.

### 2.5. Oxygen consumption

The rate of oxygen consumption was measured in a YSI-5300 Oxygraph equipped with a Clark-Type electrode (Yellow Springs Instruments Inc., OH) interfaced to a chart recorder. The sample was placed in a water-jacketed chamber at 30 °C. The phosphorylating state (III) was induced with 0.5 mM ADP. The reaction mixture was 1 M sorbitol, 10 mM maleate (pH was adjusted to 6.8 with Tris), 10 mM Tris-phosphate (Pi), 0.5 mM  $MgCl_2$  and 75 mM KCl. Mitochondrial protein (Prot) was 0.5 mg/mL; final volume was 1.5 mL. The concentrations of different respiratory substrates and inhibitors are indicated in the legends to the figures.

### 2.6. Blue native (BN) and 2D SDS-Tricine electrophoresis

BN-PAGE was performed as described in the literature [49]. The mitochondrial pellet was suspended in sample buffer (750 mM aminocaproic acid, 25 mM imidazole (pH 7.0)) and solubilized with 2.0 mg *n*-dodecyl- $\beta$ -D-maltoside (laurylmaltoside, LM)/mg Prot, or 4.0 mg digitonin (Dig)/mg Prot at 4 °C for 1 h and centrifuged at 33,000 rpm at 4 °C for 25 min. The supernatants were loaded on 4–12% (w/v) polyacrylamide gradient gels. Protein, 0.25 or 0.5 mg per lane was added to 8.5 × 6 cm or 17 × 12 cm gel sizes, respectively. The stacking gel contained 4% (w/v) polyacrylamide. Also, 0.025% digitonin was added to the gel preparation to improve protein band definition [61]. For 2D SDS-Tricine-PAGE, complete lanes from the BN-gels were loaded on 12% polyacrylamide gels to resolve the subunits that constitute each complex. 2D-gels were subjected to Coomassie-staining [61] and silver-staining [62,63]. Apparent molecular weights were estimated using Benchmark Protein (Invitrogen, CA) and Precision Plus Protein™ (BIO-RAD, Richmond, CA) standards.

### 2.7. In-gel enzymatic activities

In-gel NADH/nitrotetrazolium blue chloride (NTB) oxidoreductase activity was determined incubating native gels in a mixture of 10 mM Tris (pH 7.0), 0.5 mg NTB/mL and 1 mM NADH [64]. Inhibitors such as rotenone and flavone were not able to act on their target enzymes in the gel assays, probably due to dilution into the BN-gel incubation medium, their hydrophobicity or their specific inhibition sites on the protein i.e. the indicator (NTB) seems to receive electrons from flavin prosthetic groups [65], far from the inhibitor blocking sites (near the ubiquinone site) [66,67] (result not shown). In-gel cytochrome c oxidase (COX) activity was determined using diaminobenzidine and cytochrome c [68]. Cyanide was useful to inhibit COX (Result not shown), but cannot be used to unveil the alternative oxidase because there is no method available to measure AOX in-gel activity. In-gel ATPase activity was measured as in [61]. Oligomycin was not able to inhibit this activity (Result not shown) as previously reported in [68].

**Table 1**

Rates of oxygen consumption in isolated mitochondria from *D. hansenii* in the presence of different respiratory substrates and inhibitors.

Substrate and other additions	Rate of oxygen consumption (natgO · (min · mg Prot) <sup>-1</sup> )	Respiratory control (III/IV)
Pyruvate (10 mM) + malate (10 mM)	123 ± 10*	2.36 ± 0.07
+ ADP (500 µM)	290 ± 7**	
+ Rotenone (50 µM)	8 ± 1	
+ Flavone (500 µM)	114 ± 5	
+ Antimycin-A (5 µM)	32 ± 3	
+ NaCN (500 µM)	33 ± 2	
+ Propyl-gallate (100 µM)	108 ± 6	
Citrate (10 mM) + malate (10 mM)	138 ± 10*	2.17 ± 0.05
+ ADP (500 µM)	299 ± 12**	
+ Rotenone (50 µM)	11 ± 2	
+ Flavone (500 µM)	135 ± 5	
+ Antimycin-A (5 µM)	41 ± 3	
+ NaCN (500 µM)	39 ± 2	
+ Propyl-gallate (100 µM)	128 ± 6	
Succinate (10 mM)	143 ± 11*	1.64 ± 0.08
+ ADP (500 µM)	235 ± 14**	
+ Rotenone (50 µM)	144 ± 9	
+ Flavone (500 µM)	143 ± 11	
+ Antimycin-A (5 µM)	38 ± 3	
+ NaCN (500 µM)	39 ± 5	
+ Propyl-gallate (100 µM)	117 ± 4	
NADH (1 mM)	258 ± 9*	1.23 ± 0.05
+ ADP (500 µM)	317 ± 12**	
+ Rotenone (50 µM)	243 ± 10	
+ Flavone (500 µM)	28 ± 14	
+ Antimycin-A (5 µM)	65 ± 3	
+ NaCN (500 µM)	65 ± 4	
+ Propyl-gallate (100 µM)	204 ± 4	
Glycerol-phosphate (10 mM)	216 ± 10*	1.28 ± 0.03
+ ADP (500 µM)	276 ± 11**	
+ Rotenone (50 µM)	216 ± 10	
+ Flavone (500 µM)	216 ± 10	
+ Antimycin-A (5 µM)	39 ± 3	
+ NaCN (500 µM)	37 ± 3	
+ Propyl-gallate (100 µM)	188 ± 7	

The rates of oxygen consumption were measured in resting state (IV)\* and phosphorylating state (III)\*\*. The phosphorylating state was induced with ADP. Rates of oxygen consumption in the presence of inhibitors were measured after a steady state was reached. Reaction mixture: 1 M sorbitol, 75 mM KCl, 10 mM Tris-phosphate, 1 mM MgCl<sub>2</sub> and 10 mM maleic acid, pH 6.8 (Tris). Mitochondria 0.5 mg Prot · (mL)<sup>-1</sup> were added in each assay. Temperature 30 °C. Final volume 1.5 mL. Data from five independent experiments are expressed as the mean ± SD.

## 2.8. Protein search, alignment and sequence analysis

We used the BLAST website and the NCBI database to search and compare protein sequences from alternative respiratory enzymes. We used the known protein sequences from other yeasts [69–71] to search for possible NDH2s, AOXs and/or MitGPDHs in the *D. hansenii* NCBI database. The identified *D. hansenii* sequences were aligned against those from *S. cerevisiae*, *Y. lipolytica* and/or *C. albicans* using Clustal W 2.0 [72]. The BLAST analysis also indicated the percentages of identity and similarity between amino acid sequences.

## 2.9. Western blotting

Mitochondrial samples were diluted in 0.5 mL sample buffer (500 mM Tris pH 6.8, 10% glycerol, 10% SDS, 0.05% 2-β-mercaptoethanol and 0.01% bromophenol blue) and boiled for 5 min [73]. SDS-Tricine-PAGE was performed in a 10% polyacrylamide gel. Proteins were electrotransferred to PVDF membranes for immunoblotting using 25 mM potassium phosphate, 25 mM sodium phosphate, 12 mM Tris, 192 mM glycine and 20% methanol, pH 7.0 [74]. Membranes

were blocked with 0.5% albumin in TBS/T (50 mM Tris, 100 mM NaCl, pH 7.6, and 0.1% Tween 20) for 1 h and incubated overnight at 4 °C with the primary antibody (monoclonal mouse antibody against the AOX from the higher plant *Sauvormatum guttatum* [75]). Then, membranes were washed with TBS/T and incubated at room temperature for 1 h with the horseradish peroxidase (HRP)-conjugated secondary antibody (HRP anti-mouse-IgG). Antibodies were diluted in TBS/T. Once the membranes were washed, the bands were developed by chemiluminescence (ECL kit [76].

## 2.10. Mass spectrometry

From the BN-gels or 2D SDS-Tricine gels, the indicated bands were excised and sent for protein sequence identification by LC-MS to the University Proteomics Laboratory of the Instituto de Biotecnología, UNAM (Cuernavaca, Morelos, Mexico). Peptides were analyzed in a LC-MS system constituted by an Accela microflux liquid chromatographer (Thermo-Fisher Co., San Jose, CA, USA) with a splitter (1/20), a LTQ Orbitrap Velos mass spectrometer (Thermo-Fisher Co., San Jose, CA, USA) and a nano-electrospray ionization (ESI) system. After tryptic digestion, samples were analyzed in a tandem high-resolution mass spectrometer. Mascot and Protein-Prospector algorithms were used to search all spectrometric results against the NCBI database. Protein sequence coverage (%) is shown in Tables 3 and 5.

## 3. Results

### 3.1. *D. hansenii* contains a branched mitochondrial respiratory chain

To define the composition of the respiratory chain from *D. hansenii*, we measured the rate of oxygen consumption in isolated mitochondria using different substrates and inhibitors. To prevent the mitochondrial permeability transition (PT), 10 mM phosphate and 75 mM KCl were added (Table 1). As expected [58,59], citrate-malate and pyruvate-malate were efficiently oxidized in a rotenone-sensitive fashion by complex I while succinate was oxidized by complex II. In addition, the complex III inhibitor antimycin-A and the complex IV inhibitor NaCN partially inhibited oxygen consumption. Partial inhibitions indicated the presence of an alternative pathway for oxygen consumption [59]. The presence of an active AOX was confirmed by the partial sensitivity of the rate of oxygen consumption to propyl-gallate (PG). PG was preferred over salicylhydroxamic acid (SHAM) because full inhibition was achieved with 100 µM PG while a higher 500 µM SHAM was needed (Result not shown). Full inhibition of oxygen consumption was achieved by adding NaCN and PG together (Table 1).

The above results confirm the presence of a branched mitochondrial respiratory chain in *D. hansenii* that contains at least all four multi-subunit complexes plus an alternative AOX [55,56]. The presence of additional external alternative dehydrogenases was suggested when NADH and glycerol-phosphate were oxidized at high rates (Table 1). Oxidation of these substrates was partially sensitive to both, NaCN or PG, indicating that electrons coming from these substrates could reach either the cytochrome pathway or AOX. The external NADH dehydrogenase (NDH2e) activity was sensitive to flavone, a specific inhibitor of type II NADH dehydrogenases, but it was not sensitive to rotenone. Also, the glycerol-phosphate dehydrogenase (MitGPDH) activity was not sensitive to either rotenone or flavone. Thus, it is suggested that *D. hansenii* contains a branched mitochondrial respiratory chain composed by the four canonical complexes, alternative dehydrogenases (at least NDH2 and MitGPDH) and an AOX.

The substrates predicted to yield a higher number of protons-pumped per electron consumed in the respiratory chain ( $H^+ / e^-$ ) exhibited a higher respiratory control (RC = phosphorylating state (III)/resting state (IV)) than those with a low  $H^+ / e^-$  (Table 1), i.e., the highest respiratory controls were obtained using pyruvate-malate, RC = 2.35 ± 0.07 or citrate-malate, RC = 2.17 ± 0.05. By contrast,

with succinate a low  $RC = 1.64 \pm 0.08$  was observed, while with glycerol-phosphate  $RC = 1.28 \pm 0.03$  and with NADH  $RC = 1.23 \pm 0.05$ .

### 3.2. The putative mitochondrial NDH2e from *D. hansenii* is inhibited by flavone and exhibits a high homology with NDH2s from other sources

To confirm the presence of external NDH2(s) in *D. hansenii* the rate of oxygen consumption was titrated with rotenone to inhibit complex I or flavone to inhibit any NDH2 activity present [38]. The rate of oxygen consumption in the absence of inhibitors was taken as 100%. In the presence of pyruvate-malate, respiration was inhibited by rotenone, but it was insensitive to flavone (Fig. 1A). At 5  $\mu$ M rotenone 50% inhibition was obtained while maximum inhibition of the pyruvate-malate-supported oxygen consumption was reached at 50  $\mu$ M rotenone (Fig. 1A, full circles). By contrast, with NADH, flavone inhibited oxygen consumption while rotenone exhibited little effect (Fig. 1B). In the presence of NADH, 500  $\mu$ M flavone led to maximal inhibition (Fig. 1B, empty circles).

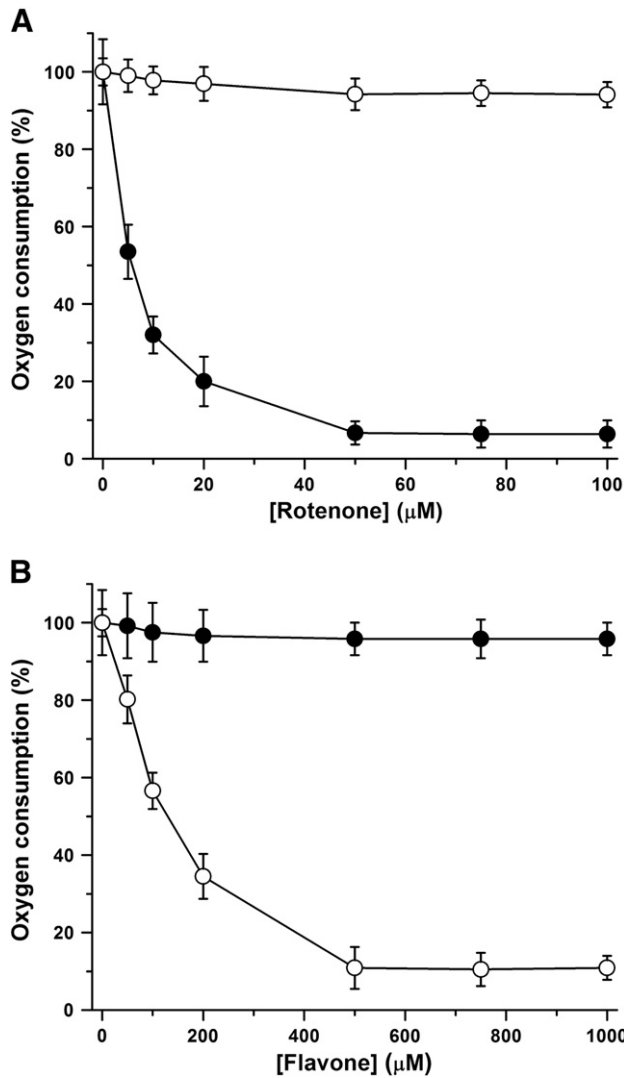


**Fig. 1.** Inhibition of oxygen consumption in isolated mitochondria from *D. hansenii* with rotenone (A) or flavone (B). The substrate was either 10 mM pyruvate-malate (●) or 1 mM NADH (○). Oxygen measurements were made in the resting state (IV). The reaction mixture was as in Table 1. Data from five independent experiments are expressed as the mean  $\pm$  SD.

Yeast species may contain different alternative dehydrogenases, e.g. *S. cerevisiae* contains three mitochondrial NDH2 isoforms plus an external MitGPDH [21,40]. To detect possible alternative dehydrogenases in the NCBI database, the genome of *D. hansenii* was analyzed for sequences homologous to those encoding for NDH2s and MitGPDHs in *Y. lipolytica* and *S. cerevisiae*. For NDH2s, the BLAST analysis unveiled a protein sequence with high homology to type II NADH dehydrogenases. This is the hypothetical protein DEHA2D07568p, a 568 amino acid (MW = 63 kDa) precursor. DEHA2D07568p was aligned against the NDH2e sequence from *Y. lipolytica* (YALI0F25135p) and the NDH2s from *S. cerevisiae*, i.e. NDI (YML120c), NDE1 (YMR145c) and NDE2 (YDL085w) (Table 2), exhibiting high sequence similarity. In addition, DEHA2D07568p closely resembles external NDH2s from several fungi and plants (Result not shown). Furthermore, when the conserved motifs described for the NDH2e from *Y. lipolytica* [77] were compared with the DEHA2D07568p, both proteins exhibited highly matching dinucleotide binding sites (for NADH or FAD) and hydrophobic regions (Fig. 2). These results plus the flavone sensitivity strongly suggest that DEHA2D07568p is an NDH2e. In addition, there is a 98.9% probability that this protein is imported into mitochondria as predicted by the MitoProt II-v1.101 program [78]. Analysis of the *D. hansenii* genome did not detect other genes coding for NDH2s.

### 3.3. *D. hansenii* has a mitochondrial glycerol-phosphate dehydrogenase (MitGPDH)

Isolated mitochondria from *D. hansenii* oxidized glycerol-phosphate at a high rate (Table 1), suggesting the presence of a mitochondrial GPDH as predicted by Adler and co-workers [79]. Thus, to look for orthologues the *D. hansenii* sequences were aligned against the corresponding genes from *S. cerevisiae* (Gut2p) and *Y. lipolytica* (YALI0B13970p). The analysis unveiled only one candidate sequence, annotated as hypothetical protein DEHA2E08624p; a 652 amino-acid precursor, MW = 72.5 kDa with a 65.9% probability of being imported by mitochondria [78]. DEHA2E08624p sequence is similar to MitGPDHs from other yeast species (Table 2) and with other MitGPDHs stored in the NCBI database. Thus, our data suggest that DEHA2E08624p is a mitochondrial GPDH.

### 3.4. The AOX in *D. hansenii* mitochondria is sensitive to AMP

In isolated mitochondria from *D. hansenii* cyanide-resistant respiration (CRR) was ~20–25% of the total. In different organisms this percentage can vary depending on different molecules or environmental

**Table 2**

*D. hansenii* putative alternative oxidoreductase sequences. Percentage of identity and similarity with those from other yeast sources.

Sequences	Identity (%)	Similarity (%)
<b>a) NDH2s</b>		
• DEHA2D07568p vs. YALI0F25135p (Y <sub>l</sub> NDH2e)	50	65
• DEHA2D07568p vs. YML120c (ScNDE1)	45	64
• DEHA2D07568p vs. YMR145c (ScNDE2)	52	69
• DEHA2D07568p vs. YDL085w (ScNDI)	50	69
<b>b) MitGPDHs</b>		
• DEHA2E08624p vs. YALI0B13970p (Y <sub>l</sub> MitGPDH)	49	64
• DEHA2E08624p vs. Gut2p (ScMitGPDH)	58	73
<b>c) AOXs</b>		
• DEHA2C03828p vs. AAQ08895 (Y <sub>l</sub> AOX1)	54	69
• DEHA2C03828p vs. AAQ08896 (Y <sub>l</sub> AOX2)	50	66
• DEHA2C03828p vs. XP_723460 (CaAOX1)	63	73
• DEHA2C03828p vs. XP_723269 (CaAOX2)	65	79

Protein sequences are shown accordingly with their NCBI definition or accession nomenclature.

Abbreviations: Sc: *S. cerevisiae*; Yl: *Y. lipolytica*; Ca: *C. albicans*; NDH2e/NDE: external alternative NADH dehydrogenase; NDI: internal alternative NADH dehydrogenase; AOX1: alternative oxidase isoform 1; AOX2: alternative oxidase isoform 2; Mit: mitochondrial isoform.

### Dinucleotide binding motif I

<i>D. hansenii</i>	90	QKKKTLVILGSGWGSISLLKNLDTTLYNVVVVSPR	124
<i>Y. lipolytica</i>	110	PSKKTLVVLGSGWGSVSFLKKLDTSNYNVIVVSPR	144
	.	:	:

### Hydrophobic motif I

<i>D. hansenii</i>	126	YFLFTPPLLPS	135
<i>Y. lipolytica</i>	146	YFLFTPPLLPS	155

### Hydrophobic motif II

<i>D. hansenii</i>	214	SLNYDYLVVGVAQPSTFGIPGVAEHSTFLKEV	246
<i>Y. lipolytica</i>	215	EIPFDYLVVGVGAMSSTFGIPGVQENACFLKEI	247
	.	:	:

### Dinucleotide binding motif II

<i>D. hansenii</i>	278	SIVVCGGGPTGVEVAGELQDYIDQDLKKWMPEVASELKVIILVEA	321
<i>Y. lipolytica</i>	278	HTVVVGGGPTGVEFAELODFFEDDLRKWIPDIRDDFKVTLVEA	321
	.	:	:

**Fig. 2.** Alignment of the conserved motifs of DEHA2D07568p and *Y. lipolytica* NDH2e amino acid sequences. (:) Conserved substitutions; (.) semi-conserved substitutions. Identical residues in both sequences are shown in gray. Numbers indicate amino acids in the linear sequence of each protein.

conditions, e.g.  $\alpha$ -ketoacids, AMP, salts, temperature and mitochondrial-matrix redox state [80–82]. In addition, many plants and microorganisms express AOX in response to ROS or cytochromic pathway inhibitors [83,84]. AOXs from yeast or from *Ustilago maydis* are activated by AMP and possibly by the redox state, but not by  $\alpha$ -ketoacids [85]. To test some of the properties of the *D. hansenii* AOX (*DhAOX*); it was decided to explore the sensitivity to AMP or pyruvate. To measure only CRR, these experiments were conducted in the presence of 500  $\mu$ M NaCN. Full oxygen consumption inhibition was achieved with 500  $\mu$ M NaCN plus 100  $\mu$ M propyl-gallate. It was observed that AMP increased CRR (~15%) while pyruvate had no effects (Fig. 3), i.e. the AOX from *D. hansenii* shares the sensitivity to AMP from other fungi AOXs.

Further analysis of AOX was conducted by comparing the *DhAOX* hypothetical protein sequence with the constitutive and inducible AOX isoforms (1 and 2, respectively) from *Yarrowia lipolytica* and *Candida albicans*. The BLAST analysis unveiled only one candidate, annotated as hypothetical protein DEHA2C03828p. This sequence corresponds to a 338 amino-acid precursor with a theoretical MW of 39.4 kDa. There is a 97.1% probability that this protein is imported by mitochondria [78]. The DEHA2C03828p sequence has high similarity to the AOXs from both yeast species (Table 2). With the above results, it may be concluded that *D. hansenii* mitochondria contain a branched respiratory chain composed by all four canonical complexes plus three alternative oxidoreductases, namely an NDH2e, a  $\text{Mit}_\text{GPDH}$  and the *DhAOX* already reported [59]. Alternative enzymes were analyzed using SDS-Tricine PAGE, western blotting and mass spectrometry (see below).

*albicans*. The BLAST analysis unveiled only one candidate, annotated as hypothetical protein DEHA2C03828p. This sequence corresponds to a 338 amino-acid precursor with a theoretical MW of 39.4 kDa. There is a 97.1% probability that this protein is imported by mitochondria [78]. The DEHA2C03828p sequence has high similarity to the AOXs from both yeast species (Table 2). With the above results, it may be concluded that *D. hansenii* mitochondria contain a branched respiratory chain composed by all four canonical complexes plus three alternative oxidoreductases, namely an NDH2e, a  $\text{Mit}_\text{GPDH}$  and the *DhAOX* already reported [59]. Alternative enzymes were analyzed using SDS-Tricine PAGE, western blotting and mass spectrometry (see below).

### 3.5. In *D. hansenii* mitochondria, respiratory complexes organize into supercomplexes

After detection of the different components of the mitochondrial respiratory chain from *D. hansenii*, it was decided to define whether the respiratory complexes were organized into supercomplexes as described for many other species [48,50,51]. Both *D. hansenii* and *Y. lipolytica* are closely related [69,70], so we decided to use *Y. lipolytica* mitochondrial respiratory complexes and supercomplexes as standards to estimate the MW of those from *D. hansenii*. For BN-PAGE, mitochondrial membranes were solubilized with either laurylmaltoside (LM) or digitonin (Dig). Digitonin was used expecting to preserve associations between respiratory complexes, while laurylmaltoside was expected to allow isolation of the individual complexes. The BN-PAGE results are shown for solubilized mitochondria from *Y. lipolytica* (Fig. 4A) and from *D. hansenii* (Fig. 4B). In LM-solubilized mitochondria, the individual complexes from either *Y. lipolytica* or *D. hansenii* were observed at different migration distances. Migration distances for complexes I, IV and V were reasonably near in both species. By contrast, the complex III band from *D. hansenii* was hardly detectable by BN-PAGE (Fig. 4B lane LM). In fact, the location of complex III was detected only in the 2D Tricine-SDS-PAGE (see below). In digitonin-solubilized mitochondria from both *Y. lipolytica* (Fig. 4A) and *D. hansenii* (Fig. 4B) several high MW bands corresponding to putative respiratory supercomplexes were revealed.

To further characterize the location and composition of each complex and supercomplex, the in-gel enzymatic activities of NADH dehydrogenase (NDH), ATPase and cytochrome c oxidase (COX) were assayed in BN-gels (Fig. 4C to E). In the LM solubilized sample, NDH activity

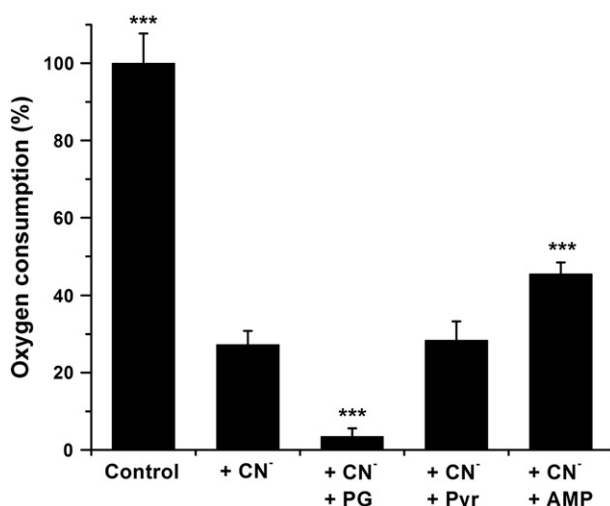


**Fig. 3.** Activation of the *D. hansenii* AOX by AMP but not by pyruvate (Pyr). Oxygen consumption was measured in state IV with 10 mM succinate as respiratory substrate. 50  $\mu$ M rotenone was added to inhibit complex I. Cytochrome-dependent oxygen consumption was inhibited with 500  $\mu$ M NaCN (CN<sup>-</sup>). 100  $\mu$ M propylgallate (PG), 10 mM pyruvate (Pyr) or 1 mM AMP was used as indicated. n = 3  $\pm$  SD. One-way ANOVA (Dunnett's multiple comparison test) \*P < 0.05 compared to the cyanide-treated sample (second bar).

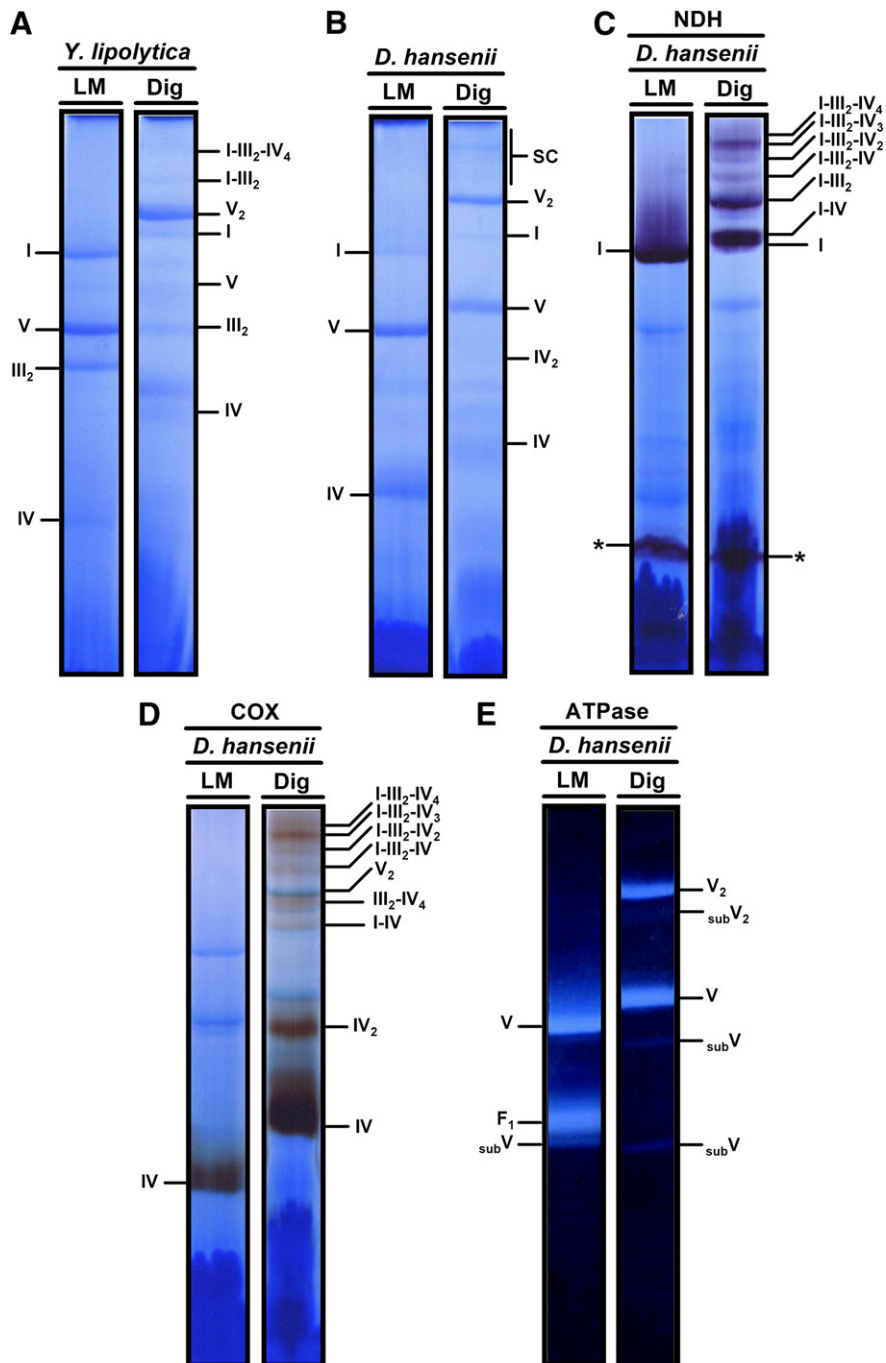


**Fig. 4.** Respiratory complexes and supercomplexes found in solubilized *D. hansenii* mitochondria. Isolated mitochondria were solubilized with laurylmaltoside (LM) 2.0 mg/mg Prot or digitonin 4.0 mg/mg Prot. (A) *Y. lipolytica* solubilizates were resolved by BN-PAGE in a 4–12% polyacrylamide gradient gel and were used as MWs standards. (B) LM- and Dig-solubilizates from *D. hansenii* mitochondria resolved by BN-PAGE. (C) In-gel NADH-dehydrogenase activity (NDH); 1 mM NADH and 0.5 mg/mL nitrotetrazolium blue chloride (NTB). (D) In-gel cytochrome c oxidase activity (COX); 0.04% diaminobenzidine and 0.02% cytochrome c. (E) In-gel ATPase activity performed in BN-gel; 35 mM Tris, 270 mM glycine, 0.2% Pb(NO<sub>3</sub>)<sub>2</sub>, 14 mM MgSO<sub>4</sub> and 8 mM ATP (pH 8.4). I, III<sub>2</sub>, IV and V are the mitochondrial mammalian-like complexes. (\*) Putative NDH2e. *D. hansenii* supercomplexes (SC) were: I-IV, I-III<sub>2</sub>, I-III<sub>2</sub>-IV, I-III<sub>2</sub>-IV<sub>2</sub>, I-III<sub>2</sub>-IV<sub>3</sub> and I-III<sub>2</sub>-IV<sub>4</sub> where stoichiometries are indicated as sub-indexes. IV<sub>2</sub>: complex IV dimer; F<sub>1</sub>: soluble domain of complex V; V<sub>2</sub>: complex V dimer; subV: complex V sub-complexes.

exhibited two purple bands corresponding to complex I and presumably to the NDH2e (Fig. 4C lane LM). When solubilized with digitonin, higher MW purple bands were detected (Fig. 4C lane Dig). These bands were assigned as supercomplexes containing complex I plus different amounts of either complex III or complex IV (see below). Also, the NDH activity seemed more intense in three bands than in all others, suggesting that complex I-containing supercomplexes were concentrated in these bands. These bands had MWs compatible with their assignment as the

complex I band running alone; as a I-IV supercomplex; a I-III<sub>2</sub> supercomplex and a I-III<sub>2</sub>-IV<sub>3</sub> supercomplex (Fig. 4C lane Dig; also see Fig. 4D which is described below).

When COX activity was measured, a single brown band was observed in the LM-solubilized lane (Fig. 4D lane LM). It is suggested that this activity is the product of monomeric complex IV. The digitonin lane revealed several brown bands corresponding to monomeric complex IV and to a number of supercomplexes containing complexes I, III<sub>2</sub>

and IV (Fig. 4D lane Dig). Supercomplex I-III<sub>2</sub>-IV<sub>3</sub> exhibited the highest activity. Also, a faint band, probably corresponding to I-IV supercomplex was detected near complex I.

In regard to in-gel ATPase activity, LM treatment revealed three activity bands that were respectively assigned as the monomeric complex V, the F<sub>1</sub> subunit and a F<sub>1</sub> subcomplex (Fig. 4E lane LM). In the first two bands the ATPase activity was much higher than the activity detected in the subcomplex, indicating that this may be at low concentrations or exhibit less activity. In the digitonin solubilized samples ATPase activity was detected in four bands (Fig. 4E lane Dig). The ATPase activity was more intense in the bands assigned as the complex V dimer and monomer, while the lower intensity bands probably were the F<sub>1</sub> subunit and an F<sub>1</sub>F<sub>0</sub>-ATP synthase sub-complex. Dimers of complex V have also been detected previously in mitochondria from beef heart, *S. cerevisiae*, *Polytomella* sp. and from other sources by digitonin solubilization or using lower LM/protein ratios [51].

To determine the location of each respiratory complex, including complex III which was not observed in the BN gels, and also whether any given complex was part of a putative supercomplex, complete BN-PAGE lanes from LM- and Dig-solubilized mitochondria were resolved by second dimension denaturing gels (2D Tricine-SDS-PAGE) and subjected to Coomassie-staining (Fig. 5) or silver-staining (Fig. 6), respectively. The second dimension gel from LM-solubilized mitochondria contains the individual subunit signatures [49] from each respiratory complex (Fig. 5). In order to confirm the assignments for complexes I, III, IV and V different bands were excised and sent to protein identification by LC-MS. The 75-kDa subunit from NADH dehydrogenase (I), the core proteins 1 and 2 from the bc<sub>1</sub> complex (III), the COX subunit 2 from cytochrome c oxidase (IV) and the gamma ( $\gamma$ ) subunit from F<sub>1</sub>F<sub>0</sub>-ATP synthase (V) were identified with a high sequence coverage (Table 3). In all cases, identified subunits were located at the lane that was previously predicted for a specific respiratory complex. Complex III, which was difficult to see before (Fig. 4B, lane LM), could be located next to the complex V monomer (Fig. 5).

In the 2D-gel obtained from digitonin-solubilized mitochondria, the subunit pattern of individual complexes was found also at high MWs indicating the presence of supercomplexes (Fig. 6). The MWs suggested that these supercomplexes contained complexes I, III and IV. In addition, a pattern corresponding to a complex V dimer (V<sub>2</sub>) was identified. It is suggested that the supercomplexes detected by BN-gels (Fig. 4) and

2D SDS-Tricine-gels (Figs. 5 and 6) were: IV<sub>2</sub>, I-IV, III<sub>2</sub>-IV<sub>4</sub>, V<sub>2</sub>, I-III<sub>2</sub>(S<sub>0</sub>), I-III<sub>2</sub>-IV(S<sub>1</sub>), I-III<sub>2</sub>-IV<sub>2</sub>(S<sub>2</sub>), I-III<sub>2</sub>-IV<sub>3</sub>(S<sub>3</sub>) and I-III<sub>2</sub>-IV<sub>4</sub>(S<sub>4</sub>).

To determine the stoichiometry and the theoretical MWs of these supercomplexes, the MWs of each complex/supercomplex were estimated by measuring the migration distance of the corresponding bands in BN-PAGE of the digitonin solubilizates from *D. hansenii* and interpolating them by linear regression in a log MW vs. migration distance plot from the solubilized mitochondrial respiratory complexes from *Y. lipolytica* that we used as MW standards (Fig. 7). The estimated MWs are shown in Table 4. The composition of each supercomplex was determined by correlating the MW estimates and the presence of NDH, COX and/or ATPase activity in each band. The calculated MWs for complex I, IV and V monomers and complex III dimer were very similar to those from *Y. lipolytica* (Fig. 7). The *D. hansenii* MWs of the supercomplexes were similar to those reported for *Y. lipolytica* [51]. By contrast, the complex V dimers from *D. hansenii* were heavier than expected (Table 4).

In mammalian systems, large supercomplexes containing I<sub>1</sub>-III<sub>2</sub>-IV<sub>4</sub> and III<sub>2</sub>-IV<sub>4</sub> have been detected in BN-gels [49]. Also, mammalian supercomplexes seem to be associated into larger “respiratory strings” [86]. In *D. hansenii*, it seems that complexes I, III<sub>2</sub> and IV organize into supercomplexes suggesting that these mitochondria also possess “respiratory strings” where chain units of the I-III<sub>2</sub>-IV<sub>3</sub> supercomplex would attach to each other. In contrast to *Y. lipolytica* [87], NDH2e seems to be detached from the cytochrome-complexes; i.e. in digitonin-treated samples in-gel NADH dehydrogenase activity was absent at the sites where cytochrome complexes migrated (Fig. 4C lane Dig).

At this point, we can conclude that the branched respiratory chain from *D. hansenii* contains a large amount of canonical respiratory complexes (I, III and IV), which may be associated in supercomplexes (Fig. 4). Alternative enzymes probably are independent from the respiratory supercomplexes (at least the NDH2e (Fig. 4C lane Dig)). Nevertheless alternative enzyme distribution needs to be explored further.

### 3.6. Identification of the alternative respiratory enzymes from *D. hansenii*

NDH2e has already been proposed to correspond to the lower NADH dehydrogenase activity band detected in a BN-gel (Fig. 4C); when this band was subjected to 2D-SDS-Tricine-PAGE different proteins were separated (Fig. 8). Three spots were selected for identification; the

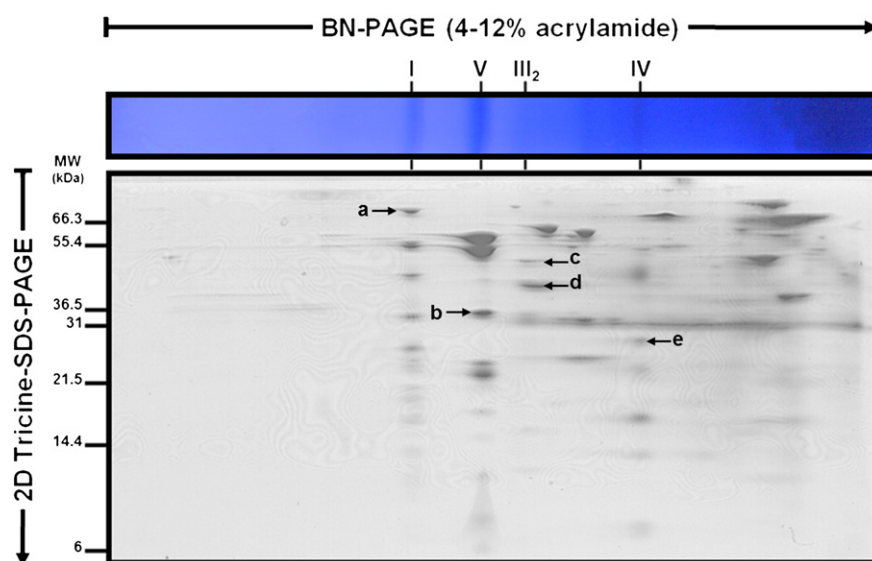


**Fig. 5.** 2D SDS-Tricine-PAGE of *D. hansenii* mitochondrial respiratory complexes. From the BN-PAGE, the lane containing the laurylmaltoside (LM) solubilized proteins was excised and subjected to 2D SDS-Tricine-PAGE. Bands that appear labeled were cut and sent for protein identification by LC-MS. These results are shown in Table 3. All SDS-Tricine-gels showed were stained with Coomassie® brilliant blue G-250. Respiratory complexes are tagged as in Fig. 4.

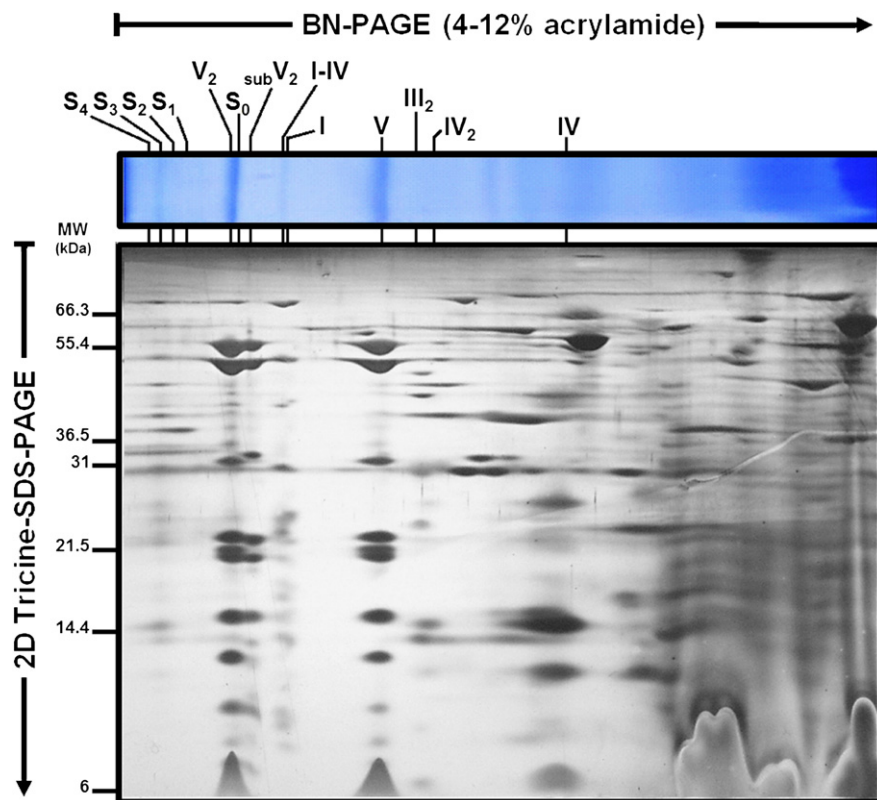


**Fig. 6.** 2D SDS-Tricine-PAGE of *D. hansenii* mitochondrial supercomplexes. After BN-PAGE, the lane containing the digitonin-solubilized proteins was excised and subjected to 2D-SDS-Tricine-PAGE followed by silver staining. Respiratory complexes are tagged as in Fig. 4. Supercomplex nomenclature: S<sub>0</sub>: I–III<sub>2</sub>, S<sub>1</sub>: I–III<sub>2</sub>–IV, S<sub>2</sub>: I–III<sub>2</sub>–IV<sub>2</sub>, S<sub>3</sub>: I–III<sub>2</sub>–IV<sub>3</sub> and S<sub>4</sub>: I–III<sub>2</sub>–IV<sub>4</sub>.

first corresponded to the hypothetical MW of NDH2e; i.e. 63 kDa (Fig. 8, f) and the other two were chosen due to their high concentration (Fig. 8, bands g and h). The spots were analyzed by LC-MS/MS and the results are shown in Table 5. The first band (f) was reported as the NDH2e hypothetical sequence (DEHA2D07568p) but surprisingly, it also contained the putative <sub>Mit</sub>GPDH (DEHA2E08624p), in spite that the predicted MWs were widely different (63 vs. 72.5 kDa, respectively) (Table 5), i.e. they were in the same spot in the 2D SDS-Tricine-gel (Fig. 8). The presence of both proteins in the asterisked band (excised from the BN-gel, Fig. 4) might reflect a physiological interaction of these alternative dehydrogenases. A similar interaction has been described in *S. cerevisiae* as part of a mitochondrial dehydrogenase membrane complex, which contains different external peripheral alternative dehydrogenases, part of the Krebs cycle enzymes (including complex II), the NDI and other NADH producing enzymes that were not defined [88]. Also, in *D. hansenii* dihydrolipoamide dehydrogenase was identified next to NDH2e and <sub>Mit</sub>GPDH (Fig. 8, g). This protein is part of the pyruvate dehydrogenase and the  $\alpha$ -ketoglutarate dehydrogenase complexes [20]. The lower band contained three proteins: the ATP/

ADP carrier (ANC); the mitochondrial porin (VDAC) and the phosphate carrier (Fig. 8, h). These proteins are involved in metabolite fluxes and have been proposed to be part of the mitochondrial unspecific channel in other yeast species [89].

In *S. cerevisiae* <sub>Mit</sub>GPDH (Gut2p) has a predicted MW = 72.4 kDa, while the mature form of this protein has a MW = 68.4 kDa [88]. This MW is close to the mature *S. cerevisiae* NDE2 with a MW = 61.7 kDa [88]. In *D. hansenii*, NDH2e exhibited an approximate MW = 60 kDa (Fig. 8) and <sub>Mit</sub>GPDH migrated very near that weight. In silico data and estimated MWs suggested that *D. hansenii* <sub>Mit</sub>GPDH contains a longer signal-sequence than the NDH2e. When both proteins mature, their MWs become similar and their electrophoretic migration coincides. As a result, both dehydrogenases appeared in the same 2D-gel spot (Fig. 8, f; Table 5).

AOX was identified by mass spectrometry (Fig. 9, upper panel) and by western blotting (WB) (Fig. 9, lower panel). For the western blot, an antibody against AOX from *S. guttatum* was used. Two bands were detected by this procedure (Fig. 9, lower panel). To determine which of these bands contains AOX, they were excised from the gel and sent

**Table 3**

Proteins identified by LC-MS analysis contained in the indicated bands from the 2D SDS-Tricine-gel (Fig. 5).

Band	Protein name	Accession no.	gl protein	Length <sup>a</sup>	Cov <sup>b</sup> (%)	MW <sup>c</sup> (kDa)
a	NADH-quinone oxidoreductase 75-kDa subunit	DEHA2G06050p	199433960	722	26.7	79
b	F <sub>1</sub> F <sub>0</sub> -ATP synthase gamma subunit	DEHA2F20658p	202953475	286	36.7	31.3
c	Ubiquinol-cytochrome c reductase core protein 1	DEHA2D13640p	199431718	445	31.7	48
d	Ubiquinol-cytochrome c reductase core protein 2	DEHA2E09834p	49655402	376	75	39.4
	IDH2 subunit of mitochondrial NAD(+) -dependent isocitrate dehydrogenase	DEHA2G05786p	49657467	365	22.2	39.5
	IDH1 subunit of mitochondrial NAD(+) -dependent isocitrate dehydrogenase	DEHA2C10758p	199430720	359	19.2	38.6
e	Cytochrome c oxidase subunit 2	YP_001621413.1	162951843	246	11.7	28.4

<sup>a</sup> Number of amino acids.

<sup>b</sup> Protein sequence coverage.

<sup>c</sup> Predicted molecular weights from the *D. hansenii* NCBI database sequences.

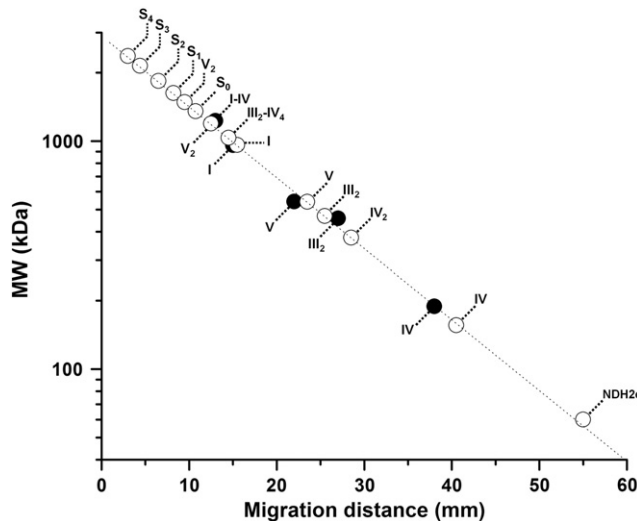


**Fig. 7.** Molecular weight (MW) estimates of the *D. hansenii* complexes and supercomplexes. The previously characterized molecular masses of *Y. lipolytica* mitochondrial complexes were plotted against their migration distance in BN-PAGE (●). Then, the migration distances of the *D. hansenii* respiratory complexes and supercomplexes (○) were interpolated and their corresponding molecular masses inferred (see values in Table 4). MW values from *Y. lipolytica* complexes I, III<sub>2</sub>, IV, V and complex V dimer (V<sub>2</sub>) were taken from the previous report by Guerrero-Castillo and co-workers [51]. (\*) Putative NDH2e. Note that y-axis is in log-scale. Nomenclature for complexes and supercomplexes is as in Figs. 4 and 6.

to LC-MS/MS analysis. AOX was the “i” band (Fig. 9, upper panel) while the “j” band contained the ANC and VDAC (Fig. 9, upper panel). Results are shown in Table 5.

Experimental evidence supports the presence of a branched mitochondrial respiratory chain in *D. hansenii*. This chain contains the multi-subunit complexes I, II, III and IV; there is also a mitochondrial F<sub>1</sub>F<sub>0</sub>-ATP synthase (complex V), which tends to be a dimer and is detached from the respiratory supercomplexes (Fig. 4E). Three alternative enzymes: NDH2e, MitGPDH and *Dh*AOX were detected as additional components of the branched respiratory chain. Preliminary evidence presented here suggests that multiprotein associations containing the alternative dehydrogenases plus at least two enzymes from the Krebs cycle do exist. Such associations have been described in *S. cerevisiae* [88].

**Table 4**  
Estimated molecular weights (MWs) of the *D. hansenii* complexes and supercomplexes by BN-PAGE.

Complex/supercomplex	Calculated MW <sup>a</sup> (kDa)	Expected MW <sup>b</sup> (kDa)
I	963 ± 49	–
III <sub>2</sub>	469 ± 24	–
IV	156 ± 12	–
V	541 ± 28	–
IV <sub>2</sub>	377 ± 19	312
I-IV	1035 ± 53	1119
III <sub>2</sub> -IV <sub>4</sub>	1196 ± 61	1223
I-III <sub>2</sub> (S <sub>0</sub> )	1356 ± 35	1432
V <sub>2</sub>	1484 ± 76	1082
I-III <sub>2</sub> -IV (S <sub>1</sub> )	1630 ± 87	1588
I-III <sub>2</sub> -IV <sub>2</sub> (S <sub>2</sub> )	1842 ± 51	1744
I-III <sub>2</sub> -IV <sub>3</sub> (S <sub>3</sub> )	2143 ± 59	1900
I-III <sub>2</sub> -IV <sub>4</sub> (S <sub>4</sub> )	2370 ± 135	2056

Complex and supercomplex nomenclature as in Figs. 4–6.

<sup>a</sup> Calculated MW of the *D. hansenii* complexes and supercomplexes correspond to the mean ± SD from three independent experiments.

<sup>b</sup> Supercomplexes expected MWs correspond to the sum of the individual MW of each respiratory complex according to their stoichiometries (subscript numbers).

#### 4. Discussion

The structure of the branched mitochondrial respiratory chain from *D. hansenii* was analyzed in isolated mitochondria. In addition, we characterized the association pattern of respiratory complexes into respiratory supercomplexes [44,48,49,86]. In agreement with Veiga and co-workers [59], we found that the *D. hansenii* respiratory chain contains all four canonical respiratory complexes I, II, III and IV plus an AOX. In addition, we detected two additional components, namely, an external type II NADH dehydrogenase (NDH2e) and a mitochondrial glycerol-phosphate dehydrogenase (<sub>Mit</sub>GPDH).

AOX activity is resistant to cyanide [58,80]; electrons reach it directly from the ubiquinone pool, as indicated by the resistance of oxygen consumption activity to the complex III inhibitor antimycin-A (Table 1, Fig. 3). Cyanide-resistant, AOX-supported respiration is found in many yeast species, including *D. hansenii* and it has been proposed that AOX regulates energy production in response to different physiological conditions [57–59]. Regulation is the result of a decrease in the electron flux to the cytochromic pathway with the concomitant increase in electron flux to AOX [34–36,87]. Here, it was observed that *D. hansenii* alternative oxidase (*Dh*AOX) is activated by AMP while it is insensitive to α-ketoacids, such as pyruvate. AMP activation is widely reported for AOXs from different yeasts and fungi [21,80,85]. It was suggested that *Dh*AOX activity is induced at the stationary growth phase [59]. In this view, the presence of the AOX could be helpful to diminish the electron flux through the cytochromic pathway and reduce the ATP/O ratio in this physiological condition. In contrast to Veiga and co-workers [59], in our hands *Dh*AOX activity was detected in isolated mitochondria from mid-exponential growth phase cultures. This is probably due to the differences in growth conditions, as we used a non-fermentable carbon source (lactate, see Materials and methods) [14]. This result suggests that *Dh*AOX is active in early growth phases and not only at the stationary phase where it probably acts as an energy sink [35,87]. In cells grown in lactate, *Dh*AOX was detected regardless of the addition of AMP (Table 1, Fig. 3). The role of *Dh*AOX in different growth phases requires further studies.

Two other alternative enzymes, a glycerol-phosphate dehydrogenase and an alternative NADH dehydrogenase were both bound to the external face of the IMM. Electrons were fed to <sub>Mit</sub>GPDH and NDH2e by external glycerol-phosphate or NADH, respectively. These electrons were used to reduce oxygen. From the BLAST analysis of the genomes, we concluded that there is a single gene codifying for each of these

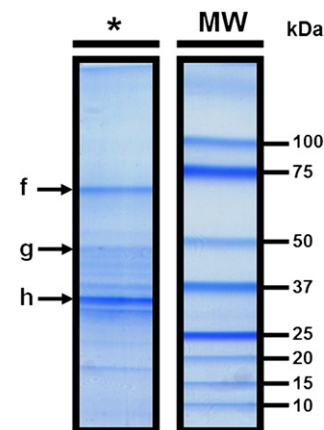


**Fig. 8.** Identification of the *D. hansenii* alternative NADH dehydrogenase (NDH2e) and the mitochondrial glycerol-phosphate dehydrogenase (<sub>Mit</sub>GPDH) by 2D SDS-Tricine-PAGE and LC-MS. (\*) NADH dehydrogenase activity band from the BN gel, which was excised and subjected to 2D SDS-Tricine-PAGE in order to separate components. SDS-Tricine-gel was stained with Coomassie® brilliant blue G-250. Both *D. hansenii*. Bands contained f: NDH2e and MitGPDH, g: dihydrolipoamide dehydrogenase (subunit from pyruvate dehydrogenase and α-keto glutarate dehydrogenase) and h: ANC, PiC and VDAC (Table 5).

**Table 5**

Proteins identified by LC-MS analysis contained in the indicated bands from the SDS-Tricine-gels (Figs. 8 and 9).

Band	Protein name	Accession no.	gi protein	Length <sup>a</sup>	Cov <sup>b</sup> (%)	MW <sup>c</sup> (kDa)
f	Glycerol-3-phosphate dehydrogenase ( <i>Mit</i> GPDH) precursor	DEHA2E08624p	49655350	652	25.3	72.5
	Mitochondrial external alternative NADH dehydrogenase (NDH2e) precursor	DEHA2D07568p	199431532	568	38.2	63
g	Dihydrolipoamide dehydrogenase	CBS767	49653406	495	58	53.2
	Major ADP/ATP carrier (ANC) of the mitochondrial inner membrane	DEHA2E12276p	49655508	301	41.5	33
h	Voltage-dependent anion channel (VDAC) of the outer mitochondrial membrane	DEHA2D16456p	49654868	282	65.6	29.9
	Mitochondrial phosphate carrier (PiC)	DEHA2B12188p	49653149	307	33.6	32.4
i	Alternative oxidase (AOX) precursor	DEHA2C03828p	199430515	338	36.7	39.4
j	Major ADP/ATP carrier (ANC) of the mitochondrial inner membrane	DEHA2E12276p	49655508	301	38.5	33
	Voltage-dependent anion channel (VDAC) of the outer mitochondrial membrane	DEHA2D16456p	49654868	282	52.1	29.9

<sup>a</sup> Amino acid sequence length.

<sup>b</sup> Protein sequence coverage.

<sup>c</sup> Predicted molecular weights from the *D. hansenii* NCBI database sequences.

proteins and we assigned DEHA2E08624p and DEHA2D07568p as the *Mit*GPDH and the NDH2e, respectively. These sequences were highly homologous to those from *Y. lipolytica* [77] and *S. cerevisiae* [90] (Fig. 2, Table 2).

NDH2e from *D. hansenii* was insensitive to rotenone while it was inhibited specifically by flavone. In isolated mitochondria from *D. hansenii*, 500 μM flavone promoted maximum inhibition of oxygen consumption (Fig. 1B, empty circles), which is similar to the concentrations reported for other organisms, e.g. in isolated mitochondria from *Plasmodium yoelii yoelii* [91] or *Paracoccidioides brasiliensis* [92] exogenous NADH-supported oxygen uptake is inhibited at similar flavone concentrations. In isolated mitochondria from *U. maydis*, complete inhibition is obtained at 250 μM flavone [85]. The flavone-mediated inhibition of the NADH:Q<sub>5</sub> oxidoreductase from *S. cerevisiae* exhibited an IC<sub>50</sub> = 95 μM, although in the presence of 300 μM flavone, activity was still at 20% [38].

NDH2e has been proposed to compensate for the absence of an aspartate-malate shuttle in ascomycetous fungi [85]. Here, we observed a high rate of exogenous NADH oxidation in isolated mitochondria from *D. hansenii*. Mitochondrial NADH oxidation probably occurs in the intact cell, establishing a NADH/NAD<sup>+</sup> recirculation cycle with the cytosol. Furthermore, probably *Mit*GPDH also constitutes an important mitochondrial sink of redox equivalents [93].

In *D. hansenii* active synthesis and accumulation of glycerol and lipids occur during growth; remarkably, these activities are stimulated by high salt concentrations [79] and *Mit*GPDH seems to participate in both processes. In addition, in *S. cerevisiae*, glycerol-phosphate dehydrogenase is finely regulated by the activity of NDHs, i.e. at saturating NADH, alternative NADH dehydrogenases physically attached to the *Mit*GPDH inhibit the use of glycerol-phosphate and transfer only

electrons that come from external NDH [39]. In fact, the presence of both enzymes, whether associated or not, causes competition for the entrance of electrons into the respiratory chain [94].

In *Y. lipolytica* growing in the exponential phase, electrons entering the respiratory chain at NDH2e are channeled to the cytochrome pathway [87]. This reflects the presence of an NDH2e-III<sub>2</sub>-IV supercomplex. By contrast, electrons coming from pyruvate-malate (Complex I) or succinate (Complex II) can reach either the cytochrome or the alternative pathways both in *Y. lipolytica* and in *D. hansenii*. The presence of unattached non proton-pumping alternative oxidoreductases (NDH2e, *Mit*GPDH, and *Dh*AOX) probably constitutes a physiological mitochondrial uncoupling mechanism [35]. This is interesting, as *Y. lipolytica* seems to lack the ability to undergo a permeability transition [51,95] while *D. hansenii* does possess a mitochondrial unspecific channel [14]. Electron transfer from the alternative oxidoreductases to AOX constitutes a futile oxygen consumption pathway that needs to be tightly regulated [89]. The presence of this pathway in *D. hansenii* during the exponential growth phase is puzzling, although it may be suggested that it participates in the modulation of ROS production as has been proposed in other branched respiratory chains [35].

In *D. hansenii*, the mammalian-like mitochondrial respiratory complexes I, III and IV are associated in supercomplexes. Supramolecular organization of the respiratory chain has been proposed to promote electron channeling, stabilization of labile multi-subunit complexes and sequestration of free radicals [48]. Consistent association patterns of supercomplexes observed by BN-PAGE, strongly suggest the existence of larger structures such as "respiratory strings" [86] or "respiratory patches" [54]. In *Y. lipolytica* supercomplexes I-III<sub>2</sub>, I-III<sub>2</sub>-IV<sub>4</sub>, I-IV, III<sub>2</sub>-IV and III<sub>2</sub>-IV<sub>2</sub> and a complex V dimer have been described [51]. In *S. cerevisiae* mitochondria a supercomplex III<sub>2</sub>-IV<sub>2</sub> has been detected [96]. In *D. hansenii* respiratory supercomplexes involving complexes I, III and IV were similar to those found in *Y. lipolytica*. Supercomplexes I-III<sub>2</sub>, I-III<sub>2</sub>-IV<sub>3</sub> and III<sub>2</sub>-IV<sub>4</sub> from *D. hansenii* contained the higher NADH dehydrogenase and COX activities as measured in BN-gels (Fig. 4C and D, lanes Dig). These supercomplexes were better observed in the activity staining experiments. In addition, the complex V dimer was easily observed both in the BN-gel and by ATPase activity staining (Fig. 4B and E, lane Dig). The *D. hansenii* F<sub>1</sub>F<sub>0</sub>-ATP synthase dimer was heavier than the V<sub>2</sub> from *Y. lipolytica*. This is probably due to stronger interactions between the subunits of complex V in these mitochondria than in other yeasts. Another explanation to this observation could be that V<sub>2</sub> may be associated to, and stabilized by the ATP/ADP carrier (ANC) and the phosphate carrier (PiC) in a structure known as the "synthasome" [97]. Molecular weights from the other respiratory complexes were similar to those from *Y. lipolytica*. Moreover, a big difference was observed between the single classical complexes from both *D. hansenii* and *Y. lipolytica* (Fig. 4A and B, lanes LM). In *D. hansenii* respiratory complexes were observed in smaller concentration than complex V. In fact, complex III was not observed in the BN-gels; it was only located by its subunit pattern in the 2D-SDS-Tricine-gels (Fig. 5) and by the identification of the core proteins 1 and 2 by mass

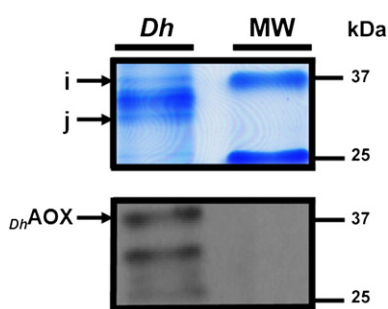


**Fig. 9.** Identification of the *D. hansenii* alternative oxidase (AOX) by SDS-Tricine-PAGE, western blotting and LC-MS. Total mitochondrial protein extract was subjected to SDS-Tricine-PAGE. SDS-Tricine-gel was stained with Coomassie® brilliant blue G-250 (upper panel). The SDS-Tricine-gel was electrotransferred onto PVDF membrane for western blotting. The membrane was decorated with a monoclonal mouse antibody against the AOX from the higher plant *S. guttatum* (lower panel). The two bands that were resulted immunoreactive in panel A (labeled as "i" and "j") were excised and subjected to identification by LC-MS. These results are shown in Table 5. At the upper panel, *D. hansenii* AOX corresponds to the "i" band. *Dh*AOX: *Debaryomyces hansenii* alternative oxidase.

spectrometry (Table 3). Cytochromic complexes III and IV are postulated to be the scaffold of the “respiratory string” [86]. In this case, our observation is unclear, as complex III does not seem to be present in the same amount as complex IV (Fig. 4B, lane LM). These results are not clearly understood and need to be explored further. Still, the electrophoretic migration of respiratory supercomplexes, their putative MWs, their enzymatic activities and the LC-MS identification of some of their subunits indicate that the mitochondrial respiratory chain from *D. hansenii* associates into supercomplexes which are very similar to those detected in organisms studied before such as mammals [44,48,68], plants [43,45,46,50] and other yeasts such as *S. cerevisiae* [44,53] and *Y. lipolytica* [51].

This is the first description of the complete structure of the branched respiratory chain from *D. hansenii*. In addition, we analyzed the supramolecular organization of the classical respiratory complexes in *D. hansenii* mitochondria. Alternative redox enzymes from this yeast do not seem to be attached to supercomplexes at least under our experimental conditions (mid-exponential phase, non-fermentable carbon source), which suggests that the *D. hansenii* alternative oxidoreductases dynamically associate/dissociate with supercomplexes. This would be in agreement with a dynamic plasticity model of the oxidative phosphorylation [55], i.e. respiratory components alternate between association in supercomplexes and free forms.

## Acknowledgements

Technical assistance was received from Martha Calahorra, Ramón Méndez-Franco and Norma Sánchez. We thank Dr Juan Pablo Pardo for the gift of the AOX antibody. Partially funded by the PAPIIT program and DGAPA/UNAM (grant IN202612). ACO, SGC and MRL are CONACYT fellows enrolled in the Biochemistry Graduate Program at UNAM. This is a partial requirement for the obtention of the PhD degree by ACO.

## References

- [1] J.C. Gonzalez-Hernandez, C.A. Cardenas-Monroy, A. Pena, Sodium and potassium transport in the halophilic yeast *Debaryomyces hansenii*, Yeast 21 (2004) 403–412.
- [2] U. Breuer, H. Harms, *Debaryomyces hansenii*—an extremophilic yeast with biotechnological potential, Yeast 23 (2006) 415–427.
- [3] B. Norkrans, Studies on marine occurring yeasts: growth related to pH, NaCl concentration and temperature, Arch. Mikrobiol. 54 (1966) 374–392.
- [4] B. Norkrans, A. Kylin, Regulation of the potassium to sodium ratio and of the osmotic potential in relation to salt tolerance in yeasts, J. Bacteriol. 100 (1969) 836–845.
- [5] C. Prista, M.C. Loureiro-Dias, V. Montiel, R. Garcia, J. Ramos, Mechanisms underlying the halotolerant way of *Debaryomyces hansenii*, FEMS Yeast Res. 5 (2005) 693–701.
- [6] J.A. Hobot, D.H. Jennings, Growth of *Debaryomyces hansenii* and *Saccharomyces cerevisiae* in relation to pH and salinity, Exp. Mycol. 5 (1981) 217–228.
- [7] H. Seiler, M. Busse, The yeasts of cheese brines, Int. J. Food Microbiol. 11 (1990) 289–303.
- [8] T. Nakase, M. Suzuki, Taxonomic studies on *Debaryomyces hansenii* (Zopf) Lodder et Kreger-Van Rij and related species. II. Practical discrimination and nomenclature, J. Gen. Appl. Microbiol. 31 (1985) 71–86.
- [9] T.v.d. Tempel, M. Jakobsen, The technological characteristics of *Debaryomyces hansenii* and *Yarrowia lipolytica* and their potential as starter cultures for production of Danablu, Int. Dairy J. 10 (2000) 263–270.
- [10] M.E. Fadda, V. Mossa, M.B. Pisano, M. Deplano, S. Cosentino, Occurrence and characterization of yeasts isolated from artisanal Fiore Sardo cheese, Int. J. Food Microbiol. 95 (2004) 51–59.
- [11] N.S. Sanchez, M. Calahorra, J.C. Gonzalez-Hernandez, A. Pena, Glycolytic sequence and respiration of *Debaryomyces hansenii* as compared to *Saccharomyces cerevisiae*, Yeast 23 (2006) 361–374.
- [12] N.S. Sanchez, R. Arreguin, M. Calahorra, A. Pena, Effects of salts on aerobic metabolism of *Debaryomyces hansenii*, FEMS Yeast Res. 8 (2008) 1303–1312.
- [13] M. Calahorra, N.S. Sanchez, A. Pena, Activation of fermentation by salts in *Debaryomyces hansenii*, FEMS Yeast Res. 9 (2009) 1293–1301.
- [14] A. Cabrera-Orefice, S. Guerrero-Castillo, L.A. Luevano-Martinez, A. Pena, S. Uribe-Carvaljal, Mitochondria from the salt-tolerant yeast *Debaryomyces hansenii* (halophilic organelles?), J. Bioenerg. Biomembr. 42 (2010) 11–19.
- [15] M. Gutierrez-Aguilar, X. Perez-Martinez, E. Chavez, S. Uribe-Carvaljal, In *Saccharomyces cerevisiae*, the phosphate carrier is a component of the mitochondrial unselective channel, Arch. Biochem. Biophys. 494 (2010) 184–191.
- [16] B. Guerin, O. Bunoust, V. Rouqueys, M. Rigoulet, ATP-induced unspecific channel in yeast mitochondria, J. Biol. Chem. 269 (1994) 25406–25410.
- [17] S. Manon, M. Guerin, Investigation of the yeast mitochondrial unselective channel in intact and permeabilized spheroplasts, Biochem. Mol. Biol. Int. 44 (1998) 565–575.
- [18] V. Perez-Vazquez, A. Saavedra-Molina, S. Uribe, In *Saccharomyces cerevisiae*, cations control the fate of the energy derived from oxidative metabolism through the opening and closing of the yeast mitochondrial unselective channel, J. Bioenerg. Biomembr. 35 (2003) 231–241.
- [19] M. Gutierrez-Aguilar, V. Perez-Vazquez, O. Bunoust, S. Manon, M. Rigoulet, S. Uribe, In yeast, Ca<sup>2+</sup> and octylguanidine interact with porin (VDAC) preventing the mitochondrial permeability transition, Biochim. Biophys. Acta 1767 (2007) 1245–1251.
- [20] D.G. Nicholls, S.J. Ferguson, Bioenergetics 3, Academic Press, London, 2002.
- [21] T. Joseph-Horne, D.W. Hollomon, P.M. Wood, Fungal respiration: a fusion of standard and alternative components, Biochim. Biophys. Acta 1504 (2001) 179–195.
- [22] I.M. Juszczuk, A.M. Rychter, Alternative oxidase in higher plants, Acta Biochim. Pol. 50 (2003) 1257–1271.
- [23] N. Sen, H.K. Majumder, Mitochondrion of protozoan parasite emerges as potent therapeutic target: exciting drugs are on the horizon, Curr. Pharm. Des. 14 (2008) 839–846.
- [24] A. McDonald, G. Vanlerberghe, Branched mitochondrial electron transport in the Animalia: presence of alternative oxidase in several animal phyla, IUBMB Life 56 (2004) 333–341.
- [25] D. Munro, N. Pichaud, F. Paquin, V. Kemeid, P.U. Blier, Low hydrogen peroxide production in mitochondria of the long-lived *Arctica islandica*: underlying mechanisms for slow aging, Aging cell 12 (2013) 584–592.
- [26] R. Buschges, G. Bahrenberg, M. Zimmermann, K. Wolf, NADH: ubiquinone oxidoreductase in obligate aerobic yeasts, Yeast 10 (1994) 475–479.
- [27] J. Nosek, H. Fukuhara, NADH dehydrogenase subunit genes in the mitochondrial DNA of yeasts, J. Bacteriol. 176 (1994) 5622–5630.
- [28] D.A. Berthold, M.E. Andersson, P. Nordlund, New insight into the structure and function of the alternative oxidase, Biochim. Biophys. Acta 1460 (2000) 241–254.
- [29] M.S. Albury, C. Affourtit, P.G. Crichton, A.L. Moore, Structure of the plant alternative oxidase, Site-directed mutagenesis provides new information on the active site and membrane topology, J. Biol. Chem. 277 (2002) 1190–1194.
- [30] M.E. Andersson, P. Nordlund, A revised model of the active site of alternative oxidase, FEBS Lett. 449 (1999) 17–22.
- [31] A.L. Moore, J.N. Siedow, The regulation and nature of the cyanide-resistant alternative oxidase of plant mitochondria, Biochim. Biophys. Acta 1059 (1991) 121–140.
- [32] H. Lambers, The physiological significance of the cyanide-resistant respiration in higher plants, Plant Cell Environ. 3 (1980) 293–302.
- [33] D.A. Day, J.T. Wiskich, Regulation of alternative oxidase activity in higher plants, J. Bioenerg. Biomembr. 27 (1995) 379–385.
- [34] D.P. Maxwell, Y. Wang, L. McIntosh, The alternative oxidase lowers mitochondrial reactive oxygen production in plant cells, Proc. Natl. Acad. Sci. U. S. A. 96 (1999) 8271–8276.
- [35] S. Guerrero-Castillo, D. Araiza-Olivera, A. Cabrera-Orefice, J. Espinasa-Jaramillo, M. Gutierrez-Aguilar, L.A. Luevano-Martinez, A. Zepeda-Bastida, S. Uribe-Carvaljal, Physiological uncoupling of mitochondrial oxidative phosphorylation. Studies in different yeast species, J. Bioenerg. Biomembr. 43 (2011) 323–331.
- [36] R. El-Khoury, E. Dufour, M. Rak, N. Ramanantsoa, N. Grandchamp, Z. Csaba, B. Duvillie, P. Benit, J. Gallego, P. Gressens, C. Sarkis, H.T. Jacobs, P. Rustin, Alternative oxidase expression in the mouse enables bypassing cytochrome c oxidase blockade and limits mitochondrial ROS overproduction, PLoS Genet. 9 (2013) e1003182.
- [37] S. Kerscher, S. Drose, V. Zickermann, U. Brandt, The three families of respiratory NADH dehydrogenases, Results Probl. Cell Differ. 45 (2008) 185–222.
- [38] S. de Vries, L.A. Grivell, Purification and characterization of a rotenone-insensitive NADH:Q6 oxidoreductase from mitochondria of *Saccharomyces cerevisiae*, Eur. J. Biochem. 176 (1988) 377–384.
- [39] I.L. Pahlman, C. Larsson, N. Averet, O. Bunoust, S. Boubeker, L. Gustafsson, M. Rigoulet, Kinetic regulation of the mitochondrial glycerol-3-phosphate dehydrogenase by the external NADH dehydrogenase in *Saccharomyces cerevisiae*, J. Biol. Chem. 277 (2002) 27991–27995.
- [40] M. Rigoulet, A. Mourier, A. Galinier, L. Casteilla, A. Devin, Electron competition process in respiratory chain: regulatory mechanisms and physiological functions, Biochim. Biophys. Acta 1797 (2010) 671–677.
- [41] B. Ronnow, M.C. Kielland-Brandt, GUT2, a gene for mitochondrial glycerol 3-phosphate dehydrogenase of *Saccharomyces cerevisiae*, Yeast 9 (1993) 1121–1130.
- [42] C.R. Hackenbrock, B. Chazotte, S.S. Gupte, The random collision model and a critical assessment of diffusion and collision in mitochondrial electron transport, J. Bioenerg. Biomembr. 18 (1986) 331–368.
- [43] H. Eubel, J. Heinemeyer, H.P. Braun, Identification and characterization of respirasomes in potato mitochondria, Plant Physiol. 134 (2004) 1450–1459.
- [44] H. Schagger, K. Pfeiffer, Supercomplexes in the respiratory chains of yeast and mammalian mitochondria, EMBO J. 19 (2000) 1777–1783.
- [45] F. Krause, N.H. Reischneider, D. Vocke, H. Seelert, S. Rexroth, N.A. Dencher, “Respirasome”-like supercomplexes in green leaf mitochondria of spinach, J. Biol. Chem. 279 (2004) 48369–48375.
- [46] H. Eubel, L. Jansch, H.P. Braun, New insights into the respiratory chain of plant mitochondria. Supercomplexes and a unique composition of complex II, Plant Physiol. 133 (2003) 274–286.
- [47] G. Lenaz, M.L. Genova, Kinetics of integrated electron transfer in the mitochondrial respiratory chain: random collisions vs. solid state electron channeling, Am. J. Physiol. Cell Physiol. 292 (2007) C1221–C1239.
- [48] H. Schagger, Respiratory chain supercomplexes of mitochondria and bacteria, Biochim. Biophys. Acta 1555 (2002) 154–159.
- [49] H. Schagger, Respiratory chain supercomplexes, IUBMB Life 52 (2001) 119–128.
- [50] N.V. Dudkina, J. Heinemeyer, S. Sunderhaus, E.J. Boekema, H.P. Braun, Respiratory chain supercomplexes in the plant mitochondrial membrane, Trends Plant Sci. 11 (2006) 232–240.

- [51] S. Guerrero-Castillo, M. Vazquez-Acevedo, D. Gonzalez-Halphen, S. Uribe-Carvajal, In *Yarrowia lipolytica* mitochondria, the alternative NADH dehydrogenase interacts specifically with the cytochrome complexes of the classic respiratory pathway, *Biochim. Biophys. Acta* 1787 (2009) 75–85.
- [52] H. Boumans, L.A. Grivell, J.A. Berden, The respiratory chain in yeast behaves as a single functional unit, *J. Biol. Chem.* 273 (1998) 4872–4877.
- [53] R.A. Stuart, Supercomplex organization of the oxidative phosphorylation enzymes in yeast mitochondria, *J. Bioenerg. Biomembr.* 40 (2008) 411–417.
- [54] E. Nubel, I. Wittig, S. Kerscher, U. Brandt, H. Schagger, Two-dimensional native electrophoretic analysis of respiratory supercomplexes from *Yarrowia lipolytica*, *Proteomics* 9 (2009) 2408–2418.
- [55] R. Acin-Perez, P. Fernandez-Silva, M.L. Peleato, A. Perez-Martos, J.A. Enriquez, Respiratory active mitochondrial supercomplexes, *Mol. Cell* 32 (2008) 529–539.
- [56] E.J. Boekema, H.P. Braun, Supramolecular structure of the mitochondrial oxidative phosphorylation system, *J. Biol. Chem.* 282 (2007) 1–4.
- [57] A. Veiga, J.D. Arrabaca, M.C. Loureiro-Dias, Cyanide-resistant respiration is frequent, but confined to yeasts incapable of aerobic fermentation, *FEMS Microbiol. Lett.* 190 (2000) 93–97.
- [58] A. Veiga, J.D. Arrabaca, M.C. Loureiro-Dias, Cyanide-resistant respiration, a very frequent metabolic pathway in yeasts, *FEMS Yeast Res.* 3 (2003) 239–245.
- [59] A. Veiga, J.D. Arrabaca, F. Sansonetty, P. Ludovico, M. Corte-Real, M.C. Loureiro-Dias, Energy conversion coupled to cyanide-resistant respiration in the yeasts *Pichia membranifaciens* and *Debaryomyces hansenii*, *FEMS Yeast Res.* 3 (2003) 141–148.
- [60] A.G. Gornall, C.J. Bardawill, M.M. David, Determination of serum proteins by means of the biuret reaction, *J. Biol. Chem.* 177 (1949) 751–766.
- [61] I. Wittig, H. Schagger, Advantages and limitations of clear-native PAGE, *Proteomics* 5 (2005) 4338–4346.
- [62] B.R. Oakley, D.R. Kirsch, N.R. Morris, A simplified ultrasensitive silver stain for detecting proteins in polyacrylamide gels, *Anal. Biochem.* 105 (1980) 361–363.
- [63] W. Wray, T. Boulikas, V.P. Wray, R. Hancock, Silver staining of proteins in polyacrylamide gels, *Anal. Biochem.* 118 (1981) 197–203.
- [64] E. Zerbetto, L. Vergani, F. Dabbeni-Sala, Quantification of muscle mitochondrial oxidative phosphorylation enzymes via histochemical staining of blue native polyacrylamide gels, *Electrophoresis* 18 (1997) 2059–2064.
- [65] M.S. Johnson, S.A. Kuby, Studies on NADH (NADPH)-cytochrome c reductase (FMN-containing) from yeast. Isolation and physicochemical properties of the enzyme from top-fermenting ale yeast, *J. Biol. Chem.* 260 (1985) 12341–12350.
- [66] U. Brandt, A two-state stabilization-change mechanism for proton-pumping complex I, *Biochim. Biophys. Acta* 1807 (2011) 1364–1369.
- [67] M. Iwata, Y. Lee, T. Yamashita, T. Yagi, S. Iwata, A.D. Cameron, M.J. Maher, The structure of the yeast NADH dehydrogenase (Ndi1) reveals overlapping binding sites for water- and lipid-soluble substrates, *Proc. Natl. Acad. Sci. U. S. A.* 109 (2012) 15247–15252.
- [68] I. Wittig, M. Karas, H. Schagger, High resolution clear native electrophoresis for in-gel functional assays and fluorescence studies of membrane protein complexes, *Mol. Cell. Proteomics* 6 (2007) 1215–1225.
- [69] B. Dujon, D. Sherman, G. Fischer, P. Durrens, S. Casaregola, I. Lafontaine, J. De Montigny, C. Marche, C. Neveuville, E. Talla, N. Goffard, L. Frangeul, M. Aigle, V. Anthouard, A. Babour, V. Barbe, S. Barnay, S. Blanchin, J.M. Beckerich, E. Beyne, C. Bleykasten, A. Boisrame, J. Boyer, L. Cattolico, F. Confaniolieri, A. De Daruvar, L. Despons, E. Fabre, C. Fairhead, H. Ferry-Dumazet, A. Groppi, F. Hantraye, C. Hennequin, N. Jauniaux, P. Joyet, R. Kachouri, A. Kerrest, R. Koszul, M. Lemaire, I. Lesur, L. Ma, H. Muller, J.M. Nicaud, M. Nikolski, S. Oztas, O. Ozier-Kalogeropoulos, S. Pellenz, S. Potier, G.F. Richard, M.L. Straub, A. Suleau, D. Swennen, F. Tekaia, M. Wesolowski-Louvel, E. Westhof, B. Wirth, M. Zeniou-Meyer, I. Zivanovic, M. Bolotin-Fukuhara, A. Thierry, C. Bouchier, B. Caudron, C. Scarpelli, C. Gaillardin, J. Weissenbach, P. Wincker, J.L. Souciet, Genome evolution in yeasts, *Nature* 430 (2004) 35–44.
- [70] D.J. Sherman, T. Martin, M. Nikolski, C. Cayla, J.L. Souciet, P. Durrens, Genolevures: protein families and synteny among complete hemiascomycetous yeast proteomes and genomes, *Nucleic Acids Res.* 37 (2009) D550–D554.
- [71] W.K. Huh, S.O. Kang, Characterization of the gene family encoding alternative oxidase from *Candida albicans*, *Biochem. J.* 356 (2001) 595–604.
- [72] M.A. Larkin, G. Blackshields, N.P. Brown, R. Chenna, P.A. McGettigan, H. McWilliam, F. Valentin, I.M. Wallace, A. Wilm, R. Lopez, J.D. Thompson, T.J. Gibson, D.G. Higgins, Clustal W and Clustal X version 2.0, *Bioinformatics* 23 (2007) 2947–2948.
- [73] U.K. Laemmli, Cleavage of structural proteins during the assembly of the head of bacteriophage T4, *Nature* 227 (1970) 680–685.
- [74] H. Towbin, T. Staehelin, J. Gordon, Electrophoretic transfer of proteins from polyacrylamide gels to nitrocellulose sheets: procedure and some applications, *Proc. Natl. Acad. Sci. U. S. A.* 76 (1979) 4350–4354.
- [75] T.E. Elthon, R.L. Nickels, L. McIntosh, Monoclonal antibodies to the alternative oxidase of higher plant mitochondria, *Plant Physiol.* 89 (1989) 1311–1317.
- [76] N. Chiquete-Felix, J.M. Hernandez, J.A. Mendez, A. Zepeda-Bastida, A. Chagolla-Lopez, A. Mujica, In guinea pig sperm, aldolase A forms a complex with actin, WASP, and Arp2/3 that plays a role in actin polymerization, *Reproduction* 137 (2009) 669–678.
- [77] S.J. Kerscher, J.G. Okun, U. Brandt, A single external enzyme confers alternative NADH:ubiquinone oxidoreductase activity in *Yarrowia lipolytica*, *J. Cell Sci.* 112 (Pt 14) (1999) 2347–2354.
- [78] M.G. Claros, P. Vincens, Computational method to predict mitochondrially imported proteins and their targeting sequences, *Eur. J. Biochem.* 241 (1996) 779–786.
- [79] L. Adler, A. Blomberg, A. Nilsson, Glycerol metabolism and osmoregulation in the salt-tolerant yeast *Debaryomyces hansenii*, *J. Bacteriol.* 162 (1985) 300–306.
- [80] A.L. Umbach, J.N. Siedow, The cyanide-resistant alternative oxidases from the fungi *Pichia stipitis* and *Neurospora crassa* are monomeric and lack regulatory features of the plant enzyme, *Arch. Biochem. Biophys.* 378 (2000) 234–245.
- [81] C. Affourtit, K. Krab, A.L. Moore, Control of plant mitochondrial respiration, *Biochim. Biophys. Acta* 1504 (2001) 58–69.
- [82] C.A. Smith, V.J. Melino, C. Sweetman, K.L. Soole, Manipulation of alternative oxidase can influence salt tolerance in *Arabidopsis thaliana*, *Physiol. Plant.* 137 (2009) 459–472.
- [83] S. Sakajo, N. Minagawa, T. Komiyama, A. Yoshimoto, Characterization of cyanide-resistant respiration and appearance of a 36 kDa protein in mitochondria isolated from antimycin A-treated *Hansenula anomala*, *J. Biochem.* 108 (1990) 166–168.
- [84] X. Huang, U. von Rad, J. Durner, Nitric oxide induces transcriptional activation of the nitric oxide-tolerant alternative oxidase in *Arabidopsis* suspension cells, *Planta* 215 (2002) 914–923.
- [85] O. Juarez, G. Guerra, F. Martinez, J.P. Pardo, The mitochondrial respiratory chain of *Ustilago maydis*, *Biochim. Biophys. Acta* 1658 (2004) 244–251.
- [86] I. Wittig, R. Carrozzo, F.M. Santorelli, H. Schagger, Supercomplexes and subcomplexes of mitochondrial oxidative phosphorylation, *Biochim. Biophys. Acta* 1757 (2006) 1066–1072.
- [87] S. Guerrero-Castillo, A. Cabrera-Orefice, M. Vazquez-Acevedo, D. Gonzalez-Halphen, S. Uribe-Carvajal, During the stationary growth phase, *Yarrowia lipolytica* prevents the overproduction of reactive oxygen species by activating an uncoupled mitochondrial respiratory pathway, *Biochim. Biophys. Acta* 1817 (2012) 353–362.
- [88] X. Grandier-Vazeille, K. Bathany, S. Chaignepain, N. Camougrand, S. Manon, J.M. Schmitter, Yeast mitochondrial dehydrogenases are associated in a supramolecular complex, *Biochemistry* 40 (2001) 9758–9769.
- [89] S. Uribe-Carvajal, L.A. Luevano-Martinez, S. Guerrero-Castillo, A. Cabrera-Orefice, N.A. Corona-de-la-Pena, M. Gutierrez-Aguilar, Mitochondrial unselective channels throughout the eukaryotic domain, *Mitochondrion* 11 (2011) 382–390.
- [90] S.J. Kerscher, Diversity and origin of alternative NADH:ubiquinone oxidoreductases, *Biochim. Biophys. Acta* 1459 (2000) 274–283.
- [91] S.A. Uyemura, S. Luo, M. Vieira, S.N. Moreno, R. Docampo, Oxidative phosphorylation and rotenone-insensitive malate- and NADH-quinone oxidoreductases in *Plasmodium yoelii yoelii* mitochondria in situ, *J. Biol. Chem.* 279 (2004) 385–393.
- [92] V.P. Martins, F.M. Soriano, T. Magnani, V.G. Tudela, G.H. Goldman, C. Curti, S.A. Uyemura, Mitochondrial function in the yeast form of the pathogenic fungus *Paracoccidioides brasiliensis*, *J. Bioenerg. Biomembr.* 40 (2008) 297–305.
- [93] M. Klingenberg, Localization of the glycerol-phosphate dehydrogenase in the outer phase of the mitochondrial inner membrane, *Eur. J. Biochem.* 13 (1970) 247–252.
- [94] O. Bunoust, A. Devin, N. Averet, N. Camougrand, M. Rigoulet, Competition of electrons to enter the respiratory chain: a new regulatory mechanism of oxidative metabolism in *Saccharomyces cerevisiae*, *J. Biol. Chem.* 280 (2005) 3407–3413.
- [95] M.V. Kovaleva, E.I. Sukhanova, T.A. Trendeleva, M.V. Zyl'kova, L.A. Ural'skaya, K.M. Popova, N.E. Saris, R.A. Zvyagilskaya, Induction of a non-specific permeability transition in mitochondria from *Yarrowia lipolytica* and *Dipodascus (Endomyces) magnusii* yeasts, *J. Bioenerg. Biomembr.* 41 (2009) 239–249.
- [96] J. Heinemeyer, H.P. Braun, E.J. Boekema, R. Kouril, A structural model of the cytochrome C reductase/oxidase supercomplex from yeast mitochondria, *J. Biol. Chem.* 282 (2007) 12240–12248.
- [97] C. Chen, Y. Ko, M. Delannoy, S.J. Ludtke, W. Chiu, P.L. Pedersen, Mitochondrial ATP synthosome: three-dimensional structure by electron microscopy of the ATP synthase in complex formation with carriers for Pi and ADP/ATP, *J. Biol. Chem.* 279 (2004) 31761–31768.



# In *Saccharomyces cerevisiae* fructose-1,6-bisphosphate contributes to the Crabtree effect through closure of the mitochondrial unspecific channel



Mónica Rosas-Lemus, Cristina Uribe-Alvarez, Natalia Chiquete-Félix, Salvador Uribe-Carvajal \*

Department of Molecular Genetics, Inst. de Fisiología Celular, Universidad Nacional Autónoma de México, Mexico

## ARTICLE INFO

### Article history:

Received 25 March 2014  
and in revised form 16 May 2014  
Available online 9 June 2014

### Keywords:

Fructose-1,6-bisphosphate  
Glucose-6-phosphate  
Crabtree effect  
Mitochondria  
*Saccharomyces cerevisiae*  
Permeability transition

## ABSTRACT

In *Saccharomyces cerevisiae* addition of glucose inhibits oxygen consumption, i.e. *S. cerevisiae* is Crabtree-positive. During active glycolysis hexoses-phosphate accumulate, and probably interact with mitochondria. In an effort to understand the mechanism underlying the Crabtree effect, the effect of two glycolysis-derived hexoses-phosphate was tested on the *S. cerevisiae* mitochondrial unspecific channel (*ScMUC*). Glucose-6-phosphate (G6P) promoted partial opening of *ScMUC*, which led to proton leakage and uncoupling which in turn resulted in, accelerated oxygen consumption. In contrast, fructose-1,6-bisphosphate (F1,6BP) closed *ScMUC* and thus inhibited the rate of oxygen consumption. When added together, F1,6BP reverted the mild G6P-induced effects. F1,6BP is proposed to be an important modulator of *ScMUC*, whose closure contributes to the "Crabtree effect".

© 2014 Elsevier Inc. All rights reserved.

## Introduction

In "Crabtree positive" yeast, the addition of glucose both increases glycolysis and inhibits the rate of oxygen consumption [1,2]. It has been proposed that glucose addition induces a rapid metabolic switch from a gluconeogenic/respiratory metabolism to a fermentative mode [3]. The Crabtree effect and the Warburg effect are different in that the Crabtree effect is immediate and reversible, while the Warburg effect is established at longer times, after the expression of different proteins that lead to its irreversibility. Both phenomena have been observed in tumor cells [1]. The Crabtree effect is triggered by different metabolic signals [2,4,5]. Among these is the accumulation of the glycolytic intermediaries glucose-6-phosphate (G6P)<sup>1</sup> [6–10 mM], and fructose-1,6-bisphosphate (F1,6BP) [5–10 mM] [6–8]. Glycolysis-derived accumulation of hexoses-phosphate complements other known signaling molecules such as fructose-2,6-biphosphate [9].

The Crabtree effect is observed in tumor cells [10,11], highly proliferating non-tumor cells [11], some yeast species [12] and some bacteria [13]. In regard to the mechanism underlying the Crabtree effect, a competition between glycolysis and oxidative phosphorylation for ADP or Pi has been proposed [14–16]. The

mechanism underlying the Crabtree effect is still elusive, although inhibition of complex III and complex IV by F1,6BP has been reported [17].

Most Crabtree positive cells accumulate F1,6BP and G6P, which seem to modulate both glycolysis and oxidative phosphorylation [17–19]. Indeed, G6P and F6P activate the mitochondrial respiratory complex III, while F1,6BP inhibits the activity of both complex III and IV [17].

In the yeast *Saccharomyces cerevisiae*, oxidative phosphorylation is strongly regulated by the mitochondrial unspecific channel (*ScMUC*) [20,21]. MUCs have been observed in animals, plants and yeast [22,23]. MUCs opening, known as the permeability transition (PT), allows the passage of molecules up to 1.5 kDa [23–27], which results in mitochondrial swelling, transmembrane potential depletion and even rupture of the outer membrane [28]. It has been suggested that PT is physiological and reversible and that its main function is to eliminate cations or to partially uncouple the respiratory chain to prevent ROS overproduction [22,24,29–31]. ATP, low Pi and the rapid flow of electrons through the respiratory chain promote opening of *ScMUC* [20,32,33], while Pi, Ca<sup>2+</sup> and Mg<sup>2+</sup> close it [26].

In order to determine the mechanism by which G6P and F1,6BP control mitochondrial metabolism and whether these molecules contribute to the Crabtree effect, their effects of these hexoses-phosphate on *ScMUC* were tested. It was observed that G6P opens *ScMUC* while F1,6BP closes it. When added together, the F1,6BP effect dominated. We propose that the closing of the *ScMUC* by F1,6BP inhibits the rate of oxygen consumption in the resting state

\* Corresponding author. Fax: +52 55 5622 5630.

E-mail address: suribe@ifc.unam.mx (S. Uribe-Carvajal).

<sup>1</sup> Abbreviations used: *ScMUC*, *S. cerevisiae* mitochondrial unspecific channel; G6P, glucose-6-phosphate; F1,6BP, fructose-1,6-bisphosphate; PT, permeability transition; CCCP, carbonyl cyanide 3-chlorophenylhydrazone.

through the tight coupling of mitochondria, i.e. F1,6BP is a Crabtree effect promoter.

## Material and methods

### Materials

All chemicals were of the highest purity commercially available. Fructose-1,6-bisphosphate, MES, mannitol, triethanolamine, safranine-O, trizma-base, dextrose, carbonyl cyanide 3-chlorophenylhydrazone (CCCP) and glucose-6-phosphate, were from Sigma-Aldrich Co. (St. Louis, MO),  $(\text{NH}_4)_2\text{SO}_4$ , D-lactic acid and ethanol were from J.T. Baker S.A. de C.V. (Xalostoc, México), yeast extract and gelatin peptone were from Bioxon Dickinson, S.A. de C.V. (Cuautitlán Izcalli, México),  $\text{KH}_2\text{PO}_4$ , KCl, and phosphoric acid were from Química Suastes S.A. de C.V. (Tlalhuac, México), BSA type V was from Research Organics (Cleveland, OH).

### Growth conditions

An industrial strain of baker's yeast "yeast foam" (YF) and the *Kluyveromyces lactis* strain 12/8 were used [34]. A 75 mL preculture in YPD (1% yeast extract, 2% gelatin peptone, 2% dextrose) was maintained for 8 h at 30 °C under agitation at 250 rpm. Subsequently, the pre-culture was added to 1L of YPLac (1% yeast extract, 1% gelatin peptone, 0.12%  $(\text{NH}_4)_2\text{SO}_4$ , 0.1%  $\text{KH}_2\text{PO}_4$  and 2% lactic acid, pH = 5.5) and incubated overnight. The cells were washed twice with distilled water by centrifugation in a F14 6x250y Sorvall rotor at 3800×g for 5 min.

### Isolation of mitochondria

Mitochondria were obtained by homogenization and differential centrifugation [35]. Briefly, cells were suspended 50% w/v in mitochondrial buffer (0.6 M mannitol, 5 mM MES pH 6.8 TEA) plus 0.1% BSA and were homogenized in a Bead Beater using 0.5 mm glass beads [36]. The homogenate was centrifuged in a F21-8x50y Sorvall rotor at 1017×g for 5 min. Then the supernatant was recovered and centrifuged at 10,700×g for 10 min. The pellet was suspended in mitochondrial buffer containing BSA, and centrifuged at 3600×g for 5 min. The supernatant was recovered and centrifuged at 17,000×g for 10 min. The resulting pellet was suspended in a small volume of mitochondrial buffer (without BSA) and protein was determined by biuret [37].

### Oxygen uptake

The rate of oxygen consumption was measured in resting state (State IV), in phosphorylating conditions (State III) and in the presence of the uncoupler CCCP (State U). We used a Strathkelvin Oximeter model 782 (Warner/Strathkelvin Instruments) with a Clark type electrode immersed in a 1 ml chamber with a water bath (PolyScience model 9000, USA) at 30 °C. The reaction mixture was 0.6 M mannitol, 5 mM MES, pH 6.8 (TEA), 10 mM KCl and 2 µl/ml ethanol. Pi concentrations used are indicated in the legends of the figures and tables. Mitochondrial protein concentration was 0.25 mg/ml.

### Mitochondrial swelling

The  $\text{K}^+$ -mediated mitochondrial swelling was determined at room temperature. The reaction mixture was 0.3 M mannitol, 5 mM MES, pH 6.8 (TEA) and 2 µl/ml, ethanol. Swelling was started with 20 mM KCl as indicated. The absorbance changes were

measured at 540 nm in a DW 2000 Aminco spectrophotometer in split mode equipped with a magnetic stirrer [38].

### Transmembrane potential

The  $\Delta\Psi$  was determined spectrophotometrically using a DW2000 Aminco spectrophotometer in dual mode. The reaction mixture was 0.6 M mannitol, 5 mM MES pH 6.8, 10 mM KCl, 2 µl/ml ethanol and 15 µM safranine-O. Absorbance changes were followed at 511–533 nm [39].

## Results and discussion

G6P increases, while F1,6BP inhibits the rate of oxygen consumption through direct inhibition of the cytochrome complexes III and IV [17]. However, a possible additional effect on  $s_c\text{MUC}$  has not been explored. The opening of  $s_c\text{MUC}$  accelerates oxygen consumption through uncoupling of oxidative phosphorylation [20,24,25,40]. By contrast, when  $s_c\text{MUC}$  is closed, oxygen consumption decreases [41]. Therefore, it was decided to explore in isolated yeast mitochondria the effect of G6P and F1,6BP on the rate of oxygen consumption (Table 1).

G6P was tested at concentrations of 2–20 mM in mitochondria where the  $s_c\text{MUC}$  was fully open (0.1 mM Pi), partially open (1 mM Pi) or fully closed (4 mM Pi). When  $s_c\text{MUC}$  was fully open, G6P had no effects (Results not shown). In mitochondria with partially closed  $s_c\text{MUC}$ , G6P increased the rate of oxygen consumption in the resting state IV while the uncoupled state was mildly accelerated only at the highest concentrations tested. These effects led to a mild decrease in the U/IV quotient (Table 1). In the conditions where  $s_c\text{MUC}$  was fully closed, only the highest concentrations of G6P resulted in a small increase in state IV respiration, while the uncoupled rate did not change significantly. Thus, a small decrease in the U/IV quotient was observed at the highest G6P concentrations tested (Table 1). In all cases, the effects of G6P on the phosphorylating state III were similar to those observed in the uncoupled state (Result not shown). The results suggest that at the tested concentrations, G6P has a mild uncoupling effect.

F1,6BP was tested at concentrations of 2–20 mM under conditions where  $s_c\text{MUC}$  was fully open (0.1 mM Pi) or fully closed (4 mM Pi) (Table 2). In mitochondria with an open  $s_c\text{MUC}$ , F1,6BP inhibited both state IV and the uncoupled state, increasing the U/IV from 1.0 in the totally uncoupled control to 2.0 at 6 mM. In mitochondria with a closed  $s_c\text{MUC}$ , F1,6BP also decreased the rates of respiration both in state IV and in the uncoupled state. The U/IV remained constant up to 6 mM F1,6BP, and it decreased at 10 and 20 mM F1,6BP (Table 2). The decrease in the rate of oxygen consumption in state IV respiration and the increase in the U/IV quotient indicated that F1,6BP is a coupling agent. Thus, the oxygen consumption results (Tables 1 and 2) indicate that G6P and F1,6BP are  $s_c\text{MUC}$  effectors, and that while the former is a mild uncoupler, the latter is an efficient coupling agent even at low concentrations.

When  $s_c\text{MUC}$  is open, mitochondria swell upon  $\text{K}^+$  addition. Thus, to further investigate whether G6P and F1,6BP modulate  $s_c\text{MUC}$ , swelling was measured. As expected from the oxygen consumption results, G6P had no effect on the opening of  $s_c\text{MUC}$  (Result not shown). However, in the presence of a partially closed  $s_c\text{MUC}$  (1 mM Pi) a slight rate of swelling was observed which increased mildly at higher G6P concentrations (Fig. 1A). In mitochondria where the  $s_c\text{MUC}$  was closed,  $\text{K}^+$ -mediated swelling was not observed and G6P did not have any effects (Fig. 1B).

The data in Table 2 suggest that F1,6BP is a coupling agent. To determine whether this effect may be related to  $s_c\text{MUC}$ , we added increasing concentrations of F1,6BP to mitochondria with open

**Table 1**

Effect of G6P on the rate of oxygen consumption under conditions where the  $s_c$ MUC is partially closed (1 mM Pi) or completely closed (Pi 4 mM).

Pi	G6P (mM)	State IV natgO(min <sup>-1</sup> mg prot) <sup>-1</sup>	Uncoupled state natgO(min <sup>-1</sup> mg prot) <sup>-1</sup>	U/IV
1 mM ( $s_c$ MUC partially closed)	0	132 ± 17.0	210 ± 19.8	1.6
	2	138 ± 19.8	198 ± 36.8	1.4
	4	150 ± 31.1	212 ± 39.6	1.4
	6	160 ± 11.3	214 ± 14.1	1.3
	10	194 ± 19.8	262 ± 14.1	1.3
	20	234 ± 14.1	280 ± 11.3	1.2
4 mM ( $s_c$ MUC closed)	0	162.9 ± 28.8	310.0 ± 45.4	1.9
	2	170.8 ± 5.25	278.8 ± 32.9	1.6
	4	196.7 ± 23.5	318.2 ± 23.6	1.6
	6	212.0 ± 18.3	333.9 ± 21.6	1.6
	10	208.7 ± 7.8	326.6 ± 11.0	1.6
	20	231.2 ± 16.5	332.8 ± 40.7	1.4

Reaction mixture: 0.6 M mannitol, 5 mM MES pH 6.8 (TEA), 2 μL ethanol/mL, 10 mM KCl and Pi as indicated. Glucose-6-phosphate (G6P) as indicated. Mitochondria (250 μg prot./mL). The uncoupled state was generated using CCCP (1.5 μM).

**Table 2**

Effect of F1,6BP on the rate of oxygen consumption under conditions where the  $s_c$ MUC is opened (Pi 0.1 mM) or closed (Pi 4 mM).

Pi	F1,6BP (mM)	State IV natgO(min <sup>-1</sup> mg prot) <sup>-1</sup>	Uncoupled state natgO(min <sup>-1</sup> mg prot) <sup>-1</sup>	U/IV
0.1 mM ( $s_c$ MUC open)	0	328.4 ± 29.0	339.2 ± 24.0	1.0
	2	167.6 ± 21.3	257.9 ± 46.0	1.5
	4	143.3 ± 27.3	263.2 ± 25.0	1.8
	6	129.4 ± 4.9	254.0 ± 43.0	2.0
	10	142.2 ± 12.5	276.7 ± 66.0	1.9
	20	140.6 ± 21.7	250.4 ± 46.0	1.8
4 mM ( $s_c$ MUC closed)	0	240.7 ± 21.1	452.5 ± 40.3	1.9
	2	214.2 ± 5.1	408.0 ± 48.5	1.9
	4	229.0 ± 19.4	422.2 ± 57.9	1.8
	6	208.3 ± 24.6	385.9 ± 8.8	1.8
	10	194.1 ± 24.4	357.3 ± 56.0	1.8
	20	192.7 ± 27.6	334.7 ± 28.3	1.7

Reaction mixture as in Table 1, except F1,6BP as indicated.

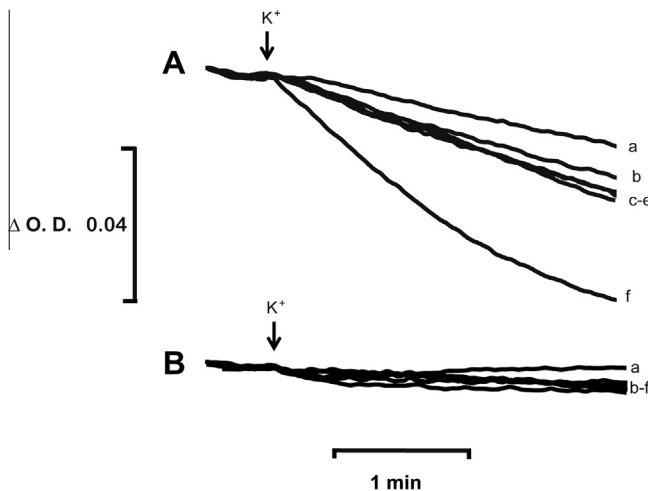


**Fig. 1.** Effects of G6P on mitochondrial swelling. Reaction mixture: 0.3 M mannitol, 5 mM MES pH 6.8 (TEA), 2 μL ethanol/mL, mitochondria 250 μg prot./mL, and Pi as indicated. Swelling was measured spectrophotometrically at 540 nm. The arrow indicates the addition of 20 mM KCl. (A) Pi 1 mM. (B) Pi 4 mM. G6P (mM) was: a, 0; b, 2; c, 4; d, 6; e, 10; f, 20.

$s_c$ MUC (0.1 mM Pi). In the absence of F1,6BP, mitochondrial swelling was large and rapid (Fig. 2A). Then, as the F1,6BP concentration increased, swelling decreased, becoming negligible at concentrations of 4 mM and above (Fig. 2A trace f). At 4 mM Pi, where  $s_c$ MUC was closed, no swelling was detected neither in the control nor at any F1,6BP concentration (Fig. 2B). Both oxygen consumption and mitochondrial swelling experiments indicate that F1,6BP promotes closure of  $s_c$ MUC, leading to coupling of oxidative phosphorylation.

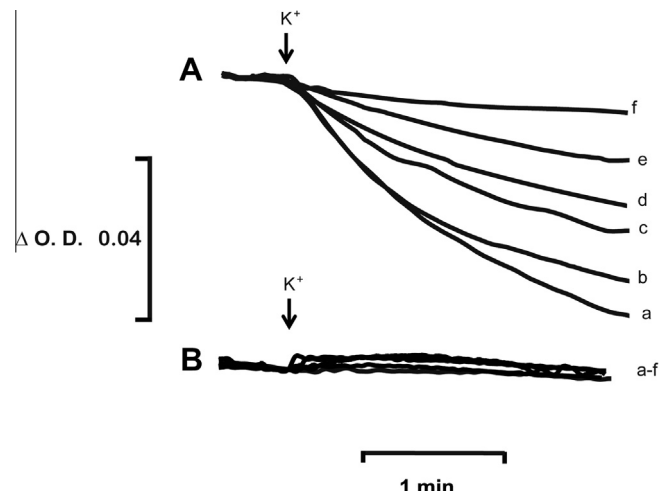


**Fig. 2.** Effects of F1,6BP on mitochondrial swelling. Reaction mixture as in Fig. 1 except (A) Pi 0.1 mM. (B) Pi 4 mM. At the arrow 20 mM KCl was added. G6P (mM) was: a, 0; b, 0.25; c, 0.5; d, 1; e, 2; f, 4.

The transmembrane potential decreases upon opening of  $s_c$ MUC [25], and thus the effect of G6P and F1,6BP on this parameter was also tested. In mitochondria with partially closed  $s_c$ MUC, G6P depleted the already-low transmembrane potential (Fig. 3A). Under conditions where  $s_c$ MUC was closed, different concentrations of G6P decreased the transmembrane potential (Fig. 3B). When assaying F1,6BP effects on mitochondria with fully open  $s_c$ MUC (Fig. 4A), the transmembrane potential increased with

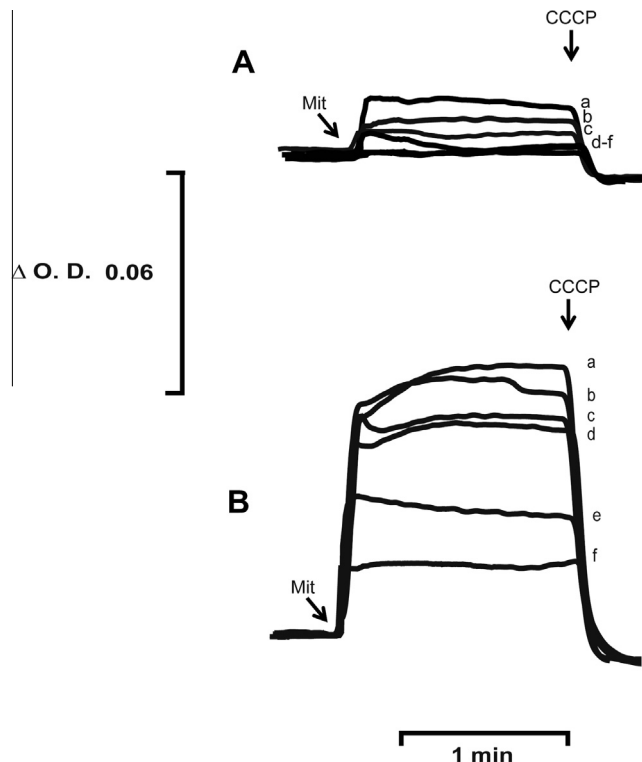


**Fig. 3.** Effects of G6P on the mitochondrial transmembrane potential. Reaction mixture as in Table 1 (except 15  $\mu$ M safranin-O), 10 mM KCl and Pi as indicated. (A) Pi 1 mM, (B) Pi 4 mM. G6P (mM) as follows: a, 0; b, 2; c, 4; d, 6; e, 10; f, 20. Where indicated, mitochondria (250  $\mu$ g prot./mL) or CCCP (1.5  $\mu$ M) were added.

increasing F1,6BP concentrations, reaching the highest value at 10 mM (Fig. 4A, trace e) and 20 mM (Fig. 4A trace f). Under closed  $s_c$ MUC conditions, a biphasic effect was observed, where a slight hyperpolarization was detected at 6 (Fig. 4B trace d) and 10 mM (Fig. 4B trace e) whereas a modest decrease in the transmembrane potential was observed at 20 mM F1,6BP (Fig. 4B trace f).

Both phosphate hexoses tested here seem to induce opposite effects. G6P is a mild uncoupler, probably opening  $s_c$ MUC, while F1,6BP has a strong coupling effect that probably results from closing  $s_c$ MUC. As both molecules are accumulated simultaneously during active glycolysis, it was decided to test which of their effects predominates when both are present.

To close  $s_c$ MUC even at low Pi (0.1 mM), 2 mM F1,6BP was added. Under these conditions  $K^+$  addition did not induce swelling (Fig. 5A, trace a). Then, increasing G6P concentrations promoted swelling, reaching a maximum at 20 mM G6P. The opposite experiment was performed under partially closed  $s_c$ MUC conditions (1 mM Pi) and in the presence of 10 mM G6P, where a slight swelling was promoted by  $K^+$  addition. Then, at increasing F1,6BP concentrations inhibition of swelling was observed, suggesting that the  $s_c$ MUC-closing effect of F1,6BP was much stronger than the  $s_c$ MUC-opening effect of G6P.

Thus, we propose that the two hexose-phosphates known to accumulate during active glycolysis are effectors of the  $s_c$ MUC. G6P is a mild uncoupler working through the opening  $s_c$ MUC while F1,6BP has stronger coupling properties that probably result in  $s_c$ MUC closure. The effect of the hexose-phosphate derivatives tested here was observed at lower concentrations than those needed to inhibit respiration.

In mammals, the mitochondrial permeability transition triggers cell death programs while in turn, a persistently closed MUC results in resistance to apoptosis. Indeed, in rat liver, overexpressed hexokinase seems to interact directly with mitochondria,

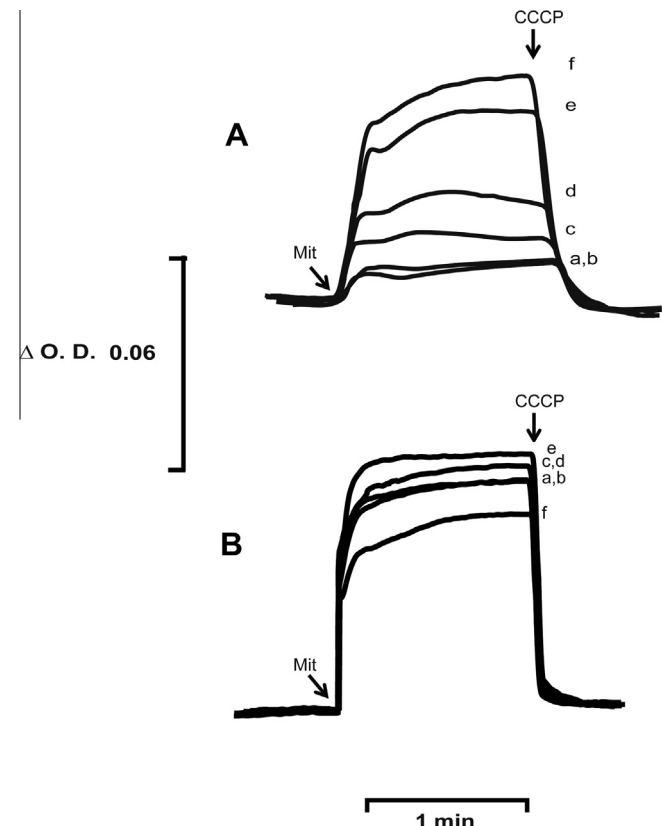


**Fig. 4.** Effects of F1,6BP on the transmembrane potential. Reaction mixture as in Fig. 3, except (A) Pi 0.1 mM and (B) Pi 4 mM. F1,6BP (mM) was: a, 0; b, 2; c, 4; d, 6; e, 10; f, 20. Mitochondria (250  $\mu$ g prot./mL), CCCP (1.5  $\mu$ M).

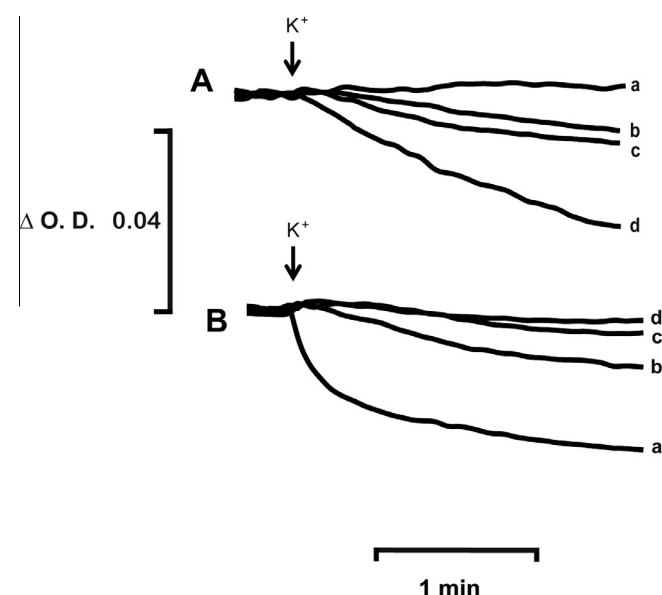


**Fig. 5.** Effects of competition between F1,6BP and G6P on mitochondrial swelling. Reaction mixture: as in Fig. 1. Pi as indicated. (A) Pi 0.1 mM, 2 mM F1,6BP. G6P (mM) was: a, 0; b, 4; c, 10; d, 20. (B) Pi 1 mM, 10 mM G6P. F1,6BP (mM) was a, 0; b, 0.5; c, 4; d, 10.

maintaining MUC in a closed state and thus inhibiting cell death [40–42]. F1,6BP promoted  $s_c$ MUC closure, therefore inhibiting the permeability transition. In addition, a closed  $s_c$ MUC inhibits apoptosis and promotes unregulated cell growth, indicating that there

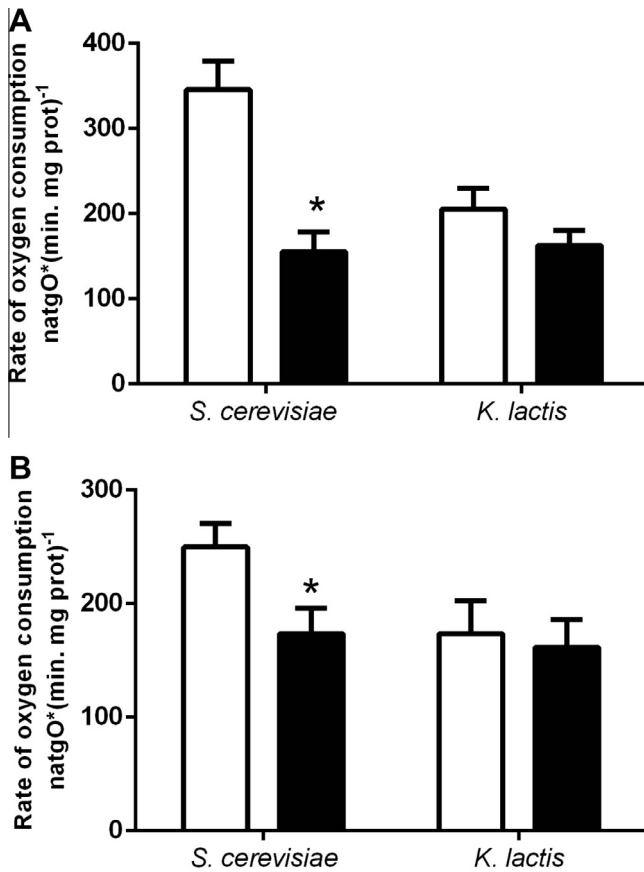


**Fig. 6.** Effect of F1,6BP on the rate of oxygen consumption of isolated mitochondria from *S. cerevisiae* or *K. lactis*. Reaction mixture as in Table 2, except (A) Pi 0.1 mM; (B) Pi 1 mM. F1,6BP was absent (empty bars) or 10 mM (black bars). \*Differences are statistically significant  $P < 0.01$ , based on ANOVA tukey's multiple comparison test.

may be a causal relationship between tumor cell immortalization and F1,6P accumulation.

If the F1,6BP-mediated inhibition of oxygen consumption by *S. cerevisiae* were related to the Crabtree effect, then Crabtree-negative yeasts should not be inhibited. To test this, we compared the effect of 10 mM F1,6BP on mitochondria isolated from either *S. cerevisiae* or from the Crabtree negative yeast *Kluyveromyces lactis* [43]. As expected from the results shown in Table 2, F1,6BP inhibited the rate of oxygen consumption in mitochondria from *S. cerevisiae* at both 0.1 mM (Fig. 6A) and 1.0 mM Pi (Fig. 6B). By contrast, in mitochondria from *K. lactis*, F1,6BP did not have any effects on the rate of oxygen consumption at either phosphate concentration (Fig. 6). These results strongly support the notion that F1,6BP is a key metabolite that signals closure of *Sc*MUC, triggering the Crabtree effect. Indeed, upon glucose addition, F1,6BP rises to 5–10 mM, which is much higher than the concentration of 0.5 mM F1,6BP needed to maintain *Sc*MUC in a closed state [7]. Furthermore, at 5 mM F1,6BP, additional mitochondrial effects are observed, such as inhibition of complex III and IV activities in the resting state IV. Further studies are needed in order to elucidate the physiological role of maintaining *Sc*MUC closed and dissect its likely relationship with the Crabtree effect.

## Acknowledgments

M.R.L. and C.U.A. are CONACYT fellows enrolled in the Biochemistry PhD program at UNAM. Partially funded by PAPIIT-DGAPA/

UNAM (grant IN202612). The authors thank Dr. Roberto Coria and Dr. Rocío Navarro for the kind donation of the *K. lactis* 12/8 strain. Dr. Diego González Halphen critically read the manuscript and participated in discussion of the data.

## References

- R. Diaz-Ruiz, M. Rigoulet, A. Devin, Biochim. Biophys. Acta 1807 (2011) 568–576.
- A. Devin, L. Dejean, B. Beauvoit, C. Chevtzoff, N. Averet, O. Bunoust, M. Rigoulet, J. Biol. Chem. 281 (2006) 26779–26784.
- J.M. Thevelein, S. Hohmann, Trends Biochem. Sci. 20 (1995) 3–10.
- B. Beauvoit, M. Rigoulet, O. Bunoust, G. Raffard, P. Canioni, B. Guerin, Eur. J. Biochem. 214 (1993) 163–172.
- N. Averet, H. Aguilaniu, O. Bunoust, L. Gustafsson, M. Rigoulet, J. Bioenerg. Biomembr. 34 (2002) 499–506.
- N. Averet, V. Fitton, O. Bunoust, M. Rigoulet, B. Guerin, Mol. Cell. Biochem. 184 (1998) 67–79.
- C. Stefan, U. Sauer, FEMS Yeast Res. 11 (2011) 263–272.
- J.R. Ermandes, C. De Meirsman, F. Rolland, J. Winderickx, J. de Winde, R.L. Brandao, J.M. Thevelein, Yeast 14 (1998) 255–269.
- J. Francois, E. Van Schaftingen, H.-G. Hers, Eur. J. Biochem. 145 (1984) 187–193.
- H.G. Crabtree, Biochem. J. 23 (1929) 536–545.
- E.F. Greiner, M. Guppy, K. Brand, J. Biol. Chem. 269 (1994) 31484–31490.
- A. Merico, P. Sullo, J. Piškar, C. Compagno, FEBS J. 274 (2007) 976–989.
- I. Mustea, T. Muresian, Cancer 20 (1967) 1499–1501.
- D.H. Koobs, Science 178 (1972) 127–133.
- R.L. Veech, J.W. Lawson, N.W. Cornell, H.A. Krebs, J. Biol. Chem. 254 (1979) 6538–6547.
- S. Rodriguez-Enriquez, O. Juarez, J.S. Rodriguez-Zavala, R. Moreno-Sanchez, Eur. J. Biochem. 268 (2001) 2512–2519.
- R. Diaz-Ruiz, N. Averet, D. Araiza, B. Pinson, S. Uribe-Carvajal, A. Devin, M. Rigoulet, J. Biol. Chem. 283 (2008) 26948–26955.
- D.H. Huberts, B. Niebel, M. Heinemann, FEMS Yeast Res. 12 (2012) 118–128.
- R. Diaz-Ruiz, S. Uribe-Carvajal, A. Devin, M. Rigoulet, Biochim. Biophys. Acta 1796 (2009) 252–265.
- B. Guerin, O. Bunoust, V. Rouqueys, M. Rigoulet, J. Biol. Chem. 269 (1994) 25406–25410.
- S. Manon, X. Roucou, M. Guerin, M. Rigoulet, B. Guerin, J. Bioenerg. Biomembr. 30 (1998) 419–429.
- S. Uribe-Carvajal, L.A. Luevano-Martinez, S. Guerrero-Castillo, A. Cabrera-Orefice, N.A. Corona-de-la-Pena, M. Gutierrez-Aguilar, Mitochondrion 11 (2011) 382–390.
- P. Bernardi, Physiol. Rev. 79 (1999) 1127–1155.
- R.A. Haworth, D.R. Hunter, Arch. Biochem. Biophys. 195 (1979) 460–467.
- V. Castrejon, C. Parra, R. Moreno, A. Pena, S. Uribe, Arch. Biochem. Biophys. 346 (1997) 37–44.
- V. Perez-Vazquez, A. Saavedra-Molina, S. Uribe, J. Bioenerg. Biomembr. 35 (2003) 231–241.
- V. Castrejon, A. Pena, S. Uribe, J. Bioenerg. Biomembr. 34 (2002) 299–306.
- P. Bernardi, M. Forte, Novartis Found. Symp. 287 (2007) 157–164 (discussion 164–159).
- M. Crompton, Biochem. J. 341 (1999) 233–249.
- J.J. Lemasters, A.L. Nieminen, T. Qian, L.C. Trost, S.P. Elmore, Y. Nishimura, R.A. Crowe, W.E. Cascio, C.A. Bradham, D.A. Brenner, B. Herman, Biochim. Biophys. Acta 1366 (1998) 177–196.
- A.P. Halestrap, Nature 430 (2004). 1 p following 983.
- S. Manon, M. Guerin, Biochem. Mol. Biol. Int. 44 (1998) 565–575.
- E. Fontaine, O. Eriksson, F. Ichas, P. Bernardi, J. Biol. Chem. 273 (1998) 12662–12668.
- R. Navarro-Olmos, L. Kawasaki, L. Dominguez-Ramirez, L. Ongay-Larios, R. Perez-Molina, R. Coria, Mol. Biol. Cell 21 (2010) 489–498.
- A. Pena, M.Z. Pina, E. Escamilla, E. Pina, FEBS Lett. 80 (1977) 209–213.
- S. Uribe, J. Ramirez, A. Pena, J. Bacteriol. 161 (1985) 1195–1200.
- A.G. Gornall, C.J. Bardawill, M.M. David, J. Biol. Chem. 177 (1949) 751–766.
- S. Prieto, F. Bouillaud, D. Ricquier, E. Rial, Eur. J. Biochem. 208 (1992) 487–491.
- K.E. Akerman, M.K. Wikstrom, FEBS Lett. 68 (1976) 191–197.
- C. Fiek, R. Benz, N. Roos, D. Brdiczka, Biomembranes 688 (1982) 429–440.
- M. Gutierrez-Aguilar, X. Perez-Martinez, E. Chavez, S. Uribe-Carvajal, Arch. Biochem. Biophys. 494 (2010) 184–191.
- H. Azoulay-Zohar, A. Israelson, S. Abu-Hamad, V. Shoshan-Barmatz, Biochem. J. 377 (2004) 347–355.
- N. Mates, K. Kettner, F. Heidenreich, T. Pursche, R. Migotti, G. Kahlert, E. Kuhlichs, K.D. Breunig, W. Schellenberger, G. Dittmar, B. Hofack, T.M. Kriegel, Mol. Cell. Proteomics 13 (2014) 860–875.

# Effects of ubiquinone derivatives on the mitochondrial unselective channel of *Saccharomyces cerevisiae*

Manuel Gutiérrez-Aguilar · Helga M. López-Carbajal ·  
Cristina Uribe-Alvarez · Emilio Espinoza-Simón · Mónica Rosas-Lemus ·  
Natalia Chiquete-Félix · Salvador Uribe-Carvajal

Received: 15 June 2014 / Accepted: 25 November 2014 / Published online: 3 December 2014  
© Springer Science+Business Media New York 2014

**Abstract** Ubiquinone derivatives modulate the mammalian mitochondrial Permeability Transition Pore (PTP). Yeast mitochondria harbor a similar structure: the respiration- and ATP-induced *Saccharomyces cerevisiae* Mitochondrial Unselective Channel (*ScMUC*). Here we show that decylubiquinone, a well-characterized inhibitor of the PTP, suppresses *ScMUC* opening in diverse strains and independently of respiratory chain modulation or redox-state. We also found that naturally occurring derivatives such as hexaprenyl and decaprenyl ubiquinones lacked effects on the *ScMUC*. The PTP-inactive ubiquinone 5 (Ub<sub>5</sub>) promoted the *ScMUC*-independent activation of the respiratory chain in most strains tested. In an industrial strain however, Ub<sub>5</sub> blocked the protection elicited by dUb. The results indicate the presence of a ubiquinone-binding site in the *ScMUC*.

**Keywords** Ubiquinone analogues · Mitochondria · Permeability transition pore · Yeast

## Abbreviations

dUb	Decylubiquinone
dVO <sub>4</sub>	Decavanadate
Δψ	Mitochondrial transmembrane potential
FCCP	Carbonyl cyanide <i>p</i> -trifluoro-methoxyphenyl-hydrazone

M. Gutiérrez-Aguilar (✉)  
Dalton Cardiovascular Research Center, University of Missouri-Columbia, 134 Research Park Dr, Columbia, MO 65211, U.S.A.  
e-mail: gutierrezaguilar@missouri.edu

H. M. López-Carbajal · C. Uribe-Alvarez · E. Espinoza-Simón ·  
M. Rosas-Lemus · N. Chiquete-Félix · S. Uribe-Carvajal  
Department of Molecular Genetics, Instituto de Fisiología Celular, Universidad Nacional Autónoma de México, UNAM, Mexico City, Mexico

Cyclosporine A	CsA
PTP	Mitochondrial permeability transition pore
<i>ScMUC</i>	<i>Saccharomyces cerevisiae</i> mitochondrial unselective channel
Ub <sub>5</sub>	Ubiquinone 5
Ub <sub>30</sub>	Hexaprenylquinone
Ub <sub>50</sub>	Decaprenylquinone

## Introduction

The mitochondrial permeability transition can be defined as the rise in unselective conductance to ions and metabolites triggered by the opening of an unidentified non-selective pore (Brenner and Moulin 2012). In mammalian mitochondria, the permeability transition pore (PTP) depletes the protonmotive force and exhibits a molecular mass cutoff of up to 1.5 kDa (Bernardi 2013). The *Saccharomyces cerevisiae* Mitochondrial Unselective Channel (*ScMUC*) is probably an equivalent of the PTP (Uribe-Carvajal et al. 2011).

The biochemistry and physiopathology of the PTP has been studied *ad extenso*. Most hypotheses suggest that this pore opens irreversibly during several disease states, inducing a collapse in mitochondrial homeostasis (for a review, see Di Lisa and Bernardi 2006). In contrast, PTP transient opening or flickering has also been proposed to regulate Ca<sup>2+</sup> homeostasis in mitochondria (Ichas and Mazat 1998). Less is known in terms of the molecular composition of the PTP; earlier models proposing that the Adenine Nucleotide Translocator and the Voltage Dependent Anion Channel could form the PTP have not successfully passed genetic tests (reviewed in Bonora et al. 2014). When the mitochondrial phosphate carrier is deleted, this results in changes in the properties of both, the PTP (Kwong et al. 2014) and the *ScMUC* (Gutiérrez-Aguilar et al. 2010) likely by controlling inorganic phosphate

(Pi) availability in mitochondria. However, a moderate change in the expression levels of the Pi carrier does not impact the  $\text{Ca}^{2+}$ -induced PTP (Gutiérrez-Aguilar et al. 2014). Up to now, Cyclophilin D (CypD) and mitochondrial Complex I are the only widely accepted modulators of the PTP (Giorgio et al. 2010; Di Lisa et al. 2011; Li et al. 2012). Topical studies suggest that CypD regulates  $\text{F}_1\text{F}_0$ -ATP synthase. In addition, the purified dimeric enzyme from both mouse and *S. cerevisiae* mitochondria forms a multiple conductance channel with PTP-like behavior (Giorgio et al. 2013; Carraro et al. 2014). This has led to propose that the unselective pores observed in yeast and higher eukaryotes are equivalent structures that form at the interface of two  $\text{F}_0$  sectors of ATP synthase and that the  $\text{F}_0$  sector may play an important role in PTP formation (Bernardi 2013; Bonora et al. 2013).

The  $s_c$ MUC probably participates in energy surplus dissipation processes (Prieto et al. 1995). Although the  $s_c$ MUC and the mammalian PTP present similar molecular exclusion properties, it was earlier proposed that the  $s_c$ MUC could be hardly considered a yeast counterpart of the PTP (Manon et al. 1998). Since *S. cerevisiae* lacks a mitochondrial  $\text{Ca}^{2+}$ -uniporter (Uribe et al. 1992),  $\text{Ca}^{2+}$  does not activate the  $s_c$ MUC unless *S. cerevisiae* mitochondria are incubated in the presence of the  $\text{Ca}^{2+}$  ionophore ETH129 (Yamada et al. 2009; Carraro et al. 2014). In regard to similarities in their properties,  $s_c$ MUC and PTP are both regulated by ADP, octylguanidine,  $\text{Mg}^{2+}$ , Pi, mercurials and mastoparan (Uribe-Carvajal et al. 2011). Indeed it has been suggested that MUCs are conserved throughout the eukaryotic domain (for reviews see Azzolin et al. 2010; Bernardi and Von Stockum 2012).

Different ubiquinone analogues seem to interact with mammalian mitochondria on a specific site. Then, depending on the analogue substituent, PTP may be activated, unaffected or inhibited (Walter et al. 2000). In addition, since ubiquinones are natural ligands of respiratory complexes I, II and III, certain analogues can also interfere with respiration thus making difficult to detect off-site effects (Walter et al. 2000). Here we aimed to determine whether ubiquinone analogues modulate the  $s_c$ MUC. This is interesting as *S. cerevisiae* mitochondria lack respiratory complex I. Our results show that known PTP inhibitors modulate  $s_c$ MUC activity and support the notion of a conserved ubiquinone-binding site on the channel.

## Materials and methods

### Materials

All chemicals were reagent grade. dUB, Ub<sub>5</sub>, Ub<sub>30</sub>, Ub<sub>50</sub>, Mannitol, MES, ethanol, safranine-O, CaCl<sub>2</sub>, MgCl<sub>2</sub>, ADP, FCCP and bovine serum albumin type V were from Sigma

Chem Co. (St. Louis, MO). All other reagents were of the highest purity commercially available.

### Industrial and laboratory yeast strains

A commercial strain of the baker's yeast *S. cerevisiae* (La Azteca) was purchased from a local bakery. The industrial strain Yeast Foam (YF) was obtained from a previous collaboration (Díaz-Ruiz et al. 2008). The laboratory strains were BY4741 (BY) (*MATA*; *his3* Δ1; *leu2* Δ0; *met15* Δ0; *ura3* Δ) and W303 (*MATα*; *ura3*-1; *trp1*Δ 2; *leu2*-3,112; *his3*-11,15; *ade2*-1; *can1*-100).

### Isolation of Yeast Mitochondria

For experiments in Figs. 1, 2A, B, C, 3, 4B and 5, an industrial strain of *S. cerevisiae* (La Azteca) was used. Cells (40 g) were suspended and incubated in a rich liquid medium under aeration (3 L/min) for 16 h, washed, suspended in distilled water and starved overnight under aeration (de Kloet et al. 1961). Cells were washed by centrifugation three times and suspended in 0.6 M mannitol, 5 mM MES, 0.1 % bovine serum albumin, pH 6.8 adjusted with triethanolamine (TEA). Cells were disrupted using a Braun cell-homogenizer and 0.45 mm diameter glass beads. Mitochondria were isolated by differential centrifugation in a SS34 rotor (Sorvall) (Cortés et al. 2000). Protein concentration was determined by a biuret method. For experiments in Figs. 2D and 4, the strains YF, W303 and BY were also used. The *S. cerevisiae* industrial strain Yeast Foam (YF) was subcultured 8 hours in YPD and cultured in YPLac until reaching an optical density of 3.0–3.5. The *S. cerevisiae* laboratory strains W303 and BY were subcultured in YPD for 24 hours and cultured in YPLac for 24 hours. All cultures were grown under constant agitation (250 rpm) at 30 °C. Mitochondria were isolated from the YF, W303 and BY strains after spheroplast homogenization and differential centrifugation (for detailed protocols see Gutiérrez-Aguilar et al. 2010).

### Oxygen consumption

The rate of oxygen consumption was measured in the resting state (State 4) and in the phosphorylating state (State 3) using an YSI model 5,300 oxygraph equipped with a Clark-Type electrode at room temperature in a 1.5 mL chamber containing mitochondria at a final concentration of 0.5 mg protein/mL. Samples were suspended in respiration buffer (0.6 M mannitol, 5 mM MES pH 6.8 (TEA) plus 5 μL/mL 96 % ethanol as respiratory substrate, unless indicated otherwise). The concentrations of Pi and K<sup>+</sup> used are indicated under each figure. Stock solutions were 1.0 M MgCl<sub>2</sub>, 2.0 M KCl, and either 1.0

or 0.1 M PO<sub>4</sub><sup>3-</sup> buffer, pH 6.8 (TEA) and 20 mM dUb, Ub<sub>5</sub>, Ub<sub>30</sub>, Ub<sub>50</sub>.

#### Transmembrane potential ( $\Delta\psi$ )

The  $\Delta\psi$  was determined using 10  $\mu$ M safranine-O, following the absorbance changes at 511–533 nm in a DW2000 Aminco spectrophotometer in dual mode (Akerman and Wikström 1976). At the end of each trace,  $\Delta\psi$  was collapsed by adding 6  $\mu$ M FCCP.

#### Mitochondrial swelling

The K<sup>+</sup>-mediated swelling of mitochondria was measured as described before (Castrejón et al. 2002). Typically, coupled isolated mitochondria are impermeable to K<sup>+</sup>. However, when the *S<sub>c</sub>MUC* opens, it allows unselective transport of externally added K<sup>+</sup> along with anions present in the medium, resulting in the transport of osmotically active species. This will result in the transport of water towards the mitochondrial matrix following swelling of the organelles, which is optically measured as a decrease in light scattering of isolated mitochondria in suspension. Swelling buffer, containing 0.3 M mannitol, 5 mM MES, pH 6.8 (TEA), plus 5  $\mu$ L/mL ethanol or NADH was used to promote swelling under energized conditions. Swelling was promoted by adding 20 mM KCl where indicated by an arrow. The absorbance changes were measured at 540 nm in a DW2 Aminco spectrophotometer in split mode equipped with a magnetic stirrer. Sample volume was kept constant at 4 mL of respiration buffer. Mitochondrial concentration was 0.5 mg protein/mL.

#### NADH:NAD<sup>+</sup> ratio determination

In order to determine whether the increase in alcohol dehydrogenase activity led to an increase in the percentage of reduced NADH, we made a NADH concentration curve, which we used to determine the amount of NADH present in samples incubated in the presence of increasing ethanol. Then, the 100 % percent NADH concentration was evaluated after adding 3  $\mu$ M sodium dithionite, which was prepared within one hour (Quinlan et al. 2013). NADH absorbance was read at 340 nm in a Varian 50 Bio-UV/Vis spectrophotometer.

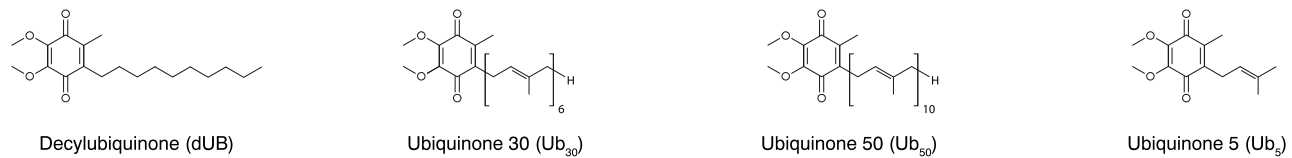
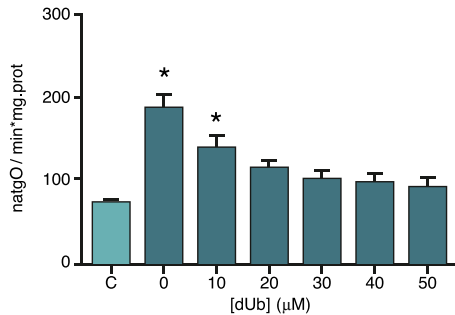
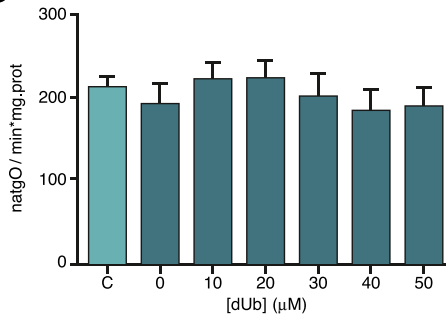
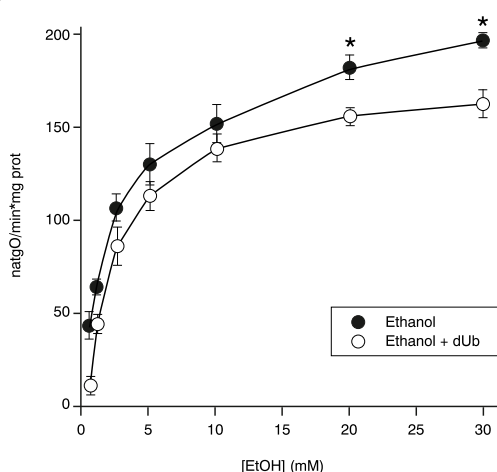
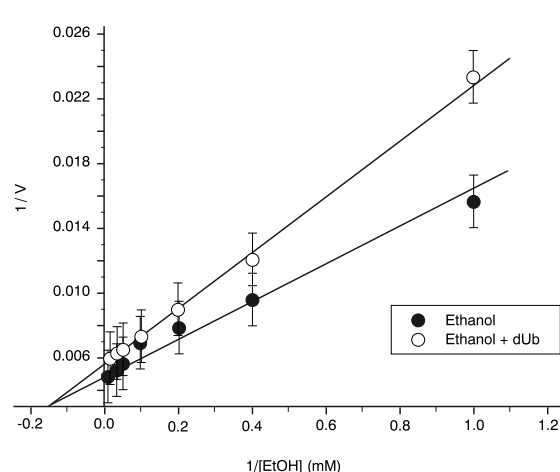
## Results

In isolated mitochondria, dUb inhibits opening of the *S<sub>c</sub>MUC*

The ubiquinone derivative dUb closes the PTP in mitochondria from different cell lines and mammalian sources (Walter

et al. 2000; Devun et al. 2010). With this in mind, we decided to assess whether other ubiquinone derivatives also regulate *S<sub>c</sub>MUC* opening (Fig. 1A). We first monitored oxygen consumption of isolated *S. cerevisiae* mitochondria from the industrial strain La Azteca under control conditions where the *S<sub>c</sub>MUC* is typically closed by high phosphate (Fig. 1B, “c”). Under these conditions, the respiration rate of isolated mitochondria remained low. Respiration was significantly increased when phosphate was decreased, indicating opening of *S<sub>c</sub>MUC* (Fig. 1B, “0”). This high respiration rate phenotype was gradually attenuated with dUb in a concentration-dependent manner (Fig. 1B “10” to “30”). We next wanted to assess if the protective effects of dUb on respiration were derived from a direct interaction with the respiratory chain (Fig. 1C). To address this possibility we tested the effects of increasing amounts of dUb in mitochondria incubated with the uncoupler FCCP. Under these conditions, dUb failed to decrease the respiration rate of isolated mitochondria suggesting that the protection was not at the level of the respiratory chain. The *S<sub>c</sub>MUC* can be regulated by fluctuations in the NADH:NAD<sup>+</sup> ratio (Bradshaw and Pfeiffer 2013). This is of particular relevance as *S. cerevisiae* lacks respiratory complex I, which has been proposed to regulate PTP opening (Li et al. 2012). To further address if dUb regulates the *S<sub>c</sub>MUC* through modifications of the NADH dehydrogenase activity, we performed state 4 oxygen consumption experiments in the presence of increasing concentrations of ethanol (which generates NADH), in the absence and presence of dUb (Fig. 1D). As expected, increasing concentrations of ethanol enhanced the rate of respiration, being maximal at 20 mM ethanol. The presence of dUb under these conditions resulted in a decreased state four respiration, reaching significance at 20 mM ethanol. Further Lineweaver-Burk processing of these results suggests that dUb behaves as a non-competitive inhibitor of NADH-linked respiration and further implying that the dUb effects on *S<sub>c</sub>MUC* activity are not related to NADH:NAD<sup>+</sup> ratio fluctuations (Fig. 1E). Furthermore, the NADH:NAD<sup>+</sup> ratio did not change in any of the ethanol concentrations tested (result not shown); this probably indicates that alcohol dehydrogenase is much slower than NADH dehydrogenase activities and thus it cannot affect the NADH reduction percentage.

Opening of the *S<sub>c</sub>MUC* prevents energized mitochondria from building up a stable  $\Delta\psi$  (Gutiérrez-Aguilar et al. 2010). With this in mind, we tested the effects of dUb on the  $\Delta\psi$  of isolated mitochondria from La Azteca strain under the same conditions as those used for oxygen consumption. The results show that in the presence of high phosphate, mitochondria are able to sustain a high, constant and FCCP-sensitive  $\Delta\psi$  (Fig. 2A trace a). Decreasing phosphate in the incubation media resulted in a fast drop in  $\Delta\psi$ , indicative of *S<sub>c</sub>MUC* opening. This  $\Delta\psi$  reading was not sensitive to further

**A****B****C****D****E**

**Fig. 1** Ubiquinone derivatives used in this study and effects of dUb on the rates of oxygen consumption in closed/open *S<sub>c</sub>MUC* conditions in mitochondria isolated from *S. cerevisiae* La Azteca strain. Chemical structures in (A) represent the ubiquinone derivatives used in this study. For panels B-E, experimental conditions were: 0.6 M Mannitol, 5 mM MES, pH 6.8, 20 mM KCl, pH 6.8 (TEA), 5  $\mu$ L ethanol /mL. To obtain the uncoupled state respiration, 6  $\mu$ M FCCP was added in the experiments on panel C. Measurements were conducted in a water-jacketed chamber (30 °C) connected to an oxymeter interfaced to a computer. Rates of oxygen consumption are expressed in natoms gram O ( $\text{min} \cdot \text{mg prot}$ ) $^{-1}$ . Isolated mitochondria were used at a final concentration of

0.5 mg prot/mL. Bars in both B and C were: “C”=4 mM Pi, no dUb, 0=0.4 mM Pi no dUb, 10=0.4 mM Pi plus 10  $\mu$ M dUb, 20=0.4 mM Pi plus 20  $\mu$ M dUb, 30=0.4 mM Pi plus 30  $\mu$ M dUb, 40=0.4 mM Pi plus 40  $\mu$ M dUb, 50=0.4 mM Pi plus 50  $\mu$ M dUb. In (D), oxygen uptake in open MUC (0.4 mM Pi) condition was evaluated in the presence (●) or absence (○) of 30  $\mu$ M dUb. Rates of respiration were calculated at different ethanol concentrations (0.5 mM, 1 mM, 2.5 mM, 5 mM, 10 mM, 20 mM, 30 mM) with and without dUb added. (E) Lineweaver-Burk plot from data presented in (D), which indicates a non-competitive inhibition of dUb. Each point represents the mean of three experiments  $\pm$  Standard Deviation. \*P<0.05 vs. “C”

addition of FCCP (Fig. 2A trace b). Under this condition, increasing dUb resulted in the gradual buildup of a  $\Delta\psi$  (Fig. 2A traces c to h), reaching maximal values at 50 and 100  $\mu$ M dUb (Fig. 2A traces g, h).

A typical parameter used to measure *S<sub>c</sub>MUC* (and PTP) activity is the swelling resulting from opening of the pore (Castrejón et al. 2002). Mitochondria suspended in buffer with ethanol as respiratory substrate and high levels of phosphate were not sensitive to K<sup>+</sup>-induced swelling (Fig. 2B trace a).

Isolated mitochondria in the presence of ethanol plus low phosphate levels rapidly swelled following K<sup>+</sup> addition (Fig. 2B trace b). Then increasing levels of dUb, attenuated mitochondrial swelling confirming a direct inhibition of the *S<sub>c</sub>MUC* (Fig. 2B traces c-h). The experiments above show that dUb closed the *S<sub>c</sub>MUC* in the presence of 0.4 mM phosphate. However, all experiments were performed in the presence of ethanol as respiratory substrate. Ethanol reduces NAD<sup>+</sup> to NADH+H<sup>+</sup>, which in turn is reoxidized by the internal

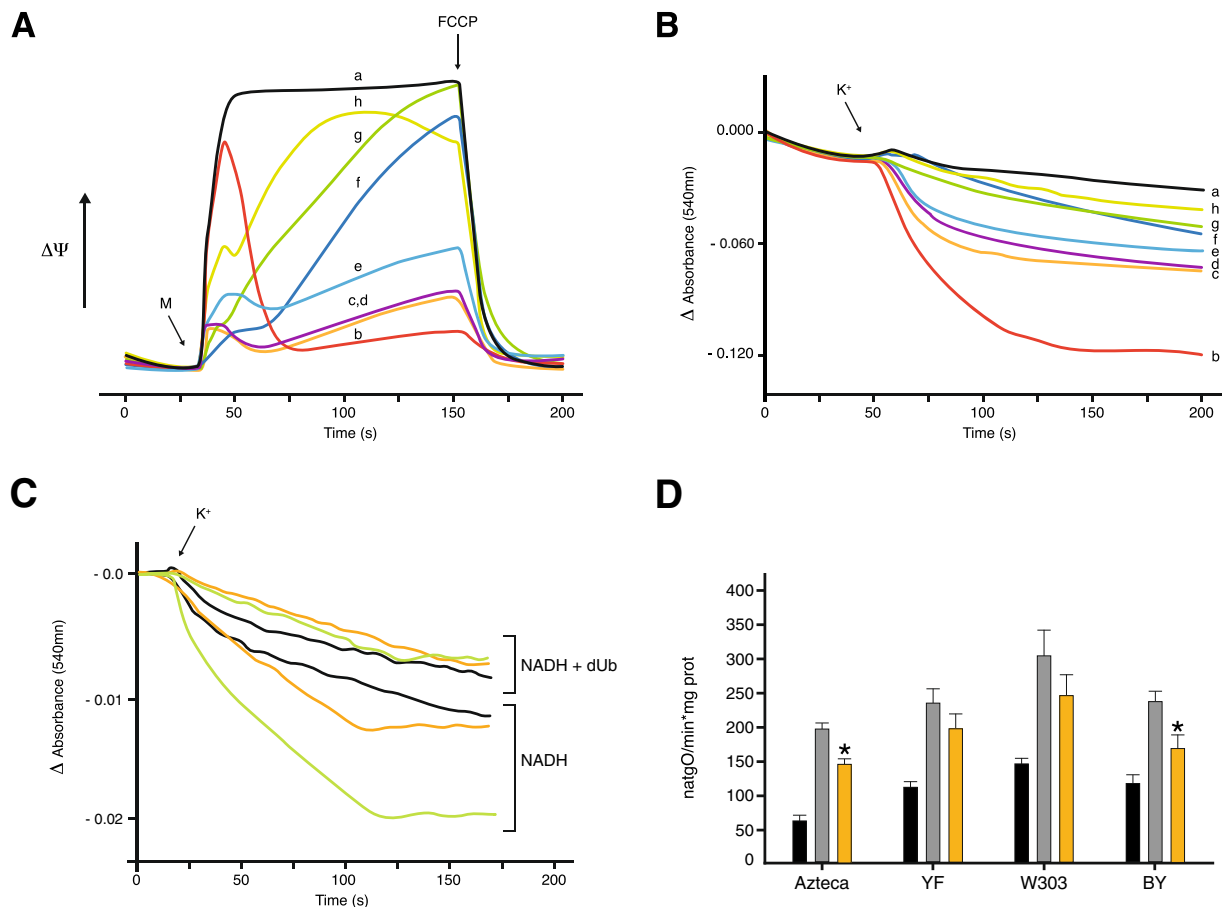


**Fig. 2** Effect of dUb on the (A)  $\Delta\Psi$  and (B) swelling of mitochondria isolated from different industrial and laboratory strains of *S. cerevisiae*. Experimental conditions: As in Fig. 1 except in (A), 10  $\mu\text{M}$  safranine-O. Traces in both (A) and (B) were: a=4 mM Pi, no dUb, b=0.4 mM Pi no dUb, c=0.4 mM Pi plus 10  $\mu\text{M}$  dUb, d=0.4 mM Pi plus 20  $\mu\text{M}$  dUb, e=0.4 mM Pi plus 30  $\mu\text{M}$  dUb, f=0.4 mM Pi plus 40  $\mu\text{M}$  dUb, g=0.4 mM Pi plus 50  $\mu\text{M}$  dUb, h=0.4 mM Pi plus 100  $\mu\text{M}$  dUb. Mitochondria (M) were added at the arrow. Representative experiment from  $n=3$ . For the experiments detailed in (C), externally added NADH was used instead of ethanol to energize mitochondria in the presence of 0.4 mM Pi being

0 mM NADH (black traces), 1 mM NADH (yellow traces) and 2 mM NADH (green traces) in the absence or presence of 30  $\mu\text{M}$  dUb as indicated. Representative experiment from  $n=3$ . In (D), data are presented as oxygen uptake rate in  $\text{natgO} (\text{min}^{-1}\text{mg prot})^{-1}$ . Bars labeled “C” represent the oxygen uptake rate in the presence of 4 mM phosphate. Bars labeled “dUb” represent the oxygen uptake rate in the presence of 30  $\mu\text{M}$  dUb. Please refer to section “Industrial and laboratory yeast strains” for information of the strains used in these experiments. Each bar represents the mean of three independent experiments  $\pm$  Standard Error. \* $P < 0.05$  vs. values of “ $ScMUC$ ” labeled bars

NADH dehydrogenase. In our hands the redox state of the pyridine nucleotides did not vary under these conditions. Nonetheless, it has been reported that increased NADH:NAD<sup>+</sup> ratios and/or high respiratory rates can result in  $ScMUC$  or PTP opening (Leverve and Fontaine 2001; Manon 1999; Manon et al. 1998). To determine whether dUb inhibited  $ScMUC$  opening in the presence of increasing NADH, we directly added NADH to isolated mitochondria (Fig. 2C). As expected, at 1 and 2 mM, NADH promoted  $ScMUC$  opening as indicated by an increase in mitochondrial swelling (Fig. 2C, “NADH” traces). In contrast, in the presence of 30  $\mu\text{M}$  dUb swelling was prevented regardless of the NADH addition (Fig. 2C, “NADH+dUb” traces). Thus it may be concluded that the effect of dUb is independent of the purine nucleotide pool redox state.

Early studies assessing the regulation and transport properties of the  $ScMUC$  concluded that industrial and laboratory strains of *S. cerevisiae* presented a mitochondrial pore with different effector sensitivities (Manon et al. 1998). These differences were later proposed to be context-specific and were abolished under appropriate experimental conditions (Bradshaw and Pfeiffer 2013). In mammalian mitochondria, cell type-dependent differential response to ubiquinone derivatives has been reported (Devun et al. 2010). With this in mind, we assessed the sensitivity of different industrial and laboratory strains of *S. cerevisiae* to dUb (Fig. 2D). We performed state 4 oxygen uptake rate experiments on the industrial strains La Azteca and Yeast Foam (YF) and the laboratory W303 and BY strains. As expected, conditions leading to closure of the  $ScMUC$  induced a typical-baseline oxygen uptake rate phenotype in isolated mitochondria from

all strains (Fig. 2D, black bars). In the presence of low phosphate loads ( $S_c$ MUC), oxygen consumption was enhanced (Fig. 2D, gray bars). In agreement with Fig. 1A, addition of 30  $\mu$ M dUb reduced the oxygen uptake rate in the industrial and laboratory strains (Fig. 2D, yellow bars). The effect was  $S_c$ MUC-specific and concentration-dependent as confirmed with  $\Delta\psi$  and swelling experiments performed in the laboratory W303 and BY strains (results not shown).

#### Effects of naturally occurring ubiquinones on the $S_c$ MUC of industrial and laboratory strains

Based on our results showing that dUb-induced  $S_c$ MUC closure does not depend on a potential interaction of the ubiquinone derivative with the respiratory chain, we next wanted to assess whether naturally occurring ubiquinones such as hexaprenyl (Ub<sub>30</sub>) and decaprenyl quinone (Ub<sub>50</sub>) could potentially influence  $S_c$ MUC activity in addition to its physiological role in the respiratory chain (Fig. 3). We performed  $\Delta\psi$  experiments on isolated mitochondria from the industrial strain La Azteca under control conditions where we detected a high and stable  $\Delta\psi$  (Fig. 3A, trace a). As shown before, opening of the  $S_c$ MUC led to a decrease in  $\Delta\psi$  (Fig. 3A, trace b). Increasing concentrations of Ub<sub>30</sub> (10–100  $\mu$ M) did not confer any potential protection on the  $S_c$ MUC-dependent  $\Delta\psi$  decrease (Fig. 3A, traces c-f). Oxygen consumption experiments in the presence of Ub<sub>30</sub> under the same experimental conditions resulted in no protection against  $S_c$ MUC-mediated increase in the oxygen consumption rate (not shown). We measured  $\Delta\psi$  of isolated mitochondria from La Azteca strain in the presence of Ub<sub>50</sub> (Fig. 3B). Although we occasionally measured weak, concentration-independent increases in  $\Delta\psi$  (see Fig. 3B, trace d), oxygen consumption experiments

evidenced lack of Ub<sub>50</sub> protection against  $S_c$ MUC-dependent increase in respiration (not shown).

#### Ub<sub>5</sub> does not modulate the $S_c$ MUC

We decided to test whether Ub<sub>5</sub>, which has been reported to behave as a PTP-inactive derivative, could modulate the  $S_c$ MUC in isolated mitochondria from the industrial and laboratory strains of *S. cerevisiae* used in this study. Consequently, we measured state 4 oxygen uptake rates of isolated mitochondria from La Azteca YF, W303 and BY strains under control conditions (C), where oxygen uptake rates were low (Fig. 4A, black bars) and in the presence of low phosphate loads, which trigger  $S_c$ MUC opening (Fig. 4A, gray bars). Addition of 200  $\mu$ M Ub<sub>5</sub> under  $S_c$ MUC conditions had no effects on the uptake rates of mitochondria from La Azteca strain. Conversely, Ub<sub>5</sub> increased oxygen uptake rates ~2–3 fold under  $S_c$ MUC conditions in the YF, W303 and BY strains (Fig. 4A, white bars). Further oxygen uptake experiments in the presence of high phosphate loads (closed  $S_c$ MUC) resulted in a concentration-dependent increase in mitochondrial respiration mediated by Ub<sub>5</sub> in all strains (Fig. 4B). The increase in oxygen uptake was significantly lower in La Azteca strain (Fig. 4B, ●). Such effects in the oxygen uptake of all strains were  $S_c$ MUC-independent, given Ub<sub>5</sub> failed to modulate  $\Delta\psi$  on isolated mitochondria from all strains in the presence of either low or high phosphate loads (not shown).

#### Ub<sub>5</sub> suppresses dUb protective effects in La Azteca strain

While dUb promoted closure of  $S_c$ MUC, Ub<sub>5</sub> did not exhibit measurable  $S_c$ MUC-related effects in La Azteca strain. Therefore, to determine if Ub<sub>5</sub> could still bind (but not

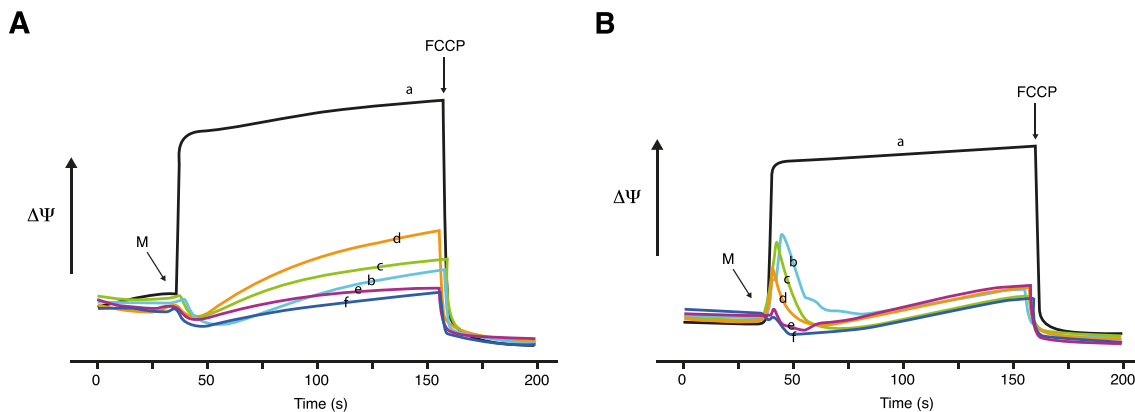


**Fig. 3** Effects of Ub<sub>30</sub> and Ub<sub>50</sub> on the  $\Delta\psi$  of isolated mitochondria of *S. cerevisiae* La Azteca strain. Experimental conditions were as in Fig. 2. Traces in (A) were: a=4 mM Pi, no Ub<sub>50</sub>, b=0.4 mM Pi, no Ub<sub>50</sub>, c=0.4 mM Pi plus 10  $\mu$ M Ub<sub>50</sub>, d=0.4 mM Pi plus 30  $\mu$ M Ub<sub>50</sub>, e=0.4 mM Pi plus 50  $\mu$ M Ub<sub>50</sub>, f=0.4 mM Pi plus 100  $\mu$ M Ub<sub>50</sub>. Traces in (B) were:

a=4 mM Pi, no Ub<sub>50</sub>, b=0.4 mM Pi, no Ub<sub>50</sub>, c=0.4 mM Pi plus 10  $\mu$ M Ub<sub>50</sub>, d=0.4 mM Pi plus 30  $\mu$ M Ub<sub>50</sub>, e=0.4 mM Pi plus 50  $\mu$ M Ub<sub>50</sub>, f=0.4 mM Pi plus 100  $\mu$ M Ub<sub>50</sub>. Mitochondria (M) were added at the arrow. Representative experiment from  $n=3$

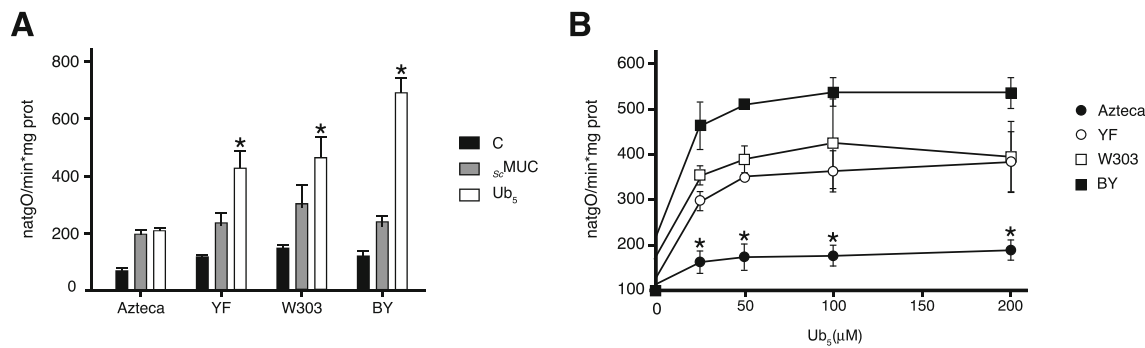


**Fig. 4** Effects of Ub<sub>5</sub> on the oxygen uptake rates of mitochondria isolated from different industrial and laboratory strains of *S. cerevisiae*. Experimental conditions: As in Fig. 2. A, B=oxygen uptake rates. Bars labeled “ $s_c$ MUC” represent oxygen uptake rates in the presence of 0.4 mM phosphate. Bars labeled “C” represent percent oxygen uptake rates in the presence of 4 mM phosphate. Bars labeled “Ub<sub>5</sub>” represent percent oxygen uptake rates in the presence of 200 μM Ub<sub>5</sub>. Please refer to section “Industrial and laboratory yeast strains” for information of the strains used in these experiments. Each bar represents the mean of three independent experiments±Standard Deviation. \*P<0.05 vs. values of “ $s_c$ MUC” labeled bars.

Deviations. \*P<0.05 vs. values of “ $s_c$ MUC” labeled bars. In (B), oxygen uptake rates were evaluated with increasing concentrations of Ub<sub>5</sub> using isolated mitochondria from La Azteca (●), YF (○), W303 (□), and by (■) strains. Data are presented as oxygen uptake rate in natgO (min\*mg prot)<sup>-1</sup>. Rates of respiration were calculated at different Ub<sub>5</sub> concentrations (0 μM, 25 μM, 50 μM, 100 μM, 200 μM). Each value represents the mean of three independent experiments±Standard Deviation. \*P<0.05 vs. values of YF, W303 and BY strains

modulate) the  $s_c$ MUC in this strain, we designed a competition protocol measuring the rate of oxygen consumption in the presence of dUb and increasing concentrations of Ub<sub>5</sub> (Fig. 5). At 0.4 mM Pi, addition of 50 μM dUb promoted the return to a basal rate. Further additions of Ub<sub>5</sub> from 25 to 200 μM increased oxygen consumption similarly to uncoupled rates (Fig. 5A). These results were confirmed with Δψ experiments under the same conditions. At 4 mM Pi, Δψ values were high and stable but low at 0.4 mM Pi. Δψ values returned to high values at 0.4 mM Pi plus 50 μM dUb. Then, in the presence of increasing Ub<sub>5</sub> concentrations Δψ values decreased again

(Fig. 5B). These results indicate that dUb-mediated closure of  $s_c$ MUC was reverted by Ub<sub>5</sub>, suggesting that these ubiquinone derivatives compete for the same binding site.

## Discussion

The PTP-modulating effects of ubiquinone analogues have been proposed to be downstream from the regulatory role of CypD (Basso *et al.* 2005). Fontaine *et al.* (1998) previously proposed that the ubiquinone effect-site was respiratory

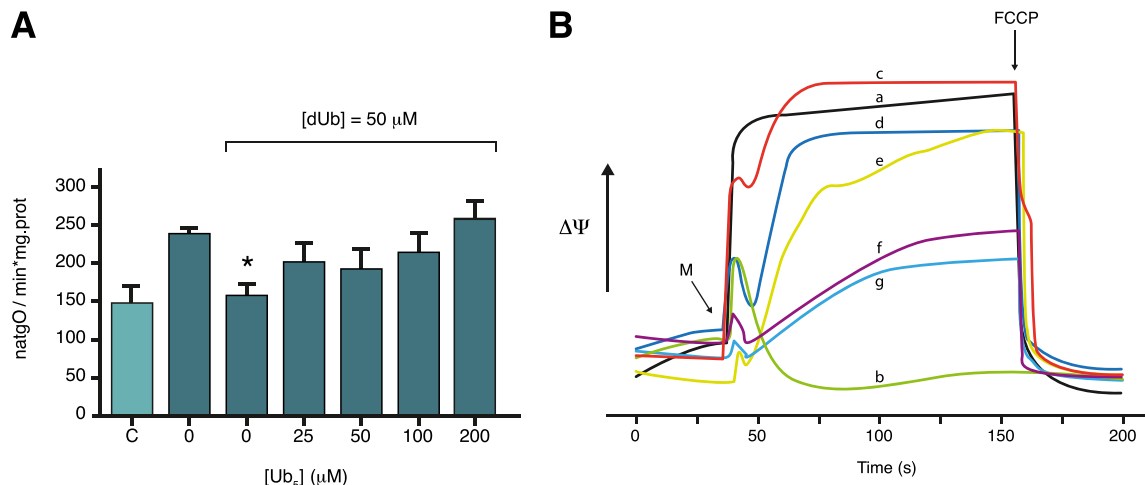


**Fig. 5** Combined effects of dUb and Ub<sub>5</sub> on the rates of oxygen consumption and Δψ of mitochondria isolated from *S. cerevisiae* La Azteca strain. Experimental conditions: As in Fig. 2. A=oxygen consumption, B=Δψ. Bars in A were: “C”=4 mM Pi, no Ub<sub>5</sub> or dUb, 0=0.4 mM Pi no Ub<sub>5</sub> or dUb, 25=0.4 mM Pi plus 25 μM Ub<sub>5</sub>, 50=0.4 mM Pi plus 50 μM Ub<sub>5</sub>, 100=0.4 mM Pi plus 100 μM Ub<sub>5</sub>, 200=0.4 mM Pi plus 200 μM Ub<sub>5</sub>. Where indicated, 50 μM dUb was present

in the reaction mixture. Each point represents the mean of three experiments±Standard Deviation. \*P<0.05 vs. C. Traces in B were: a= 4 mM Pi, no Ub<sub>5</sub>, b=0.4 mM Pi and no Ub<sub>5</sub>, c=0.4 mM Pi and no Ub<sub>5</sub>, d=0.4 mM Pi plus 25 μM Ub<sub>5</sub> e=0.4 mM Pi plus 50 μM Ub<sub>5</sub>, f=0.4 mM Pi plus 100 μM Ub<sub>5</sub>, g=0.4 mM Pi plus 200 μM Ub<sub>5</sub>. For traces c-g, 50 μM dUb was present in the reaction mixture. Mitochondria (M) were added where indicated by an arrow. Representative experiment from n=3

complex I. It is important to note that these analogues present divergent modulating properties depending on the ubiquinone side chain (Walter et al. 2002). In addition such divergent properties are cell line-specific (Devun et al. 2010). This implies that PTPs (and probably the *S. cerevisiae* MUC) may present context-specific accessory components. Indeed, (Li et al. 2012) proposed that rotenone-mediated inhibition of complex I may be even more protective against PTP opening than CsA as long as CypD levels do not exceed those of discrete complex I subunits. Manon (1999) also concluded that *S. cerevisiae* MUC activity is strictly dependent on respiratory chain activity. These data suggest that MUCs are likely modulated by the pyridine nucleotide redox state. In fact, Hunter and Haworth (1979) were the first to report NADH-induced PTP inhibition indicating that the PTP remained closed upon inhibition of complex I with rotenone or through the regulation of the NADH:NAD<sup>+</sup> ratio using β-hydroxybutyrate and acetoacetate. Ubiquinone derivatives regulate the PTP downstream of mitochondrial CypD, strongly indicating that these molecules bind directly to the pore or to another regulatory factor (Basso et al. 2005). Since the *S. cerevisiae* MUC is probably not regulated by the yeast mitochondrial Cyclophilin (Cpr3), but is still sensitive to ubiquinone derivatives, the *S. cerevisiae* MUC and the PTP still present conserved characteristics. To this, the utilization of *S. cerevisiae* as a model to understand the PTP constitutes a powerful genetic tool to unveil the molecular componentry of the *S. cerevisiae* MUC as recently proposed by Carraro et al. (2014). Here, we provide evidence supporting the notion that the *S. cerevisiae* MUC presents a conserved ubiquinone-sensitive site and that the effects of ubiquinone derivatives are independent of the presence of mitochondrial complex I, which is naturally absent in our yeast model. We also show that dUb blocks the *S. cerevisiae* MUC, like the PTP, in a similar concentration range. Then we confirm that the effects of dUb are not related to the regulation of the mitochondrial respiration nor changes in the matrix NADH:NAD<sup>+</sup> ratio, which are also known pore effectors (Leverve and Fontaine 2001). This suggests that respiration-induced *S. cerevisiae* MUC opening and dUb-mediated *S. cerevisiae* MUC closure likely occur through unrelated mechanisms.

We finally show that although the PTP-inactive Ub<sub>5</sub> counteracts the effects of dUb on the *S. cerevisiae* MUC of La Azteca strain, this derivative also strongly activates *S. cerevisiae* MUC-independent respiration in several yeast strains tested. To this, the Ub<sub>5</sub>-mediated increase in respiration has also been reported for the laboratory CEN.PK2–1C strain of *S. cerevisiae* (James et al. 2005). Although the cause for such divergent phenotype between La Azteca and the rest of the strains tested is unknown and is subject of further research in our laboratory, adaptive evolution could account for the differences monitored herein, where close to 22 % of the total transcripts detected in industrial strains do not match annotated sequences for laboratory strains (Varela et al. 2005).

We have discussed this possibility for the strain-specific differences in *S. cerevisiae* MUC activity reported before (Uribe-Carvajal et al. 2011).

Altogether, our results suggest that ubiquinone analogues can regulate the *S. cerevisiae* MUC as seen with the mammalian PTP. Consequently, ubiquinone analogues may bind to a conserved/discrete site and its lateral chain may be involved in the gating of the *S. cerevisiae* MUC as well as the PTP. This likely explains why ubiquinone derivatives with disparate side chains have similar properties on the PTP and the *S. cerevisiae* MUC. The results presented here also imply that ubiquinone analogues display its permeability-modulating effects in a complex I-independent context.

**Acknowledgments** M.G.-A. is currently supported by an American Heart Association Midwest Affiliate Postdoctoral Fellowship (13POST14060013). HLC is a CONACyT fellow enrolled in the Ms. Sc. Biochemistry program at UNAM. CUA, EGS and MRL are CONACyT fellows enrolled in the Ph. D. Biochemistry program at UNAM. Partially funded by DGAPA/PAPIIT Project IN202612. We acknowledge the technical assistance of Ramón Méndez. Mariana Valenzuela kindly helped to build the figures.

## References

- Akerman KE, Wikström MK (1976) Safranine as a probe of the mitochondrial membrane potential. FEBS Lett 68:191–197
- Azzolin L, Von Stockum S, Basso E et al (2010) The mitochondrial permeability transition from yeast to mammals. FEBS Lett 584: 2504–2509
- Basso E, Fante L, Fowlkes J et al (2005) Properties of the permeability transition pore in mitochondria devoid of Cyclophilin D. J Biol Chem 280:18558–18561
- Bernardi P (2013) The mitochondrial permeability transition pore: a mystery solved? Front Physiol 4:95
- Bernardi P, Von Stockum S (2012) The permeability transition pore as a Ca<sup>2+</sup> release channel: new answers to an old question. Cell Calcium 52:22–27
- Bonora M, Bononi A, De Marchi E et al (2013) Role of the c subunit of the F<sub>0</sub> ATP synthase in mitochondrial permeability transition. Cell Cycle 12:674–683
- Bonora M, Wieckowski MR, Chinopoulos C, et al. (2014) Molecular mechanisms of cell death: central implication of ATP synthase in mitochondrial permeability transition. Oncogene. doi:doi:10.1038/onc.2014.96
- Bradshaw PC, Pfeiffer DR (2013) Characterization of the respiration-induced yeast mitochondrial permeability transition pore. Yeast 30: 471–483
- Brenner C, Moulin M (2012) Physiological roles of the permeability transition pore. Circ Res 111:1237–1247
- Carraro M, Giorgio V, Sileikyté J, et al. (2014) Channel Formation by Yeast F-ATP Synthase and the Role of Dimerization in the Mitochondrial Permeability Transition. J Biol Chem 289:15980–15985
- Castrejón V, Peña A, Uribe S (2002) Closure of the yeast mitochondria unselective channel (YMUC) unmasks a Mg<sup>2+</sup> and quinine sensitive K<sup>+</sup> uptake pathway in *Saccharomyces cerevisiae*. J Bioenerg Biomembr 34:299–306

- Cortés P, Castrejón V, Sampedro JG, Uribe S (2000) Interactions of arsenate, sulfate and phosphate with yeast mitochondria. *Biochim Biophys Acta* 1456:67–76
- de Kloet S, van Wermeskerken R, Koningsberger VV (1961) Studies on protein synthesis by protoplasts of *Saccharomyces carlsbergensis*. I. The effect of ribonuclease on protein synthesis. *Biochim Biophys Acta* 47:138–143
- Devun F, Walter L, Belliere J et al (2010) Ubiquinone analogs: a mitochondrial permeability transition pore-dependent pathway to selective cell death. *PLoS ONE* 5:e11792
- Díaz-Ruiz R, Averet N, Araiza D, Pinson B, Uribe-Carvajal S, Devin A et al (2008) Mitochondrial oxidative phosphorylation is regulated by fructose 1,6-bisphosphate. A possible role in Crabtree effect induction? *J Biol Chem* 283:26948–26955
- Di Lisa F, Bernardi P (2006) Mitochondria and ischemia-reperfusion injury of the heart: fixing a hole. *Cardiovasc Res* 70:191–199
- Di Lisa F, Carpi A, Giorgio V, Bernardi P (2011) The mitochondrial permeability transition pore and cyclophilin D in cardioprotection. *Biochim Biophys Acta* 1813:1316–1322
- Fontaine E, Eriksson O, Ichas F, Bernardi P (1998) Regulation of the permeability transition pore in skeletal muscle mitochondria. Modulation By electron flow through the respiratory chain complex I. *J Biol Chem* 273:12662–12668
- Giorgio V, Soriano ME, Basso E et al (2010) Cyclophilin D in mitochondrial pathophysiology. *Biochim Biophys Acta* 1797:1113–1118
- Giorgio V, Von Stockum S, Antoniel M et al (2013) Dimers of mitochondrial ATP synthase form the permeability transition pore. *Proc Natl Acad Sci U S A* 110:5887–5892
- Gutiérrez-Aguilar M, Douglas DL, Gibson AK et al (2014) Genetic manipulation of the cardiac mitochondrial phosphate carrier does not affect permeability transition. *J Mol Cell Cardiol* 72:316–325
- Gutiérrez-Aguilar M, Pérez-Martínez X, Chávez E, Uribe-Carvajal S (2010) In *Saccharomyces cerevisiae*, the phosphate carrier is a component of the mitochondrial unselective channel. *Arch Biochem Biophys* 494:184–191
- Hunter DR, Haworth RA (1979) The  $\text{Ca}^{2+}$ -induced membrane transition in mitochondria. I. The protective mechanisms. *Arch Biochem Biophys* 195:453–459
- Ichas F, Mazat JP (1998) From calcium signaling to cell death: two conformations for the mitochondrial permeability transition pore. Switching from low- to high-conductance state. *Biochim Biophys Acta* 1366:33–50
- James AM, Cochemé HM, Smith RAJ, Murphy MP (2005) Interactions of mitochondria-targeted and untargeted ubiquinones with the mitochondrial respiratory chain and reactive oxygen species. Implications for the use of exogenous ubiquinones as therapies and experimental tools. *J Biol Chem* 280:21295–21312
- Kwong JQ, Davis J, Baines CP et al (2014) Genetic deletion of the mitochondrial phosphate carrier desensitizes the mitochondrial permeability transition pore and causes cardiomyopathy. *Cell Death Differ* 21(8):1209–1217
- Leverve XM, Fontaine E (2001) Role of substrates in the regulation of mitochondrial function in situ. *IUBMB Life* 52(3–5):221–229
- Li B, Chauvin C, De Paulis D et al (2012) Inhibition of complex I regulates the mitochondrial permeability transition through a phosphate-sensitive inhibitory site masked by cyclophilin D. *Biochim Biophys Acta* 1817:1628–1634
- Manon S (1999) Dependence of yeast mitochondrial unselective channel activity on the respiratory chain. *Biochim Biophys Acta* 1410:85–90
- Manon S, Roucou X, Guérin M et al (1998) Characterization of the yeast mitochondria unselective channel: a counterpart to the mammalian permeability transition pore? *J Bioenerg Biomembr* 30:419–429
- Prieto S, Bouillaud F, Rial E (1995) The mechanism for the ATP-induced uncoupling of respiration in mitochondria of the yeast *Saccharomyces cerevisiae*. *Biochem J* 307(Pt 3):657–661
- Quinlan CL, Peresvoshchikova IV, Hey-Mogensen M, Orr AL, Brand MD (2013) Sites of reactive oxygen species generation by mitochondria oxidizing different substrates. *Redox Biol* 1:304–312
- Uribe S, Rangel P, Pardo JP (1992) Interactions of calcium with yeast mitochondria. *Cell Calcium* 13:211–217
- Uribe-Carvajal S, Luévanos-Martínez LA, Guerrero-Castillo S et al (2011) Mitochondrial unselective channels throughout the eukaryotic domain. *Mitochondrion* 11:382–390
- Varela C, Cárdenas J, Melo F, Agosin E (2005) Quantitative analysis of wine yeast gene expression profiles under winemaking conditions. *Yeast* 22:369–383
- Walter L, Miyoshi H, Leverve X et al (2002) Regulation of the mitochondrial permeability transition pore by ubiquinone analogs. a progress report. *Free Radic Res* 36:405–412
- Walter L, Nogueira V, Leverve X et al (2000) Three classes of ubiquinone analogs regulate the mitochondrial permeability transition pore through a common site. *J Biol Chem* 275:29521–29527
- Yamada A, Yamamoto T, Yoshimura Y et al (2009)  $\text{Ca}^{2+}$ -induced permeability transition can be observed even in yeast mitochondria under optimized experimental conditions. *Biochim Biophys Acta* 1787: 1486–1491

## OXYGEN: FROM TOXIC WASTE TO OPTIMAL (TOXIC) FUEL OF LIFE.

Mónica Rosas-Lemus<sup>1</sup>, Cristina Uribe-Alvarez<sup>1</sup>, Martha Contreras-Zentella<sup>2</sup>, Luis Alberto Luévano-Martínez<sup>3</sup>, Natalia Chiquete-Félix<sup>1</sup>, Adriana Muhlia-Almazán<sup>4</sup>, Edgardo Escamilla-Marván<sup>2</sup> and Salvador Uribe-Carvajal<sup>1\*</sup>.

<sup>1</sup> Dept Genética Molecular, Inst de Fisiología Celular, UNAM México.

<sup>2</sup> Dept Biología Celular y del desarrollo, Inst de Fisiología Celular, UNAM México.

<sup>3</sup> Dept Bioquímica, Inst de Química, U de Sao Paulo, Sao Paulo, SP, Brazil.

<sup>4</sup> Lab Bioenergética y Genética Molecular, CIAD, Hermosillo, Sonora, México.

**\*Correspondence:** Dept Genética Molecular, Inst Fisiología Celular, UNAM, AP 70-214, Circ Ext, 04510 Mexico DF, Mexico. Tel: +52 55 56225632. e-mail: suribe@ifc.unam.mx.

**Keywords:** Oxygen, ROS, oxydative stress, oxyconformers, oxyregulators, adaptative metabolism.

**ABSTRACT:**

Some 2.5 billion years ago the great oxygenation event (GOE) led to a  $10^5$ -fold rise in atmospheric oxygen [ $O_2$ ] killing most species on Earth. In spite of the tendency to produce toxic Reactive Oxygen Species (ROS), the highly exergonic reduction of  $O_2$  made it the ideal biological electron acceptor. During aerobic metabolism,  $O_2$  is reduced to water liberating energy, which is coupled to ATP synthesis. Today all organisms aerobic or not need to deal with  $O_2$  toxicity. Avoiding exposure to high  $O_2$  is important for all organisms.  $O_2$ -permeant organisms need to seek adequate [ $O_2$ ], e.g. aquatic crustaceans bury themselves in the sea bottom where  $O_2$  is scarce. Also, the intestinal lumen is a micro-aerobic environment where many facultative bacteria live. Another example is the cytoplasm of eukaryotes where intracellular symbionts such as *Rickettsia* hide from oxygen. Organisms such as plants, fish, reptiles and mammals developed  $O_2$ -impermeable epithelia, plus specialized external respiratory systems that in combination with  $O_2$ -binding proteins such as hemoglobin or leg-hemoglobin control  $O_2$  in tissues. Once inside the cell, ROS production is prevented by rapid  $O_2$  consumption during the oxidative phosphorylation (OxPhos) of ATP. When ATP is in excess, OxPhos becomes uncoupled in an effort to continue eliminating  $O_2$ . Branched respiratory chains, unspecific pores and uncoupling proteins (UCPs) uncouple OxPhos. One last line of resistance against ROS is deactivation by enzymes such as Super Oxide dismutase and catalase. Aerobic species profit from the high electron affinity of  $O_2$ , while at the same time they need to avoid the toxicity of its reduction by-products.

## 1. At the beginning, all life was anaerobic.

The early Earth atmosphere contained high  $[H_2]$ ,  $[NH_3]$  and  $[CH_4]$ , while  $[O_2]$  was less than  $10^{-5}$  the Present Atmospheric Level (PAL) [1, 2]. Thus, all life forms were anaerobic [3, 4]. Early redox reactions involved electron donors such as  $H_2$ ,  $CO_2$  or  $HS$  [5, 6] while electron acceptors probably were sulfur and  $NO_3$  [7]. Eukaryotes were present before  $O_2$  rose [8, 9] and contained anaerobic mitochondrion-like organelles [10-15].

## 2. The massive increase in $[O_2]$ and the need to counteract its toxicity.

Approximately 2.5 billion years ago, the Great Oxygenation Event (GOE) was precipitated by both geological [16] and biological processes such as the photosynthetic activity of Cyanobacteria [17, 18]. Today,  $O_2$  is the preferred electron acceptor used by facultative microorganisms and the only one used by aerobes. The highly exergonic reduction of  $O_2$  provided the energy needed for the development of multicellular organisms. In addition, the high energy of activation required for  $O_2$  reduction ensures that this reaction occurs mostly through catalyzed reactions. For instance, oxidases bind their substrate tightly, preventing the liberation of ROS [19]. At low concentrations, ROS are useful as signaling molecules, while at higher concentrations ROS damage and kill cells. Cells need much less  $[O_2]$  than what is found in the atmosphere and thus, to prevent ROS production they maintain internal  $O_2$  low [20]. Cells have developed two mechanisms to deal with surplus  $O_2$ : 1) avoiding it, and 2) rapidly reducing it. Furthermore, cellular  $O_2$  is found mostly bound to proteins such as hemoglobin, leg-hemoglobin and myoglobin. Early oxy-conformer organisms are permeant to  $O_2$  and thus at different stages in their life cycle they have to migrate to micro-aerobic or

anaerobic spaces (Table 1).have to cope with variations in O<sub>2</sub>. More evolved oxy-regulator organisms from fish to mammals, enveloped themselves in an O<sub>2</sub>-impermeable epithelium, while at the same time developing highly specialized systems that control tissue [O<sub>2</sub>] (Fig. 1). Oxyconformers and oxyregulators display different strategies to manage O<sub>2</sub>-byproduct toxicity (Fig. 1).

**Oxy-conformers.** All cells in these organisms are exposed to environmental [O<sub>2</sub>]. O<sub>2</sub>-permeable organisms do have O<sub>2</sub> transport proteins and intracellular O<sub>2</sub> binding proteins, but in addition they need to implement diverse strategies to deal with changing O<sub>2</sub>. These include searching for microaerophilic or anaerobic environments. Among oxyconformers are Arthropoda, the most abundant and widely distributed phylum on Earth; it comprises subphyla Chelicerata (spiders), Myriapoda (centi- and millipedes), Hexapoda (Insects) and Crustacea, all of them protected by an exoskeleton. Non-aquatic insects possess a hard waterproof cuticle and branched invaginated tubules forming a specialized respiratory structure that works well at constant [O<sub>2</sub>]. Aquatic organisms, including most of the Crustacea are exposed to highly variant [O<sub>2</sub>], which may be 26-times lower than in the atmosphere [22, 23]. In water, [O<sub>2</sub>] varies with temperature, depth, mechanical aeration and tidal movements. Only few invertebrates (Plathelmythes, Nematoda, Mollusca, Anellida, and Sypuncula) have been thoroughly studied in regard to their mechanisms to deal with fluctuating [O<sub>2</sub>] [15, 24]. Remarkably, very few studies on Crustacea are available.

Most marine invertebrates, including crustaceans are oxy-conformers [25]. Oxyconformity forces organisms to reduce aerobic activity during hypoxia/ anoxia cycles, in order to control the release of ROS and thus it would be expected to find lower ROS production in species that both, inhabit low oxygen-contant environments and exhibit low

oxygen consumption rates [26]. It is not clear how mitochondria from oxyconformers respond to hypoxia, how respiratory activity adapts to reduced metabolic rates, and how the cellular redox balance and energetic homeostasis are preserved [27].

Marine crustaceans display different responses to hypoxia/ anoxia. To avoid hyperoxygenated or anoxic waters, crustaceans migrate between open sea and coastal lagoons (Fig. 2), or migrate vertically through the water column to flee the O<sub>2</sub>-minimum zone (OMZ) and into [O<sub>2</sub>] compatible with their metabolic needs [28, 29]. Some shrimp species, such as the burrowing thalassinids *Upogebia major*, and *Callianasa japonica*, which commonly inhabit the extremely hypoxic or even anoxic intertidal flats, can reduce their respiratory rate in dugout burrows, surviving up to 5 h of anoxia for *U. major*, and 19 h for *C. japonica* [30]. *Artemia franciscana* is well known for its high tolerance to anoxia; the embryos of this species survive without O<sub>2</sub> for years through the complete depression of their metabolic rates [31, 32]. Metabolic rate depression is also observed in ectotherms, which lower their mitochondrial activity in function of temperature adjusting their O<sub>2</sub> consumption machinery accordingly [33].

Among uni-cellular organisms, diverse yeast species can survive at almost any [O<sub>2</sub>]. *Saccharomyces cerevisiae* can thrive in very low [O<sub>2</sub>] through fermentation, although it does possess a facultative aerobic metabolism. The anaerobic metabolism of *S. cerevisiae*, *D. hansenii* and other yeast is the basis for the fermentation industry of bread, wine and cheese. Yeast and other organisms have developed diverse systems to detoxify oxygen through physiological uncoupling and these will be discussed below.

Many bacteria are facultative. Among these *Escherichia coli* is a very illustrative representant that may thrive both in microaerobic environments such as the intestinal

lumen or and survive in the external environment in a wide range of [O<sub>2</sub>]. Bacteria respond to environmental [O<sub>2</sub>] variations or other conditions such the need to fixate N<sub>2</sub> [34, 35] by varying the composition of their branched respiratory chains (Fig. 3A), which may pump as little as zero protons or as many as those in orthodox respiratory chains [36, 37]. Still, when motile, bacteria will swim towards environments containing the ideal [O<sub>2</sub>].

Intracellular Rickettsiae, such as *R. prowazekii*, *Wolbachia* sp. or *Sodalis*, are endosymbiotic bacteria living in the cytoplasm of multicellular organisms. The cytoplasm is a micro-aerophilic environment equipped with oxygen consuming organelles and ROS-detoxifying enzymes. Remarkably, most endosymbionts contain a respiratory chain that at least in the case of *Wolbachia* seems to aid host mitochondria to deplete intracellular O<sub>2</sub> (Fig. 3B). Upon oxygen exposure *Wolbachia* develops a proton-pumping, oxygen-consuming respiratory chain (to be published).

Many parasites exhibit various life-cycle stages, which have different sensitivities to ROS engineered to endure different attacks from macrophages. *Leishmania* sp. undergoes a relatively simple life cycle with two stages: the flagellated mobile promastigote living in the gut of the sand fly vector and the intracellular amastigote within phagolysosomal vesicles of the vertebrate host macrophage[38]. Promastigotes contain respiratory complexes I, II, III and IV, while it is not clear whether amastigotes possess an oxidative phosphorylation machinery. Strikingly, amastigotes exhibit a succinate-dependent, uncoupler-sensitive transmembrane potential. Differences in sensitivity to oxidants are also observed between them, *in vitro*, promastigotes are more resistant to H<sub>2</sub>O<sub>2</sub> than amastigotes [39].

In the bloodstream, *Trypanosoma cruzi* trypomastigotes contain high complex II-III activities. Interestingly, cytochrome c oxidase (COX) activity decreases, creating an “electron

bottleneck” that favors an increase in electron leakage, thus overproducing ROS. Goncalves *et al.* (2011) propose that the oxidative preconditioning provided by this mechanism confers protection to bloodstream trypomastigotes against ROS liberated by the host immune system. Mitochondrial remodeling during the *T. cruzi* life cycle is probably a key metabolic adaptation for survival in different hosts [40].

Malaria parasites are vulnerable to oxidative stress during their intraerythrocytic life stages. They contain the canonical respiratory chain (complex I, II, III and IV) plus an alternative electron transport pathway. Moreover, malaria mitochondria, coordinate the biosynthesis of pyrimidine, haem and coenzyme Q [41]. *Plasmodium falciparum* possesses genes for two different superoxide dismutases (SOD), a cytosolic, Fe<sup>2+</sup>-dependent, (SOD-1) expressed throughout the intraerythrocytic life of the parasite. The second, SOD-2, is mitochondrial and possesses a reminiscent apicoplast targeting sequence. The host immune response to malaria involves phagocytosis as well as the production of nitric oxide and ROS that end up contributing to the pathology of the disease [42].

Regardless the organism studied, cytoplasmic [O<sub>2</sub>] can vary widely, so damage control is needed at two levels. Either O<sub>2</sub> is reduced independently of ATP production in a process known as physiological uncoupling, or the ROS-handling enzymes are activated. Many reviews on ROS-handling enzymes, such as superoxide dismutase and catalase are found elsewhere [43, 44].

### **3. Physiological uncoupling as an oxygen depleting mechanism.**

Both in oxyconformers and oxyregulators, once O<sub>2</sub> enters the cell it has to be reduced at a high rate. When ATP is needed the respiratory chain rapidly catalyzes this reduction;

otherwise O<sub>2</sub> consumption has to be uncoupled from ATP synthesis with the aim of preventing ROS overproduction [45]. A review on the physiological uncoupling mechanisms observed in mitochondria from different species of yeasts has been published recently [46]. Yeast mitochondrial uncoupling mechanisms may be a) proton sinks, such as the mitochondrial unspecific channels [47-49] and the UCP [50, 51] or b) non-pumping redox alternative enzymes found in branched respiratory chains [49]. In *Yarrowia lipolytica* during the stationary growth phase electron passage from alternative NADH dehydrogenases (NDH2) to alternative oxidases (AOX) uncouples oxidative phosphorylation and decreases the production of ROS [52, 53]. Here, the possibility that physiological uncoupling systems are present in all living organisms is revised. Both proton sinks and branched chains are observed.

**Proton sinks:** First detected in mammalian mitochondria as a response to the disruption of intracellular calcium homeostasis, the opening of the mitochondrial permeability transition pore (MPTP) leads to mitochondrial uncoupling and to the activation of signaling events leading to apoptosis [54]. In crustaceans subjected to hypoxia, mitochondrial functions are downregulated [55-57] and there is an anoxia-triggered intracellular increase in both calcium and phosphate, while ATP production is inhibited, probably as a result of the opening of a MPTP. In *Artemia franciscana* [32] and in the ghost shrimp *Lepidophthalmus louisianensis* [58] the proteins needed to form the MPTP are present. However, whether these crustaceans possess MPTPs is to be defined. Both in crustacean mitochondria and in other known hypoxia-tolerant invertebrates (mussels, oysters, and cnidarians among others) the role of a putative MPTP is an interesting question.

**Branched Respiratory Chains.** Bacteria do not exhibit a permeability transition. This seems to be a mitochondrial trait. Instead, bacteria (and many mitochondria) exhibit branched respiratory chains. Indeed, different species of mitochondria may exhibit from none to three alternative enzymes. In contrast, bacteria may contain as much as twenty electron entry ports and as many exits. Thus, in most prokaryotes branched respiratory chains seem to be the mechanism of choice to maintain a high rate of O<sub>2</sub> consumption, while adjusting ATP production to the energy requirements of the cell. In this regard, the bioenergetic efficiency for each entry point is defined as the stoichiometry of H<sup>+</sup> pumped per e<sup>-</sup> traveling through the respiratory chain [59]. In addition, terminal oxidases are remarkably varied and their active site orientation, to the cytoplasm or to the periplasm determines their pumping efficiency [37].

Alternative oxidoreductases is the term designating all components of the respiratory chain different to the usual complexes I through IV. Most alternative oxidoreductases lack proton-pumping activity and may coexist with, or substitute for the respiratory proton-pumping complexes. Alternative enzymes catalyze the rapid, uncoupled flow of electrons towards O<sub>2</sub>. Alternative NADH dehydrogenases may either substitute for (*S. cerevisiae*) or coexist with (bacteria, plants and diverse fungi) complex I [60, 61].

Alternative oxidases (AOXs) catalize the oxidation of ubiquinol to quinone and the reduction of O<sub>2</sub> to H<sub>2</sub>O in the absence of proton translocation [62]. Although highly represented among plants, fungi and protist species, animal AOXs have been predicted to exist only in in Molluska, Nematoda and Chordata [63]. Recently, the number of phyla that probably possess AOX has increased including Placozoa, Porifera, Cnidaria, Annelida, Echinodermata, Hemichordata and Chordata In some marine vertebrates such as sipunculids, annelids (*Nereis pelagica*, and *Arenicola marina*) and in bivalves (*Arctica islandica*) AOX

has been detected [64-66]. However, there are no confirmed reports for AOX in mitochondria from crustaceans [67]. In different plant and animal species, cells lacking AOX show an increased susceptibility to death due to H<sub>2</sub>O<sub>2</sub>, hypoxia and pathogens [68]. The ultimate decoupling of electron flow occurs when NADH dehydrogenases act in concert with alternative oxidases.

Bacterial cytochrome-containing oxidases are many. These enzymes are differentially expressed in response to different oxygen concentrations and on whether an organism is an obligate aerobic or a facultative species. In addition, oxidases may coexist depending on the species under study and they may play different roles in the cell [69]. In *E. coli*, different oxidases are expressed depending on [O<sub>2</sub>]. At high O<sub>2</sub>, bo3 is expressed, while at low O<sub>2</sub> bd cytochromes are observed (Fig. 3 A). Furthermore, *E. coli* is capable of growth under anaerobiosis, using respiratory chains reminiscent of the early Earth that use ubiquinone, menaquinone or demethyl-menaquinone to donate electrons to enzymes that use terminal acceptors different to O<sub>2</sub> (Fig. 3-B) [36, 37].

Branched respiratory chains provide the possibility of consuming O<sub>2</sub> without producing ATP. In the yeast *Y. lipolytica*, in the bacterium *E. coli* and probably in the Rickettsial *Wolbachia* sp., the arrangement of the respiratory chain varies such that when [O<sub>2</sub>] is high, or ATP is needed, high proton pumping efficiency is observed. In contrast, factors such as arrival to the stationary phase or microaerophilic conditions probably trigger overexpression of the alternative NADH dehydrogenase and/or the AOX leading to the futile reduction of O<sub>2</sub> [60]. A possible arrangement of the respiratory chain of *Wolbachia* sp is illustrated (fig. 3C) where a large number of possible electron donating enzymes reduce menaquinone or

ubiquinone that in turn reduce final electron accepting enzymes that are expressed according to the presence of O<sub>2</sub> in the cytoplasm of the host [70, 71].

N-fixating bacteria are a special case. These may be facultative as *Klebsiella pneumonia* or strict aerobics such as *Azotobacter vinelandii* or *Gluconobacter diazotrophicus*. As they contain fragile, oxygen-sensitive nitrogen fixating enzymes that need to be protected, these bacteria have developed many strategies to detoxify [O<sub>2</sub>]. Thus, in N-fixating bacteria, both N-reductases and different oxidases are expressed: *A. vinelandii* contains a highly active respiratory chain and is able to adjust the expression of its three oxidases to a wide range of [O<sub>2</sub>]. Among these, cytochrome *bd* has high O<sub>2</sub> affinity (Km<sub>O<sub>2</sub></sub>= 5 μM) and becomes active during N fixation [19, 72-74]. Indeed, during N fixation the H<sup>+</sup>/O index is low, at 1 [75]. In *Ga. diazotrophicus* different periplasmic membrane enzymes such as glucose-, acetaldehyde- or ethanol-dehydrogenases reduce a quinone, which in turn donates its electrons to two different oxidases, *ba* which is coupled to ATP synthesis and *bb<sub>3</sub>* which is not coupled but its role is to deplete O<sub>2</sub> in the vicinity of nitrogen reductases [76].

**ROS detoxification:** In spite of the production-prevention mechanisms outlined above, ROS may reach high concentrations, e.g. during ischemia-reperfusion. The last line of defense is detoxification. Enzymes such as Superoxide dismutases (SODs) and catalases deactivate ROS. SODs have been grouped on the basis of the metal cofactor, which can be Fe, Mn, Ni or Cu/Zn (Whittaker and Whittaker 1998). The Fe-SODs, are mostly found in microaerophiles and anaerobes. Microorganisms in aerobic environments prefer Mn-SOD (Cannio, Fiorentino et al. 2000). Catalase dismutates hydrogen peroxide to water plus O<sub>2</sub> (Klotz and Loewen 2003). Several genes capable of H<sub>2</sub>O<sub>2</sub> dismutation evolved from ancestral genomes. The

most abundant were heme-containing enzymes spread among bacteria, Archaea and Eukarya (Zamocky, Furtmuller et al. 2008).

Catalase dismutates hydrogen peroxide to water plus O<sub>2</sub> (Klotz and Loewen 2003). Several genes capable of H<sub>2</sub>O<sub>2</sub> dismutation evolved from ancestral genomes. The most abundant were heme-containing enzymes spread among bacteria, Archaea and Eukarya (Zamocky, Furtmuller et al. 2008). In *Clostridium acetobutylicum*, a strict anaerobic that survives little time when exposed to O<sub>2</sub>, no catalases are found (Nölling et al., 2001), and a function has yet to be found for the annotated SODs.

#### **4. Conclusion.**

During the early paleoproterozoic period, a massive death toll resulted from a 10<sup>5</sup> times-rise in atmospheric O<sub>2</sub>. In order to survive, organisms had to learn to cope with O<sub>2</sub> toxicity while profiting from the large energy release coupled to its reduction. Several O<sub>2</sub>-management strategies are revised here. Among these is hiding away from O<sub>2</sub>, moving to adequate O<sub>2</sub> concentrations or excluding O<sub>2</sub> with impermeable epithelia. Once O<sub>2</sub> enters the cell, other mechanisms are designed to handle it. Its reactivity is controlled by O<sub>2</sub>-quenching proteins or by rapidly reducing it with specific oxidases. In order to avoid side reactions, the rate of reduction had to be kept at optimal pace, independently of ATP production and thus several mechanisms of physiological uncoupling of oxidative phosphorylation evolved. Physiological uncoupling was achieved either by opening proton sinks or by using O<sub>2</sub> independently of the proton gradient. Today, these mechanisms are expressed in many cells. Proton sinks include unspecific channels and uncoupling proteins, while proton gradient-independent consumption

of O<sub>2</sub> involved alternative oxido-reductases found in the branched respiratory chains of fungi, plants and arthropods. In spite of the function of all these O<sub>2</sub>-management machines, O<sub>2</sub> can still react unspecifically to form ROS, which destroy the cell through processes such as aging, apoptosis or necrosis. Once formed, ROS may still be eliminated by enzymes such as SOD and catalase, which are reviewed elsewhere [44] O<sub>2</sub> is a great source of energy for the cell, but its high toxicity has to be dealt with, through mechanisms that we are only beginning to understand.

**Acknowledgements.** Authors thank Ramón Méndez-Franco for technical assistance. Partially funded by the PAPIIT program and DGAPA/UNAM (grant IN202612). MRL and CUA are CONACYT fellows enrolled in the Biochemistry Graduate Program at UNAM.

**Declaration of Interest Policy.** The authors do not have any interests to disclose.

#### 4. REFERENCES.

- [1] Lane, N. Oxygen the molecule that made the world. Oxford: Oxford University Press; 2002: 384.
- [2] Sessions, A. L.; Doughty, D. M.; Welander, P. V.; Summons, R. E. and Newman, D. K. The continuing puzzle of the great oxidation event. *Curr Biol* 2009; 19:R567-574.
- [3] Pavlov, A. A. and Kasting, J. F. Mass-independent fractionation of sulfur isotopes in Archean sediments: strong evidence for an anoxic Archean atmosphere. *Astrobiology* 2002; 2:27-41.
- [4] Martin, W.; Rotte, C.; Hoffmeister, M.; Theissen, U.; Gelius-Dietrich, G.; Ahr, S. and Henze, K. Early cell evolution, eukaryotes, anoxia, sulfide, oxygen, fungi first (?), and a tree of genomes revisited. *IUBMB Life* 2003; 55:193-204.
- [5] Nisbet, E. G. and Sleep, N. H. The habitat and nature of early life. *Nature* 2001; 409:1083-1091.
- [6] Martin, W. and Muller, M. The hydrogen hypothesis for the first eukaryote. *Nature* 1998; 392:37-41.
- [7] Castresana, J. and Saraste, M. Evolution of energetic metabolism: the respiration-early hypothesis. *Trends Biochem Sci* 1995; 20:443-448.
- [8] Gray, M. W. Evolution of organellar genomes. *Curr Opin Genet Dev* 1999; 9:678-687.
- [9] Kurland, C. G. and Andersson, S. G. Origin and evolution of the mitochondrial proteome. *Microbiol Mol Biol Rev* 2000; 64:786-820.
- [10] Hellemond, J. J. v.; Klei, A. v. d.; Weelden, S. H. v. and Tielens, A. G. M. Biochemical and evolutionary aspects of anaerobically functioning mitochondria. *Philosophical Transactions of the Royal Society of London. Series B: Biological Sciences* 2003; 358:205-215.
- [11] Mentel, M. and Martin, W. Energy metabolism among eukaryotic anaerobes in light of Proterozoic ocean chemistry. *Philos Trans R Soc Lond B Biol Sci* 2008; 363:2717-2729.
- [12] Tielens, A. G.; Rotte, C.; van Hellemond, J. J. and Martin, W. Mitochondria as we don't know them. *Trends Biochem Sci* 2002; 27:564-572.
- [13] Zhou, Z.; Takaya, N.; Nakamura, A.; Yamaguchi, M.; Takeo, K. and Shoun, H. Ammonia Fermentation, a Novel Anoxic Metabolism of Nitrate by Fungi. *Journal of Biological Chemistry* 2002; 277:1892-1896.
- [14] Abe, K.; Hattori, H. and Hirano, M. Accumulation and antioxidant activity of secondary carotenoids in the aerial microalga *Coelastrella striolata* var. *multistriata*. *Food Chemistry* 2007; 100:656-661.
- [15] Müller, M.; Mentel, M.; van Hellemond, J. J.; Henze, K.; Woehle, C.; Gould, S. B.; Yu, R.-Y., et al. Biochemistry and Evolution of Anaerobic Energy Metabolism in Eukaryotes. *Microbiology and Molecular Biology Reviews* 2012; 76:444-495.
- [16] Hayes, J. M. and Waldbauer, J. R. The carbon cycle and associated redox processes through time. *Philosophical Transactions of the Royal Society B: Biological Sciences* 2006; 361:931-950.

- [17] Holland, H. D. The oxygenation of the atmosphere and oceans. *Philos Trans R Soc Lond B Biol Sci* 2006; 361:903-915.
- [18] Golblatt C; Lenton, T. M. and Watson, A. J. Bistability of atmospheric oxygen and the Great Oxidation. *Nature* 2006; 443:683-686.
- [19] Poole, R. K.; D'Mello, R.; Hill, S.; Ioannidis, N.; Leung, D. and Wu, G. The oxygen reactivity of bacterial respiratory haemoproteins: oxidases and globins. *Biochim Biophys Acta* 1994; 1187:226-231.
- [20] Hinton, H. E. Respiratory systems of insect egg shells. *Annu Rev Entomol* 1969; 14:343-368.
- [21] Hall, G. a. Unit VII Respiration. In: Hall, J., ed. *Textbook of Medical Physiology*. Philadelphia Pennsylvania, USA: Elsevier; 2012.
- [22] Hill, R. W., Wyse, G. A., Anderson, M. Animal Physiology. MA, USA. : Inc. publishers; 2004: 770 pp.
- [23] Abele, D. Toxic oxygen: the radical life-giver. *Nature* 2002; 420:27.
- [24] Martinez-Cruz, O.; Calderon de la Barca, A. M.; Uribe-Carvajal, S. and Muhlia-Almazan, A. The function of mitochondrial F(O)F(1) ATP-synthase from the whiteleg shrimp Litopenaeus vannamei muscle during hypoxia. *Comp Biochem Physiol B Biochem Mol Biol* 162:107-112.
- [25] Hochachka P. W., S., G.N. Biochemical Adaptation: Mechanism and Process in Physiological Evolution.In: Published, 2002.p
- [26] Buttemer, W. A.; Abele, D. and Costantini, D. From bivalves to birds: oxidative stress and longevity. *Functional Ecology* 2010; 24:971-983.
- [27] Strahl, J.; Dringen, R.; Schmidt, M. M.; Hardenberg, S. and Abele, D. Metabolic and physiological responses in tissues of the long-lived bivalve Arctica islandica to oxygen deficiency. *Comp Biochem Physiol A Mol Integr Physiol* 2011; 158:513-519.
- [28] Ekau, W.; Auel, H.; Pörtner, H. O. and Gilbert, D. Impacts of hypoxia on the structure and processes in pelagic communities (zooplankton, macro-invertebrates and fish). *Biogeosciences* 2010; 7:1669-1699.
- [29] W. Dall, B. J. H. P. C. R. and Sharples, D. J. 8. Life Histories. *Advances in Marine Biology*. Academic Press; 1991: 283-314.
- [30] Mukai, H. and Koike, I. Behavior and Respiration of the Burrowing Shrimps Upogebia major (de Haan) and Callianassa japonica (de Haan). *Journal of Crustacean Biology* 1984; 4:191-200.
- [31] Clegg, J. Embryos of Artemia franciscana survive four years of continuous anoxia: the case for complete metabolic rate depression. *Journal of Experimental Biology* 1997; 200:467-475.
- [32] Menze, M. A.; Hutchinson, K.; Laborde, S. M. and Hand, S. C. Mitochondrial permeability transition in the crustacean Artemia franciscana: absence of a calcium-regulated pore in the face of profound calcium storage. *American Journal of Physiology - Regulatory, Integrative and Comparative Physiology* 2005; 289:R68-R76.
- [33] Galli, G. L. and Richards, J. G. Mitochondria from anoxia-tolerant animals reveal common strategies to survive without oxygen. *J Comp Physiol B*.

- [34] Baracchini, O. and Sherris, J. C. The chemotactic effect of oxygen on bacteria. *J Pathol Bacteriol* 1959; 77:565-574.
- [35] Ulloa, O.; Canfield, D. E.; DeLong, E. F.; Letelier, R. M. and Stewart, F. J. Microbial oceanography of anoxic oxygen minimum zones. *Proc Natl Acad Sci U S A* 2012; 109:15996-16003.
- [36] Ingledew, W. J. and Poole, R. K. The respiratory chains of *Escherichia coli*. *Microbiol Rev* 1984; 48:222-271.
- [37] Unden, G. and Bongaerts, J. Alternative respiratory pathways of *Escherichia coli*: energetics and transcriptional regulation in response to electron acceptors. *Biochim Biophys Acta* 1997; 1320:217-234.
- [38] Chakraborty, B.; Biswas, S.; Mondal, S. and Bera, T. Stage specific developmental changes in the mitochondrial and surface membrane associated redox systems of *Leishmania donovani* promastigote and amastigote. *Biochemistry (Mosc)* 2010; 75:494-518.
- [39] Van Assche, T.; Deschacht, M.; da Luz, R. A.; Maes, L. and Cos, P. *Leishmania-macrophage* interactions: insights into the redox biology. *Free Radic Biol Med* 2011; 51:337-351.
- [40] Goncalves, R. L.; Barreto, R. F.; Polycarpo, C. R.; Gadelha, F. R.; Castro, S. L. and Oliveira, M. F. A comparative assessment of mitochondrial function in epimastigotes and bloodstream tryptomastigotes of *Trypanosoma cruzi*. *J Bioenerg Biomembr* 2011; 43:651-661.
- [41] Krungkrai, J. The multiple roles of the mitochondrion of the malarial parasite. *Parasitology* 2004; 129:511-524.
- [42] Muller, S. Redox and antioxidant systems of the malaria parasite *Plasmodium falciparum*. *Mol Microbiol* 2004; 53:1291-1305.
- [43] McCord, J. M.; Keele, B. B., Jr. and Fridovich, I. An enzyme-based theory of obligate anaerobiosis: the physiological function of superoxide dismutase. *Proc Natl Acad Sci U S A* 1971; 68:1024-1027.
- [44] D'Autreux, B. and Toledo, M. B. ROS as signalling molecules: mechanisms that generate specificity in ROS homeostasis. *Nat Rev Mol Cell Biol* 2007; 8:813-824.
- [45] Kadenbach, B. Intrinsic and extrinsic uncoupling of oxidative phosphorylation. *Biochim Biophys Acta* 2003; 1604:77-94.
- [46] Guerrero-Castillo, S.; Araiza-Olivera, D.; Cabrera-Orefice, A.; Espinasa-Jaramillo, J.; Gutierrez-Aguilar, M.; Luevano-Martinez, L. A.; Zepeda-Bastida, A., et al. Physiological uncoupling of mitochondrial oxidative phosphorylation. Studies in different yeast species. *J Bioenerg Biomembr* 2011; 43:323-331.
- [47] Manon, S.; Roucou, X.; Guerin, M.; Rigoulet, M. and Guerin, B. Characterization of the yeast mitochondria unselective channel: a counterpart to the mammalian permeability transition pore? *Journal of Bioenergetics Biomembranes* 1998; 30:419-429.
- [48] Bernardi, P. The mitochondrial permeability transition pore: a mystery solved? *Front Physiol* 2013; 4:95.
- [49] Uribe-Carvajal, S.; Luevano-Martinez, L. A.; Guerrero-Castillo, S.; Cabrera-Orefice, A.; Corona-de-la-Pena, N. A. and Gutierrez-Aguilar, M. Mitochondrial Unselective Channels throughout the eukaryotic domain. *Mitochondrion* 2011; 11:382-390.

- [50] Nicholls, D. G. and Rial, E. A history of the first uncoupling protein, UCP1. *J Bioenerg Biomembr* 1999; 31:399-406.
- [51] Luevano-Martinez, L. A.; Moyano, E.; de Lacoba, M. G.; Rial, E. and Uribe-Carvajal, S. Identification of the mitochondrial carrier that provides *Yarrowia lipolytica* with a fatty acid-induced and nucleotide-sensitive uncoupling protein-like activity. *Biochim Biophys Acta* 2010; 1797:81-88.
- [52] Guerrero-Castillo, S.; Cabrera-Orefice, A.; Vazquez-Acevedo, M.; Gonzalez-Halphen, D. and Uribe-Carvajal, S. During the stationary growth phase, *Yarrowia lipolytica* prevents the overproduction of reactive oxygen species by activating an uncoupled mitochondrial respiratory pathway. *Biochim Biophys Acta* 2012; 1817:353-362.
- [53] Cabrera-Orefice, A.; Chiquete-Felix, N.; Espinasa-Jaramillo, J.; Rosas-Lemus, M.; Guerrero-Castillo, S.; Pena, A. and Uribe-Carvajal, S. The branched mitochondrial respiratory chain from *Debaryomyces hansenii*: components and supramolecular organization. *Biochim Biophys Acta* 2013; 1837:73-84.
- [54] Bernardi, P. Mitochondrial transport of cations: channels, exchangers, and permeability transition. *Physiol Rev* 1999; 79:1127-1155.
- [55] Kwast, K. E. and Hand, S. C. Acute depression of mitochondrial protein synthesis during anoxia: contributions of oxygen sensing, matrix acidification, and redox state. *J Biol Chem* 1996; 271:7313-7319.
- [56] Eads, B. D. and Hand, S. C. Mitochondrial mRNA stability and polyadenylation during anoxia-induced quiescence in the brine shrimp *Artemia franciscana*. *J Exp Biol* 2003; 206:3681-3692.
- [57] Martinez-Cruz, O.; Calderon de la Barca, A. M.; Uribe-Carvajal, S. and Muhlia-Almazan, A. The function of mitochondrial F(O)F(1) ATP-synthase from the whiteleg shrimp *Litopenaeus vannamei* muscle during hypoxia. *Comp Biochem Physiol B Biochem Mol Biol* 2012; 162:107-112.
- [58] Holman, J. D. and Hand, S. C. Metabolic Depression is Delayed and Mitochondrial Impairment Averted during Prolonged Anoxia in the ghost shrimp, *Lepidophthalmus louisianensis* (Schmitt, 1935). *J Exp Mar Bio Ecol* 2009; 376:85-93.
- [59] Borisov, V. B.; Murali, R.; Verkhovskaya, M. L.; Bloch, D. A.; Han, H.; Gennis, R. B. and Verkhovsky, M. I. Aerobic respiratory chain of *Escherichia coli* is not allowed to work in fully uncoupled mode. *Proceedings of the National Academy of Sciences* 2011; 108:17320-17324.
- [60] Kerscher, S. J. Diversity and origin of alternative NADH:ubiquinone oxidoreductases. *Biochimica et Biophysica Acta (BBA) - Bioenergetics* 2000; 1459:274-283.
- [61] Büschges, R.; Bahrenberg, G.; Zimmermann, M. and Wolf, K. Nadh: Ubiquinone oxidoreductase in obligate aerobic yeasts. *Yeast* 1994; 10:475-479.
- [62] Vanlerberghe, G. C. and McIntosh, L. Alternative Oxydase: From Gene to Function. *Annu Rev Plant Physiol Plant Mol Biol* 1997; 48:703-734.
- [63] McDonald, A. and Vanlerberghe, G. Branched mitochondrial electron transport in the Animalia: presence of alternative oxidase in several animal phyla. *IUBMB Life* 2004; 56:333-341.
- [64] Tschischka, K.; Abele, D. and Portner, H. O. Mitochondrial oxyconformity and cold adaptation in the polychaete *Nereis pelagica* and the bivalve *Arctica islandica* from the Baltic and White Seas. *J Exp Biol* 2000; 203:3355-3368.

- [65] Buchner, T.; Abele, D. and Portner, H. O. Oxyconformity in the intertidal worm *Sipunculus nudus*: the mitochondrial background and energetic consequences. *Comp Biochem Physiol B Biochem Mol Biol* 2001; 129:109-120.
- [66] Hildebrandt, T. M. and Grieshaber, M. K. Three enzymatic activities catalyze the oxidation of sulfide to thiosulfate in mammalian and invertebrate mitochondria. *FEBS Journal* 2008; 275:3352-3361.
- [67] McDonald, A. E.; Vanlerberghe, G. C. and Staples, J. F. Alternative oxidase in animals: unique characteristics and taxonomic distribution. *Journal of Experimental Biology* 2009; 212:2627-2634.
- [68] Vanlerberghe, G. C.; Robson, C. A. and Yip, J. Y. Induction of mitochondrial alternative oxidase in response to a cell signal pathway down-regulating the cytochrome pathway prevents programmed cell death. *Plant Physiol* 2002; 129:1829-1842.
- [69] Cook, G. M. and Poole, R. K. Oxidase and periplasmic cytochrome assembly in *Escherichia coli* K-12: CydDC and CcmAB are not required for haem-membrane association. *Microbiology* 2000; 146 ( Pt 2):527-536.
- [70] Wu, M.; Sun, L. V.; Vamathevan, J.; Riegler, M.; Deboy, R.; Brownlie, J. C.; McGraw, E. A., et al. Phylogenomics of the reproductive parasite *Wolbachia* *pipientis* wMel: a streamlined genome overrun by mobile genetic elements. *PLoS Biol* 2004; 2:E69.
- [71] Klasson, L.; Walker, T.; Sebaihia, M.; Sanders, M. J.; Quail, M. A.; Lord, A.; Sanders, S., et al. Genome evolution of *Wolbachia* strain wPip from the *Culex pipiens* group. *Mol Biol Evol* 2008; 25:1877-1887.
- [72] Haddock, B. A. and Jones, C. W. Bacterial respiration. *Bacteriol Rev* 1977; 41:47-99.
- [73] Jones, K. Acetilene reduction by mats of blue-green algae in sub-tropical grassland: Possible contribution by other micro-organisms. *New Phytologist* 1977; 78:437-440.
- [74] Ng, T. C. N.; Laheri, A. N. and Maier, R. J. Cloning, sequencing, and mutagenesis of the cytochrome c4 gene from *Azotobacter vinelandii*: characterization of the mutant strain and a proposed new branch in the respiratory chain. *Biochimica et Biophysica Acta (BBA) - Bioenergetics* 1995; 1230:119-129.
- [75] Bertsova, Y. V.; Bogachev, A. V. and Skulachev, V. P. Two NADH:ubiquinone oxidoreductases of *Azotobacter vinelandii* and their role in the respiratory protection. *Biochim Biophys Acta* 1998; 1363:125-133.
- [76] González, P. J.; Correia, C.; Moura, I.; Brondino, C. D. and Moura, J. J. G. Bacterial nitrate reductases: Molecular and biological aspects of nitrate reduction. *J Inorg Biochem* 2006; 100:1015-1023.
- [77] Peacock, A. J. ABC of oxygen: oxygen at high altitude. *Br Med J* 1998; 317:1063-1066.
- [78] Popel, A. S. Theory of oxygen transport to tissue. *Crit Rev Biomed Eng* 1989; 17:257-321.
- [79] Wilson, D. F.; Rumsey, W. L.; Green, T. J. and Vanderkooi, J. M. The oxygen dependence of mitochondrial oxidative phosphorylation measured by a new optical method for measuring oxygen concentration. *J Biol Chem* 1988; 263:2712-2718.
- [80] Geng, M. and Duan, Z. Prediction of oxygen solubility in pure water and brines up to high temperatures and pressures. *Geochimica et Cosmochimica Acta* 2010; 74:5631-5640.

- [81] Chapelle, G. and Peck, L. S. Amphipod Crustacean Size Spectra: New Insights in the Relationship between Size and Oxygen. *Oikos* 2004; 106:167-175.
- [82] Beman, J. M. and Carolan, M. T. Deoxygenation alters bacterial diversity and community composition in the ocean's largest oxygen minimum zone. *Nat Commun* 2013; 4:2705.
- [83] Borsuk, M. E.; Stow, C. A.; Luettich Jr, R. A.; Paerl, H. W. and Pinckney, J. L. Modelling Oxygen Dynamics in an Intermittently Stratified Estuary: Estimation of Process Rates Using Field Data. *Estuarine, Coastal and Shelf Science* 2001; 52:33-49.
- [84] Engle, V. and Summers, J. K. Refinement, validation, and application of a benthic condition index for Northern Gulf of Mexico estuaries. *Estuaries* 1999; 22:624-635.

**Table 1: Oxygen Concentrations in Different Environments.**

Environment	Oxygen concentration ( $\mu\text{M}$ )		References
<b>Atmosphere</b>	1000m ASL	256.0	[77]
	Sea level	1028.0	
<b>Alveoles</b>		143.0	[21]
<b>Arteries</b>		123.0	[21]
	<i>Hb bound</i>	120.5	[78]
	<i>Not bound</i>	2.5	
<b>Capillaries</b>		130.0	[21]
<b>Interstitial fluid</b>		55.0	[21]
<b>Tissue cells</b>		31.0	[21]
<b>Veins</b>		59.0	[21]
<b>Mitochondria</b>	Minimal for coupling	0.1	[79]
	Minimal reported	20.0	
<b>Distilled water</b>		223.0	[80]
<b>Sea water</b>	Surface	198-397.0	[81]
		250.0	[35]
	MOZ	< 20.0	[82]
<b>Estuaries</b>	Surface	375.0	[83]
	Bottom	62.5	[84]

Oxygen concentrations reported were modified from partial pressures to micromolar concentration ( $\mu\text{M}$ ) using Henry's law at 310.15 K.ASL, (above sea level).

**FIGURE LEGENDS :**

**Fig. 1. Oxygen management strategies in different organisms.** Organisms need to adapt to the O<sub>2</sub> concentration in the environment. Therefore, either they move to environments with adequate O<sub>2</sub> or they engineer different mechanisms to process O<sub>2</sub> at varying rates (Electron transport chain (ETC) activity, mitochondrial unspecific channels (MUC), uncoupling proteins (UCPs)). Additionally, oxyregulators have developed O<sub>2</sub>-excluding mechanisms such as impermeable epithelia, external respiratory systems (Lungs, gills, stomas) and O<sub>2</sub>-transporting proteins (Hemoglobin, myoglobin).

**Fig. 2. Migration of Shrimp during their life cycle.** Shrimp spend most of their life in the open sea, where they mate and lay eggs which hatch and undergo different larval stages (Nauplius, Protozoa, Mysis). Once in the poslarval stage, they travel to estuaries where they mature reaching the juvenile stage, and burying themselves in the sand for long periods. Once maturity is reached, they begin the cycle again returning to the open sea. This migration pattern takes shrimp to waters with widely different O<sub>2</sub> concentrations.

**Fig. 3. Diversity of bacterial respiratory chains at different [O<sub>2</sub>]. A.** The respiratory chain from *Escherichia coli* during aerobiosis, micro-aerobiosis and anaerobiosis. Modified from [36, 37]. Ubiquinone is expressed at high [O<sub>2</sub>] and NADH DH type II is overexpressed as compared to the NADH DH type I, which in turn is expressed at low [O<sub>2</sub>]. The major final oxidase is cytochrome *bo*. During anaerobiosis, the respiratory chain in *Escherichia coli* succinate dehydrogenase is not expressed, whereas fumarate reductase or nitrate reductase may be the final electron acceptors. **B,** Hypothetical respiratory chain of *Wolbachia pipiensis* constructed from BLAST and genome sequences reported in [70, 71]. At high [O<sub>2</sub>] cytochrome bc1 and different cytochrome oxidases are expressed. Under micro-aerobic conditions cytochrome *bd* is expressed. Then under anaerobiosis, nitrate reductase is expressed.

Oxygen  
management  
strategies

Oxyconformers

- Modulation of respiratory metabolism
- Physiological uncoupling mechanisms
- Migration to adequate oxygen concentrations
- Different life stages

Crustacea (Hollman, 2009)  
Yeast (Díaz-Ruiz *et al*, 2010)  
Bacteria (Unden *et al*, 1997)

Yeast (Guerrero-Castillo *et al*, 2011)  
Plants (Vanlenberghe *et al*, 1997)  
Endoparasites (Müller *et al*, 2004)

Crustacea (Ekau, 2010)  
Bacteria (Baracchini and Sherris, 1959)

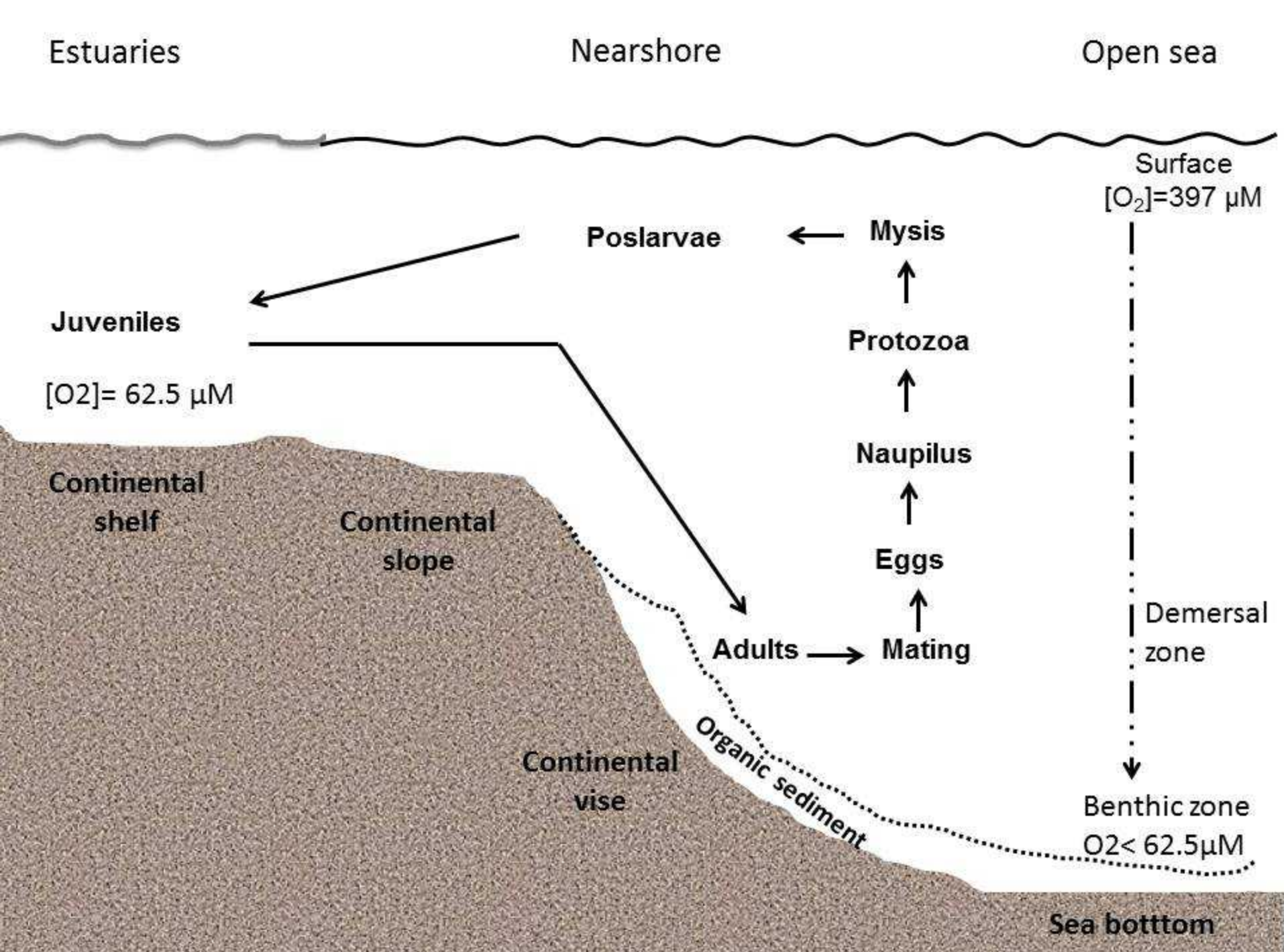
Endoparasites (Krunkrai, 2004)  
Endosymbionts (Uribe-Álvarez, personal communication)  
Crustacea (Dall *et al*, 1990)

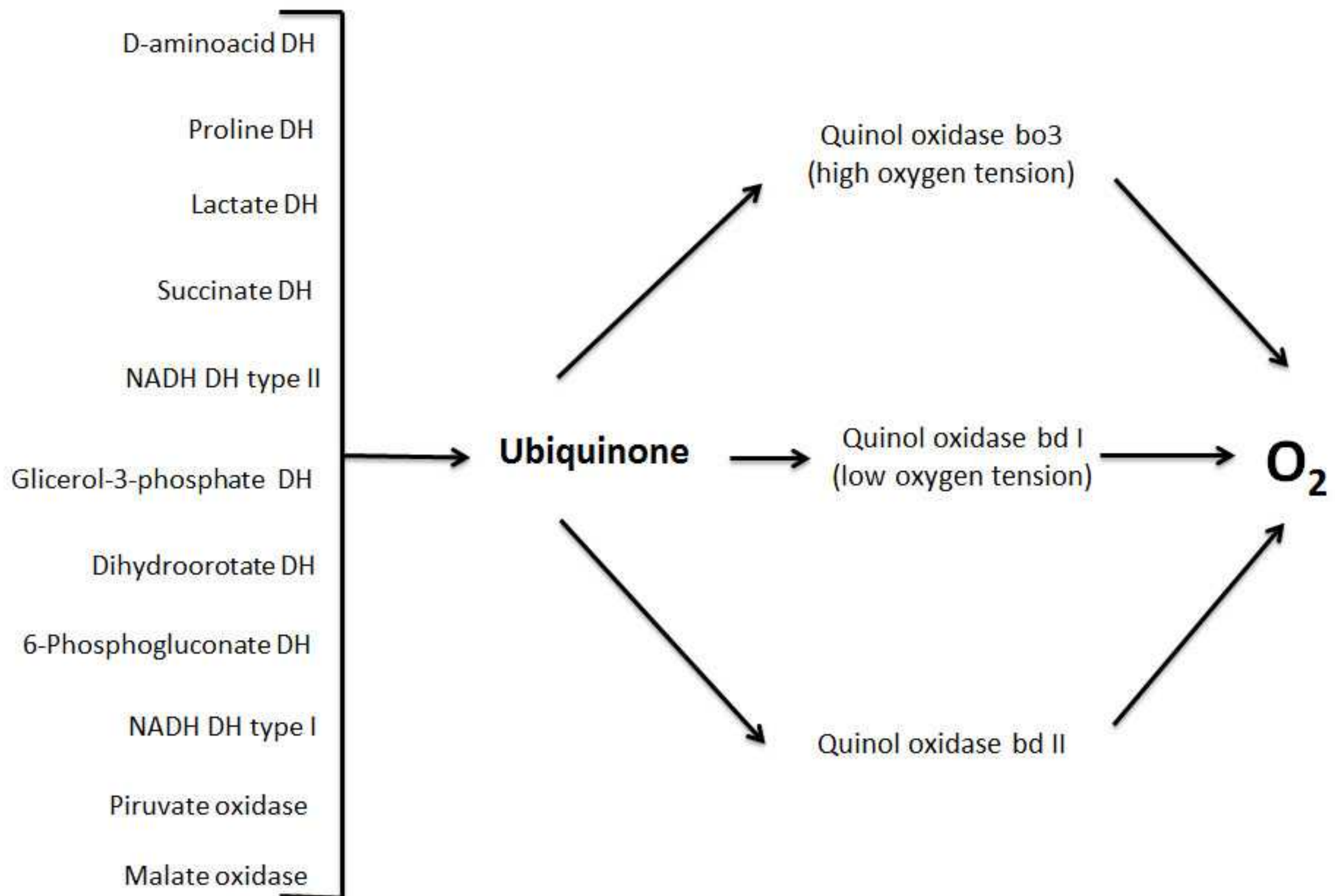
Oxyregulators

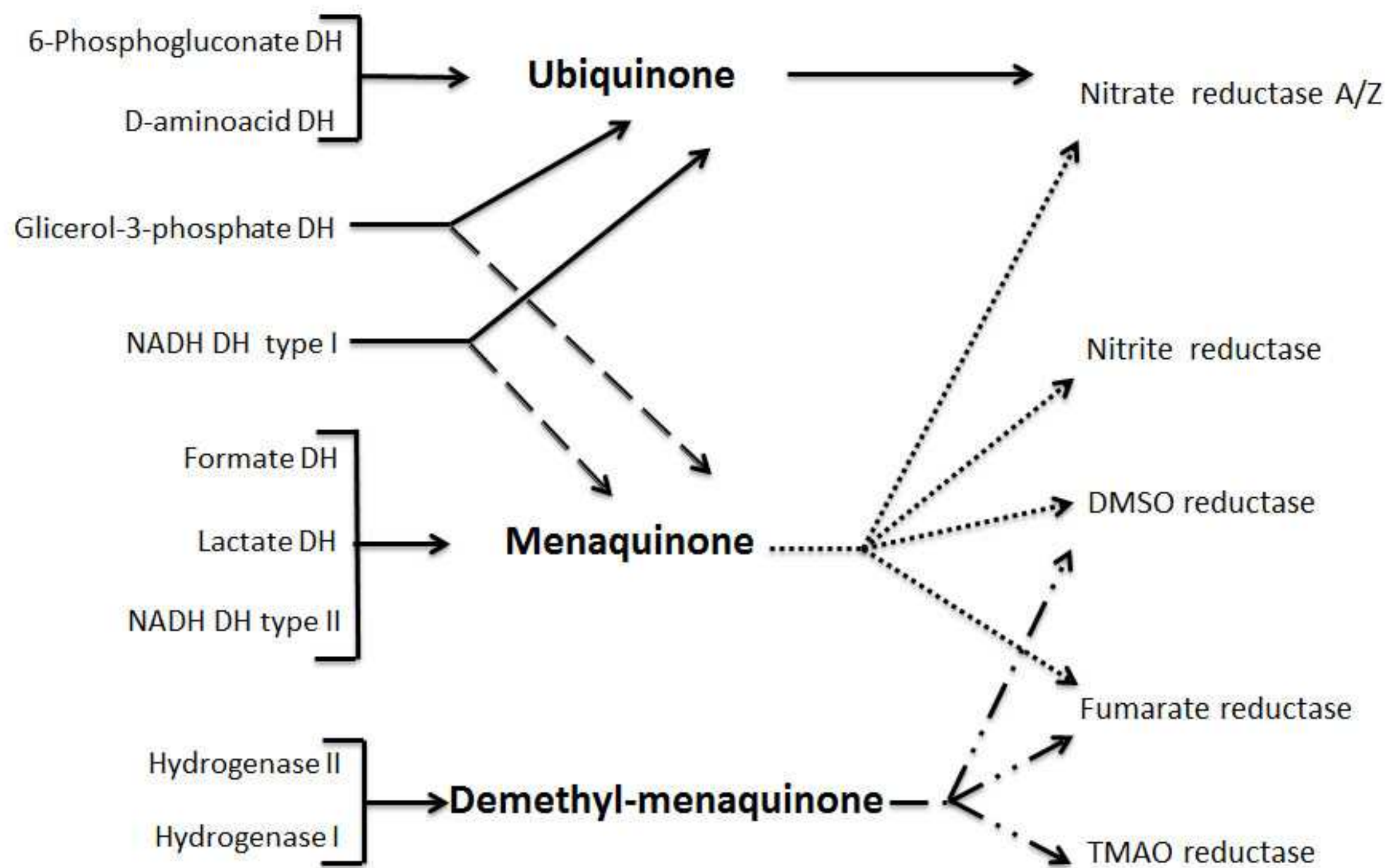
- Impermeable epithelia
- Protein buffers
- Sophisticated respiratory systems

Hemoglobin (Hinton, 1969)  
Myoglobin (Hinton, 1969)

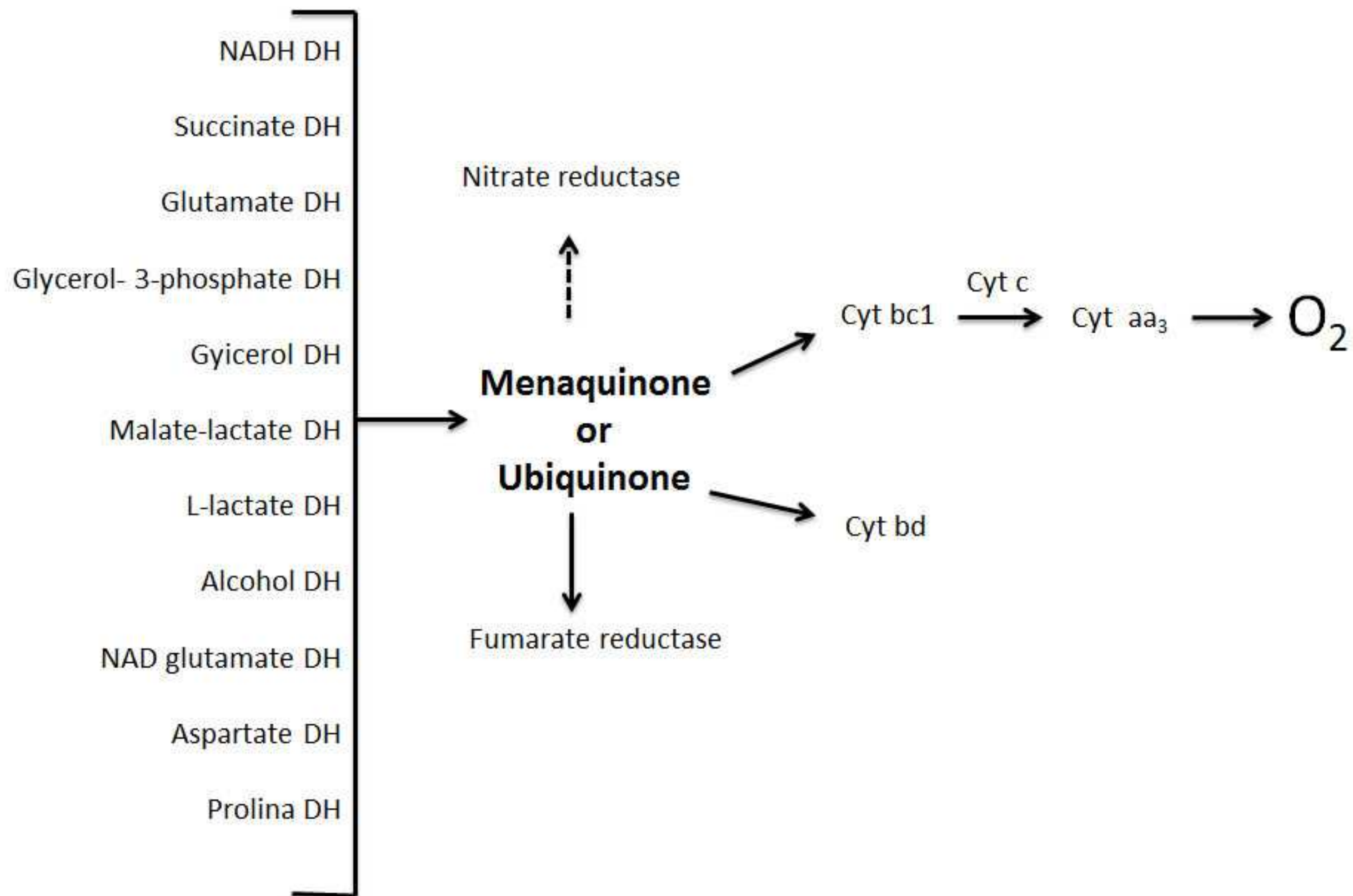
Gills (Hill *et al*, 2004)  
Lungs (Hill *et al*, 2004)  
Stomas (Hill *et al*, 2004)



**A**FIG. 3 A. Rosas-Lemus *et al.*, 2014

**B**FIG. 3 B. Rosas-Lemus *et al.*, 2014

C

FIG. 3 C. Rosas-Lemus *et al.*, 2014